Performance Evaluation of Active Chilled Beam in Cooling and Heating Operation under Actual Field Boundary Conditions

Rohit Kumar Upadhyay

A Thesis

in the

Building Science Graduate Program

Presented in Partial Fulfillment of the Requirements for the

Degree of Master of Applied Science in Building Engineering/Building Science

at the

British Columbia Institute of Technology

Burnaby, British Columbia, Canada

October, 2018

BRITISH COLUMBIA
INSTITUTE OF TECHNOLOGY

Building Science Graduate Program
School of Construction
and the Environment
3700 Willingdon Avenue
Burnaby, British Columbia
Canada V5G 3H2

bcit.ca

This is to certify that the thesis prepared

By: ROHIT UPADHYAY Student Number:

Entitled: PERFORMANCE EVALUATION OF ACTIVE CHILLED BEAM IN COOLING AND HEATING OPERATION UNDER ACTUAL FIELD BOUNDARY CONDITIONS

And submitted in partial fulfillment of the requirement for the degree of:

Master of Applied Science in Building Engineering/Building Science

Complies with the regulations of the Institute and meets the accepted standards with respect to originality and quality.

Signed by the final Examining Committee:

Bo Li, MASc, P.Eng., Chair

Weimin Wang, PhD, University of North Carolina, Examiner, external to program

M. Kavgic

Miroslava Kavgic, PhD, University of Manitoba, Examiner, external to program

Rodrigo Mora, PhD, Supervisor

Approved by:

Graduate Program Director

ABSTRACT

People spend most of their time indoors and often share the same environment; therefore, knowledge and prediction of the indoor conditions are important to optimize the indoor conditions for the occupants at the building design phase. A range of parameters like air velocity, temperature and relative humidity determines the indoor climate and are important for the comfort of the occupant of a room in terms of thermal comfort and indoor air quality.

Active Chilled Beam (ACB), a high-performance air distribution system has gained popularity as an energy efficient, sustainable comfort cooling technology with favourable performance in term of thermal comfort to occupants. ACB is wildly utilized in a variety of commercial buildings, schools, laboratories and hospitals. However, in-depth investigations on the performance of these systems under different boundary conditions are still inadequate.

Many studies have been conducted on ACB in cooling mode. However, the performance and efficiency of active beams under different real-life boundary conditions (cooling and heating mode) have not been documented. Studying performance of ACB under real boundary conditions is critical because, unlike typical ceiling air diffusers, the performance of ACB (i.e. induction ratio) is tightly coupled with the conditions of the room it serves, and the ACB performance effects, in turn, the quality of air distribution in the room. The focus of the study is not measuring the performance of ACB through thermal comfort or draft rate as previously done in many studies. The study is focused on characterization of room level by mapping the airflow and temperature distribution in the room and to gather data to perform numerical simulations to visualize the various characteristics of air in the space by CFD modelling.

Therefore, this research follows a field-study approach in two offices to investigate the performance of ACB in a high-performance building under cooling and heating operation. The performance matrix used in this study is thermal stratification and the temperature difference between the ankle and head for a sitting and a standing person in the occupied zone and ventilation efficiency by numerical simulations. The ACB used in the case study is 4 – pipe, cooling and heating type. The performance of ACB is assessed at two levels: 1) at the ACB level, using ACB measurements and metrics; and 2) at the room level, using measurements and metrics that assess room thermal uniformity and airflow conditions for comfort and air quality.

ACB measurements include supply and induced air velocities and temperatures. Room-level microclimatic measurements include air velocities, air temperatures, operative temperatures, and surface temperatures at selected locations. Comparisons are made to evaluate the ACB performance through a performance matrix. CFD models are created and validated with data with two purposes: to help gain insights into the physical phenomena and to investigate suitable models that could potentially be used to help inform design decisions at the room level. A high-performance LEED Gold building at British Columbia Institute of Technology (BCIT) at Burnaby, B.C. Canada is used for the field study.

The findings from the experiments show that the performance of ACB is affected by factors of varying nature; firstly the design of ACB itself, the operation mode (heating and cooling) and the room level conditions (enclosure, occupants and other loads). The experimental analyses of ACB indicate discharge temperatures and velocities at both ACB slots are not equal in both the cooling and heating operations, which affects the room air distribution. In the heating operation, in particular, a stratified layer is created and air movement in the occupied zone (for heights 0.1 m. 0.6 m and 1.1 m) becomes almost negligible and zero. The difference in velocity at both ACB slots could be owing to the design of primary air plenum and connection of air duct to the ACB plenum. The difference in discharge temperature is due to the design of circuits in the heat exchanger for cooling and heating, this difference in temperature is further affected by the difference in air velocities at both the ends. The difference in temperature and velocity needs thorough research in a controlled environment to study plenum pressure, outlet velocities and temperatures at discharge slots.

The findings from surface temperature distribution under steady state condition show that the ACB is effective in cooling and heating as the surface temperatures are in line with the room setpoint. The data from room air distribution indicates that the air velocities in the occupied zone are well below the maximum air velocities specified in the occupied zone in ASHRAE 55 Standard for thermal comfort. However, the standard does not set any lower limit for air velocities. The air velocity in the heating case in the occupied zone for a sitting person was found negligible and close to zero. This could cause the air stagnation in the occupied zone and the air full of contaminants could lead to poor indoor air quality which needs further investigation in a controlled environment under heating mode.

CFD model of the whole ACB with the room was found challenging to couple with the room level analyses. ACB is a complex structure with a heat exchanger and many tiny nozzles on either side, the size of the nozzles is much smaller as compare to the room dimensions and therefore meshing such geometry with room creates complexity. Therefore, a simplified model of the beam was created with flat panels. The air was assumed to be delivered through the flat panels (slots) with a constant velocity all over the face of the slot instead of nozzles as in case of ACB. The induction was found varying along the induction surface of the ACB during the experiment, was assumed constant in the model with average induction velocity along the surface of the ACB based on the experiment was used as a boundary condition.

The experimental results for air temperature were compared with the CFD simulation to determine the validity of the model and how far the results are matched. Significant agreement was achieved between the CFD simulation and experimental values. The recorded air temperature measurement in office space showed a high level of uniformity and consistency with the CFD results. The average percentage error varied from 0% to 5% with an absolute error of 1°C. However, the CFD model predicted higher air velocities throughout the room, particularly at the 0.1 m height in the occupied zone. The experimental values are almost negligible and close to zero and similarly, the predicted values in the CFD model are much lower than ASHRAE 55: 2017 velocity comfort limits. An average percentage error for air velocities in the order of 250% was found at the 0.1 m height and isolated occurrences of errors in excess of 600% with an absolute error of 0.08 m/s. The difference in predicted and actual measured values could be due to the many constraints like leakages from the ceiling and the cracks from the room which is not considered in the model. Another aspect, as discussed above is the modelling of ACB through simple slots (flat panels) with fixed face velocities, however, the room air in actual is delivered through nozzles and velocity and temperature of air is not constant all along the slots with difference in temperature and velocity in either slot as well, therefore, resulted in significant error. CFD model was further used to find the ventilation efficiency with performance indices like the age of air and the residual lifetime of air which further proved that the age of air in heating is higher than in cooling and air stagnant zone was clearly visible in the contours.

Keywords: Active Chilled Beam, ACB under Cooling, ACB under heating, CFD, Room Airflow, Ventilation Efficiency.

ACKNOWLEDGEMENTS

I would like to express my sincere gratitude to all those who guided me throughout my time at BCIT. First and foremost, I would like to thank my supervisor, Dr. Rodrigo Mora, for accepting me as his student, he has been a guide and mentor in my academic and professional development. His tremendous support at BCIT enabled me to pursue this project and finish it on time. Without his supervision and guidance, the thesis would not be possible.

I thank the Building Science department, Dr. Fitsum Tariku, Bo Li, Ellen Scobie, the whole Building Science staff, my colleague and friends. Special thanks to Mr. Doug Horn, for his help to set up the instruments for field experiments. Without their support in various aspect, this study could not have been successfully completed.

Finally, I want to thank my parents, my wife and kids who are the constant source of support, encouragement and inspiration during these two years.

TABLE OF CONTENTS

ABSTRACT **3**

ACKNOWLEDGEMENTS **6**

1. INTRODUCTION **23**

2. OVERVIEW OF CHILLED BEAM SYSTEMS **25**

2.1 HISTORY OF CHILLED BEAM 25
2.1.1 TYPES OF CHILLED BEAM 27
2.1.2 CONSTRUCTION 30
2.1.3 WORKING PRINCIPLE OF ACTIVE BEAMS 31
2.1.4 CONTROL STRATEGIES IN ACB 34
2.1.5 ADVANTAGES OF ACTIVE BEAM SYSTEMS 35

3. LITERATURE REVIEW **37**

3.1 CHILLED BEAM PERFORMANCE 38
3.2 INDUCTION RATIO MEASUREMENT METHODS 40
3.3 THERMAL COMFORT 43
3.4 SPACE AIR DISTRIBUTION 46
3.5 NUMERICAL STUDIES 50
3.5.1 CFD IN ROOMS WITH CHILLED BEAMS 51
3.5.2 CFD IN ROOMS 52
3.6 SUMMARY OF LITERATURE REVIEW 56

4. PROBLEM STATEMENT **58**

5. RESEARCH APPROACH **60**

5.1 RESEARCH OBJECTIVES 60
5.2 SCOPE AND LIMITATIONS 61

6. RESEARCH METHODOLOGY **62**

6.1 CASE STUDY BUILDING 64

7. EXPERIMENTS AND METHODOLOGY 65

7.1 EXPERIMENTAL FACILITY 65
7.1.1 OFFICES (TEST ROOMS) 65
7.1.2 MEASUREMENTS 73
7.1.3 EXPERIMENTAL PROCEDURE 88
7.2 TEST METHODOLOGY 89
7.2.1 VALIDATION 89
7.2.2 TEST SETUP 89

8. CFD MODELLING 91

8.1 CFD SOFTWARE 91
8.2 MATHEMATICAL FORMULATION 92
8.3 TURBULENCE MODEL 93
8.4 ASSUMPTIONS IN CFD MODELLING 96
8.5 PREPROCESSING 97
8.5.1 GEOMETRY CREATION 97
8.5.2 BOUNDARY CONDITIONS 97
8.5.3 MESHING 100
8.5.4 SOLVING 103
8.5.5 GRID DEPENDENCY TEST 104
8.6 VENTILATION EFFICIENCY 104

9. EXPERIMENTAL RESULTS & DISCUSSION 108

9.1 TEST ROOM 1 – HEATING MODE 108
9.1.1 COANDA EFFECT 108
9.1.2 DISCHARGE AIR VELOCITY 109
9.1.3 DISCHARGE AIR TEMPERATURE 110
9.1.4 SURFACE TEMPERATURE DISTRIBUTION 111
9.1.5 ROOM AIR DISTRIBUTION 113
9.1.6 OPERATIVE TEMPERATURE 117
9.2 TEST ROOM 2 – COOLING MODE 119
9.2.1 DISCHARGE AIR VELOCITY 119

9.2.2 DISCHARGE AIR TEMPERATURE 121
9.2.3 INDUCED AIR VELOCITY & TEMPERATURE 123
9.2.4 SURFACE TEMPERATURE DISTRIBUTION 124
9.2.5 ROOM AIR DISTRIBUTION 128
9.2.6 OPERATIVE TEMPERATURE 134
9.3 AIR VELOCITY IN HEATING AND THERMAL STRATIFICATION 134
9.4 HEAT EXCHANGER – HEATING MODE 135
9.5 CFD MODEL 141
9.5.1 CFD MODEL OF TEST ROOM 1 (UNDER HEATING) 150
9.5.2 CFD MODEL OF TEST ROOM 2 (UNDER COOLING) 162
9.6 VENTILATION EFFECTIVENESS IN HEATING AND COOLING 171

10. CONCLUSIONS 177

11. FURTHER WORK 179

REFERENCES 180

APPENDIX A – ROOM AIR DISTRIBUTION – HEATING 187

APPENDIX B – ROOM AIR DISTRIBUTION – COOLING 194

APPENDIX C – ACB DETAILS (TROX) 218

LIST OF FIGURES

Figures **Page**

Figure 2.1 – Schematic Diagram of an Induction Unit 26

Figure 2.2 – Schematic operation of a passive chilled beam [6] 27

Figure 2.3 - Schematic Operation of an active beam. [9] 29

Figure 2.4 – Multiservice Beam (TROX) [61] 29

Figure 2.5 - Typical Construction of Active chilled beam Unit [10] 30

Figure 2.6 - Schematic diagram of a 2-way Discharge Active Chilled Beam Unit [11] 31

Figure 2.7 - Low pressure kernel at the outlet of the nozzle [11] 32

Figure 2.8 - Induction effect of Active Beam [11] 32

Figure 2.9 - Heat Exchanger Operations [11] 33

Figure 2.10 - Mixing Valve Operation [11] 33

Figure 2.11 – Separate Chillers Loop Operation [11] 34

Figure 2.12 - Typical fan and motor savings for office building dedicated outdoor air systems vs. conventional HVAC systems [9] 36

Figure 3.1 - Principle behind the induction ratio adjustment 1) adjustment on 2) adjustment off 39

Figure 3.2 - Typical trajectory of airflow discharged from Active Chilled Beam Unit (ACB) 46

Figure 3.3 - ACB Model Proposed by Guan et al. [20] 52

Figure 6.1 - Research Methodology Flow Chart 62

Figure 6.2 - The Gateway Building – BCIT, Burnaby, Canada 64

Figure 7.1 - BCIT Gateway Building and the perimeter Office (Test Room 1) at second floor. 65

Figure 7.2 - Dimensions and Layout of the Office (Test Room 1) at Second Floor 66

Figure 7.3 - Test Room - 1 Exposure 67

Figure 7.4 – Active Chilled Beam installed in the Ceiling 67

Figure 7.5 - Location of Test Room 1 & Test Room 2 68

Figure 7.6 - Dimensions and Layout of the Office (Test Room 2) at Second Floor 69

Figure 7.7 - Test Room - 2 Exposures 70

Figure 7.8 – Active Chilled Beam 2 (ACB 2) Installed near the Glass Partition in the Ceiling 70

Figure 7.9 – Active Chilled Beam 1 (ACB 1) Installed near Window in the Ceiling 71

Figure 7.10 - Schematic Illustration of TROX DID632 Active Chilled Beam [Appendix C] . 72

Figure 7.11 - Manifold to Measure Air Velocity and Air Temperature at 4 Different Heights 74

Figure 7.12 – Wiring Connections for Measurement of Air Velocity and Temperature 74

Figure 7.13 - Illustration of Sensoanemo5100LSF air speed/temperature sensor 75

Figure 7.14 - Measurement of Discharge and Induced Air Velocities at Active Chilled Beam 77

Figure 7.15 - Measurement of Induced Air Velocities at Different Sections of ACB 77

Figure 7.16 – Placement of Anemometers at Induced Surface of ACB 78

Figure 7.17 - Measurement of Discharge Air Velocity inside Supply Slot 78

Figure 7.18 - Measurement of Discharge Air Velocity at the Outlet of Supply Slot 79

Figure 7.19 - Magnitude of Typical Discharge (0.93 m/s) and Induced Air Velocity (0.18 m/s) 79

Figure 7.20 - Return Air Grille Velocity and Air Temperature Measurement 80

Figure 7.21 – Placement of HOBO for Discharge and Induced Air Temperature Measurement 81

Figure 7.22 - Outdoor Air Temperature Measurement 81

Figure 7.23 - Operative Temperature Measurement Globe 82

Figure 7.24 - Operative Temperature Measurement at 3 different location. 82

Figure 7.25 - Surface Temperature Measurement Thermistor 84

Figure 7.26 - Temperature Sensors Location in the room surfaces (Test Room 1) 84

Figure 7.27 - Surface Temperature Measurement - Window and Wall 85

Figure 7.28 - Plenum Pressure Measurement 85

Figure 7.29 - On-Coil and Off-Coil Air Temperature Measurement 86

Figure 7.30 - Supply and Return Water Temperature Measurement 86

Figure 7.31 - Coil Surface Temperature Measurement 87

Figure 7.32 – Placement of External Temperature Sensor at Coil Surface 87

Figure 7.33 - Possible Occupant's Location in Test Room 1 (Heating) 89

Figure 8.1 - Simulation Process 92

Figure 8.2 - Mesh Model of Test Room 2 (Internal Surfaces) 102

Figure 8.3 - Mesh Model of Test Room 2 (External Surface) 103

Figure 8.4 - Age of Air and Residual Lifetime of Air [62] 105

Figure 8.5 – CFD Contour of Age of Air [62] 105

Figure 8.6 – CFD Contour of Residual Lifetime of Air [62] 106

Figure 8.7 – CFD Contour of Contribution of Supply Opening [62] 107

Figure 8.8 – CFD Contour of Contribution of Exhaust Opening [62] 107

Figure 9.1 - Coanda Effect through Thermal Image Camera (Heating) 108

Figure 9.2 - Coanda Effect (Heating) 109

Figure 9.3 - Discharge Air Velocity at the Two Slots 109

Figure 9.4 - Discharge Velocity & Temperatures 110

Figure 9.5 - Discharge Air Temperatures at the Two Slots (Heating) 111

Figure 9.6 - Surface Temperatures in Heating for Room Setpoint 20°C 112

Figure 9.7 - Surface Temperatures for Room Setpoint 20°C 112

Figure 9.8 - Window Temperatures at the Top, Bottom and Center for Room Setpoint 20°C 113

Figure 9.9 - Aluminum Extended Profile Obstructing Airflow at the Bottom Portion of the Window 113

Figure 9.10 - Possible Occupant's Location 114

Figure 9.11 - Average / Maximum Air Velocity and Temperature Distribution (at Setpoint 20°C) 114

Figure 9.12 - Air Temperatures & Air Velocity at 0.1, 0.6, 1.1 and 1.7 m Heights at 20°C (Heating) 115

Figure 9.13 - Air Temperatures & Air Velocity at 0.1, 0.6, 1.1 and 1.7 m Heights at 21°C (Heating) 115

Figure 9.14 - Air Temperatures & Air Velocity at 0.1, 0.6, 1.1 and 1.7 m Heights at 22°C (Heating) 116

Figure 9.15 - Air Temperatures & Air Velocity at 0.1, 0.6, 1.1 and 1.7 m Heights at 24°C at Window (Heating) 116

Figure 9.16 – Location of Operative Temperature Measurement (Heating) 117

Figure 9.17 - Room Setpoint and Room Temperature (Heating) 118

Figure 9.18 - Room Setpoint and Operative Temperature at Desk 1 118

Figure 9.19 - Room Setpoint and Operative Temperature at Desk 2 118

Figure 9.20 - Room Setpoint and Operative Temperature at Desk 3 119

Figure 9.21 - Discharge Air Velocities at One Slot (Cooling) 119

Figure 9.22 - Location of Anemometers at Supply Slots and Induction Surface of ACB 120

Figure 9.23 - Discharge Air Velocities at the Other Slot (Cooling) 120

Figure 9.24 - Difference in Average Air Velocities at 2 Slots of ACB (Cooling) 121

Figure 9.25 - Discharge Temperature at Slot 1 at 3 Different Locations 121

Figure 9.26 - Discharge Temperature at Slot 2 at 2 different locations 122

Figure 9.27 - Difference in Discharge Air Temperature & Induced Air Temperature (Cooling) 122

Figure 9.28 - Difference in Discharge Air Temperature (Cooling) 123

Figure 9.29 - Induced Air Velocity at ACB 1 (Cooling) 123

Figure 9.30 - Induced Air Temperature at ACB 1 (Cooling) 124

Figure 9.31 - Floor Surface Temperature Measured at 2 Locations (Cooling) 125

Figure 9.32 - Ceiling Temperatures Measured at 5 Locations (Cooling) 125

Figure 9.33 - Glass Partition Surface Temperatures Measured at 3 Locations (Cooling)..... 126

Figure 9.34 - Window Temperatures Measured at 6 Locations (Cooling)..... 126

Figure 9.35 - Internal Partition Temperature Measured at 4 Locations (Cooling)..... 126

Figure 9.36 - Internal Concrete Wall Temperature Measured at 6 Locations (Cooling) 127

Figure 9.37 - Average Surface Temperatures (Cooling) 127

Figure 9.38 - Measurement Points in the Test Room 2 for Room Air Distribution (Cooling) 128

Figure 9.39 - Average Air Velocity & Air Temperature at Section 3 (1.6 m) in Cooling 130

Figure 9.40 - Air Temperature at Section 3 of Test Room 2 (Setpoint 22°C in Cooling) 131

Figure 9.41 - Air Velocity at Section 3 of Test Room 2 (Setpoint 22°C in Cooling) 131

Figure 9.42 - Air Temperature at 4 Different Heights across Section 3 of Test Room 2 (Setpoint 22°C in Cooling)..... 132

Figure 9.43 - Air Velocity at 4 Different Heights across Section 3 of Test Room 2 (Setpoint 22°C in Cooling)..... 132

Figure 9.44 - Air Velocities & Temperatures at Section 1, 2 and 3 respectively at SP 22°C 133

Figure 9.45 - Room Setpoint and Operative Temperature (Near Occupant, In Cooling) 134

Figure 9.46 - Typical Average Air Velocities in Heating at 0.1, 0.6, 1.1, 1.7 m 135

Figure 9.47 - Vertical Cross Section of Heat Exchanger of ACB 136

Figure 9.48 - Top View of Heat Exchanger of ACB with Temperature Sensor Location 136

Figure 9.49 - Cross-Section of Heat Exchanger and Temperature Sensor Location..... 137

Figure 9.50 - Air Temperature above the Coil at Different Locations (Cooling) 137

Figure 9.51 - Air Temperature above the Coil at Different Locations (Heating)..... 137

Figure 9.52 - Difference between Top Center & End Surface Temperature of the Coil (Cooling) 138

Figure 9.53 - Difference between Top Center & End Surface Temperature of the Coil (Heating) 138

Figure 9.54 - Difference in Bottom Surface Temperature of the Heat Exchanger (Heating) 139

Figure 9.55 - Lengthwise Difference in Air Temperature of the Heat Exchanger 139

Figure 9.56 - Widthwise Temperature Difference of Heat Exchanger (Heating) 140

Figure 9.57 - Active Chilled Beam Complex Geometry Model in CFD 141

Figure 9.58 - Active Chilled Beam Flat Panel Model 143

Figure 9.59 - Section of ACB with One Nozzle on Each Side 144

Figure 9.60 - Velocity Profile inside an ACB 145

Figure 9.61 - Velocity Contour and Velocity Vectors at 26° Discharge Angle 146

Figure 9.62 - Velocity Contour and Velocity Vectors at 45° Discharge Angle 147

Figure 9.63 - Velocity Contour and Velocity Vectors at 60° Discharge Angle 148

Figure 9.64 - CFD Model of Test Room 1 (Heating) 150

Figure 9.65 - Temperature Contour Plot at Different Room Sections at Setpoint 20 °C (Heating) 151

Figure 9.66 - Velocity Vector Plot at 20°C (Heating) 151

Figure 9.67 - Temperature Contour Plot at Room Height 0.1 m, 0.6 m, 1.1 m and 1.7 m at 20°C (Heating) 152

Figure 9.68 - Velocity Contour Plot – Room Sections - at Different Range of Velocity at 20°C (Heating) 153

Figure 9.69 - Velocity Contour Plot at 2.945 m Height at 20°C (Heating) 154

Figure 9.70 - Velocity Contour Plot at 2.9 m Height (Left) and 1.8 m Height (Right) at 20°C (Heating) 154

Figure 9.71 - Temperature Contour Plot - Different Room Sections at Setpoint 24°C (Heating) 156

Figure 9.72 - Temperature Contour Plot at Different Room Heights at SP 24°C (Heating) .. 157

Figure 9.73 - Velocity Contour Plot at Different Room Heights at SP 24°C (Heating) 158

Figure 9.74 - Velocity Contour Plot at Different Room Sections at SP 24°C (Heating) 159

Figure 9.75 - CFD Model of Test Room 2 162

Figure 9.76 - Temperature Contour Plot at Room Setpoint 22 °C 163

Figure 9.77 - Velocity Contour Plot at Room Setpoint 22 °C 164

Figure 9.78 - Temperature Contour Plot at the Occupant in Y Direction 165

Figure 9.79 - Velocity Vector Plot at Section 1 and 4 165

Figure 9.80 - Temperature Plot at Different Heights in the Room 166

Figure 9.81 - Velocity Vectors Higher Than 0.2 m/s at 4 Different Sections in Occupied Zone 167

Figure 9.82 - Age of Air at Test Room 1 (Heating) 171

Figure 9.83 - Age of Air at Test Room 2 (Cooling) 172

Figure 9.84 - Residual Lifetime of Air at Test Room 1 (Heating) 173

Figure 9.85 - Residual Lifetime of Air at Test Room 2 (Cooling) 173

Figure 9.86 - Contribution Ratio of Supply Openings in Heating and Cooling 174

Figure 9.87 - Contribution Ratio of Exhaust Grille 175

Figure 9.88 - Contribution Ratio of Induction Surface (Heating) 176

Figure 9.89 - Contribution Ratio of Induction Surface (Cooling) 176

Figure A.1 - Air Temperature and Velocity Distribution at Room Setpoint 21 (°C) 187

Figure A.2 - Air Temperature and Velocity Distribution at Room Setpoint 22 (°C) 188

Figure A.3 - Air Temperature and Velocity Distribution at the Window with Room SP 24 (°C) 189

Figure A.4 - Grid Points in the Test Room 1 for Measurement of Air Temperature and Velocity 190

Figure A.5 - Section 1 – Air Temperature and Air Velocity at Room SP 24 (°C) 191

Figure A.6 - Section 2 – Air Temperature and Air Velocity at Room SP 24 (°C) 192

Figure A.7 - Section 3 – Air Temperature and Air Velocity at Room SP 24 (°C) 193

Figure B.1 - Grid Points in the Test Room 2 for Measurement of Air Temperature & Velocity 194

Figure B.2 - Average Air Velocity & Air Temperature at Section 1 (0.75 m) in Cooling 196

Figure B.3 - Average Air Velocity & Air Temperature at Section 2 (1.2 m) in Cooling 197

Figure B.4 - Air Temperature at Section 1 of Test Room 2 (Setpoint 22°C in Cooling) 198

Figure B.5 - Air Velocities at Section 1 of Test Room 2 (Setpoint 22°C in Cooling) 198

Figure B.6 - Air Temperatures at 4 Different Heights and Room Setpoint (Section 1 @22°C) 199

Figure B.7 - Air Velocities at 4 Different Heights and Room Setpoint (Section 1 @22°C) .. 199

Figure B.8 - Air Velocities & Temperatures at Section 1, 2 and 3 respectively at SP 22°C . 200

Figure B.9 - Air Temperature at Section 2 of Test Room 2 (Setpoint 22°C in Cooling) 201

Figure B.10 - Air Velocity at Section 2 of Test Room 2 (Setpoint 22°C in Cooling) 201

Figure B.11 - Air Temperature at 4 Different Heights across Section 2 of Test Room 2 (Setpoint 22°C in Cooling).....201

Figure B.12 - Air Velocity at 4 Different Heights across Section 2 of Test Room 2 (Setpoint 22°C in Cooling).....202

Figure B.13 - Spatial Distribution of Air Temperature and Velocity at Room SP Setpoint 24 (°C) (Section 1).....204

Figure B.14 - Section 1 – Graphs for Air Velocity and Temperature at 4 Different Heights SP 24(°C) 205

Figure B.15 - Section 1 – Graphs for Air Velocity and Temperature at SP 24(°C) 206

Figure B.16 - Spatial Distribution of Air Temperature and Velocity at Room SP Setpoint 24 (°C) (Section 2).....207

Figure B.17 - Section 2 – Graphs for Air Velocity and Temperature at 4 Different Heights SP 24(°C) 208

Figure B.18 - Section 2 – Graphs for Air Velocity and Temperature at SP 24(°C) 209

Figure B.19 - Spatial Distribution of Air Temperature and Velocity at Room SP Setpoint 24 (°C) (Section 3).....210

Figure B.20 - Section 3 – Graphs for Air Velocity and Temperature at 4 Different Heights at SP 24(°C).....211

Figure B.21 - Section 3 – Graphs for Air Velocity and Temperature at SP 24(°C) 212

Figure B.22 - Spatial Distribution of Air Temperature and Velocity at Room SP Setpoint 20 (°C) (Section 1).....214

Figure B.23 - Spatial Distribution of Air Temperature and Velocity at Room SP Setpoint 20 (°C) (Section 2).....215

Figure B.24 - Spatial Distribution of Air Temperature and Velocity at Room SP Setpoint 20 (°C) (Section 3).....216

Figure B.25 - Section 1, 2 and 3 – Graphs for Air Velocity and Temperature at SP 20(°C) .217

LIST OF TABLES

Table **Page**

Table 3.1. – Studies Related to Chilled Beam Performance 38

Table 3.2 – Studies Related to Induction Ratio Measurements 40

Table 3.3 – Studies Related to Thermal Comfort 43

Table 3.4 – Studies Related to Room Air Distribution 47

Table 7.1 - Building Design Summary 71

Table 7.2 - Specifications of the Active Chilled Beam in Test Rooms 72

Table 7.3 - Specification of Anemometer 76

Table 7.4 - Sensor Specifications for Office Experiment 83

Table 8.1 – Constants of the Standard k – ε Model 95

Table 8.2 – Reynolds Number at the ACB Outlet 96

Table 8.3 – Volume Conditioner Properties 98

Table 8.4 – Fluid (Air) Properties 98

Table 8.5 - Boundary Conditions for CFD Model 99

Table 8.6 - Heat Transfer Coefficient (U Value) of Thermal Boundaries 99

Table 8.7 - Internal Heat Load in Test Rooms 100

Table 8.8 - Details of Meshing 102

Table 8.9 – Solver Details 103

Table 9.1 - Air Velocity and Air Temperature in Cooling at Setpoint Temperature 22°C (Cooling) 129

Table 9.2 - Temperature and Velocity Comparison of Experiment and CFD Model at 20°C (Heating) 155

Table 9.3 - Temperature & Velocity Comparison of Experiment and CFD Model at 24°C .. 160

Table 9.4 - Temperature & Velocity Comparison of Experiment and CFD Model at 24°C (Section 2 - Heating) 161

Table 9.5 - Air Characteristics Comparison of Experiment and CFD Model (Section 1) 168

Table 9.6 - Air Characteristics Comparison of Experiment and CFD Model (Section 2) 169

Table 9.7 - Air Characteristics Comparison of Experiment and CFD Model (Section 3) 170

Table B.1 - Air Velocity and Air Temperature in Cooling at Setpoint 22°C (Cooling) 195

Table B.2 - Air Velocity and Air Temperature in Cooling at Setpoint 24°C (Cooling) 203

Table B.3 - Air Velocity and Air Temperature in Cooling at Setpoint 24°C (Cooling) 213

1. INTRODUCTION

HVAC system has gradually become an indispensable part of our daily life. The main purpose of air HVAC system is to provide appropriate indoor environmental conditions for human thermal comfort [1]. Research shows that comfortable conditions maximize learning ability and working productivities of occupants [2]. Moreover, the HVAC systems are also critical to maintain conditioned spaces healthy to avoid diseases with long-time indoor environmental exposure [1]. To achieve such comfortable and healthy conditions, HVAC systems are employed which consume the largest percentage of building energy.

The 2014 report by the U.S. Energy Information Administration estimates that commercial building energy consumption will grow by 0.6% per year, commercial floor space will increase an average of 1% per year and the energy intensity (energy/square foot) will decrease by 0.4% per year, between 2012 and 2040 [3]. This decline is expected to come from federally mandated improvements in equipment efficiency and reduced consumption by space cooling, heating, lighting, and plug loads. Therefore, many researchers have been working for more economical, energy efficient and sustainable systems related to the buildings and for society.

In recent decades, energy efficient HVAC systems are developed at a very fast pace. Many innovative features, controls and optimization strategies are constantly added into systems which made them very complex. In almost every HVAC application, several options are available to employ and satisfy the building load, which make the decision to select the optimal system a challenging task. Generally, the choice of a good HVAC system often starts with the appropriate selection of indoor terminal units. These terminal units are desired to deliver air in an effective and efficient manner and must match with central equipment to provide superior thermal comfort, healthy indoor environment with lower energy usage [4].

Many types of HVAC indoor terminal units are employed in HVAC applications including diffusers, fan coil units, unit ventilators, active and passive chilled beams, radiant ceiling etc. Currently, Active Chilled Beam (ACB) is considered as one of the leading energy saving systems because energy is transferred through water instead of air. ACB was also listed as one of the 15 most promising HVAC related technologies by American Council for Energy-Efficient Economy (ACEEE) in 2009 [5]. Many studies have claimed that ACB can provide

improved Indoor Environment Quality (IEQ) with great energy saving potentials. Although the experience with such unit is growing worldwide, it is necessary to research and analyze the performance of ACB under different conditions. ACB systems are employed commonly in North America for heating and cooling in commercial buildings especially in a high-performance building where ACB saves fan energy and scores credits to achieve ratings. Although many studies have been done in past in cooling mode, the coupling of the ACB with the room under changing boundary conditions especially in heating mode was not studied in detail.

Therefore, this study assesses the performance of Active Chilled Beam under real operating conditions in an academic building at the British Columbia Institute of Technology, Greater Vancouver, Canada under changing boundary conditions. This study is an initial investigation of ACB performance under heating mode. The study is accomplished by characterization of the room by investigating and mapping the airflow and temperature distribution at the outlet of the ACB and inside the office environment under heating mode and cooling mode and further through CFD simulation.

2. OVERVIEW OF CHILLED BEAM SYSTEMS

A chilled beam is an air distribution unit with an integral coil that can be used in a space to provide sensible cooling and heating. The system is designed for buildings with a relatively large sensible cooling load ratio compared to a conventional all-air system. Chilled beams are generally mounted to ceilings in an occupied zone and provide chilled water flowing through the coils. This cooling strategy is an energy-saving method because chilled beams can provide larger thermal energy at higher chilled water supply temperature compared to the conventional air system.

2.1 History of Chilled Beam

Although utilizing chilled beams is relatively new in North America, chilled beam design has been in use in Europe for decades. The technology was originated in Scandinavia and has been widely accepted in Europe and Australia. More recently, the technology is penetrating North America and Asia. The concepts have been understood in America since early 1900 with Willis Carrier's introduction of HVAC induction units. Induction units also induced the space air across a coil by throwing high-velocity jet air but were used as under-window units like today's fan coil units. Figure 2.1 illustrates an induction unit; high-velocity jet nozzles were used to entrain room air across the secondary heat exchanger through which the induced room air was conditioned. As only the primary air was recirculated through central air handling units, the size of air handling units and associated ductwork could be reduced. These space savings were quite valuable for high-rise skyscrapers, so induction units were widely deployed during 1930 – 1970.

In the 1940s, mechanical system to heat and cool with ceiling radiation was first used by Gunnar Frenger, a Norwegian engineer who developed and patented a device made of a pipe attached to an aluminum profile. The first radiant ceiling was installed in Gothenburg, Sweden, in the late 1960s. [6] Induction units became less favoured in the late 1960's -1970 because of the energy crisis and due to energy efficiency (high inlet static pressure 1.5 – 3.0 in), maintenance issues and initial cost. Moreover, induction units allowed condensation on exposed surfaces of the heat exchanger, which required regular maintenance of keeping the nozzles clean [7]. The

first radiant cooling device with supply air incorporated into its design was installed in Gothenburg in 1972. The predecessor to today's passive chilled beams considered to be first installed in Stockholm, Sweden, in 1986. [6] Chilled beam technology is emerged after combining the concepts behind Carrier's induction unit and Gunnar Frenger's applications of radiant panel cooling within the ceiling.

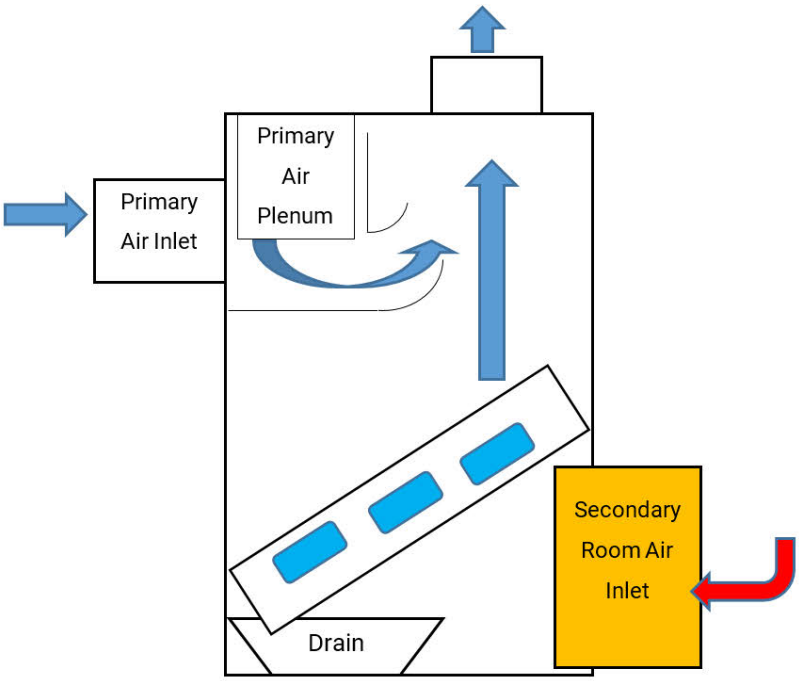

Figure 2.1 – Schematic Diagram of an Induction Unit

By the mid-1970's, induction unit based HVAC systems were virtually stopped and replaced by more energy efficient Variable Air Volume (VAV) systems. In the early 1990s, a variation of induction units in a more advanced form was introduced as Active Chilled Beam units. There were many changes adopted like Improvements in the design of induction nozzles and terminal units, employing dry operations of secondary heat exchangers and integrations with central equipment.

With these changes, the inlet pressure to supply the primary air was lowered and the need to clean, maintain or replace the heat exchanger and condensate water drainage pan was eliminated. The most negative concerns of induction units were addressed in Active Chilled Beam units but the innovative use of induction nozzles to entrain the room air across the secondary heat exchanger was kept.

2.1.1 Types of Chilled Beam

There are two main types of chilled beams, passive and active.

a) Passive Beam
b) Active Beam

Passive Beam

Passive beams are the simplest types of chilled beams and provide sensible cooling and must be used in conjunction with another HVAC system to meet ventilation and latent load requirements, therefore, a passive chilled beam is not ducted, does not supply primary air, and does not utilize fan powered equipment for any portion of the air that crosses the coil. It is based on the principle of natural convection; induction air being drawn across the coil by the natural gravitational forces and buoyancy of air. Figure 2.2 illustrates that the warm air rising to the ceiling enters the beam from the top and the cool air that has passed through the coil drops down; the motion of the cool air dropping creates a pressure drop behind it that draws more warm air through the coil [6].

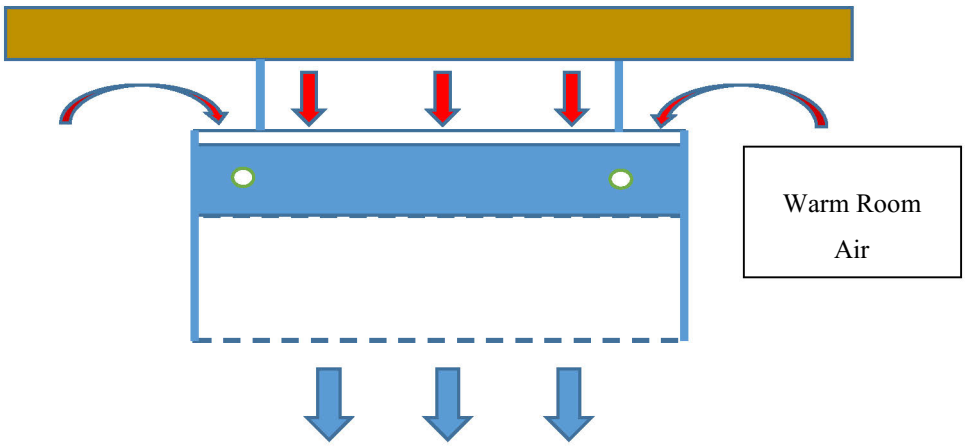

Figure 2.2 – Schematic operation of a passive chilled beam [6]

The air flow through the chilled beam is determined by the temperature difference inside and outside the coil. Cooling output capacity requirements are met by maintaining and regulating the flow of chilled water through the coil. The thermostat and a 2-way valve control the flow of water for desired cooling output.

Passive chilled beams are a good solution to provide sensible cooling to spaces where processes and people generate high heat loads, especially those that are sensitive to changes in pressure or ventilation and require no additional airflow. Passive beams could be used with traditional HVAC system for supplementary cooling for applications which have high ventilation rate or have a high latent load but could benefit from the use. Building retrofits where additional cooling is required but the original ventilation system will remain in place are also good passive beam applications. [6]

If the discharge air temperature is too high or discharge velocity is too low, stratification is possible due to the rise of warm air to the ceiling with all air distribution devices. Stratification is possible in chilled beams if water temperature entering to the heat exchanger is too high and therefore passive beams should not be used for heating applications.

Active Beam

Active Chilled Beam Unit (ACB) can be divided into two parts namely the induction area and the diffusion area. It is a device where a specific amount of primary air is supplied to the plenum of an active beam by ducts from a central air handling unit. This air is then discharged through induction nozzles in the unit which induces indoor room air. The induced air flows through the integral water coil, where it is either heated or cooled based on the water temperature. Then primary air (from air handling unit) and secondary air (induced through the coil) are mixed in the beam and diffused to the room space through slots located at the bottom of the beam [8]. Schematic operation of an Active Beam is illustrated in Figure 2.3.

Usually, the temperature of the water is 14-18°C for cooling and 30-45°C for heating application. The water flow rate is regulated for the control of indoor room temperature. Modern ACBs have one or two coils which imply that the 2 pipe units are capable of either heating or cooling only and 4 pipe units are capable of both cooling and heating.

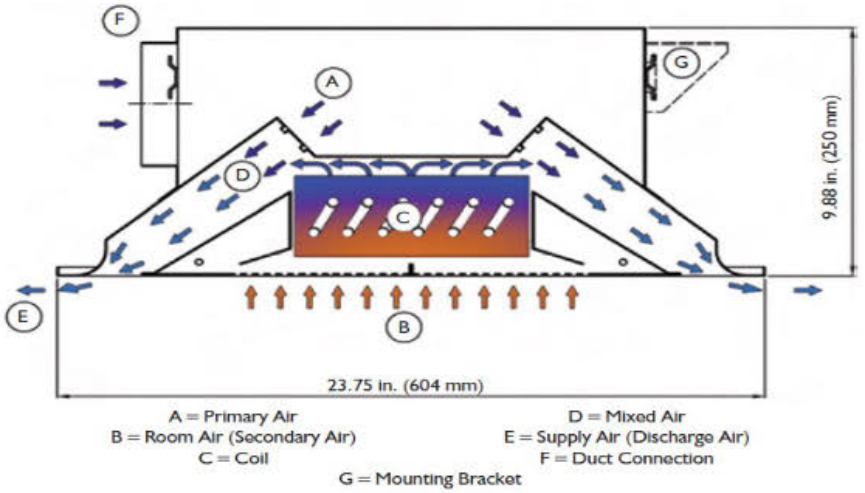

Figure 2.3 - Schematic Operation of an active beam. [9]

Multiservice Chilled Beam

They are another type of chilled beam as shown in Figure 2.4 which could be active or passive. As the name indicates, these beams incorporate different building services or functions into the beam in a prefabricated unit. This prefabricated unit reduces the amount of time required to install the building systems at a project site. Lighting fixtures and controls, speakers, motion detectors, smoke detectors, fire sprinklers and other services could be incorporated into the chilled beam. To properly select and implement multiservice beam designs, extensive integrated building design is necessary. They are utilized for applications that could benefit from off-site manufacturing of installed technical services, application due to space constraint for several high technology systems, and designs to create aesthetic interior architecture in case of lower floor heights [6].

Figure 2.4 – Multiservice Beam (TROX) [61]

2.1.2 Construction

The ACB is made of an insulated sealed primary air plenum containing a primary air connection spigot and an arrangement of primary air nozzles through which the primary air is delivered to space. The lower part of the unit is a sheet metal mixing chamber where the secondary heat exchanger is housed with supply air outlet slots as shown in Figure 2.5.

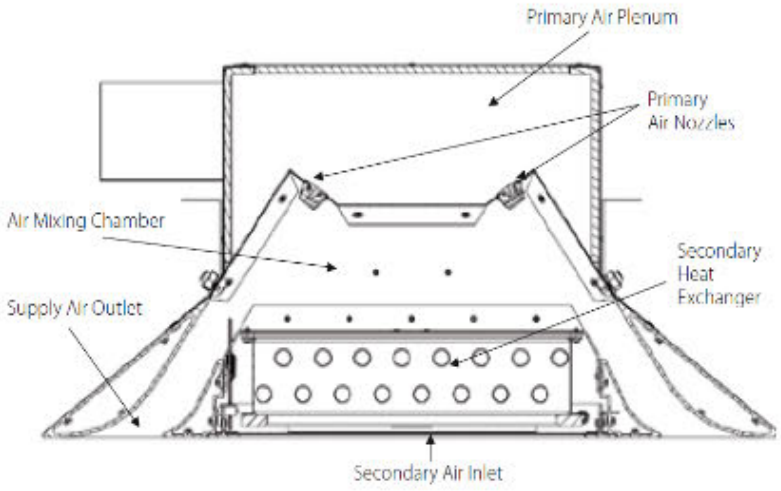

Figure 2.5 - Typical Construction of Active chilled beam Unit [10]

The secondary air heat exchanger coil is centrally located in the mixing chamber of the unit and is accessible through a perforated metal return air grille panel. The heat exchanger coil and mixing chamber are separated from the primary air plenum by the nozzle plate to ensure the mixing chamber is exposed only to room air from the space to be conditioned. ACB is equipped with mounting brackets to facilitate installation [10].

ACB should be utilized when sensible cooling, heating, and ventilation air are required in an application. Classrooms, private and public office buildings, meeting facilities, health care facilities and other application that may have moderate to high sensible heat ratios and building retrofits where space for new mechanical equipment may be limited are all good applications for active beams.

2.1.3 Working Principle of Active Beams

Figure 2.6 shows that the primary air is delivered into the primary air plenum and out through the nozzles into the mixing chamber and finally to the conditioned space. The intended force in an ACB is to create the induction effect by the nozzles. The primary air delivered to ACB can be at any temperature, but it is beneficial to use a lower temperature. This would ensure adequate latent capacity is delivered in the primary air and allow the primary air to handle a proportion of the required sensible cooling of the space.

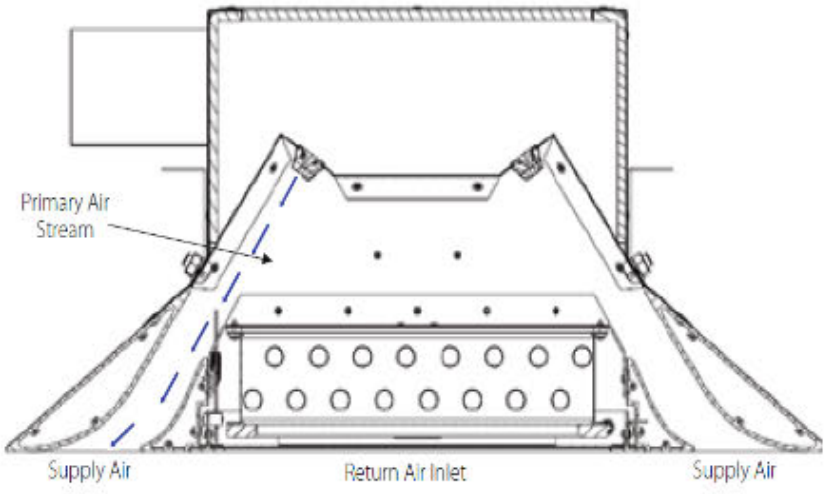

Figure 2.6 - Schematic diagram of a 2-way Discharge Active Chilled Beam Unit [11]

As shown in Figure 2.7 at the outlet of the nozzle, a low-pressure kernel is created as the pressure at the nozzle is degraded when air flows through the nozzle. All pressure degradation occurs at the primary air nozzle which results in a low-pressure area immediately at the nozzle outlet. This low-pressure area is slightly lower in pressure than the surrounding room air and therefore this low-pressure area attracts the surrounding air which is at a slightly higher pressure as shown in Figure 2.8. Secondary air from the conditioned space is drawn or induced into the low-pressure kernel through the heat exchanger coil.

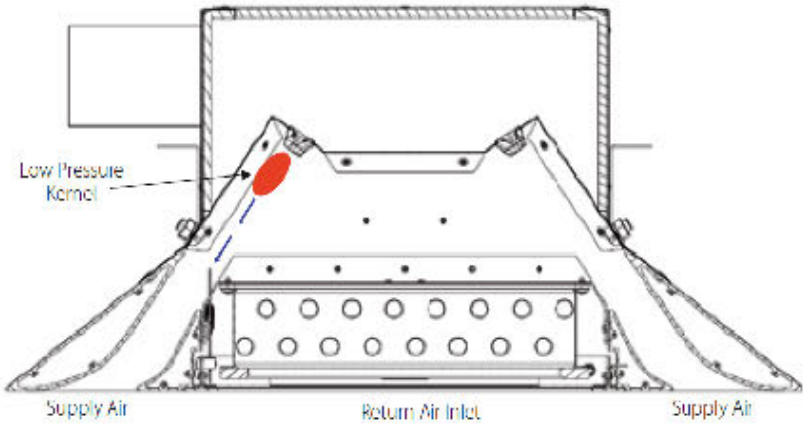

Figure 2.7 - Low pressure kernel at the outlet of the nozzle [11]

The efficiency of the induction effect is dependent on the number, size, efficiency of the nozzles and the density and geometry of the secondary cooling coil. This secondary air from the conditioned space is moved across the heat exchanger without the need of any fan energy. Therefore, the induction effect is a significant contributor to the energy reduction potential of active beams. Typically, an active beam can induce the secondary air of up to 2 - 5 times the primary air quantity.

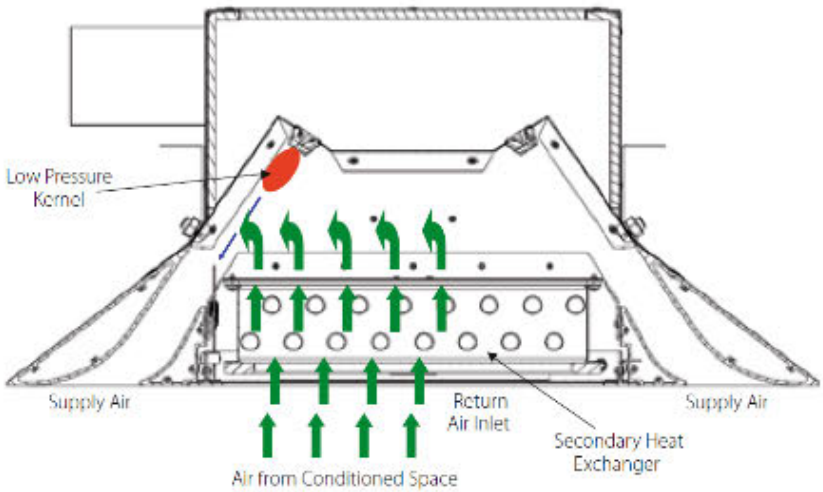

Figure 2.8 - Induction effect of Active Beam [11]

The primary air and secondary air are mixed in a mixing chamber prior to delivery to space, therefore, the total supply air quantity delivered by the ACB is the sum of the primary and secondary air quantities. Primary air is a function of the primary air quantity and the temperature difference between the primary air and room air temperatures, this air provides around 25-35% of the ACB sensible capacity. The secondary air that passes over a localized cooling coil operating with 14°C-18°C chilled water provides 65-75% of the ACB sensible cooling capacity.

It must be noted that this capacity is assumed when the primary air is being delivered cold and dry to the Active Beams. If the primary air is being delivered at a neutral temperature 18°C-20°C the secondary water coil in the Active Beams would provide essentially 100% of the zone sensible cooling capacity. By adjusting the water temperature of the heat exchanger, it is operated at the dry condition and consequently, there is no condensate water.

There are three methods for maintaining the temperature of the secondary water loop for the active beam as described below:

1. By using a water to water heat exchanger as shown in Figure 2.9. A secondary water pump circulates the secondary water in the ABC circuit while a modulating valve controls the primary water flow to achieve the design secondary water temperature.

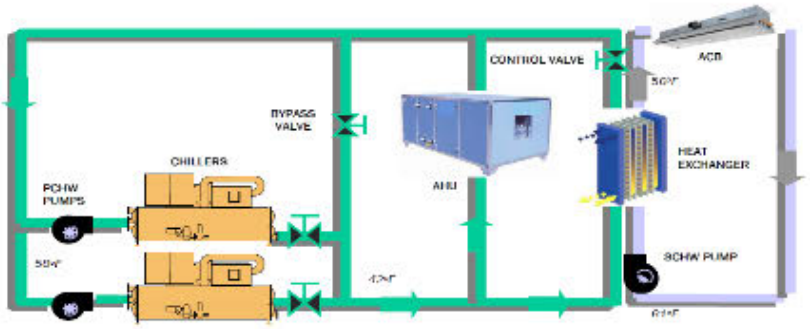

Figure 2.9 - Heat Exchanger Operations [11]

2. By using a mixing valve as shown in Figure 2.10 that allows primary water into the suction side of the secondary water circulating pump. The case study building uses a combination of a heat exchanger and mixing valve configuration to supply chilled water generated by heat pump on a higher temperature to Active Chilled Beams to avoid condensation in space.

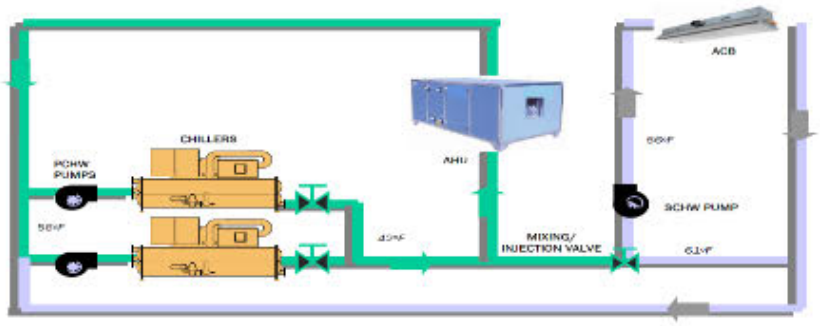

Figure 2.10 - Mixing Valve Operation [11]

3. By using separate chillers for the primary and secondary water loops as shown in Figure 2.11. This option provides the ultimate energy efficiency of the chiller plant but has a higher installed cost.

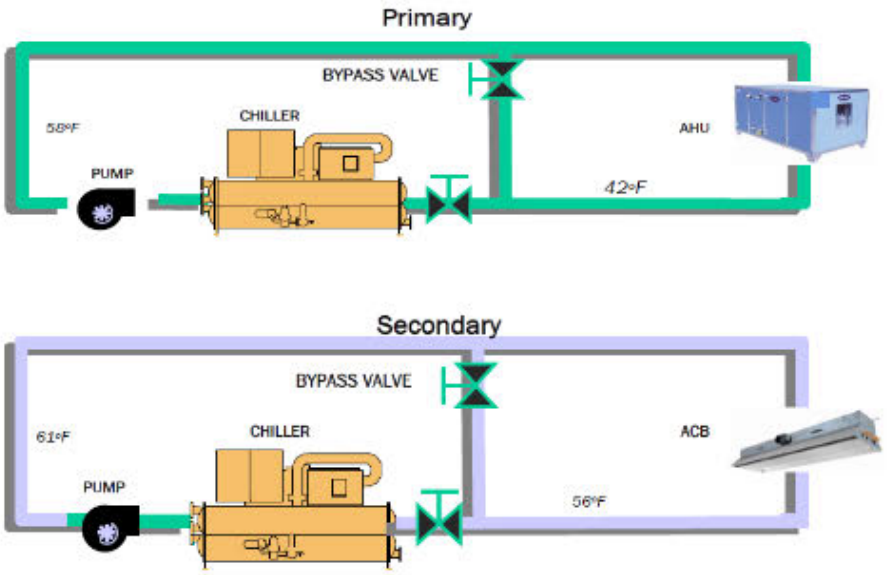

Figure 2.11 – Separate Chillers Loop Operation [11]

2.1.4 Control Strategies in ACB

Primary air

Primary airflow in the active chilled beam is kept constant most of the time unless it is designed with a variable air volume system. The primary airflow can be regulated by a fully self-contained volume flow limiter which is a mechanical device and requires no electrical or control connections and can be easily installed in the duct to maintain a volume flow rate to the active beam. The volume flow limiter also compensates for any changes in system pressure and maintains the beam's design airflow rate.

Room Temperature

The control of room temperature is mainly accomplished by varying the water flow rate or its supply temperature to the active chilled beam coil in response to a room thermostat feedback. The chilled or hot water flow rate is varied through a modulated or on/off type valves until the temperature is achieved in the room in cooling and heating operation respectively.

2.1.5 Advantages of Active Beam Systems

Compared with conventional HVAC systems, the active beam systems offer several advantages that are briefly summarized as below:

IEQ improvement

Overall IEQ can be substantially improved by ACB systems as below:

- Active beams improve comfort within the building spaces because the discharge air velocity is slower than the all air system.
- ACB also provides better mixing of the primary air and room air because of the induction principle which results in uniform temperature throughout the room, in other terms higher Air Diffusion Performance Index (ADPI), can be achieved.
- ACB also provides the ventilation air to the spaces at all times and at all loads which results in excellent indoor air quality and odor control.
- ACB operates without a fan and therefore typically operates with sound levels under 20 Noise Criterion (NC) whereas traditional overhead terminal units produce sound levels in the range of 35-40 NC.

Energy efficiency

Active beam systems can significantly reduce the air requirement as compared to a conventional all air system. The required primary air is usually reduced by 75-85% when compared to an all air system [11]. Case studies have shown that active beam systems can save 20-40% energy consumption when compared to an all air system. According to several energies retrofit projects in North America, the total power demand for active beam systems is about 25%-30% less than that for conventional VAV systems [5]. That means 8-10 LEED credits can be awarded through the optimizing energy performance section. This energy savings is also threefold:

- The system requires lesser air flow (primary air) than VAV system for the same building load and therefore reduces the fan energy.
- The chilled water is supplied at a higher temperature which increases the efficiency of chiller plant by 15%-20%.
- The requirement for reheat energy to over cooled supply air is eliminated.

Figure 2.12 below is from ASHRAE Journal demonstrating typical power savings with chilled beam systems versus a conventional all air system.

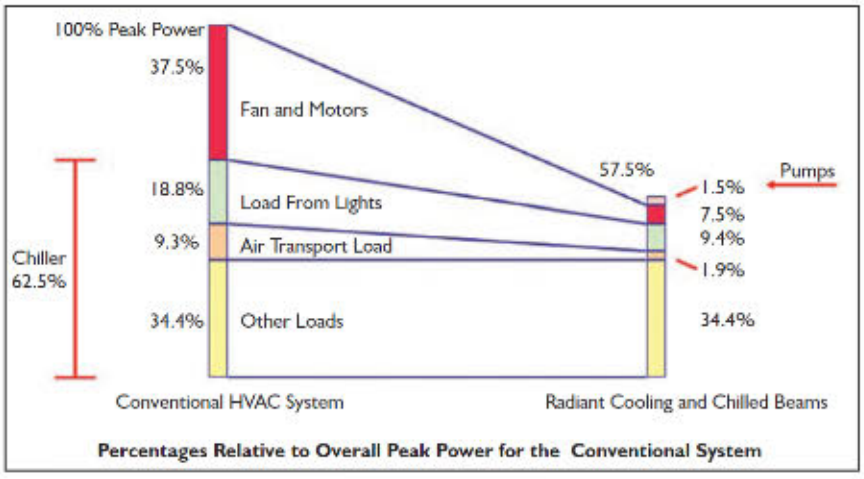

Figure 2.12 - Typical fan and motor savings for office building dedicated outdoor air systems vs. conventional HVAC systems [9]

Space savings

- ACB technology provides an opportunity to replace large supply and return air ductworks with small chilled water pipes. That results in significant space savings above the ceiling. Reduction in airflow also reduces the footprint of AHU.
- No electrical power connections are needed to run a chilled beam. This decreases the coordination between electrical services at the project site and reduces electrical switchgear.
- Controls are simpler and cheaper for chilled beams as compared to VAV or other systems.
- ACB provides easy commissioning process. ACB requires adjustments of the water balancing valves and primary air balancing dampers through simple static pressure readings.
- ACB required no or very minimum maintenance as there are no moving parts. Cleaning of the coil is usually required only after 4-5 years unless the beams are used in a dirty environment.

3. LITERATURE REVIEW

The literature review for the study started with the background information of ACB, the history of the chilled beam, types, application, advantages and their utilization in the building which is already discussed in detail in the second chapter. Further literature review starts with technological advancement over the years and numerous studies were done by researchers on efficient beams. A table is provided in each section to summarize the literature to evaluate different performances of active beams.

Alexander et al. [9] presented various considerations for active beams about the duct design and working static pressures, terminal unit placement and room air distribution, chilled water side control. Suitability of the systems for various spaces was also briefly discussed in the literature. Loudermilk et al. [12] studied 4 cases and concluded that low dew-point primary air temperatures are often associated with chilled beam systems, but they are often not a necessity. An alternative is to relax space design humidity levels, which may offer savings in fan and chiller energy, as well as reducing the required number of beams.

Livchark et al. [13] emphasized using ACB systems with the minimum primary air volume flow rate. The lack of programs considering transient heat transfer effect and design tendency of engineers to apply safety margins leads to high volume flow rates which result in space cooling or heating by primary air while keeping the water valves shut. They recommended that if the volume of air could not be minimized then VAV must be used in conjunction to ACB. They define a parameter called Coil Output to Primary Airflow Ratio (COPA) which represents the amount of cooling or heating, the energy produced by the active beam coil (P_w: Btu/h) per volume of primary air used (q_p: cfm). The higher the COPA ratio, the more efficient chilled beam design, the more effectively primary air is used.

$$\mathrm{COPA} = \frac{P_W}{q_p} \qquad 1$$

They derived equations describing active beam cooling/heating output, along with empirical formulae for coil heat transfer coefficient that can be used to represent active beams in energy simulation programs.

3.1 Chilled Beam Performance

Table 3.1. – Studies Related to Chilled Beam Performance

Method	Evaluation	Author(s)	Title of the Literature
Numerical CFD Simulation	Cooling Performance	Livtchak A. Horttanainen P. Yankov G. Artemov V.	The Effect of Room Thermal Environment on the Performance of Cooled Beams.
Field Study	Airflow control, temperature of water and air.	R. Kosonen	An analysis of a flexibility chilled beam system in hot and humid climate.

Livtchak et al [14] compared the cooling performance of static (passive) and active beams and showed that the latter had the higher cooling capacity. *They stressed that the performance of chilled beam depends on the thermal environment of the room. The location of air distribution devices and heat sources in a room must be considered for better performance of chilled beam and to achieve thermal comfort.*

Kosonen [15] investigated the flexibility to control throw pattern and air flow rate of the active beam in an organization change environment where the traditional one-person office areas, or cells, and open offices changing into spaces that are more suited to teamwork referred to as dens or clubs or vice versa. He suggested that the primary airflow rate of each beam could be reduced by using an air quality control unit in the space and room space air velocities could be reduced by reducing the induction ratio of the active beam to an appropriate level.

Many manufacturers developed adjustable blades as illustrated in Figure 3.1 to handle the changes in the space layout. The indoor airflow patterns can be optimized as per the requirements and provide flexibilities in adopting ACB for such changes. Kosonen concluded his field study in an office building in hot and humid climate concluded that the room design conditions of 23 ^{0}C and 65 % is attainable with the water inlet and the supply temperatures 17 ^{0}C and 14 ^{0}C when the specific supply air flow rate is 10 l/s per person and proper

dehumidification of indoor air before using water-based cooling systems in tropical climate. He also proposed to mix return air with fresh air supply.

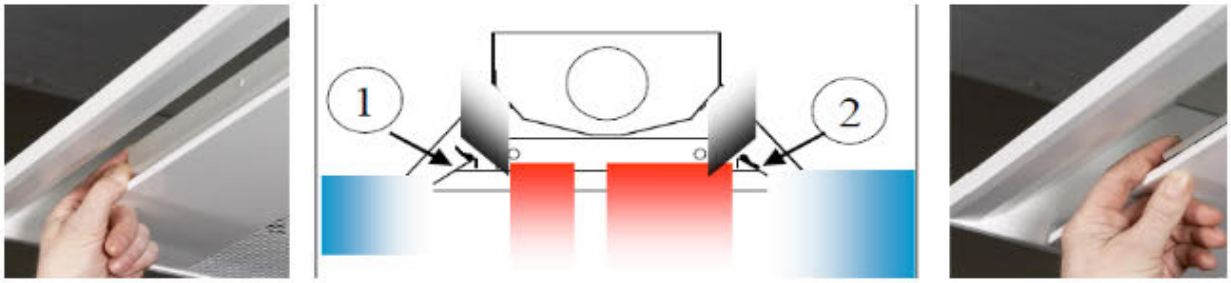

Figure 3.1 - Principle behind the induction ratio adjustment 1) adjustment on 2) adjustment off

3.2 Induction ratio measurement methods

Using the entrainment effect of the induction nozzle to throw the primary air and induce the secondary air is the innovation of ACB. This effect is a measure of the efficiency of the ACB and the cause of cooling/heating capacity which can be achieved. The entrainment ratio is affected by many factors like nozzle arrangement, geometries of the casing, etc.

Table 3.2 – Studies Related to Induction Ratio Measurements

Method	Author(s)	Title of the Literature
Laboratory Experiment	Peter Filipsson, Anders Truschel, Jonas Graslund and Jan-Olof Dalenback.	Induction ratio of active chilled beams-Measurement methods and influencing parameters.
Laboratory Experiment	M. Ruponen and J.A. Tinker	A novel method to measure the air entrainment ratio of an active chilled beam
Laboratory Experiment and Simulation	C. Chen, W. Cai, Y. Wang, C. Lin	Further study on the heat exchanger circuitry arrangement for an active chilled beam terminal unit
Laboratory Experiment and CFD Simulation	Z. Guan and C. Wen	Geometric optimization on active chilled beam terminal unit to achieve high entrainment efficiency.
Numerical CFD Simulation	Z. Guan and C. Wen	Numerical investigation of geometry parameters for designing efficient terminal units in active chilled beam

Filipsson et al. [16] investigated other factors and conditions that influence the induction ratio. They compared three methods of determining the IR and concluded that the IR is influenced by the chilled water temperature due to buoyant forces. Novel methods of determining the IR were presented and it was concluded that current methods may lead to overestimation. The 3 methods used are explained on the next page.

If m is mass flow, c_p is specific capacity and t temperature. Index w is chilled water, p is primary air, s is supply air, i, out is induced air downstream the coil, and r is room air

Capacity method

Uses an energy balance over the chilled beam coil. By measuring the flow and the temperature rise of the chilled water and the temperature drop of the induced air the flow of induced air can be determined by the equation below

$$IR = \frac{\dot{m}_w \,.\, c_{p,w} \,.\, (t_{w,out} - t_{w,in})}{\dot{m}_p \,.\, c_{p,a} \,.\, (t_r - t_{i,out})} \qquad 2$$

A major drawback of this method is the issue of measuring the temperature of the induced air down-stream the coil and this method overestimated the IR by 25% estimated by Ruponen and Tinker [17]

Temperature Method

Temperature method is a method of measuring the temperature of the mixed supply air, the primary air and the induced air down-stream the coil to calculate the IR. Just as the capacity method, this method suffers from the problem of measuring the induced air temperature downstream of the coil.

$$IR = \frac{t_p - t_s}{t_s - t_{i,out}} \qquad 3$$

Modified capacity method

Both the capacity method and the temperature method suffer from the difficulties of measuring the temperature of the induced air downstream the coil. But by combining the two methods it is possible to find an expression for IR without that problem. The capacity method (Eq. (1)) and the temperature method (Eq. (2)) are combined into the modified capacity method (Eq. (3)). However, this method did not account for radiation effect and therefore the IR calculated was overestimated.

$$IR = \frac{t_s - t_p}{t_r - t_s} + \frac{\dot{m}_w \cdot c_{p,w} \cdot (t_{w,out} - t_{w,in})}{\dot{m}_p \cdot c_{p,a} \cdot (t_r - t_s)} \quad (4)$$

Velocity method

Ruponen et al. [17] presented a single purpose built measurement venturi with which it is possible to determine the induced air flow rate as a function of the air velocity measured in one point in the throat of the venturi. It was concluded that the method produces reliable and consistent results.

Chen et al. [18] used a velocity transducer to scan the induced air velocity in a dense grid under the beam. The purpose of the study was to determine the velocity profile but the method can be used to determine airflow rate as well.

Guan et al. [19] investigated the influences of the geometry of the terminal unit on entrainment ratio through CFD simulations. It was found that the nozzle radius was negatively correlated to the entrainment ratio, while the nozzle spacing was positively correlated to the entrainment ratio, and the former has a higher influence on ER.

Guan and Wen [20] proposed an innovative method of acquiring entrainment ratio by using an external hood at the supply air outlets. The hood was long enough to reduce the turbulence of the supply air and the velocity at the end of the hood was measured with a velocity transducer at 19 points along each long side of the beam.

3.3 Thermal Comfort

Table 3.3 – Studies Related to Thermal Comfort

Method	Author(s)	Title of the Literature
Full Scale Laboratory Experiments	Jérôme Le Dréau, Per Heiselberg and Rasmus Lund Jensen.	A full-scale experimental set up for assessing the energy performance of radiant wall and active chilled beam for cooling buildings.
Numerical CFD Simulation	Jérôme Le Dréau and Per Heiselberg,	Sensitivity analysis of the thermal performance of radiant and convective terminals for cooling buildings
Laboratory Experiments	Mustakallio et al., Panu Mustakallio, Zhecho Bolashikov, Kalin Kostov, Arsen Melikov and Risto Kosonen.	Thermal environment in simulated offices with convective and radiant cooling systems under cooling (summer) mode of operation.
Laboratory Experiments (Test Bed)	Kyu-Nam Rhee, Mi-Su Shin and Sun-Ho Choi.	Thermal uniformity in an open plan room with an active chilled beam system and conventional air distribution systems.

Active Beams have been developed to promote the use of low-temperature heating and high-temperature cooling systems [21]. Though ACB has many advantages like the uniformity of comfort level and increased efficiency with the optimized convective flow but many performance gaps have been reported, Jérôme Le Dréau [22] illustrated following with experiments in his thesis.

- ACB are not efficient at a high outdoor temperature
- No air temperature gradient
- Risk of draught
- Risk of short-circuiting between the air inlet and outlet

Aleksejs Prozuments [23] tested an active chilled beam in a hospital ward mock-up room and found the risk of stratification in heating and insufficient mixing of ventilation air.

Dréau et al. [24] performed full-scale experiments under both steady-state and dynamic conditions in cooling mode in a test room with a thermal manikin and a window to compare the energy performance of a radiant wall and an active beam. It was observed that the radiant wall was more energy efficient to remove heat than the active beam. The energy savings in case of the radiant wall of 10% was due to increased ventilation losses in active beams. The local comfort conditions (radiant asymmetry, vertical air temperature gradient, the risk of draught) were also evaluated and the measured parameters were within the comfort range.

Dréau et al. [25] performed steady-state numerical simulation on in-house software "BSim" of a typical office using four types of terminals including active beam, radiant floor, wall and ceiling. A sensitivity analysis was conducted; the air change rate, the outdoor temperature and the air temperature stratification have the largest effect on the cooling requirement. The radiant ceiling achieves the most uniform comfort conditions in the space followed by the active beam. The active beam achieves uniform comfort conditions in theory, but CFD simulations are needed to validate these results and account for the draught risk.

Mustakallio et al. [26] evaluated thermal environment through experiments in a double office room with 2 thermal manikins and in a six-person meeting room with convective and radiant cooling systems like chilled beam (CB), chilled beam with radiant panel (CBR), chilled ceiling with ceiling installed mixing ventilation (CCMV) and desk mounted local radiant cooling panels with mixing ventilation (MVRC) under summer condition. Active beam system with convective cooling was able to provide good thermal environment but more homogeneous thermal environment within the occupied zone was achieved by active beam integrated radiant panel (CBR), chilled ceiling with overhead mixing ventilation (CCMV).

Rhee et al. [27] conducted experiments in a full-scale test-bed to evaluate thermal comfort in open-plan office building conditions with multiple ACB and compared with conventional air distribution systems. Air diffusion performance index (ADPI), air velocity for the local discomfort due to cold draught, and vertical air temperature difference to evaluate stratification was measured. The results showed that the ACB system can provide acceptable thermal uniformity, even with less air flow rate than other conventional air distribution systems.

Arsen et al. [28] studied the impact of the airflow interaction on occupant's thermal comfort in rooms with active beams. They used thermal mannequins, artificial windows, ceiling lights as

heat sources inside the room. CFD was not performed. They studied impact of primary air flow rate and heat load strength on the thermal environment in space, speed and temperature measurements were done to calculate air diffusion performance index (ADPI) and draught rating index (DR). They concluded that heat load and the supplied flow rate have substantial impact on the air distribution in rooms with chilled beams. Non-uniformity of the thermal environment and the risk of draught discomfort increases when the heat load and the flow rate of the supplied primary air increases.

3.4 Space Air Distribution

A comprehensive understanding of room air flow distribution by active beam unit is an important criterion for indoor thermal comfort design for the systems. The air velocity in the zone must be accurately predicted and controlled in the design phase to strictly avoid draught sensation in the occupied zone. The experimental data and models are needed to improve the accuracy of CFD simulations to attain the optimal thermal comfort.

The typical room air distribution from an Active Chilled Beam unit is shown below in Figure 3.2. The air flow jet attaches to the ceiling (i.e. Coanda effect) then impinges on the ceiling wall corner, follows the vertical wall, impinges on the wall floor corner and finally enters the occupied zone. An occupied zone is defined as the area 0.3 meter from the internal wall, 1.0 meter from the external wall, and 1.8 meters from the floor as per ASHRAE 55 Standard [29]

Outside the occupied zone, the focus is the air flow pattern. Many studies were conducted using Particle Image Velocimetry (PIV). PIV is an innovative technology to study indoor air flow for the measurement of whole air flow fields in fractions of a second.

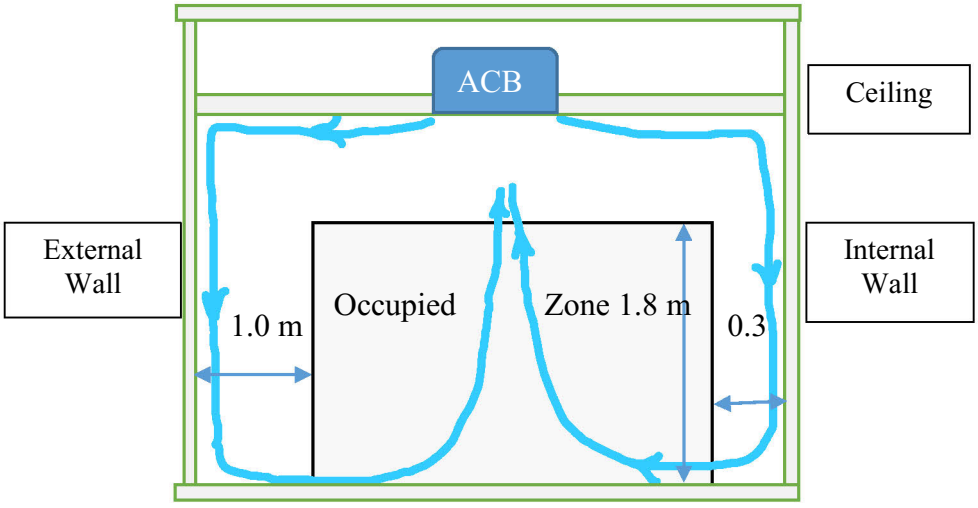

Figure 3.2 - Typical trajectory of airflow discharged from Active Chilled Beam Unit (ACB)

Table 3.4 – Studies Related to Room Air Distribution

Methods	Author(s)	Title of the Literature
Laboratory Experiment	G. Cao, M. Sivukari, J. Kurnitski, M. Ruponen, and O. Seppänen	Particle Image Velocimetry (PIV) application in the measurement of indoor air distribution by an active chilled beam
Laboratory Experiment	G. Cao, M. Ruponen, R. Paavilainen, and J. Kurnitski	Modelling and simulation of the near-wall velocity of a turbulent ceiling attached plane jet after its impingement with the corner
Experiment and Numerical CFD Simulation	G. Cao, M. Ruponen, and J. Kurnitski	Experimental investigation of the velocity distribution of the attached plane jet after impingement with the corner in a high room
Experiment & Numerical CFD Simulation	G. Cao, J. Kurnitski, P. Mustakallio, and O. Seppänen	Active chilled beam wall jet prediction by the free convection model
Experiment and CFD Simulation	G. Cao, J. Kurnitski, M. Ruponen, P. Mustakallio, and O. Seppänen	Plane-air-jet corner zone modelling in a room ventilated by an active chilled beam
Laboratory Experiments and CFD Simulation	H. Koskela, H. Häggblom, R. Kosonen, and M. Ruponen	Air distribution in office environment with asymmetric workstation layout using chilled beams
Laboratory Experiments and CFD Simulation	H. Koskela, H. Häggblom, R. Kosonen, and M. Ruponen	Flow pattern and thermal comfort in office environment with active chilled beams
Laboratory Experiment with CFD Simulation	Risto Kosonen,Arsen Melikov, Boryana Yordanova and Lyuben Bozkhov.	Impact of heat load distribution and strength on airflow pattern in rooms with exposed chilled beams.
Laboratory Experiment with CFD Simulation	Risto Kosonen, Maija Virta and Arsen Melikov.	The impact of thermal loads on indoor airflow.

Cao et al. [30, 31] performed many studies on airflow behaviours of the attached plane jet discharged from an active beam in a room using PIV. The air turbulence structure, airflow features, velocity distribution and maximum velocity decay were investigated. Impact of Reynolds number and turbulence intensity level was addressed. Each step along the trajectory was reflected by a model and then the model was experimentally verified. The PIV visualization results proved that the jet will attach to the ceiling and become fully turbulent a short distance downstream from the slot.

Cao et al. [32, 33] further studied the airflow patterns of attached plane jets and set up an efficient model to predict the maximum jet velocity decay of an attached plane jet after its impingement with the corner in a high room. It was proved that the jet would attach to the ceiling because of the Coanda effect and became fully turbulent in a short distance. The room air was constantly entrained into the jet and the jet grew at a certain rate. Then, the impingement of the attached plane jet on the ceiling wall corner was identified. The jet behaviours were found to be different from those obtained in a relatively low room. An efficient model was set up to predict the maximum air jet velocity decay after the jet impingement and a CFD tool, CFX 11.0, was shown to be effective to describe the process.

Cao et al. [34] proposed a free convection model by superposing a free convection velocity and an isothermal jet velocity. It was found the air velocities decreased quasi-linearly when approaching the floor level below the height of 1.7 m. The introduced model could be used for prediction of the maximum velocity of the wall jet. The result showed that the returning corner air flow reattached to the floor surface after separation from the wall. The maximum air velocity was very close to the floor [35].

Koskela et al. [36, 37] evaluated the air distribution in mock-up open plan office with asymmetric workstation layout using chilled beams for summer, winter and spring/autumn. They found that the heat sources had a notable influence on the flow pattern in the room causing large-scale circulation and affecting the direction of inlet jets. It was concluded that the risk of draught was caused by the downfall of colliding inlet jets and large recirculation due to asymmetric heat load distribution. The result indicated that the mean air velocity was high when the air flows discharged from two adjacent terminal units collided with each other and turned down into the occupied zone together. As a consequence, active beam systems were difficult to fulfil the targets of the existing standards, especially with high cooling loads. CFD-simulation

was able to predict the general flow pattern but somewhat overestimated the airspeed compared to measurements.

Kosonen et al. [38] with the physical measurements and the performed smoke visualization investigated various heat load strengths in a room with length-wise installed ACB. Results showed that the flow from the ACB was not disturbed with the heat load of 56W/m2. However higher loads depicted the significant impact of the convective flow and thus increased the draught risk and local velocities in the occupied zone.

Kosonen et al. [39] stressed that convection flows caused by thermal loads may significantly affect the air flow conditions in the room and assist the occurrence of high velocity near occupants. The results with full-scale measurements with ACBs revealed that the installations with possibilities of convection flow opposing the supplied flow should be avoided. They generalized that convection flows have less impact on air distribution in rooms with chilled beams installed in lengthwise direction than when installed crosswise in rooms.

Jan et al. [40] studied the various consideration for minimizing draught discomfort in rooms with ACB. They conducted a full-scale office room experiment with 3 to 4 ACB in ceiling with Halton Velocity Control Device. Different factors were analyzed like placement of ACB, different strength of heat load and location, primary air flow, induced airflow. Practical guidelines to minimize draught discomfort in rooms were given. They concluded that room height should not be more than 3.5 meters, air flow from ACB being dispersed from slot has velocity decay which can be described as a plane wall jet and is inverse proportional to the square root of the distance. Ceiling mounted obstacles can influence the ACB airflow and ACB should be installed perpendicular to the window façade.

Risto et al. [41] studied the impact of heat load location and strength on air flow pattern with a passive chilled beam system. They used two passive chilled beams, three light fittings and a swirl diffuser. Experiments were executed in a mock-up of an office room to study the air velocities in the occupied spaces, velocity profiles were noted when underneath heat loads exist, and the cool and warm air flows interact. No upward plume was generated, and the dummy only acted as a flow obstacle, having a significant effect on the velocity profile, they concluded that the full-scale tests and CFD predictions are recommended. The maximum air velocity measured was below 0.25 m/s with heat gain of 164 W/m2.

Nygaard and Uth [42] reported that occupants were satisfied with the thermal micro-environment established by the localized ACB. However, the results of their study show that the conditions outside of the micro-climate were evaluated as unacceptable by the subjects. No results were reported in heating mode.

3.5 Numerical Studies

Computational Fluid Dynamics is used to analyze the indoor environment and room air diffusion since 1970s after the development of computer programing and turbulence models. P.V. Nielsen being the pioneer initiating such studies in 1974. CFD solves fluid flow, heat transfer and chemical species transport. The parameters such as air velocity, air temperature, contaminant concentrations, relative humidity and turbulence quantities, are critical for designing a comfortable indoor environment. This is because the design of appropriate ventilation systems and the development of control strategies require detailed knowledge of airflow, contaminant dispersion and temperature distribution in a building.

In recent years, due to the continuous research and development in CFD, it has emerged as the dominating simulation technique for modelling indoor airflows because of the ability to accurately model extremely complex flows with computational power that has dramatically increased in the last twenty years [43]. Many simplification methodologies have been developed that enable solutions of complex airflows that reduce the modeling effort and the overall time and cost [44].

The air movement in interior spaces of a building is called room air diffusion. Indoor airflow modeling characterizes room conditions by solving the fundamental principles of energy, momentum and mass flow [45] to predict the interactions of inlet and outlet mass flows with the heat sources and sinks. Air is introduced in the interior space through 2 supply outlets (slots) of ACB in order to provide thermal comfort and improve indoor environmental quality. Accurate predictions of room airflow and air temperature distribution in the space is not feasible by experimental methods due to the complexity involved in room air flows, limitation on the number of equipment/sensors, placement of the sensors at different positions and at different intervals which results in longer time frame [46]. Therefore, CFD has gained popularity as a design and analytical tool to visualize and predict the air movement inside the room. It helps to

predict local air velocity and temperature distribution in a particular space. Parameters like airflow rates, inlet temperature, heat load and other boundary conditions are varied to predict the impact of such variation on boundary conditions on indoor climate and energy management in buildings. CFD simulation helps to ensure that the ACB system creates the proper indoor climate conditions.

The numerical studies reviewed are briefly mentioned below. The studies are divided into two groups to gain understating of boundary conditions, convergence models used, and various assumptions made.

a) CFD in rooms with Chilled Beams
b) CFD in rooms

3.5.1 CFD in rooms with Chilled Beams

Cammarata et al. [47] conducted a numerical investigation on active beams for indoor air conditioning. A standard room with physical fluid properties and structural element properties were assumed, the chilled beam was located at the room ceiling incompressible fluid modelled by a k-ε turbulent scheme. They studied the fluid-dynamical and thermal performance of ACB by 2D and 3D modelling in COMSOL Multiphysics in winter and summer with 3 different configurations of nozzles. They achieved stationary conditions for air temperature in the occupied region of the room in about 30 minutes since initial time and applying the hardest climatic conditions both in winter and in summer, almost constant velocity distribution in the occupied portion of the conditioned space was also established.

Guan et al. [20] investigated a novel structure of ACB as illustrated in Figure 3.3 to achieve high entrainment ratio to increase the energy efficiency of the ACB system. They tested the ER of a commercially available unit physically and then an innovative method to find ER was proposed and validated. The CFD model of the unit was made and experimental data was validated. Further, the ACB was modified in the CFD model and found that by changing the geometry of the mixing chamber and length of the nozzle, the ER could be increased by 30% with previous conditions. They proposed that the Induction can be increased by relocating the

nozzles and the induction kernel closer to the center of ACB. This provides effective air mixing and entrainment. The turbulence of the flow is modelled by the standard k-ε model.

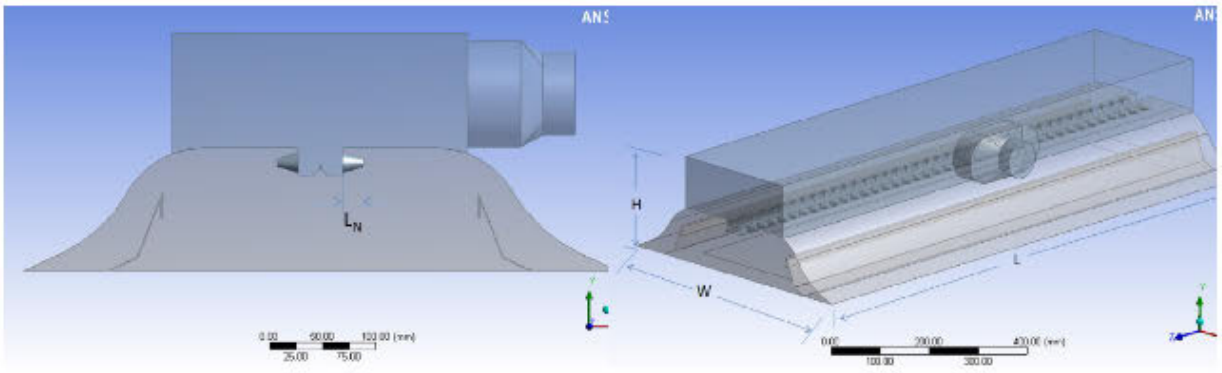

Figure 3.3 - ACB Model Proposed by Guan et al. [20]

3.5.2 CFD in rooms

Some researchers have set up fine examples on how to verify, validate, and report CFD results in order to help engineers to perform CFD correctly and effectively. But, these examples were for specific applications and may not be used as a general guide to verify, validate, and report CFD analyses of indoor environment. Qingyan Chen and Jelena Srebric presented a manual illustrating the steps necessary to verify, validate, and report CFD analyses in the indoor environment through ASHRAE RP-1133. [48]

Verification involves following

a) Identifying related physical phenomena for an indoor environmental analysis.
b) Assessing if the CFD code has the capability of accounting for the identified physical phenomena.

Validation involves demonstrating the coupled ability of a user and a CFD code to accurately conduct a simulation of a representative indoor environment.

Reporting results involve summarizing the CFD analysis so that others can make informed assessments of the value and quality of the CFD.

The following can be deduced from an example being given for office ventilation: [49]

1) The airflow in an indoor environment is controlled by the Navier-Stokes Equation of mass, momentum, and energy, which can be expressed in a common form as below. The variable φ represents, predicted quantities like air velocity, temperature, or species concentration at any point in the 3D space. The equation refers to the change in time of a variable at a location is equal to the amount of the variable-flux (i.e., momentum, mass, thermal energy).

$$\frac{\partial}{\partial t}(\rho\phi) + \frac{\partial}{\partial x_j}(\rho U_j \phi) = \frac{\partial}{\partial x_j}\left(\Gamma_\phi \frac{\partial \phi}{\partial x_j}\right) + S_\phi \quad (5)$$

Transient + Convection = Diffusion + Source

2) Most indoor airflows are turbulent because of high Rayleigh (Ra) high Reynolds (Re) number. The Ra and Re numbers as:

$$R_a = \frac{\beta g \Delta T L^2}{\nu k} \quad (6)$$

$$R_e = \frac{UL}{\nu} \quad (7)$$

In some regions, the airflow can be weak turbulent or laminar, however, overall flow is often considered as turbulent.

3) It is feasible to compute the indoor airflow with the capacity and speed of present computers by using turbulence models. Turbulence modeling approximations are needed for CFD.

   The turbulence models can be divided into two groups:
   a) Large-Eddy Simulations (LES)
   b) Turbulent transport models (Reynolds averaged Navier-Stokes equation modeling (RANS))

4) LES models have only one or no empirical coefficients; few modeling assumptions are involved and require a great deal of computing time and high computing cost. Therefore, only few LES applications have been performed.

5) In RANS modeling, the mean flow variables are found by using turbulent-transport models which are further classified as
   a) Eddy-Viscosity Models (k-ε model)
   b) Reynolds-stress models.

6) An early and popular eddy viscosity model is the k-ε model from Launder and Spalding (1974) and a basic Reynolds-stress model is the one summarized by Launder (1989). The Reynolds-stress models are superior and produce better accuracy to the eddy viscosity models because the Reynolds-stress models do not use the Boussinesq approximation. However, there is a penalty in terms of complexity, computing requirements, and numeric algorithm stability with the Reynolds-stress models.

7) Simple k-ε model and the renormalization group k-ε model can provide satisfactory results for most simple indoor air simulations. However, the k-ε model is inaccurate for flows with adverse pressure gradients.

8) LES is suitable for transient simulation because it always calculates the flow in a transient form. It uses a finer grid distribution which will dramatically increase the computing time and accuracy.

9) For complex steady-airflow simulations, RANS equations with turbulent transport models are recommended.

10) The indoor environment consists of complicated radiative, conductive and convective heat transfer. Sometimes physical phenomenon includes combustion, participating media radiation, and particle transport in multiphase like air-liquid, air-solid, and air-liquid-solid, therefore, it is important to verify if these can be modeled by a CFD code.

11) Accurate specifications of boundary conditions to interpret the specific physical phenomena into a computer model or mathematical equations are crucial in CFD modeling of indoor environments.

12) A steady-state flow simulation is sufficient for an office environment to find out the mechanical ventilation for summer and winter conditions.

13) The CFD analysis assumes non-slip condition for the velocity, constant temperature condition, and zero kinetic energy at walls.

14) The experimental data can give the wall surface temperatures that have already considered radiation and therefore radiation model or auxiliary model is not required.

15) The numerical procedures with a finite-volume method usually converge much faster, therefore, the Cartesian coordinate system with structured mesh system is selected to represent the human bodies.

16) The first-order differencing scheme and SIMPLE algorithms seem to be more stable. Therefore, they can be selected for the office design simulation.

17) The boundary conditions for a room include flow obstacles of all solid objects, heat transfer from heated objects and walls, tracer gas sources, supply airflow, and exhausted flow.

18) Zero pressure and zero gradient for all other flow parameters were used as boundary conditions for the exhaust.

19) For such a complicated system, it is very difficult to reach grid independent results and the uncertainty and error for turbulent intensity are the largest in both the CFD model and the measurements.

Few pieces of literature which were studied to gain insight into CFD in rooms are below.

Abanto et al. [50] conducted a study on airflow modelling in a computer room with ceiling diffusers. They used pre-processor Gambit and Rhinoceros NURBS, Fluent commercial flow solver and Vu as post-processor. The results were validated with a MINIBAT. Re-normalization group (RNG) k-ε model was used in the study. Through numerical simulations, four indoor air-quality parameters were estimated - mean age of air, mean radiant temperature, predicted mean vote and predicted percentage of dissatisfied. They concluded that boundary conditions and the inclusion of real-world geometries like diffuser inlets have a major impact on fluid-flow. Segregated pressure-based solver, SIMPLE pressure-velocity coupling and finite -volume approach, Discrete Ordinates (DO) radiation model and H20 was used in species transport equations. They modeled computers and human beings (through thermal mannequins). Room boundaries were modeled as adiabatic walls and were considered diffuse with ε= 0.9 -1.0. No modeling was conducted for the heating scenario.

Zhu et al. [51] conducted a numerical analysis of a cold air distribution system with ceiling diffuser. Fluent CFD Software was used. 2 equation k-ε turbulence model was used. Simulated model results were compared with experimental set up with multi-anemometer to measure the temperature and velocity in the room. The experimental result matched the numerical simulation with FLUENT. Assumptions made in the study were incompressible, invariable and steady-state flow. No air leakage, no solar radiation, no internal heat source, high Reynolds number, Doors, and windows were considered as closed. CFD was done for cooling mode only.

Muller et al. [52] stated that the RANS model could not predict the effect of thermal plumes to ventilation air. Therefore, a suitable model must be selected for the different type of research. Gilani et al. [53] in their study on stratified indoor environment concluded that out of the five commonly used turbulence models tested, the S k-ε, R k-ε, RNG k-ε, S k-ω and SST k-ω model, only the two k-ω models succeeded in reproducing the thermal plume structure and the associated thermal stratification, while the three k-ε models clearly failed in doing so.

Sadrizadeh et al. [54] studied nine turbulence models by numerical simulation with a focus on accuracy and computing cost. They worked on turbulent-viscosity and Reynolds-stress of RANS modelling. The experiment consisted of thermal manikin in a box-shaped wind tunnel and concluded that the RNG k-ε, v2-f models showed the best overall performance. The Realizable k-ε model is the most robust and easy convergence turbulence model and can be used as good initial fields for more advanced models to achieve converged results.

Zhang et al. [55] studied the performance of eight turbulence models for indoor airflow in terms of accuracy and computing cost. These models covered RANS modeling, hybrid RANS and LES. The results revealed that LES provides the most detailed flow features, but the computing time was high. RNG k-ω and a modified v2-f model provided the best result in studied cases.

3.6 Summary of Literature Review

Water is approximately 4000 times more efficient to remove the generated heat in a space compared to air for the same volume of water and air and, therefore, the transfer of energy through water is energy efficient and therefore the Active Beams are energy efficient units as tested and verified by many researchers. Livchak and Lowell [13] showed that active beams

would perform poorly if the primary air supply is oversized and therefore COPA (Coil Output to Primary Airflow Ratio) was given by them. Alexander and O'Rourke [9] observed that decreasing the pressure at the nozzle level lowers cooling capacity and thus lower the efficiency of the active beam. Active beams are not recommended for buildings with high indoor latent loads, such as restaurants, sports facilities, theatres and hospitals.

Indoor environment of a space is influenced by personal variables like Met rate, Clo value, air temperature, radiant temperature, velocity and RH. The literature review shows that Active beams fulfill the general thermal comfort criteria defined by ASHRAE Standard 55, but few studies show draught risk, local discomfort and high air movement generated by ACB under cooling mode condition [22, 23]. Many studies iterated that though active beam achieves uniform comfort conditions in theory, but further simulations like CFD are needed to validate these results to account for the non-uniform air distribution and the draught risk.

Literature review on room air distribution shows that the regions of higher draught risk in rooms with active beams were estimated with all these studies. There is a risk of local discomfort due to higher air velocities under the ACB due to induction of room air. It is also important to trace the heat sources evenly distributed because asymmetric layout may cause opposing upward buoyancy flow that deflects ventilation air into the occupied zone or large recirculation that creates draught risk at the ankle level.

Literature review on the measurement of induction ratio of active beam units shows that the velocity method was considered as the most suitable method as both capacity method and temperature method suffer from difficulty to measure induced air temperature downstream the coil as it is non-uniform and varies both along and across the coil. Although none of the methods could be regarded as best practice and therefore the induction ratio measurement needs more investigation due to the complexity involved.

Literature review on CFD performed on active beam shows that many of the studies considered the perforated grill, the induction phenomenon simply by adding pressure loss. CFD simulation with change of the boundary conditions and in heating mode was not performed in past. It was also noted that RNG k-ε and standard k-ε turbulence model is used in many studies.

4. PROBLEM STATEMENT

Nowadays, decreasing the energy consumption in residential and commercial buildings has become very important and many organizations and governments are continuously working to reduce it further by different means within the building industry. It is documented that energy consumption in such buildings is much more compared to the energy used for transportation [56]. Therefore, a push to optimize the energy consumption by applying active and passive design energy-saving strategies is growing rapidly.

HVAC system consumes approx. 60% – 70% of total energy of a building and thus play a major role in terms of decreasing the energy consumption in buildings. Although decreasing the supply airflow rate from ventilation systems save energy but several studies show that reducing the supply flow rate has a negative impact on indoor air quality affecting negatively human performance and health [57]. Therefore, new technologies to remove heat between the human body and its environment efficiently have taken considerable notice. Among various methods for cooling and heating the spaces, high-temperature water cooling and low-temperature water heating systems like Active Chilled Beam Units have become popular.

The reference case study building, a high-performance LEED Gold building also employs ACB with cooling and heating capabilities and primary air is supplied by central air handling units. Even though the reference case study building is operational and there are no apparent complaints, the building is far from being a high-performance building that fully meets the climate and occupancy needs. Preliminary observations on building suggest that the energy efficient systems like ACB with cooling and heating coil do not provide uniform air distribution and cause thermal discomfort. The effect is more prominent in heating mode operation and for the offices at the perimeter of the building having operable windows. Anecdotal evidence also suggests that the perimeter office on the first floor has more discomfort which has windows next to the occupant. The offices on the second floor also have the windows but the effect of radiation is minimized owing to the double façade installed at the second, and third floor of the building.

Many studies have been conducted on ACB technology in cooling mode as presented in literature review but the performance and efficiency of active beams and its coupling with the room under varying boundary conditions have not been documented in detail. Some literature

on chilled beam systems suggested that ACB have limited heating capacities [21], the risk of stratification, insufficient mixing and temperature gradient (> 3 °C) under heating mode [23]. Due to the tendency of warm air to rise to the ceiling, stratification is possible if the discharge air temperature is too high or discharge velocity is too low. With chilled beams, stratification is likely if the temperature of the water entering the coil is too high.

Literature review on ACB shows [21] that ACB often require a separate perimeter heating system. This increases the total cost of the HVAC system. However, *no other heating system was employed in case study building and many occupants were found using personal heaters in perimeter offices, therefore a detailed study of ACB under heating mode is a must.*

Literature review on thermal comfort from ACB shows that many studies have bee n conducted with different office configurations under cooling mode while performance of ACB under heating mode was not documented. Literature review in cooling showed risk of draught, short circuiting of air stream, less efficient at high outdoor temperature.

Literature review on numerical studies shows that most of the studies were conducted to find out the room air distribution, to understand the airflow patterns of attached plane jets and predict the velocity decay of an attached plane jet after it impinges on the wall and then reaches to the floor to determine the thermal comfort. Most of the studies through numerical CFD simulation were primarily focused to optimize the performance of ACB through changing geometry, nozzles, and enhancing the induction ratio. Many of these studies were conducted under cooling mode operation.

Therefore, this study aims to gain insight of performance of ACB under cooling and heating mode. The focus of study is not measuring the performance of ACB through thermal comfort or draft rate rather to focus on characterization of room level by mapping the airflow and temperature distribution in the room and to gather data to perform numerical simulations to visualize the various characteristics of air in the space by CFD modelling. The research follows a field-study approach on two offices to investigate the performance of ACB in a high-performance building under varying boundary conditions. The performance matrix used in this study is thermal stratification and temperature difference between ankle and head for sitting and standing person in occupied zone and to assess the ventilation efficiency by beam in cooling and heating modes of operation.

5. RESEARCH APPROACH

5.1 Research Objectives

The objectives of this research are to address the performance gaps described in the problem statement. These objectives include the use of offices into the case study building and conduct experiment changing various boundary conditions and to get answers of some overarching goals as described below:

1) To study and explore the functioning of Active Chilled Beam and find out various factors affecting its performance.
2) To study few offices in real time with and without the double façade through experimentation and evaluate the air velocity and temperature distribution in cooling and heating mode.
3) To assess the risk of stratification and temperature gradient in heating mode.
4) To develop and validate a CFD model coupling a chilled beam and an office under varying boundary conditions. The model will be used to help understand room air and temperature distribution to assess active beam performance with the change of various boundary conditions.
5) To assess the comparative performance of ACB by investigating the ventilation efficiency in cooling and heating mode with calibrated CFD models for both the test rooms.

5.2 Scope and Limitations

The scope of the study is as follows:

1) **Field studies:**

- Field studies are conducted in the Gateway Building at BCIT. The Micro-climatic analyses are limited in time by the availability of offices i.e. when employees are on vacation or during the period before a new employee is hired. The extent of the measurements is also limited by the number of instruments available.

2) **CFD:**

- To develop a CFD model of the active chilled beam coupled with the room. The initial intent of this research was to conduct a room level analyses only and use CFD models of ACB from manufacturers. However, manufacturers were reluctant to share their models. Therefore, a simplified approach to develop a CFD model of the ACB model is adopted for the study with a discussion with manufacturers.

The main limitation of the study was the time frame to study building, the mechanical system installed in the building and conducting experiments in a running building with heavy instrumentation in offices. The building facility was in use at the time of study and proper access to the building was also the limitation of the study. Same offices were not available to test the ACB in winter and summer and therefore the winter experiment was conducted in a perimeter office covered by double façade and summer experiment in perimeter office at first floor and is not covered by double façade. The major task was to learn CFD modelling and develop a CFD model of a complex Active Beam Unit. Many assumptions were made to model the ACB to predict airflow distribution in a space.

6. RESEARCH METHODOLOGY

As indicated in Figure 6.1, the main focus of this research is on ACB performance through ACB characteristics and Room level analyses of Active Chilled Beams. ***Room Level*** analysis is performed to get the data in an uncontrolled real environment through field experiments. The data gathered from the experiments is used to set up the boundary conditions for the CFD model and further used to validate the model and compare the results in heating and cooling mode of operation of ACB. The CFD of ACB was validated against the manufacturer software for isothermal condition and then it was coupled with the test rooms.

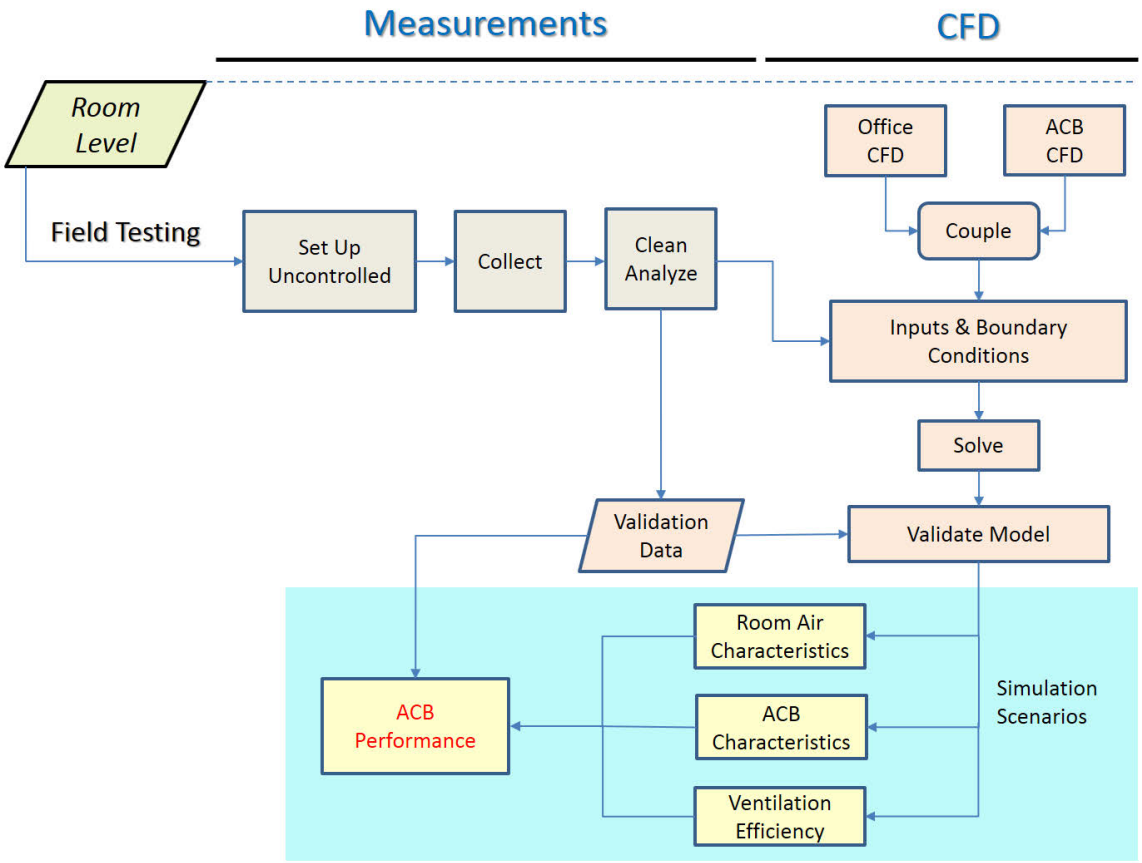

Figure 6.1 - Research Methodology Flow Chart

The ***Room Level*** analysis will to be conducted in 2 steps.

1) In field,

2) Through CFD simulation.

1. Field Study –For field study, 2 offices were instrumented to measure and record the wall temperature, air temperature and velocities at different levels, room return and supply air velocity, flow and temperatures from the active beam. Limitation of this study was the availability of offices in a fast-paced occupied building and therefore all the experiments were intended to be executed during vacations. Another limitation was that the same office could not be used for another season to record the data. Therefore, only one season data could be recorded. During the field study, the thermostat setpoint was changed from initial condition to a set condition and response of active beam was studied. The goal of field study is to assess actual field operation, response under varying boundary conditions.

2. Computational Fluid Dynamics Modeling – The CFD model of the experimented offices with Active Beam was developed and calibrated to use for analyzing further room configurations, thermal loads, and varying boundary conditions. CFD models are studied under steady state condition. The CFD model is made on the Cradle "scStream" software. The model of the chilled beam was planned to be obtained from a manufacturer however manufacturer were reluctant to share the model. The simple k-ε turbulence model is used in the study as the same was used previously by different researchers for room airflow.

Hence, the study is accomplished by investigating the air velocity and temperature distribution inside a room with active beams through a combination of field study and CFD simulations under different modes to evaluate the thermal comfort and other parameters. The study also utilized the data from the Building Automation System (BAS). Temperature sensors and anemometers with data loggers are also placed to record air temperature, operative temperature, window temperatures, and relative humidity in the testing offices. The recorded data is used to analyze the performance of ACB and set up boundary conditions to simulate different scenarios in CFD model.

6.1 Case Study Building

The building to be used in the study is located at BCIT Campus in British Columbia, Canada is shown in Figure 6.2. The BCIT Gateway Building is a three-storey structure and courtyard that includes office, study and gathering space. The building is composed of a concrete frame with a steel roof structure, supported by a typical strip and pad footings. The exterior cladding consists of aluminum curtain walls, punched windows, metal cladding and a galvanized steel frame. The interior construction is primarily metal stud partitions with glazing frames. Some of the building materials were reclaimed from demolished west wing building and 2010 Olympics sites, including carpet tiles and fixtures.

**Facility data and Image Source: BCIT website*

Figure 6.2 - The Gateway Building – BCIT, Burnaby, Canada

The Gateway building included 6,860 m^2 of new construction, 1,035m^2 of student service department renovations, and 1,892 m^2 of lab and classroom renovations. The project delivered 33 new multi-use rooms and additional study areas, as well as seismic and electrical upgrades. Some of the unique features of this building include a ventilated double façade along the full length of the west exposure to control the amount of direct solar gain. A dedicated relief air heat recovery system redirects 10,000 liters per second of the existing building relief air into the new atrium and a custom rooftop air handling unit. Over 250 new active beams are also used in the occupied spaces of the new building to provide heating and air conditioning. The Gateway building integrates several features of Intelligent Micro Grid project, which monitors energy demand, manages onsite energy plants and provides users with control of energy consumption, modeling and simulations.

7. EXPERIMENTS AND METHODOLOGY

7.1 Experimental Facility

7.1.1 Offices (Test Rooms)

As mentioned earlier, the study was carried out in a 3 story high-performance LEED Gold Building at British Columbia Institute of Technology in Burnaby City, province of British Columbia, Canada as shown in Figure 7.1. The building is located in 49° 14' N and 123° W, 20 km away from the Vancouver International Airport.

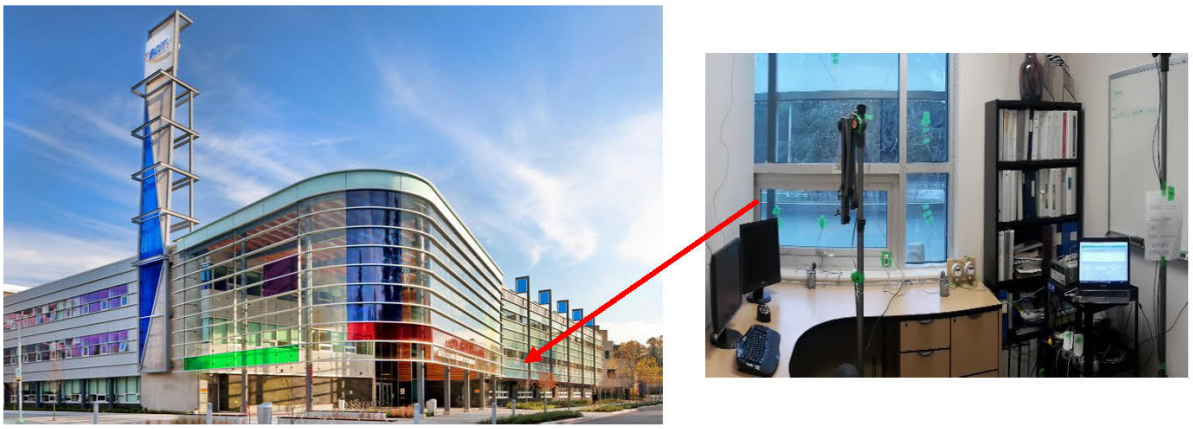

Figure 7.1 - BCIT Gateway Building and the perimeter Office (Test Room 1) at second floor.

Test Room 1

2 offices were selected for the study. This section describes the second-floor perimeter office room (Test Room 1) with the size of 4.60 m long x 3.00 m wide x 3.55 m high, as shown in Figure 7.2. A suspended ceiling is installed which reduces the actual room height to 2.95 m. The suspended ceiling is made of acoustic tiles where ACB, ceiling lights and return grille is installed. This perimeter office is covered by double façade as shown in Figure 7.1. The west and north walls are exterior walls, and the east and south walls are interior as shown in Figure 7.3. The exterior walls are made of reinforced concrete. The walls are highly insulated and calculated U values of walls and windows are shown in Table 7.1. The window of the office at the external wall is shaded by the structure of double façade and partially by trees to protect the

office from direct sunlight and therefore the room temperature is fairly stable at all time. The office is illuminated by two ceiling mounted lights. The room has its own supply and return air system. The cooling and heating in the office room were realized with 2 –way flush mounted Active Chilled Beam installed in the acoustic tile ceiling. The return from the room is facilitated by a return grille of size 0.3 x 0.125 m installed in the ceiling. The beam dimensions were 2.40 m long x 0.60 m wide and 0.21 m high. The ACB details are presented in Table 7.2. The length of the inlet slot was equal to the length of the beam and it was located symmetrically in relation to the centerline of the room and parallel to the window as illustrated in Figure 7.2. The primary air is supplied by central air handling unit and the flow and temperature of primary air are recorded in Building Automation System (BAS) system. The chilled beam is connected to a water source heat pump and both hot water and chilled water temperature supply to the chilled beam were recorded in the BAS system. The west exposed wall had a fixed window of size 2.00 m wide and 2.15 m high wide with an operable sash of size 1.4 m wide x 0.5 m high.

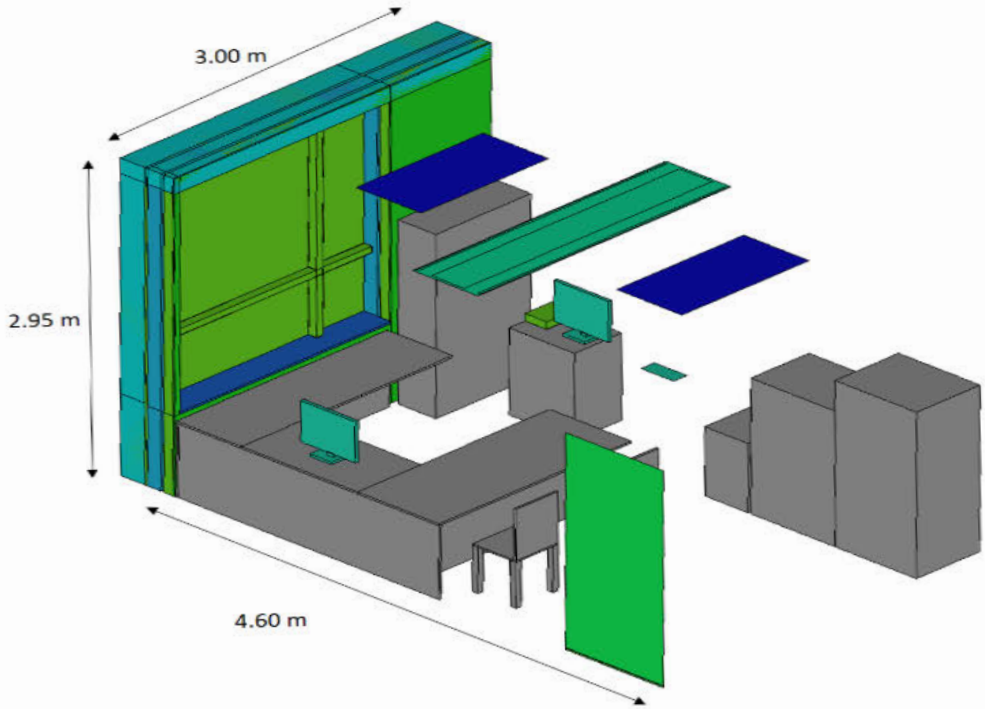

Figure 7.2 - Dimensions and Layout of the Office (Test Room 1) at Second Floor

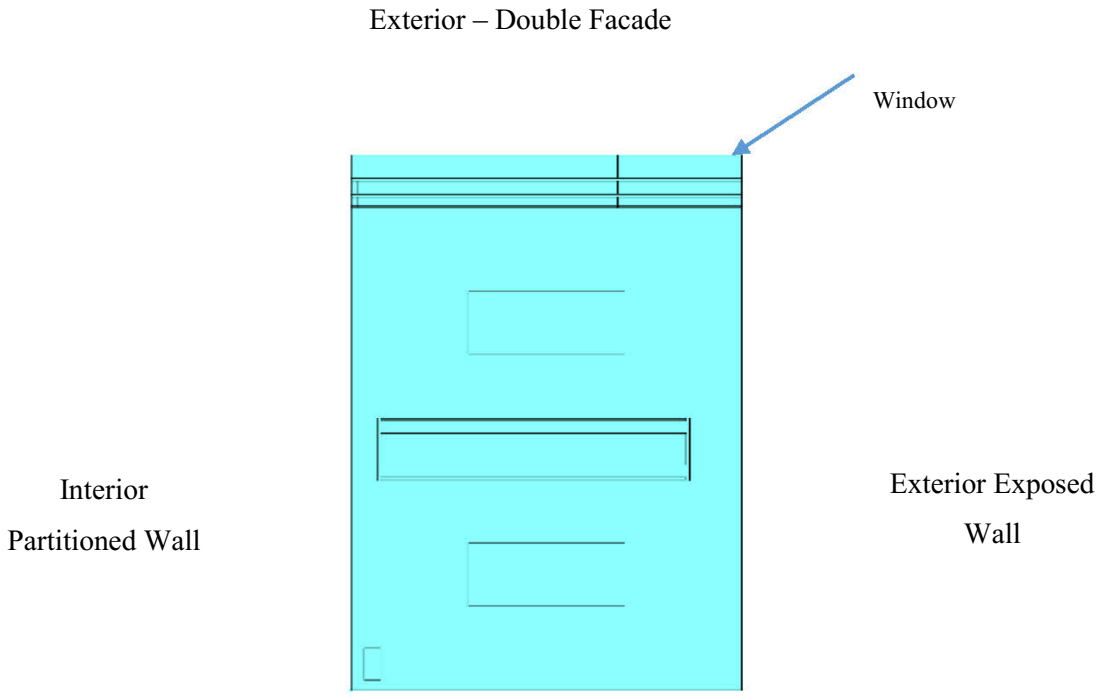

Figure 7.3 - Test Room - 1 Exposure

Figure 7.4 – Active Chilled Beam installed in the Ceiling

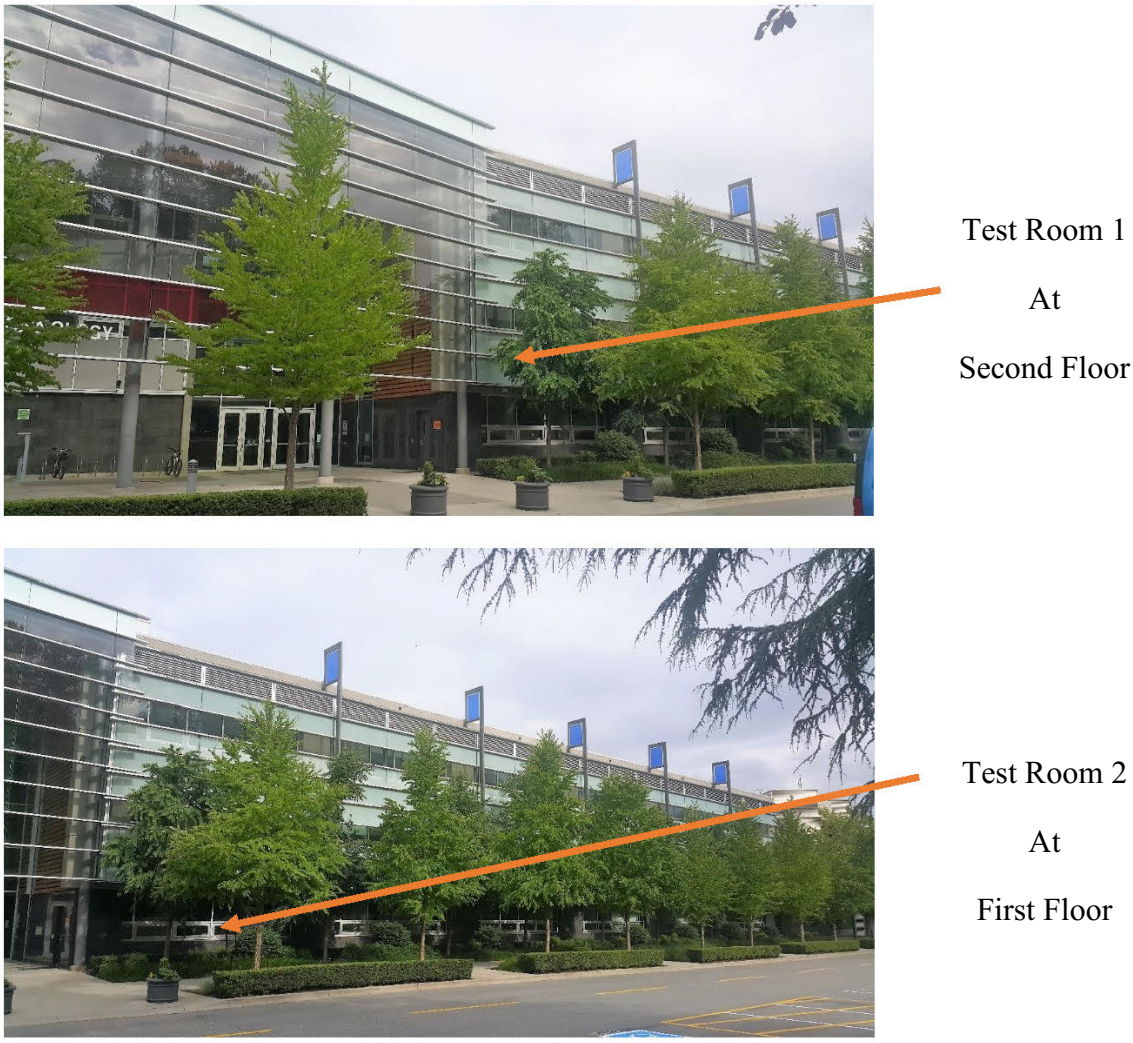

Figure 7.5 - Location of Test Room 1 & Test Room 2

Test Room 2

Test Room 2 with the size of 4.85 m long x 3.07 m wide x 3.55 m high, as shown in Figure 7.6. A suspended ceiling is installed similarly Test Room 1 at a room height of 2.95 m. This perimeter office is at the first floor and is open to the atmosphere on the west side. This test room is different from the test room 1 which is covered by double façade at the west as shown in Figure 7.5. The west wall is an exterior wall, and the other walls are interior. The construction is similar to the previous test room. The window of the office at the external wall is shaded by the extended base of double façade and partially by trees to protect the office from direct sunlight and therefore the room temperature is fairly stable most of the time during summers.

The office is illuminated by two ceiling mounted lights. The room has its own supply and return air system. The cooling and heating in the office room were realized with 2 units of 2 –way flush mounted Active Chilled Beam installed in the acoustic tile ceiling. The return from the room is facilitated by a return grille of size 0.6 x 0.125 m installed in the ceiling. The beam dimensions were 2.40 m long x 0.60 m wide and 0.21 m high. The ACB was not located symmetrically in relation to the centerline of the room and one ACB is installed closed to the glass portioned wall as illustrated in Figure 7.6. The west exposed wall had a fixed window of size 2.90 m wide and 1.75 m high with an operable sash of size 1.4 m wide x 0.5 m high.

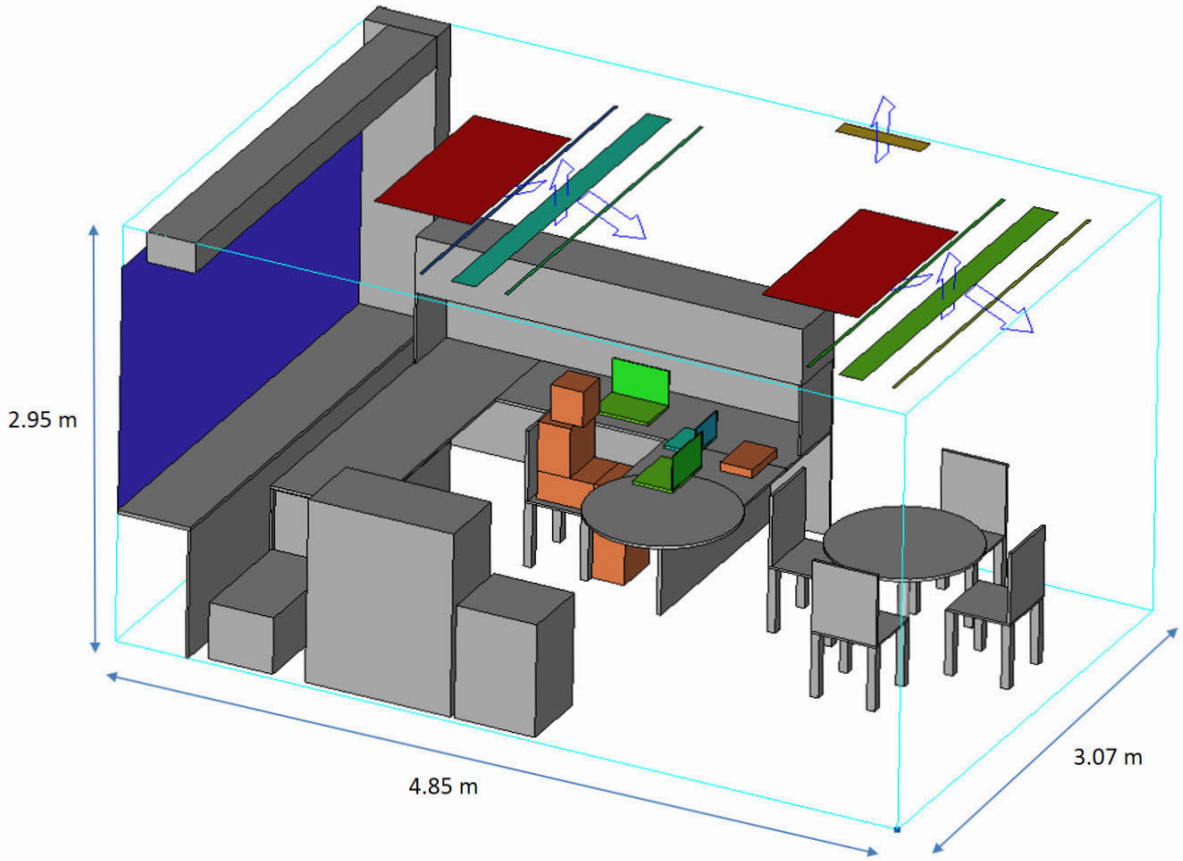

Figure 7.6 - Dimensions and Layout of the Office (Test Room 2) at Second Floor

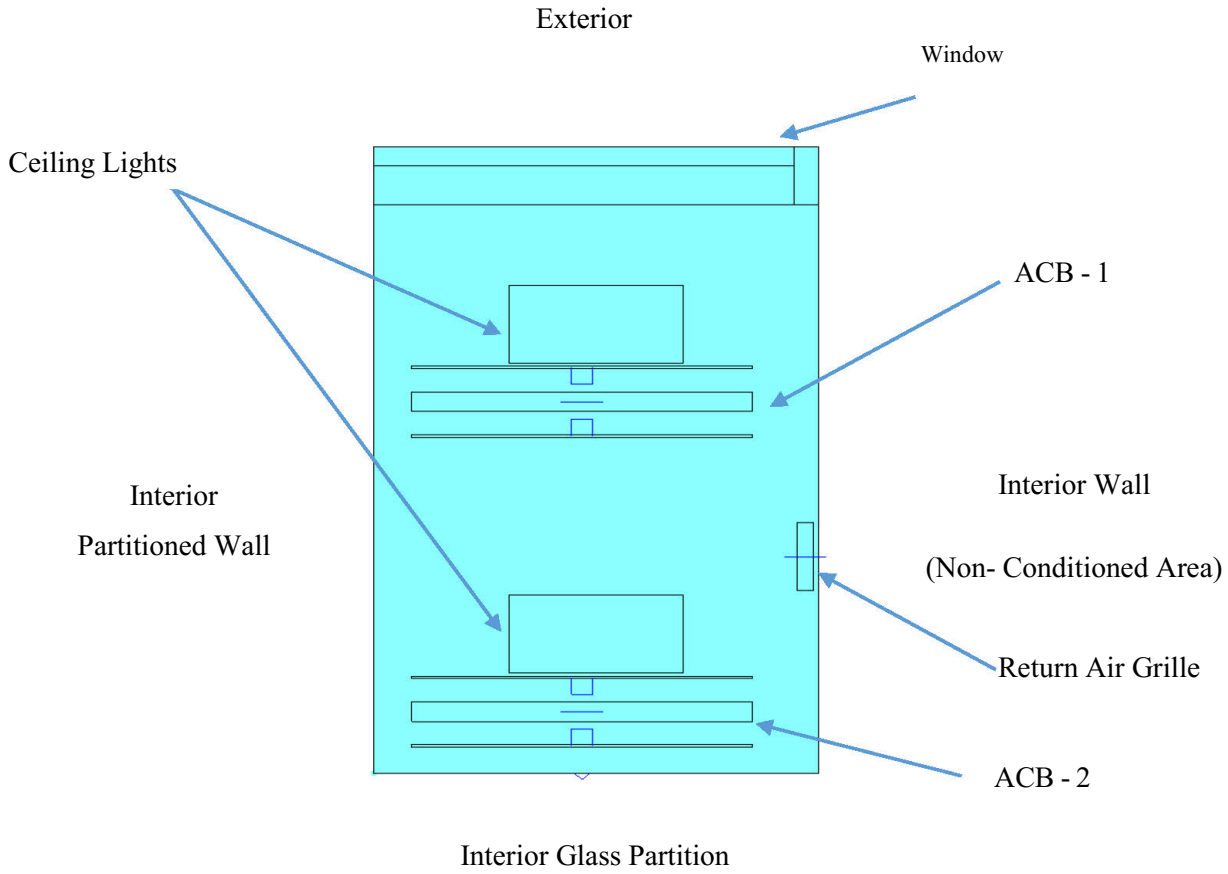

Figure 7.7 - Test Room - 2 Exposures

Figure 7.8 – Active Chilled Beam 2 (ACB 2) Installed near the Glass Partition in the Ceiling

Figure 7.9 – Active Chilled Beam 1 (ACB 1) Installed near Window in the Ceiling

Table 7.1 - Building Design Summary

Mechanical Ventilation System	Central Air Handling Units
Cooling and Heating System	Water Source Heat Pump - WSHP
Terminal Units	Active Chilled Beam – 4 pipe – Cooling & Heating
Interior Partitioned Wall	U Value - 0.73 W/m^{2}K
Exposed Wall	U Value - 0.30 W/m^{2}K
Interior Concrete Wall	U Value - 1.86 W/m^{2}K
Slab (Top and Bottom)	U Value - 0.80 W/m^{2}K
Overall Window	U Value – 2.61 W/m^{2}K

Active Chilled beam

The Active Chilled Beam (ACB) used in the study is shown in Figure 7.10. The chilled beam is manufactured by TROX (DID632). More information about the design, selection and specification, of used ACB can be found in Appendix C. The beam was constructed of ½" (12.7 mm) diameter copper tubing with aluminum extruded fins with 8 fins per inch and the fin thickness is at least 0.0055 inches (0.14 mm). The beam was a two-row, 16-passes coil. 12 passes are dedicated to cooling and 4 passes for heating.

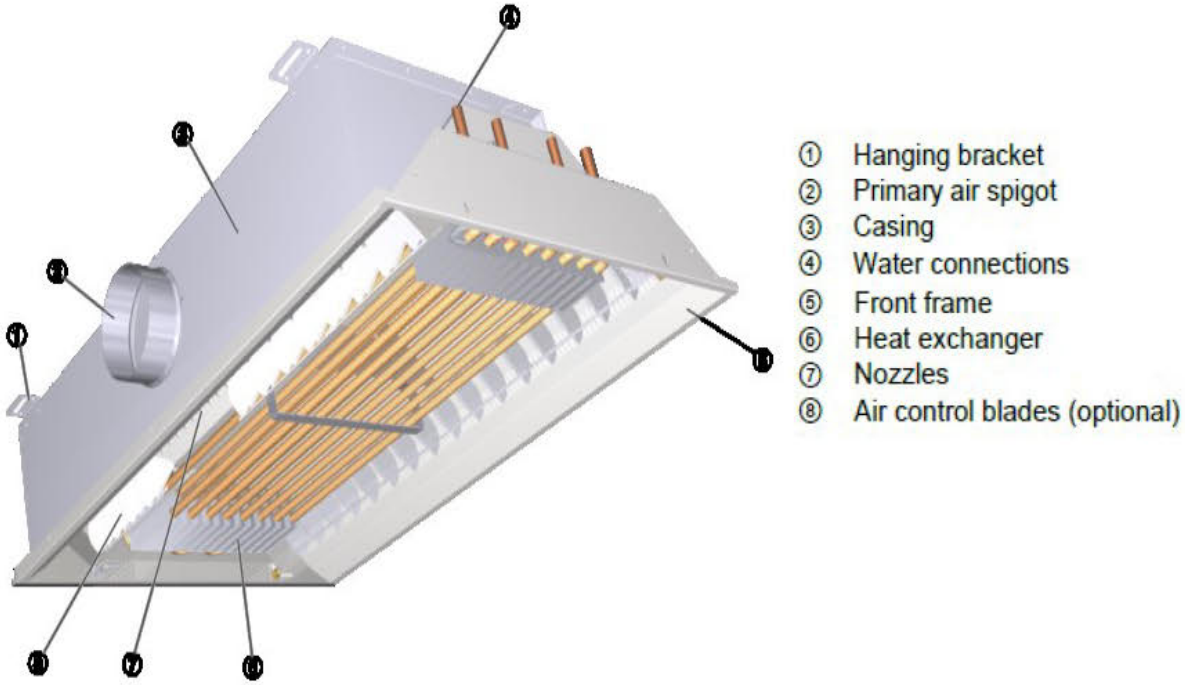

Figure 7.10 - Schematic Illustration of TROX DID632 Active Chilled Beam [Appendix C]

Table 7.2 - Specifications of the Active Chilled Beam in Test Rooms

		Test Room 1	Test Room 2
Overall Size	2.40 m x 0.60 m x 0.21 m		
Number of Chilled Beam		1	2
Cooling Capacity (W)		1154.0	2308
Heating Capacity (W)		1422.0	2844
	Design	Measured	Measured
ACB Plenum Pressure Design (Pa)	158.0	140.0	130.0
Supply Chilled Water Temperature (°C)	15.8	16.0 (±1°C)	14.5 (±1°C)
Supply Hot Water Temperature (°C)	48.9	45.0(±1°C)	44.0(±1°C)
Primary Air Flow (l/s)	28.0	23.5	22.8
Primary Air Temperature (°C)	18.0	18.0 (±1°C)	18.0 (±1°C)
Operation Schedule	5.00 AM – 10.00 PM		

7.1.2 Measurements

This section describes the experimental measurements, various sensors used, design and measurement systems.

Experiments have been conducted with two primary purposes in mind.

a) To gain an understanding of air velocity and temperature distribution in the occupied zone to assess the performance ACB in heating mode in a typical high-performance building.

b) To collect data that can be used to provide boundary conditions for numerical modelling and compare results.

Room Air Temperature and Velocity measurements

The measurement of air temperatures and air velocities at different heights were carried out by omnidirectional calibrated anemometers SensoAnemo 5100LSF as shown in Figure 7.13. The anemometers were placed on a manifold at 0.1 m, 0.6 m, 1.1 m and 1.7 m heights on a movable stand above the floor as shown in Figure 7.11 and moved manually at possible occupant's location in the room. The velocity sensor was spherical with a diameter of 2 mm. Therefore, the effect of disturbance could be neglected because of the small dimensions of the equipment. The averaging time at each point was 180 seconds. The velocity was measured with an accuracy of 0.02 m/s ±1.5% in the range of 0.05-5 m/s. All anemometers had been calibrated before the measurements. The supply and return air velocity of the beam were measured by TSI 8475 anemometers and recorded on Agilent 34972A Data logger at every 60 seconds. The details about anemometers are given in Table 7.3.

Series of airspeed and temperature measurements were made. The anemometers standard configuration for room measurement is shown in Figure 7.12.

Figure 7.11 - Manifold to Measure Air Velocity and Air Temperature at 4 Different Heights

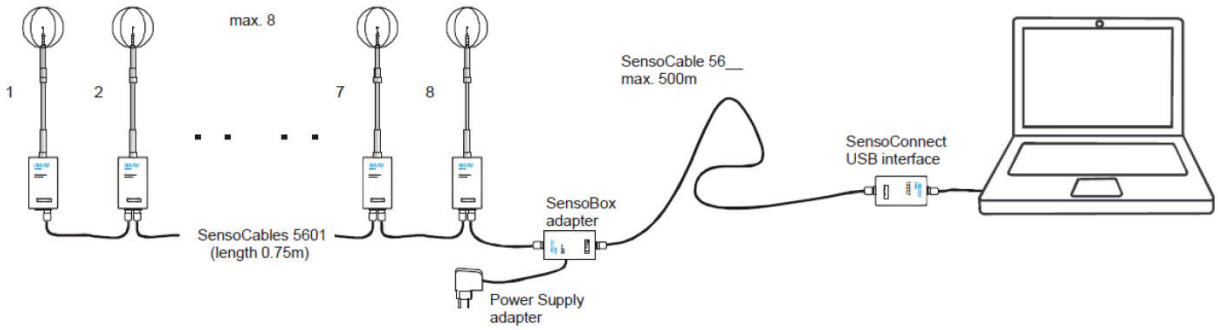

Figure 7.12 – Wiring Connections for Measurement of Air Velocity and Temperature

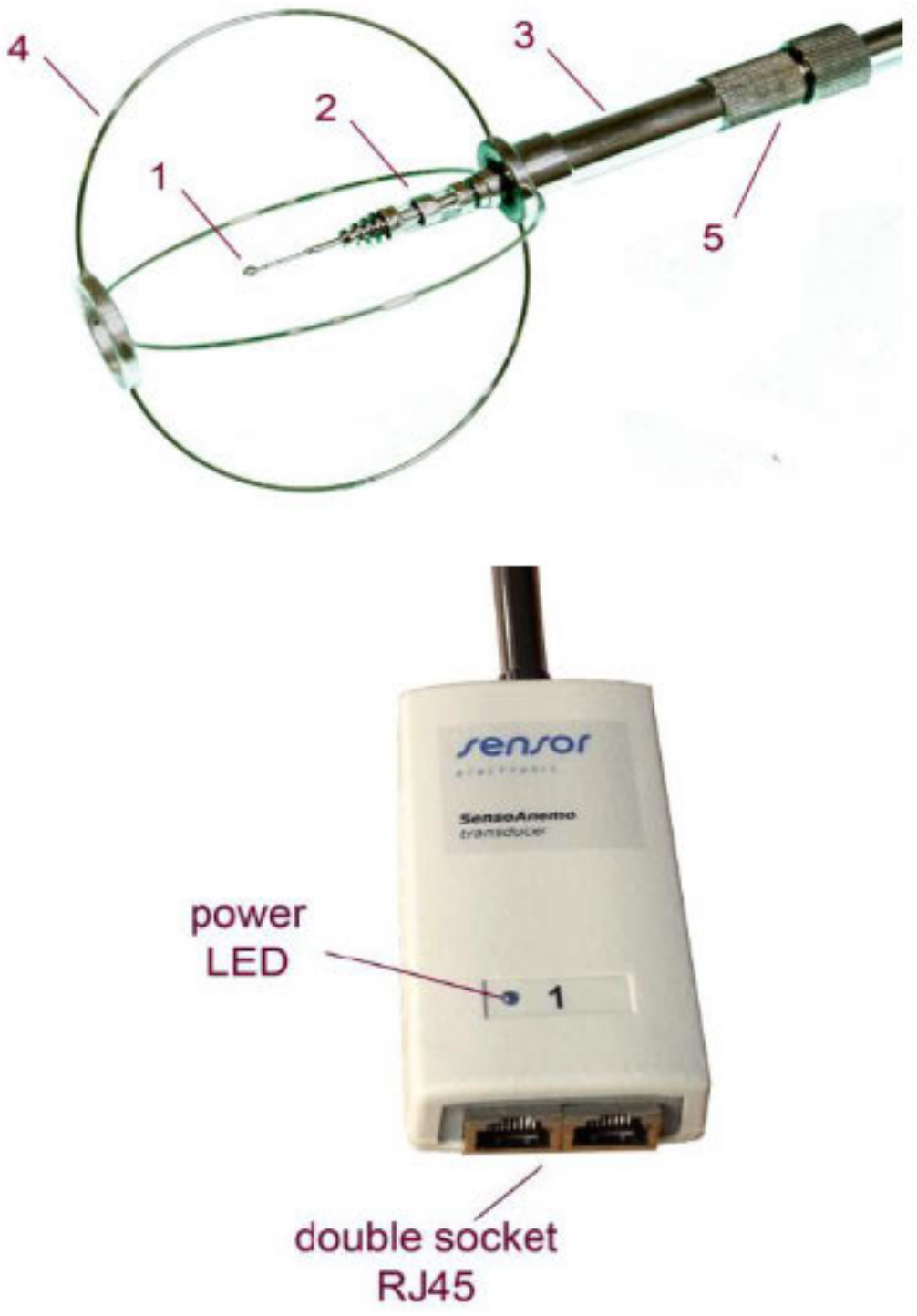

Figure 7.13 - Illustration of Sensoanemo5100LSF air speed/temperature sensor

SensoAnemo5100LSF is a transducer with omnidirectional (spherical) sensor for measurement of airspeed (magnitude of the velocity vector). The transducer measures instantaneous speed, mean airspeed and standard deviation of airspeed as well as the air temperature, draught rate

and turbulence intensity. Each probe is individually calibrated and compensated for the impact of temperature changes on velocity measurements (air temperature different than the air temperature during calibration). The compensation and calibration coefficients are programmed into EEPROM memory. The probe is shown in the Figure 7.13. The velocity sensor (1) is made of special wire pressed into the shape of a sphere with a diameter of 2 mm. The temperature sensor (2) is made of the thin nickel wire and its shape is cylindrical. The temperature sensor measures the temperature of the ambient air. The two sensors are vacuum covered with a special aluminum coating that increases their resistance to contamination and decreases the effect of thermal radiation on the accuracy of velocity measurement. Both sensors can be also protected against mechanical damage using an openwork basket (4) made with wire circles and can be locked at a certain position by a clamp screw (5). The transducer has a digital output RS485.

Table 7.3 - Specification of Anemometer

Type of speed sensor	Omnidirectional, Spherical
Diameter of speed sensor	2 mm
Measurement speed range	0.05… 5 m/s (expanded: 0.05…10m/s)
Accuracy of speed measurement	±0.02 m/s ±1.5% of readings (±0.02 m/s ±3%)
Directional sensitivity error (for v>2m/s)	±2.5% the actual value
Automatic temperature compensation	< ±0.1%/K
Upper frequency of speed fluctuation	typ. 1.5 Hz, min. 1 Hz
Response time 90%:	typ. 0.2s, max. 0.3s
Temperature range	-10…+50 °C
Accuracy of temperature	0.2 °C
Sampling rate	8 Hz
Interface	port RS485
Baud rate	115000 bps
Optional analog output	voltage 0...2V, 0...5V or current 0...20 mA
Max analog output resistance	100 Ohm
Power supply	3.3…9 VDC
power consumption	typ.60mA, peak. 110mA, economy mode 6mA

Supply and Induced Air Velocity Measurement at Active Chilled Beam

SensoAnemo5100LSF and TSI 5475 were also used to measure the supply velocity and induced velocity at ACB. 6 units of Anemometers (3 unit at each slot) were placed in supply slot of ACB and 3 anemometers were placed at induction (return) surface. The placement of anemometers at different locations in ACB during experiments is illustrated in Figure 7.14 – Figure 7.18.

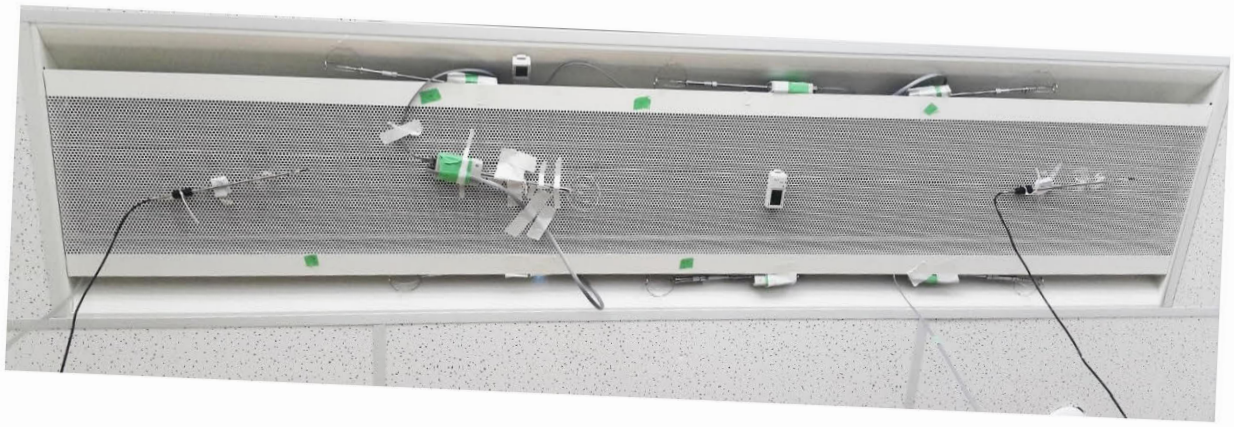

Figure 7.14 - Measurement of Discharge and Induced Air Velocities at Active Chilled Beam

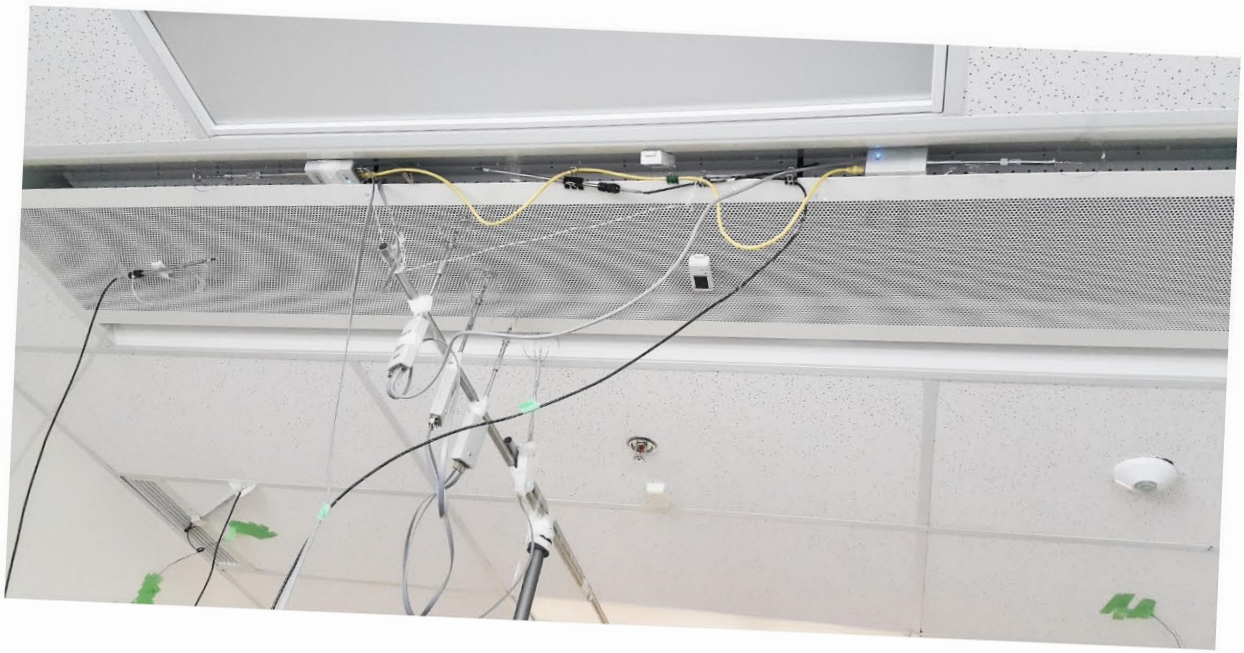

Figure 7.15 - Measurement of Induced Air Velocities at Different Sections of ACB

Figure 7.16 – Placement of Anemometers at Induced Surface of ACB

Figure 7.17 - Measurement of Discharge Air Velocity inside Supply Slot

Figure 7.18 - Measurement of Discharge Air Velocity at the Outlet of Supply Slot

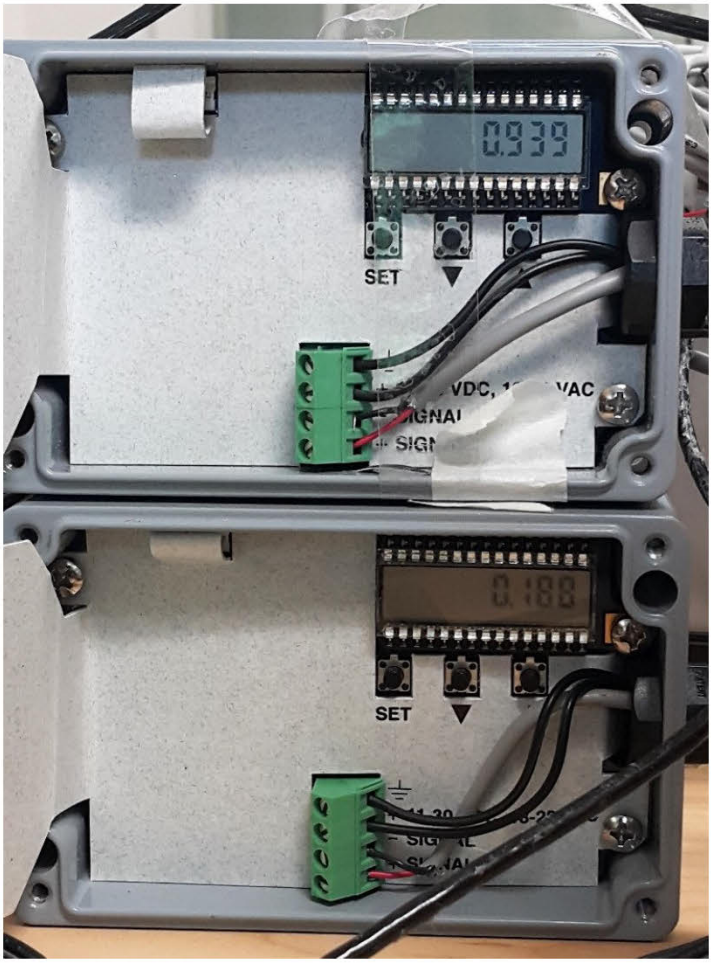

Figure 7.19 - Magnitude of Typical Discharge (0.93 m/s) and Induced Air Velocity (0.18 m/s)

Return Air Velocity and Temperature Measurement at Return Grille

REED Thermal Anemometer SD 4214 was used to measure the return air velocity and temperature at return air grille at the ceiling. Anemometer is shown in Figure 7.20

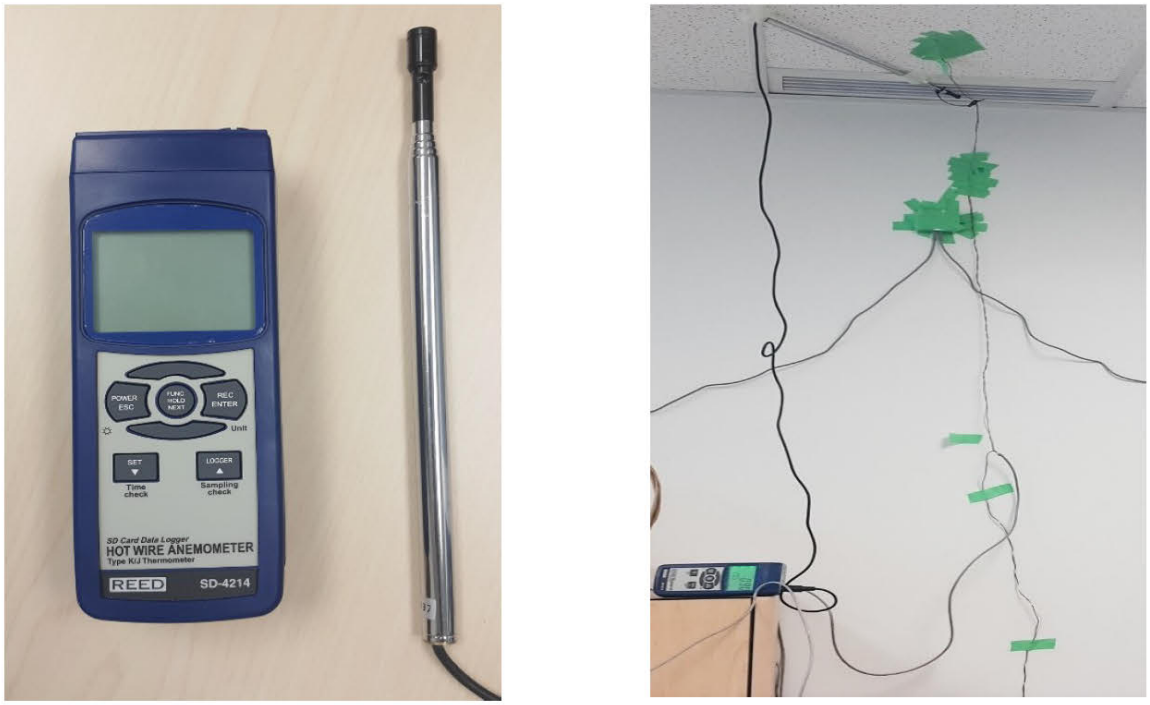

Figure 7.20 - Return Air Grille Velocity and Air Temperature Measurement

Temperature Measurement

Outdoor temperature, operating temperature and room temperature at different locations in the office room, chilled beam supply temperatures at the two slots, chilled beam return (induced) air temperature, surface temperatures, local air velocity and air temperature at different points were recorded during the experiment, sensor specifications are described in Table 7.4. The differential pressure at the ACB plenum, door and window were also recorded. The pressure difference across the door and window was found very low (negligible) and is not reported in the study. Coil on-coil, off-coil air temperatures, coil surface temperatures were also recorded to study the heat exchanger design and its effect on discharge air temperatures.

Figure 7.21 – Placement of HOBO for Discharge and Induced Air Temperature Measurement

Figure 7.22 - Outdoor Air Temperature Measurement

Operative temperature

Operative temperatures at different locations in the room were measured by a gray globe sensor of 4 cm diameter connected to a HOBO logger. The logged voltage was recorded in real time by the portable data logger via two separate voltage channels. In addition to logging data, the HOBO logger itself had an embedded sensor able to measure the air temperature and relative humidity of the air. Three HOBO devices were placed at points 1, 2 and 3 as shown in Figure 7.24. The measurement interval for all mentioned instruments was 60 seconds.

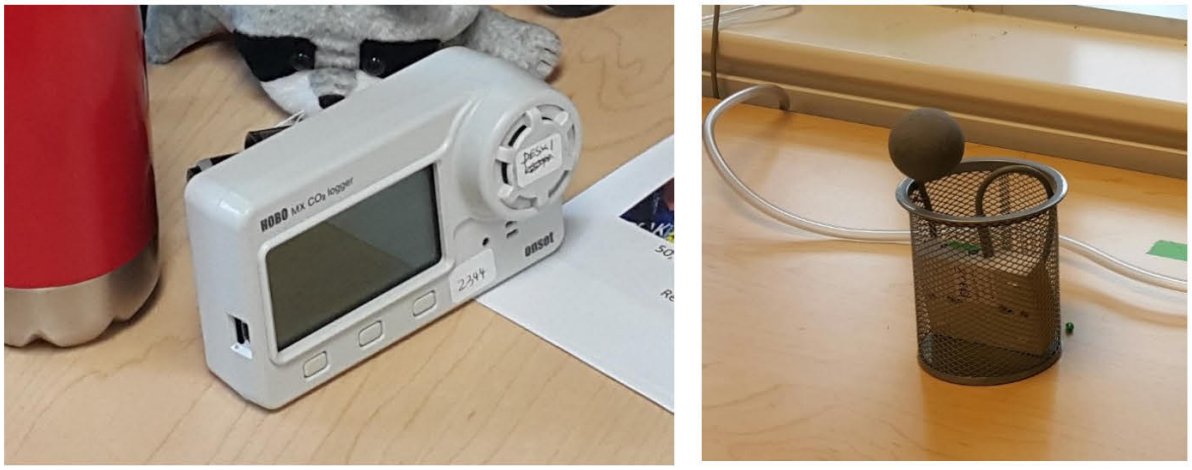

Figure 7.23 - Operative Temperature Measurement Globe

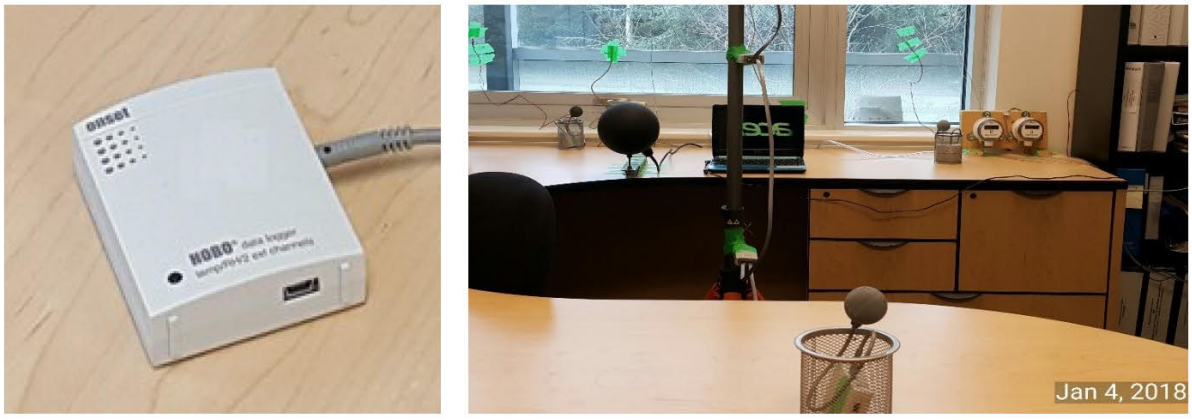

Figure 7.24 - Operative Temperature Measurement at 3 different location.

Table 7.4 - Sensor Specifications for Office Experiment

Sensor	Application	Type	Range	Accuracy
Temperature	ACB Supply / Return Air Temperature	HOBO MX1101	-20° - 70°C (-4° - 158°F)	±0.21°C from 0° to 50°C (±0.38°F from 32° to 122°F)
Temperature	Air Temperatures	HOBO U12-013	-20° - 70°C (-4° - 158°F)	±0.35°C from 0° to 50°C (±0.63°F from 32° to 122°F)
Temperature	Operative Temperatures	HOBO U12-013 with TMC6-HD	- 40° - 100°C (-40° - 212°F)	±0.25°C from 0° to 50°C (±0.45°F from 32° to 122°F)
Temperature	Outdoor Temperature	HOBO MX2302	-40 to 70°C (-40 to 158°F)	±0.2°C from 0 to 70°C (±0.36 from 32 to 158°F)
Surface Temperature	Wall & Window Temperatures	NXFT15XH103FA2B050 Thermistor	-40°C - 125°C	±0.2 °C
Air Velocity Transducer	Room Air Velocity	SensoAnemo 5100LSF	0.05 - 5 m/s	±0.02 m/s ±1.5% of readings (±0.02 m/s ±3%)
Air Velocity Transducer	ACB Supply & Return Velocity	TSI 8475	0 - 2.5 m/s	±3.0% of reading, ±1.0% of full scale
Differential Pressure	Plenum Pressure of ACB	EXTECH HD 755	±3.447 kPa	±0.3% FS + 1d (@ 25°C)
Thermo-Anemometer Data Logger	Return Air Velocity and Temperature	REED SD 4214	0.2 to 25 m/s (40 to 3940 fpm) 0 to 50°C (32 to 122°F)	±2.0% of reading
Differential Pressure Transmitter	Differential pressure between Office and Corridor, Window and Ambient	Dwyer MS-121-LCD	25 Pa – 100 Pa	±1.0% for 50 Pa

Surface Temperature measurements

Wall and window surface temperatures were recorded by NTC thermistors as shown in Figure 7.25 at numerous points in the office. Each sensor was first placed directly on to the surface after cleaning the desired spot to make better contact with the surface and it was taped by a thick layer of tape to act as insulation to avoid heat exchange with nearby air flow. The location of surface temperature sensors is shown in Figure 7.26. Mean Radiant Temperature was measured by globe thermometer. Data from thermistors and globe were recorded by Agilent 34972A data logger at every 60 seconds. The details of the sensor used in the experiment are

given in Table 7.4. To study the heat exchanger, the external surface temperature sensor TMC6-HD connected with HOBO U12-013 data logger was used as shown in Figure 7.30, Figure 7.31 and Figure 7.32.

Figure 7.25 - Surface Temperature Measurement Thermistor

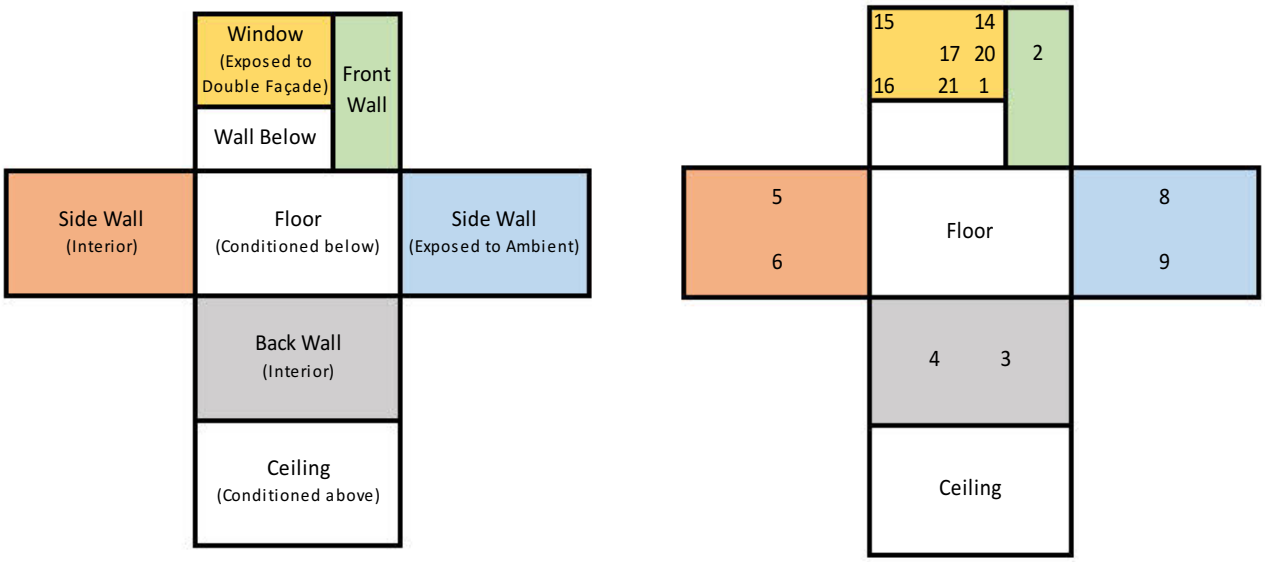

(a) Surface Labelling (b) Unfolded Surfaces with Temperature Sensors

Figure 7.26 - Temperature Sensors Location in the room surfaces (Test Room 1)

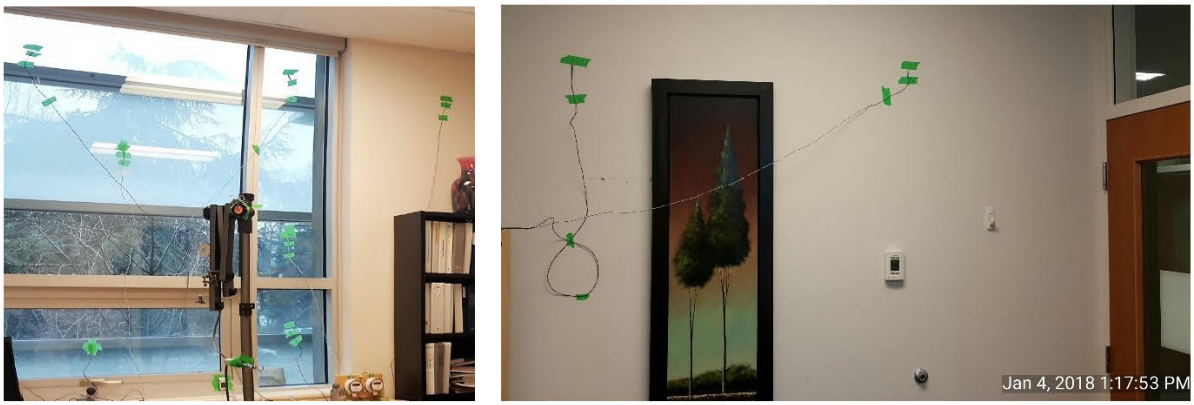

Figure 7.27 - Surface Temperature Measurement - Window and Wall

Figure 7.28 - Plenum Pressure Measurement

Figure 7.29 - On-Coil and Off-Coil Air Temperature Measurement

Figure 7.30 - Supply and Return Water Temperature Measurement

Figure 7.31 - Coil Surface Temperature Measurement

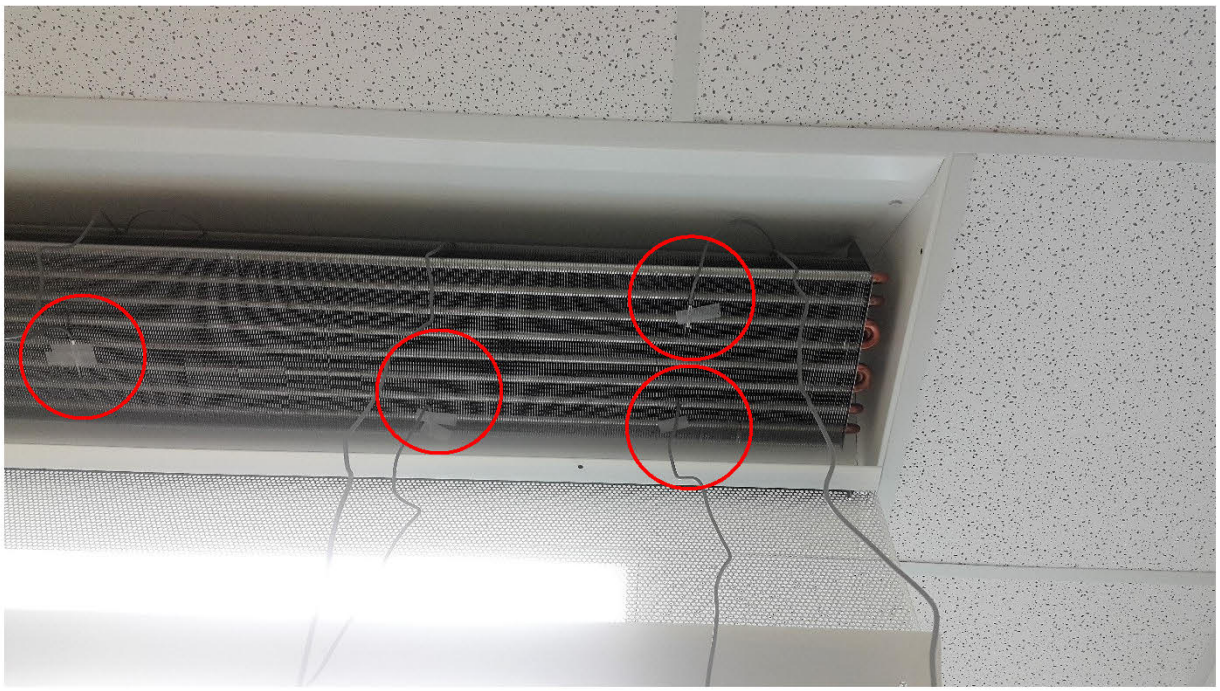

Figure 7.32 – Placement of External Temperature Sensor at Coil Surface

7.1.3 Experimental Procedure

Steady State Condition - The main experiments in this work consisted of a series of experiments on the ACB system in 2 offices (Test Rooms) conducted under steady state conditions. To obtain the data, the set temperature of the room was varied with constant internal load and air supply flow rate. Prior to recording any measurements, the office was set to run at the required set temperature for hours to allow the office to reach a quasi-steady state. The state of the office was monitored by the thermostat, temperature sensor at different surfaces, locations and heights in the room. Truly steady-state conditions in an uncontrolled environment like a running building could never be reached, as the environment surrounding the office might be changed by other occupants and one wall was exposed to external conditions, however, when the temperatures at the thermostat, the operative temperature at the desk in front of occupant and surface temperatures were pretty constant with minor fluctuations, the state of the room was assumed as steady state.

To collect each set of data, measurements were logged for 40-45 minutes. Data logging for SensoAnemo5100LSF anemometers was done in a laptop which is shown previously where all anemometers were connected in a daisy chain. Data logging for the surface temperature sensor (NTC thermistor) and TSI 8475 anemometers was carried out by Agilent data logger by scanning and logging for each channel after every 60 seconds. All other instruments and sensors had the inbuilt data logger to record the data. Measurements of the room air temperature and velocity were made with the movable stand holding the anemometers at different locations as shown in Figure 7.11 earlier. When measurements were made by the movable stand at one location, it was necessary for the occupant sitting inside the office to pick and move the stand manually to other location and therefore the next measurement was taken again after a waiting period of 300 seconds to re-stabilize the air flow pattern. Although 300 seconds is not enough for re-stabilization of an indoor environment but the fluctuations were not noticed at different heights and the velocities were fairly stable after 300 seconds while doing the experiments and therefore the waiting period of 300 seconds was chosen.

The Figure 7.33 shows the possible points where the local air velocity and temperature measurement were taken in Test Room 1.

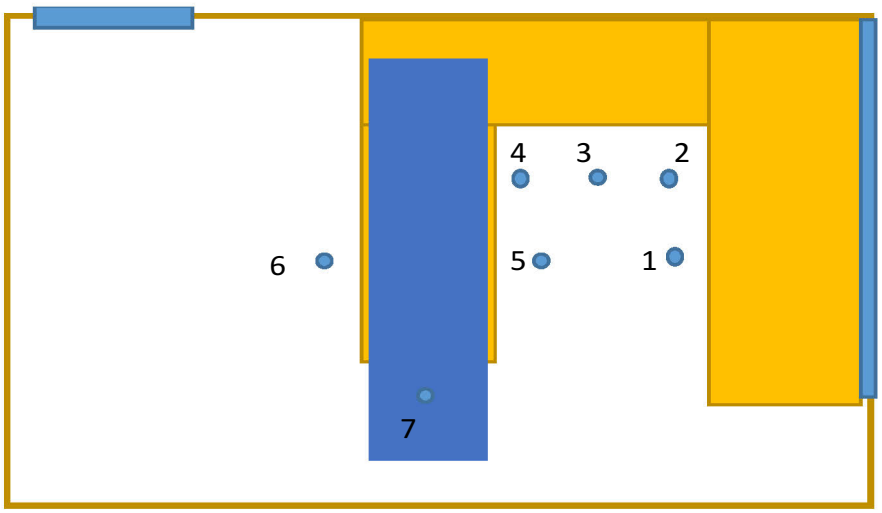

Figure 7.33 - Possible Occupant's Location in Test Room 1 (Heating)

7.2 Test Methodology

7.2.1 Validation

In order to validate the CFD model, the Active Chilled Beam in the office was tested with the usual heat load and the air characteristics were predicted at different locations in the room at 3 different heights as mentioned earlier. The air characteristics in the vicinity of the beam (supply slot, return surface and below the beam on desk) were recorded. The experimental set points are the minimum and maximum temperature in an office set by the occupant normally which is between the 20 – 24 °C. The surface temperatures of the inside walls and window of the offices were recorded to compare with the CFD model predictions. The CFD model was also used to predict the airflow characteristics and compare with experimentally recorded data.

7.2.2 Test Setup

The primary objective for these tests was to collect air temperature and velocity measurements in the space that would be used to compare with predicted values of the CFD model. The beam supply water temperature and flow rate were nearly constant during the test and was modulated by the thermostat to achieve a set temperature in the office. Once the setpoint values were achieved at the room thermostat, and on the temperature sensor placed near occupant on the

desk, the office was assumed to achieve the quasi-steady state, the data was recorded by all measurement sensors as described earlier and the manifold was moved to different locations in the Test Rooms to record the local air velocity and temperature.

Each test required between 6 to 8 hours to complete. During each test, the measured values from the thermistors, HOBO and anemometers were recorded at 60 seconds increments.

8. CFD MODELLING

8.1 CFD Software

A commercial CFD software Cradle scSTREAM V.13, based on finite-volume method, was used to solve governing Navier-Stokes equations in the three-dimensional computational domain to predict the temperature and airflow distribution in the perimeter office. scSTREAM consists of three applications: STpre, STsolver, and STpost. A finite volume method solves the governing equations by converting them into an integral conservation form that is expressed on each fractional unit of decomposed elements, or control volume. The finite volume method is used in STsolver (solver of scStream software) to solve the governing equations. The equations used in scSTREAM include mass conservation, momentum conservation, energy conservation, turbulent equations, and the conservation of diffusive species.

Steps involved in the simulation process is shown in Figure 8.1 and is explained below:

Pre-processing (STpre)

STpre helps to create the input data. It helps in creating the geometry of the model and establishing of the flow domain. The preprocessor also enables a user to set the initial conditions and boundary conditions. Once the boundary conditions are set the gridding and meshing is done.

Solving (STsolver)

STsolver loads the input data and checks the gridding of the geometry. It establishes the simulation strategy and input parameters and executes the calculation. While calculating it monitor the calculation for convergence and then output the results.

Post-processing (STpost)

STpost reads the output file from STsolver and loads the output results and helps to visualize them in form of graphs, contour plots, velocity vector etc.

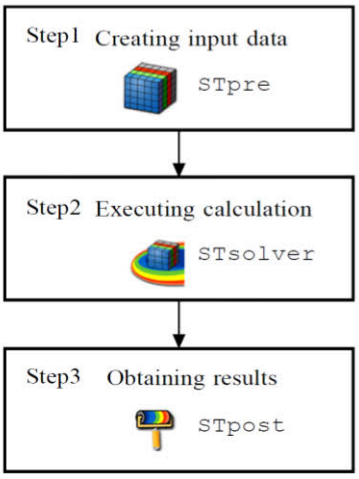

Figure 8.1 - Simulation Process

8.2 Mathematical Formulation

Governing Equations

In numerical simulations to reproduce physical phenomena, such as the air flow and temperature distribution in a room, we need to solve the fundamental equations that govern these physical problems under the given boundary conditions and initial conditions. The following governing equations are used in thermos-fluid analyses.

- Momentum conservation equations (The Navier-Stokes Equations)
- Continuity equation
- Energy conservation equation
- Model equations to represent turbulent transport

Conservation of Mass

The change in mass flow within a control volume must be equal to the mass flow in minus the mass flow out through the control volume surfaces since mass cannot be created or destroyed. This can be expressed mathematically for an incompressible fluid as below

$$\frac{\partial u}{\partial x}+\frac{\partial v}{\partial y}+\frac{\partial w}{\partial z}=0 \quad or \quad \frac{\partial u_i}{\partial x_i}=0 \tag{8.1}$$

where u, v and w were the three components of velocity corresponding to the x, y and z respectively.

Conservation of momentum (Navier–Stokes equations)

The momentum equations that govern the flow of fluid are derived from Newton's second law of motion (the conservation of momentum). The equations are called Navier-Stokes equations, and for a three-dimensional incompressible fluid take the form as below.

$$\frac{\partial \rho u_i}{\partial t} + \frac{\partial u_j \rho u_i}{\partial x_j} = -\frac{\partial p}{\partial x_i} + \frac{\partial}{\partial x_j}\mu \frac{\partial u_i}{\partial x_j} - \rho g_i \beta (T - T_0) \quad 8.2$$

Conservation of Energy

The following equation represents the transport of energy within the flow field. For incompressible fluids, it can be given as

$$\frac{\partial \rho C_p T}{\partial t} + \frac{\partial u_j \rho C_p T}{\partial x_j} = \frac{\partial}{\partial x_j} K \frac{\partial T}{\partial x_j} + \dot{q} \quad 8.3$$

Equation for Diffusive species conservation

For incompressible fluids, it is given as

$$\frac{\partial C}{\partial t} + \frac{\partial u_j C}{\partial x_j} = \frac{\partial}{\partial x_j} D_m \frac{\partial C}{\partial x_j} + \dot{d} \quad 8.4$$

8.3 Turbulence Model

A turbulence model in CFD calculation is a computational procedure to close the system of mean flow equations to enable numerical calculation of these equations. For most practical purposes it is not necessary to resolve the details of the turbulent fluctuations and only the effect on the mean flow is all that is normally required. The task of a turbulence model, therefore, is to express the Reynolds stresses in the conservation of momentum equations and the turbulent heat fluxes in the conservation of energy equation by a set of auxiliary equations (differential and/or algebraic) containing time-mean quantities of the flow [58]. The choice of models used to solve the Navier-Stokes equations depends on the type of flow in CFD. Many types of different turbulence models have been applied to characterize the room airflow. Reynolds-Averaged Navier-Stokes (RANS) and Large-eddy simulation (LES) methods have been the predominant approaches used in indoor air simulations.

The model used in the present study has been the most widely applied for describing turbulent flow phenomena and is commonly referred to as the standard k-ε model. However, the eddy viscosity strongly depends on the situation of the turbulent flow field, i.e., functions of location, velocity, etc., it needs to be redefined for each problem. Moreover, even in a uniform flow passing through a mesh, it is necessary to consider the advection effect of turbulence since turbulence is washed downstream after passing through the mesh. Thus, a "characteristic quantity of turbulence" is selected, and the "governing equations for advection, diffusion, production, and dissipation" relating to the respective quantities are being solved, and then the eddy viscosity from the "characteristic quantity of turbulence" is being determined. This characteristic quantity is the following turbulent kinetic energy (k) and its dissipation rate (ε)

Turbulent kinetic energy k and its dissipation rate ε is given by

$$k = \frac{1}{2}\overline{u_i' u_i'} \tag{8.5}$$

$$\varepsilon = \nu \overline{\frac{\partial u_i'}{\partial x_j}\frac{\partial u_i'}{\partial x_j}} \tag{8.6}$$

The equations for k and ε through advection, diffusion, production and dissipation effects are known as k- ε equations, and are usually expressed as follows.

For incompressible fluids it is given as:

$$\frac{\partial \rho k}{\partial t} + \frac{\partial u_i \rho k}{\partial x_i} = \frac{\partial}{\partial x_i}\left(\frac{\mu_t}{\sigma_k}\frac{\partial k}{\partial x_i}\right) + G_S + G_T - \rho\varepsilon \tag{8.7}$$

$$\frac{\partial \rho\varepsilon}{\partial t} + \frac{\partial u_i \rho\varepsilon}{\partial \mathrm{x_i}} = \frac{\partial}{\partial \mathrm{x_i}}\left(\frac{\mu_t}{\sigma_\varepsilon}\frac{\partial \varepsilon}{\partial \mathrm{x_i}}\right) + \mathrm{C_1}\frac{\varepsilon}{\mathrm{k}}(\mathrm{G_S} + \mathrm{G_T})(1 + \mathrm{C_3 R_f}) - \mathrm{C_2}\frac{\rho\varepsilon^2}{\mathrm{k}} \tag{8.8}$$

where,

$$\mathrm{G_S} = \mu_t\left(\frac{\partial \mathrm{u_i}}{\partial \mathrm{x_j}} + \frac{\partial \mathrm{u_j}}{\partial \mathrm{x_i}}\right)\frac{\partial \mathrm{u_i}}{\partial \mathrm{x_j}} \tag{8.9}$$

$$\mathrm{G_T} = \mathrm{g_i}\beta\frac{\mu_t}{\mathrm{P_{rt}}}\frac{\partial \mathrm{T}}{\partial \mathrm{x_i}} \tag{8.10}$$

$$\mathrm{R_f} = -\frac{\mathrm{G_T}}{\mathrm{G_S} + \mathrm{G_T}} \tag{8.11}$$

Note that the time-averaged symbol $\overline{\ }$ is omitted for $\overline{\mu_i}, \overline{T}, \overline{\rho}, \overline{P}$ and the time-averaged variables are all expressed simply by μ_i, T,ρ,P in the above equations. From k and ε a dimensional analysis of the eddy viscosity μ_t, we obtain

$$\mu_t = C_\mu \rho \frac{k^2}{\varepsilon} \qquad 8.12$$

These equations include many empirical constants such as σ_k,σ_ϵ ,C_1 . However, as virtually the same values are used for these empirical constants in a large number of reports, it would be fair to conclude that the use of empirical constants yields greater accuracy than empirically determining the eddy viscosity for each problem. The constants of the standard k- ε model are shown in the table below.

Table 8.1 – Constants of the Standard k – ε Model

σ_k	σ_ε	C_1	C_2	C_3	C_μ	σ_t
1	1.3	1.44	1.92	0.0	0.09	0.9

Reynolds Number Calculation

Reynolds number is given by

$$Re_L = \frac{\rho \vartheta L}{\mu} \qquad 8.13$$

where

$\rho =$ density of air
$\vartheta =$ mean velocity of fluid (air) at the outlet of ACB
$L =$ length (width) of ACB at discharge slot
$\mu =$ dynamic viscosity of fluid (air)

Reynolds number was calculated based on above to confirm if the flow at the outlet of ACB is turbulent and it was found that the flow regime is turbulent as per Table 8.2

Table 8.2 – Reynolds Number at the ACB Outlet

Temperature of Air	ρ (kg/m^3)	ϑ (m/s)	L (m)	μ (kg/m.s)	Re_L
15 °C	1.225	0.9	0.075	1.802 x 10^{-5}	4589
20 °C	1.204	0.9	0.075	1.825 x 10^{-5}	4453
30 °C	1.164	0.9	0.075	1.872 x 10^{-5}	4249
35 °C	1.146	0.9	0.075	1.895 x 10^{-5}	4082

8.4 Assumptions in CFD Modelling

The user should not be afraid of making assumptions. Good assumptions can simplify the complex physical phenomena in the real world with a negligible effect on the accuracy of the CFD prediction as iterated by Srebric and Chen [49].

a) The k-ε model was used to simulate steady-state airflow distribution of an ACB system in a typical 3D office space with the assumptions that the air is incompressible, the density of air is constant, the Boussinesq approximation is applicable, and the airflow is steadily turbulent with a high Reynolds number.

b) The ACB inlet was assumed as flat panel through the length of ACB instead of nozzles in simplified beam model and discharge was modelled at the same angle of discharge as in actual beam geometry.

c) The interior walls, exterior wall, window, ceiling and floor were assigned with thermal boundaries obtained by the experimentation with the heat transfer coefficients of each surface calculated from construction layers of the building.

d) Steady State and heating simulation of the office environment.

e) Usual internal heat sources of an office are considered which is detailed in Table 8.7.

f) Finite Volume approach is considered.

g) To simplify the analysis, leakage from the space is considered as negligible.

h) The only inlet and outlet at the room is from the ACB and return grille.

i) Solar radiation is negligible and is not considered.

j) The suspended ceiling was set as the upper boundary of the CFD model, and the return air plenum above the ceiling was neglected to simplify the model.

8.5 Preprocessing

8.5.1 Geometry Creation

Preprocessing analysis starts with creating the geometry. The geometry of any model can be either created in scSTREAM with its functionalities or output from CAD. In the present study, the model is created by inbuilt functionalities of scStream. The geometry of the office was built in STpre, the geometry of parts are expressed by a combination of cuboids or sections of the cylinder. Once model data is built, analysis conditions including material properties and boundary conditions are set, and the mesh is generated to form input data. These procedures, such as setting analysis conditions and generating the mesh, are called preprocessing, and a program that helps complete these procedures is called a preprocessor. All assumptions for simplifying the geometry to ease the computational effort as specified in the previous section were used while creating the geometry and setting up the conditions for the model which is discussed in detailed in next section.

8.5.2 Boundary Conditions

One of the critical tasks is defining the correct boundary conditions for HVAC air terminal devices like diffusers, ACB etc. The boundary conditions for the numerical model are important in-room airflow simulation to obtain an accurate solution. Any boundary conditions if not modelled correctly could lead to failure of simulation and misleading results for velocity and temperature distribution in the space. [59]

Velocities at the walls are considered as zero because of the no-slip condition. The no-slip boundary condition was also applied to the surfaces of the person, furniture and heat source. The furniture was considered an obstacle. In scStream, an obstacle is an object without material property, and the interior of an obstacle is treated as being outside the computational domain where the temperature inside the object is not of interest and only the flow around it is analyzed. The volume conditioner properties of the blocks are shown in Table 8.3. The boundary conditions for the CFD model were provided by the experimental measurements as shown in Table 8.5. The summary of heat loads of the office is reported in Table 8.7.

Table 8.3 – Volume Conditioner Properties

Space	3D
Flow	Incompressible
Flow Field	Turbulent flow
Turbulence Model	k- ε model
Algorithm	Steady State - Simpler
Analyzed Area	Test Room 1 & 2
Time Analyses (State)	Steady State Analyses
Gravity	Considered
Initial Condition	18°C
Wall Boundary Condition	No Slip
Meshing Method	Voxel Method
Radiation	Not Considered
Solar Radiation	Not Considered

Material Properties

The working fluid is air. The fluid properties for air are held constant and are shown in Table 8.4.

Table 8.4 – Fluid (Air) Properties

Material	**Air**
Density (kg/m3)	1.206
Specific Heat (J/(kg.K))	1007
Thermal conductivity (W/(m.K))	0.0256
Viscosity (Pa.s)	1.83e-05
Thermal Expansion Coefficient (1/K)	0.003495

Boundary condition were set as follows

Table 8.5 - Boundary Conditions for CFD Model

Boundary	Boundary Type (ScStream)
Inlet (ACB Supply Slot 1 & 2)	Volume flow rate
Induction Surface (ACB Perforated Surface)	Velocity / Volume flow rate
Outlet (Exhaust/Return Grille)	0 pressure
Wall	No Slip
Heat Sources	Volumetric Heat Sources
Furniture	Obstacle
Beam Elements	Flat Panels (Condition Region)

Thermal Boundary

The thermal conditions recorded during the experiment are used as thermal boundary conditions for the CFD model for walls, floor and ceiling surfaces. For different experiments and different set points, the thermal conditions were recorded and used in the model. The walls, ceiling and floor was modelled with heat transfer coefficients which are shown in Table 8.6.

Table 8.6 - Heat Transfer Coefficient (U Value) of Thermal Boundaries

Interior Partitioned Wall	0.73 W/m^{2}K (0.13 Btu/hr-ft^2 °F)
Exposed Wall	0.30 W/m^{2}K (0.053 Btu/hr-ft^2 °F)
Interior Concrete Wall	1.86 W/m^{2}K (0.33 Btu/hr-ft^2 °F)
Slab (Top and Bottom)	0.80 W/m^{2}K (0.14 Btu/hr-ft^2 °F)
Overall Window	2.61 W/m^{2}K (0.46 Btu/hr-ft^2 °F)

Table 8.7 - Internal Heat Load in Test Rooms

Test Room 1	
Lighting Load	2 units - 40.0 W each
Laptop	2 units – 35.0 W each
Data logger	1 unit – 20.0 W
Occupant	1 person – 45.0 W
Test Room 2	
Lighting Load	2 units - 40.0 W each
Laptop	3 units – 35.0 W each
Data logger	1 unit – 20.0 W
Occupant	1 person – 45.0 W

Convergence Criteria

The prediction of room airflow is based on a solution of the fundamental flow equations which consist of the equation of continuity, three momentum equations and the energy equation. Convergence is considered to be reached when the residuals of each of these equations are below 10^{-4}.

8.5.3 Meshing

In order to simulate airflow in the office space (Test Rooms), mesh generation was required. The mesh divides the office space into mesh elements as shown in Figure 8.2, enabling the CFD software to calculate the flow at each element of the mesh. If the mesh division becomes finer, the accuracy of the solution is improved. Meshing was a quite challenge as discussed earlier to simulate airflow with small nozzles of the beam. Therefore, mesh refinement was executed in areas of objects and with complicated geometry (near the outlet and inlet of the ACB) to capture the intricate flow structures which are produced within regions close to the object since flow velocity temperature and other physical quantities show large variation around objects.

For an accurate analysis, fine mesh elements should be generated in regions where the gradient of computed variables is expected to be large. In general, mesh elements fine enough for such regions are used to improve accuracy. However, the improvement in accuracy with finer mesh elements comes with penalties. Dividing the entire computational domain into finer mesh elements results in an unnecessary increase in memory consumption and in time of computation. Therefore, meshes can be and may as well be coarser at regions where the gradient of calculated variables is expected to be small. This operation is sometimes called a "determination of mesh refinement level", and is an important operation in STpre. [62]

Overall, optimum mesh depends on conditions and the purpose of analysis. But the minimum number of meshes required for an analysis actually exists due to the limitation of the calculation method. For example, if there is a narrow path of fluid between walls, it is recommended that there are at least three mesh elements in between the walls.

The gradient of fluid velocity is large in the vicinity of walls because of the friction between fluid and walls. Fluid velocity is zero on walls, and it approaches the mainstream velocity as the distance from walls increases. Calculating the magnitude of this wall friction is essential to estimating the resistance of the flow path as a whole. In a fluid analysis, the accuracy of this calculation near walls is maintained by dividing meshes fine near walls.

More generally, regions, where the gradient of calculated variables becomes large includes the following:

1. In the vicinity of the walls
2. Wake flow region downstream of flow separation
3. The region with a sudden change in the cross section of the flow path
4. Region of confluence

The coarsened mesh was used in areas where there were no object or complex geometries were located to produce results with cost-effective analysis. The effect of gravity was also included to account for the effects buoyancy. The total number of mesh elements used within the domain was approximately 5 million. The details of the mesh used in the study are shown in Table 8.8. The study chose a threshold size of 0.05 mm to achieve a more accurate solution.

Table 8.8 - Details of Meshing

Meshing Type	Detailed Mesh Settings
Standard Length	1.0 mm
Geometric Ratio	1.0
Threshold Size	0.05 mm
No of elements	4987983

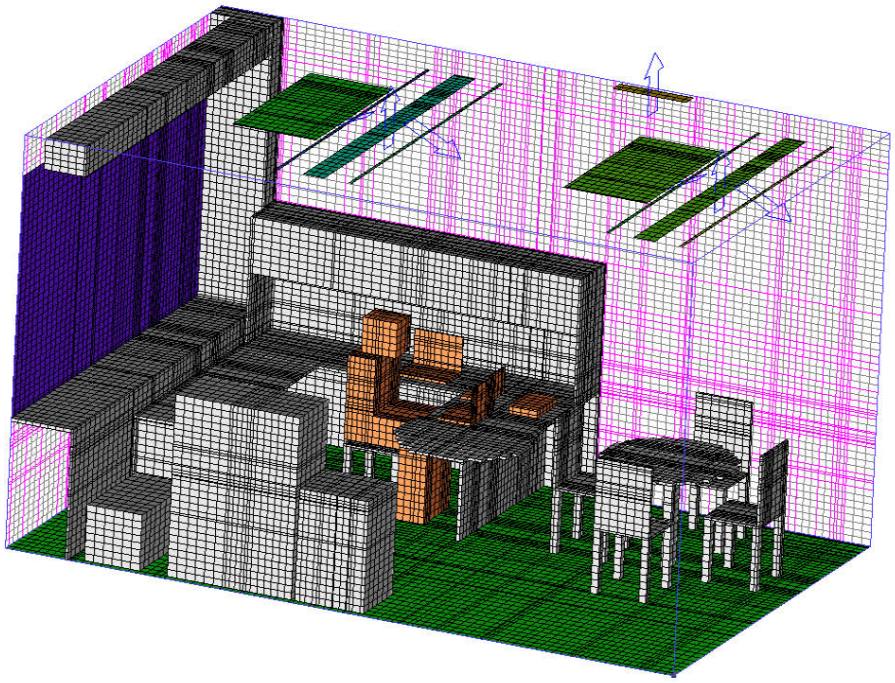

Figure 8.2 - Mesh Model of Test Room 2 (Internal Surfaces)

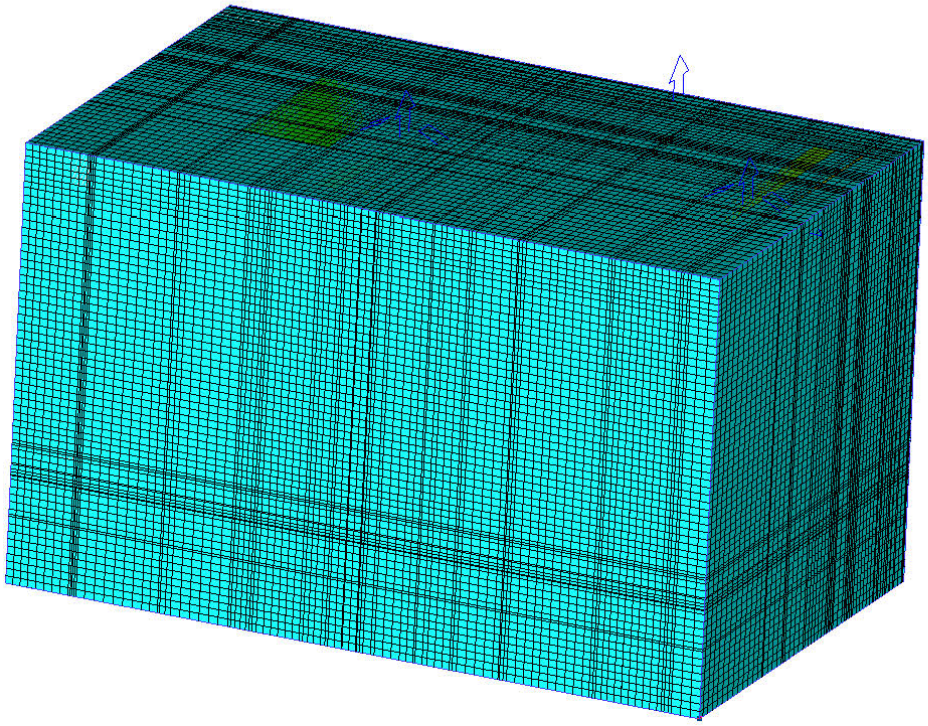

Figure 8.3 - Mesh Model of Test Room 2 (External Surface)

8.5.4 Solving

Once the model is created by STpre, the solver of scStream, STsolver analyze the data and calculation is executed. The solver is equipped with a graphical interface which monitors and helps to set the parameters of calculation and shows the status of ongoing calculation. scStream has a pressure based solver which is recommended to use for indoor incompressible flow.

Table 8.9 – Solver Details

Variable	**Solution Method**
Solver Type	Default (Simpler)
Temperature	1st Order Upwind
Pressure	1st Order Upwind
Turbulent Kinetic Energy	1st Order Upwind
Turbulent Dissipation Rate	1st Order Upwind

After calculation, results are stored in output data files. To comprehend the results, it is necessary to visualize them using graphs, contours, and so on. This process of visualizing analysis results is called post-processing. Postprocessor for scSTREAM is STpost. The results are visualized and are described in detail in the next section.

8.5.5 Grid Dependency Test

Grid dependency tests were performed to ensure that the results achieved from a simulation were appropriate and would not vary upon varying the grid density. Due attention was given to the inlet, outlet and heat sources in the test rooms. The grid density was varied and the results were found appropriate.

8.6 Ventilation Efficiency

Numerical modelling can be used to determine the ventilation effectiveness through ACB. The following indices can be determined through numerical modelling to find out the ventilation efficiency in a space. These indices are also called Scale for Ventilation Efficiency (SVE)

1) Age of air
2) Residual lifetime of air
3) Contribution ratio of supply openings or exhaust openings

Age of Air and Residual Lifetime of Air

Clean and fresh air is supplied from ACB which reaches any point in a room via the various paths. After that, air is exhausted out via various path in the room. The time taken for the air to travel from the ACB slot to any particular point in the room is called the age of (supply) air as shown in Figure 8.4 and the time taken for air to flow from the chosen point out to the exhaust opening is called the residual lifetime of air as shown in Figure 8.5. Index for Age of Air is dimensionless but can be converted to a unit of time.

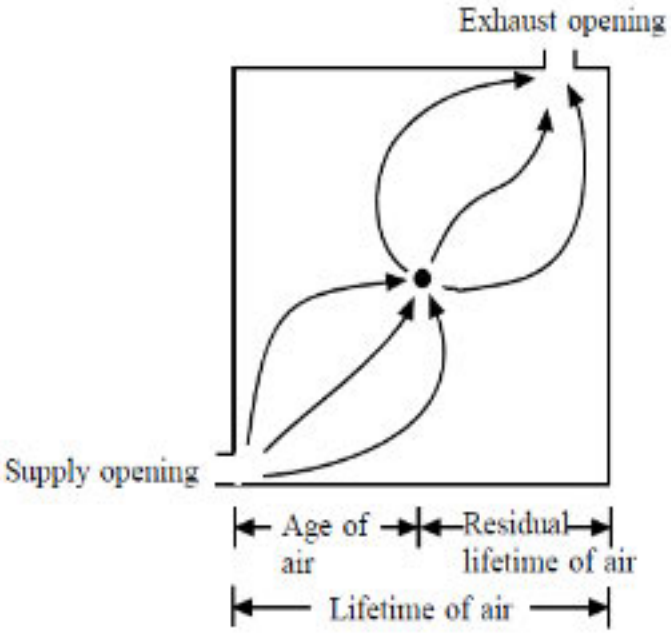

Figure 8.4 - Age of Air and Residual Lifetime of Air [62]

$$\text{Index of Age of Air} = \frac{C(X)}{C_S}$$

Where,

C(X) : Concentration of contaminant at point X [kg/m^3]

C_s : Instantaneous and uniform concentration of contaminants [kg/m^3]

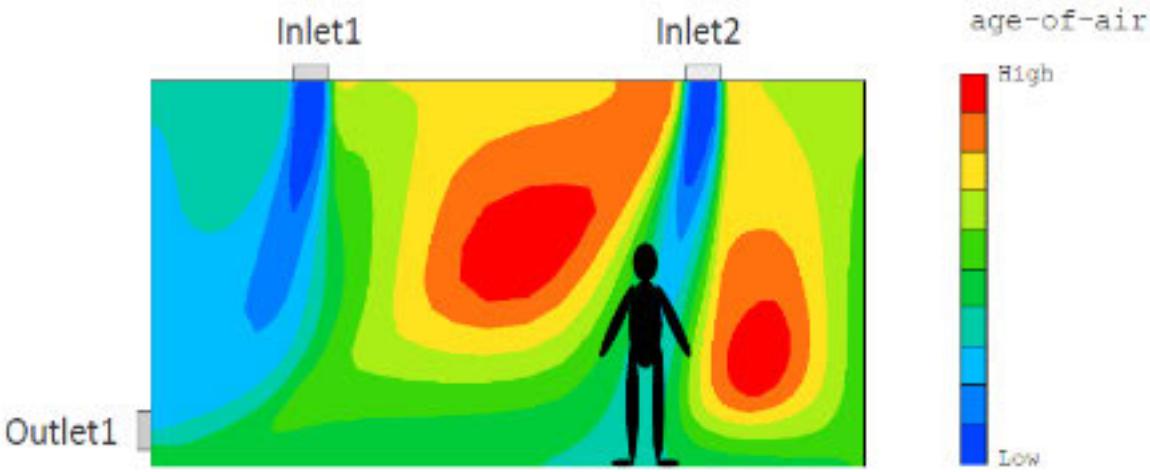

Figure 8.5 – CFD Contour of Age of Air [62]

When comparing the age of air between arbitrary two points, the point that the age of air is higher than the other is considered to be more contaminated as shown in Figure 8.5. The reason is that clean and fresh air reaches the point only having spent longer traveling in (polluted) air. As a result, the likelihood of air getting polluted increases. On the other hand, as shown in Figure 8.6, the smaller the residual lifetime of air is, the faster the contaminated air exits from the point. The sum of these indices is the index of a lifetime of air which means time to spend traveling from supply openings to exhaust openings.

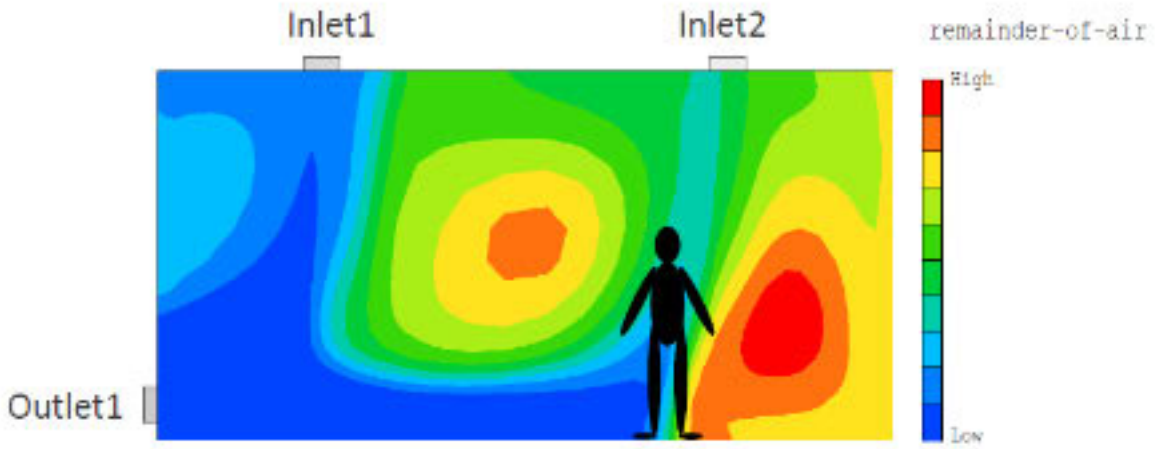

Figure 8.6 – CFD Contour of Residual Lifetime of Air [62]

Contribution Ratio of Supply Openings or Exhaust Openings

When more than two supply openings exist, it is often required to know that what region is ventilated by which of the supply openings. It is important to know the same so that the opening with efficient ventilation and with a larger contribution can be adjusted, and this index is known as Contribution ratio of supply openings. Contribution ratio of supply opening is shown in Figure 8.7. Similarly, the contribution ratio of exhaust opening can be defined when more than two exhaust openings are present as shown in Figure 8.8.

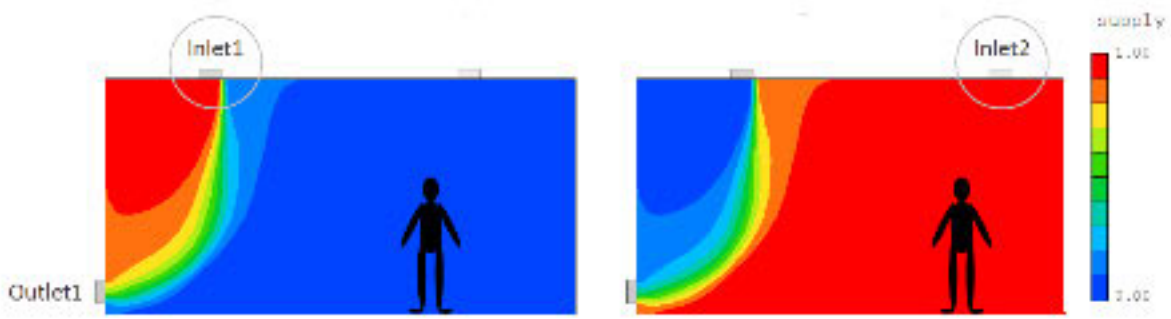

Figure 8.7 – CFD Contour of Contribution of Supply Opening [62]

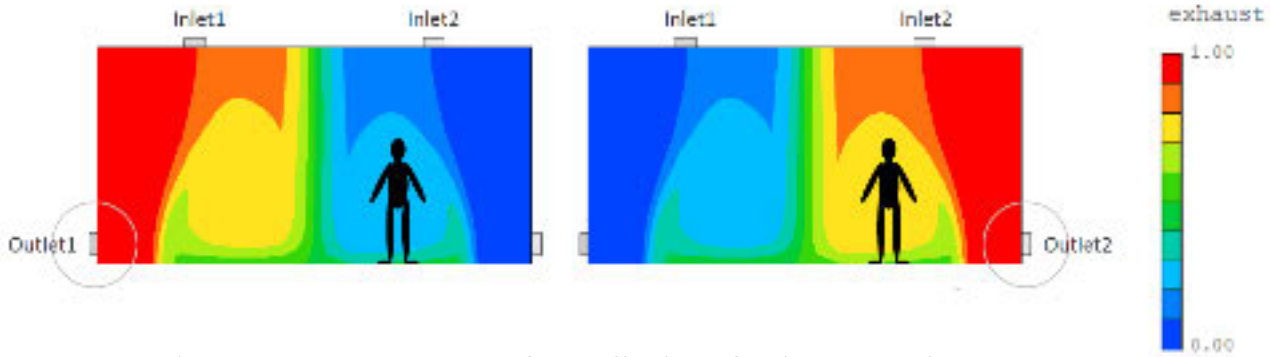

Figure 8.8 – CFD Contour of Contribution of Exhaust Opening [62]

9. EXPERIMENTAL RESULTS & DISCUSSION

9.1 Test Room 1 – Heating Mode

9.1.1 Coanda Effect

The temperature of the air jet discharged through the ACB is different from the ambient (room) air and therefore these experiments illustrated the case of a non-isothermal jet behavior in office. The Coanda effect was seen at the exit of ACB slots. Coanda effect is the tendency of the free jet attached to the ceiling. As soon as the high-velocity jet is discharged from the nozzles and further through the ACB system the air jet is seen attached to the ceiling due to low-pressure region creation above the jet. This attachment of air jet ensure good thermal comfort and avoid direct throw of cold or hot air to the occupied zone. This effect was visualized in the heating experiment through a thermal image camera which nicely captured the air jet attachment to the ceiling. The Coanda effect is shown in Figures 9.1 and Figure 9.2.

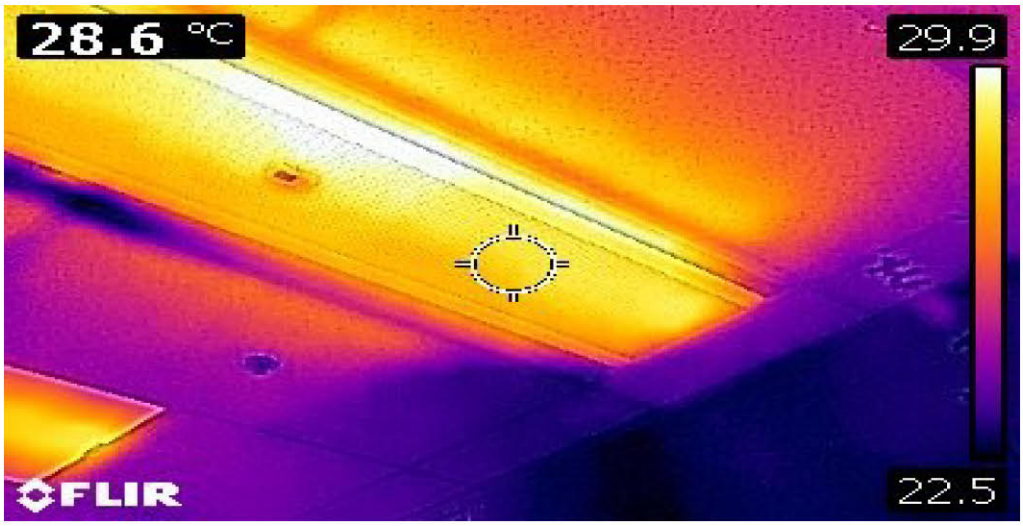

Figure 9.1 - Coanda Effect through Thermal Image Camera (Heating)

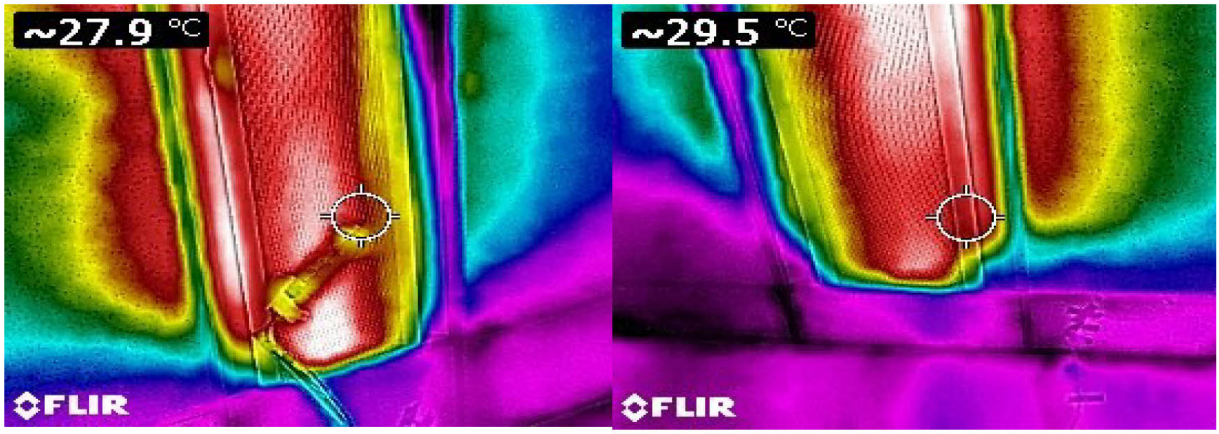

Figure 9.2 - Coanda Effect (Heating)

9.1.2 Discharge Air Velocity

The discharge air velocities were recorded during the test at both the supply slots. The velocity at one slot was found always higher than the air velocity at the other slot as shown in Figure 9.3. This phenomenon is due to the uneven pressure distribution at the nozzles in the ACB primary air plenum box as shown in Figure 9.4.

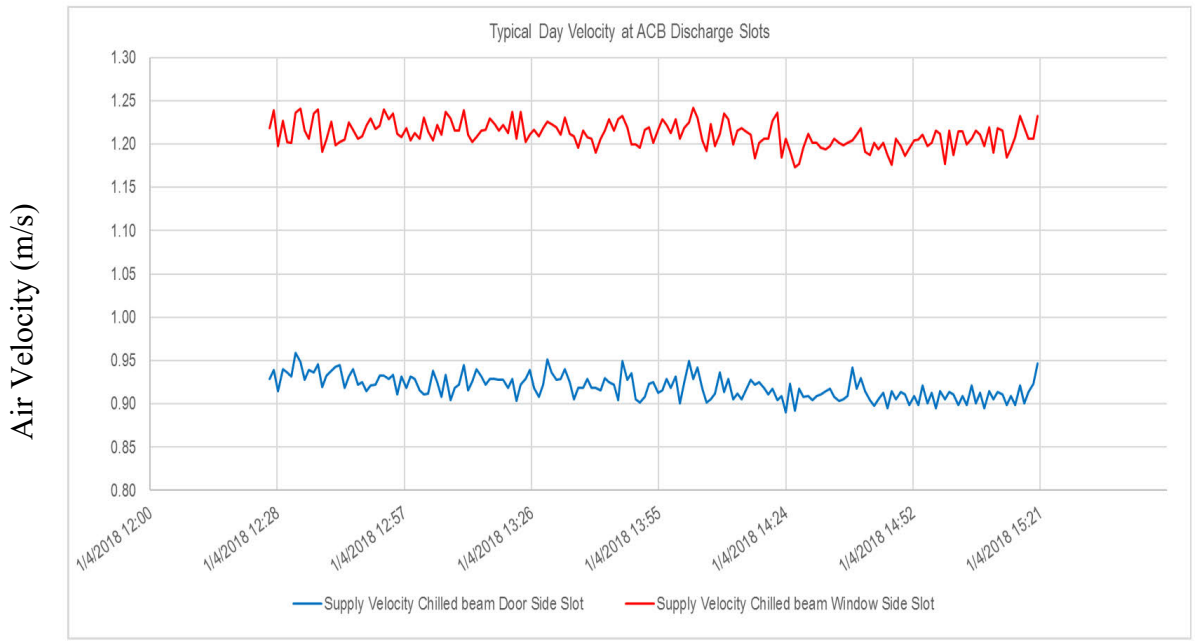

Figure 9.3 - Discharge Air Velocity at the Two Slots

The primary air supply is connected to the ACB plenum at one side and the airflow is directed towards the other end of the plenum which exerts more pressure at the nozzles at the other end. This causes the uneven air velocity distribution across the beam. The difference in velocities was also shown by Wu et al. [60] in their experiment and further in CFD modelling.

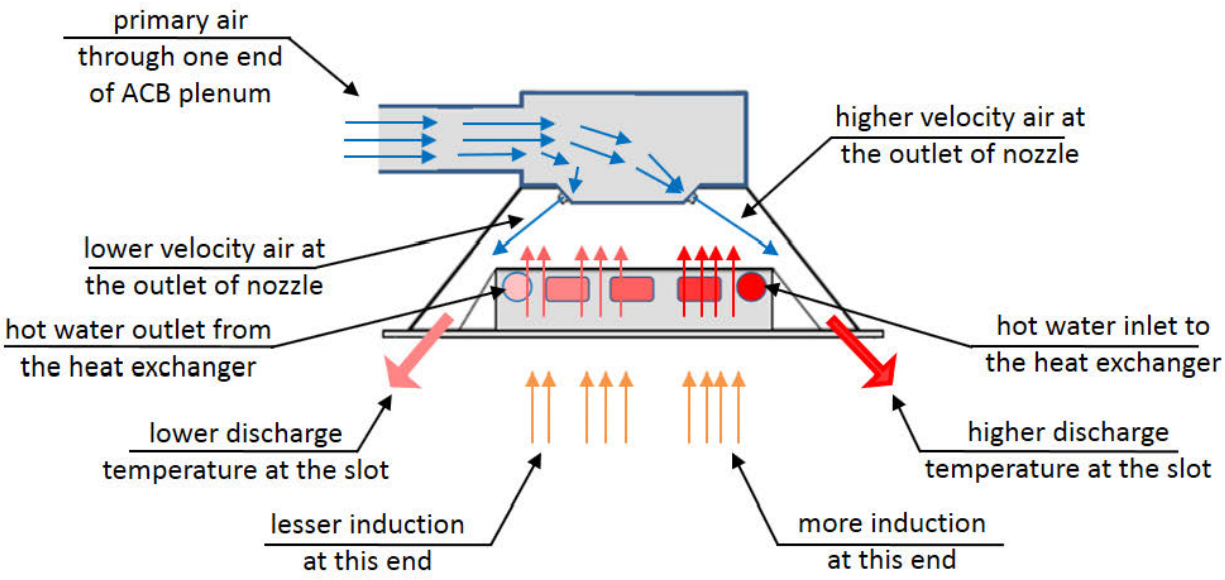

Figure 9.4 - Discharge Velocity & Temperatures

9.1.3 Discharge Air Temperature

The discharge air temperatures were recorded at both the slots and found unequal which can be seen in Figure 9.5. This could be due to the design and layout of the heat exchanger. The heat exchanger is placed horizontally in the ACB as shown in Figure 9.4. The water flowing into the heat exchanger gradually loses its heat while travelling; therefore, the temperature of the air passing through the heat exchanger is uneven, which in turn causes uneven discharge air temperatures. This effect is enhanced by the different discharge velocities at the two slots as explained above which enhances induction at one end and hence more heat transfer. The hot water inlet to the heat exchanger, higher discharge nozzle velocity (in turn higher induction) coincided at the same side of the tested beam in the experiment and therefore this phenomenon deserves further investigation in a controlled environment with ACB from different manufacturers to compare and analyze. When the room reaches steady state, the non-isothermal jet from ACB turns into an isothermal jet (water flow across the heat exchanger

stops or reduced to minimum flow) this phenomenon is then minimized and temperature at both the discharged slots becomes nearly equal as shown in Figure 9.5.

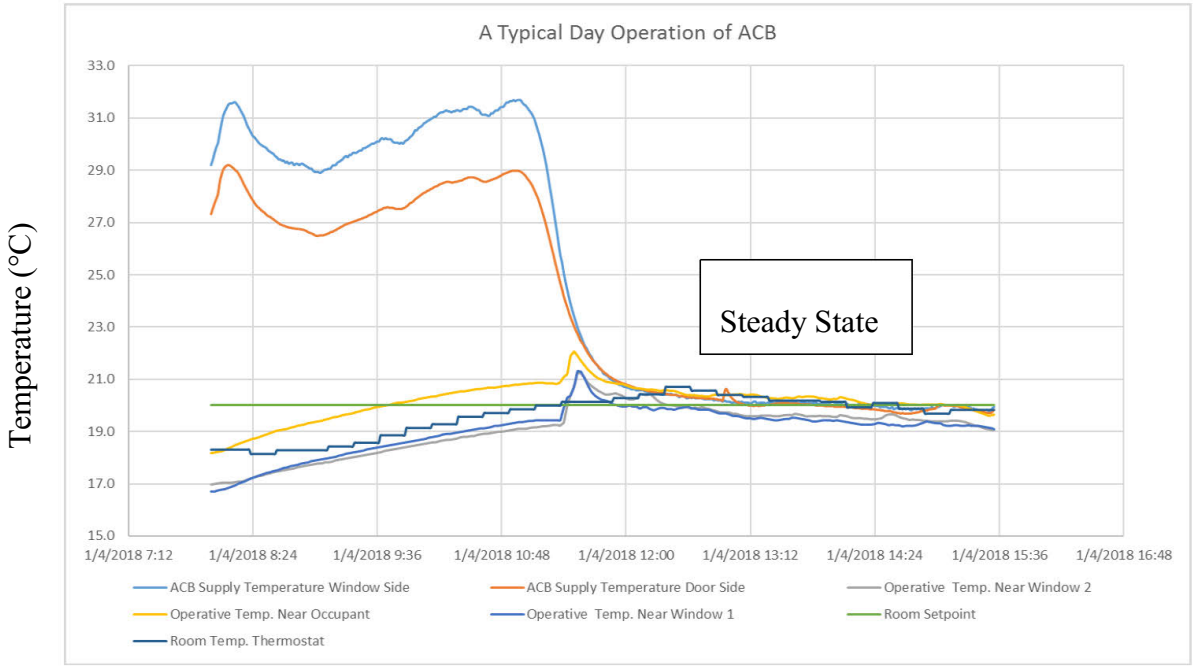

Figure 9.5 - Discharge Air Temperatures at the Two Slots (Heating)

9.1.4 Surface Temperature Distribution

Figures 9.6, Figure 9.7 and Figure 9.8 show the surface temperature distribution of room surfaces after attaining the steady state. Each set of temperatures are an average of 15 minutes measured from 12.31 to 4.15 PM as shown in Figure 9.6. The temperatures of all surfaces were found in line and within ±1°C (±1.8°F) range versus the room setpoint of 20°C (68°F) except the window which can be seen in Figure 9.7. The window temperature at the top and center were recorded close to the room setpoint temperature but the bottom of the window was found within -2.5°C (-4.5°F) range of setpoint temperature as shown in Figure 9.8. The reason of such variation in temperature is the extended aluminum profile of size 0.1 m (0.33 ft.) depth attached to the window as shown in Figure 9.9 which causes the obstruction to the airflow down the window and destroys the momentum of hot air flowing down.

No.	Time	Set Point	Window	Front Wall	Side Wall (Exposed)	Back Wall	Side Wall (Interior)
1	12:31 - 12:45	20.0	18.6	19.9	20.1	20.1	20.8
2	12:45 - 13:00	20.0	18.7	20.3	20.5	20.2	21.5
3	13:01 - 13:15	20.0	18.6	20.2	20.4	20.2	21.3
4	13:16 - 13:30	20.0	18.6	20.1	20.3	20.2	21.2
5	13:31 - 13:45	20.0	18.5	20.0	20.2	20.1	21.1
6	13:46 - 14:00	20.0	18.5	19.9	20.2	20.1	21.0
7	14.01 - 14:15	20.0	18.5	19.9	20.1	20.0	20.9
8	14:16 - 14:30	20.0	18.4	19.8	20.1	20.0	20.9
9	14:31 - 14:45	20.0	18.4	19.7	20.0	20.0	20.8
10	14:46 - 15:00	20.0	18.3	19.7	20.0	20.0	20.7
11	15.01 - 15:15	20.0	18.3	19.7	20.0	20.0	20.7
12	15:16 - 15:30	20.0	18.2	19.6	19.9	19.8	20.6
13	15:31 - 15:45	20.0	18.3	20.0	20.0	20.1	20.7
14	15:46 - 16:00	20.0	18.6	20.2	20.2	20.3	20.9
15	16:01 - 16:15	20.0	18.5	20.0	20.1	20.1	20.8

Figure 9.6 - Surface Temperatures in Heating for Room Setpoint 20°C

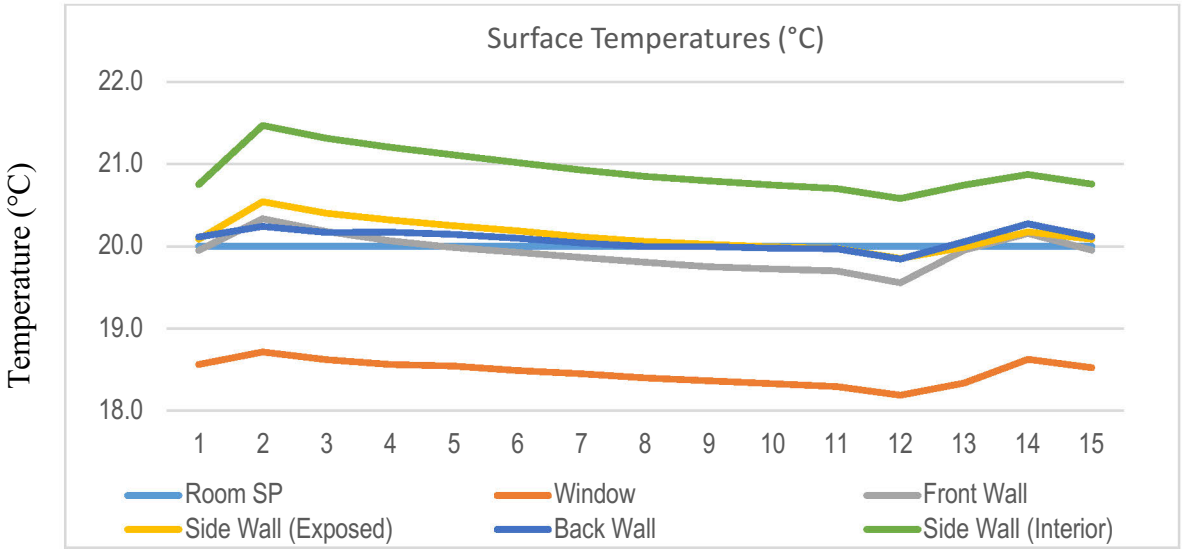

Figure 9.7 - Surface Temperatures for Room Setpoint 20°C

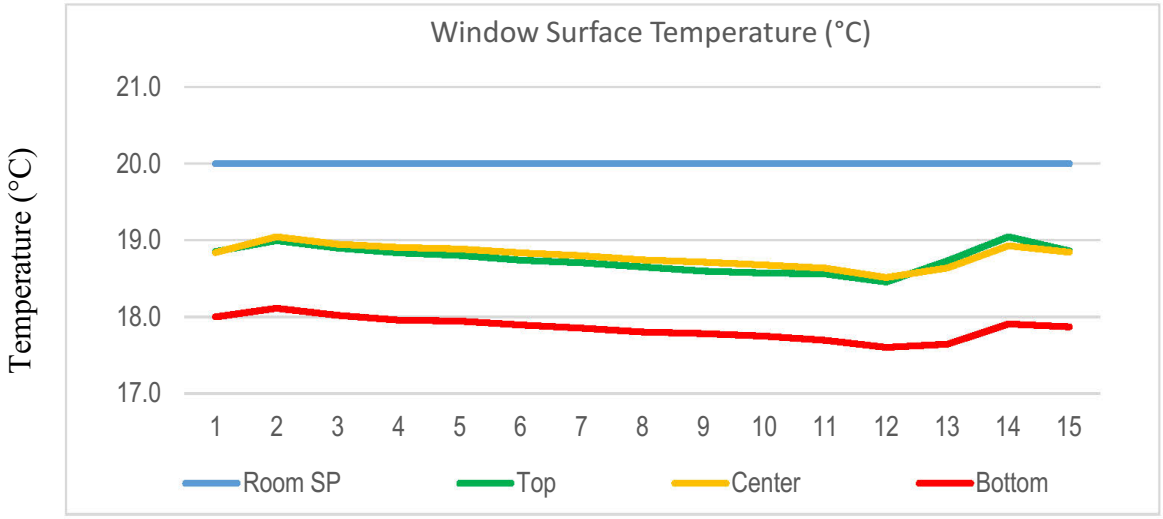

Figure 9.8 - Window Temperatures at the Top, Bottom and Center for Room Setpoint 20°C

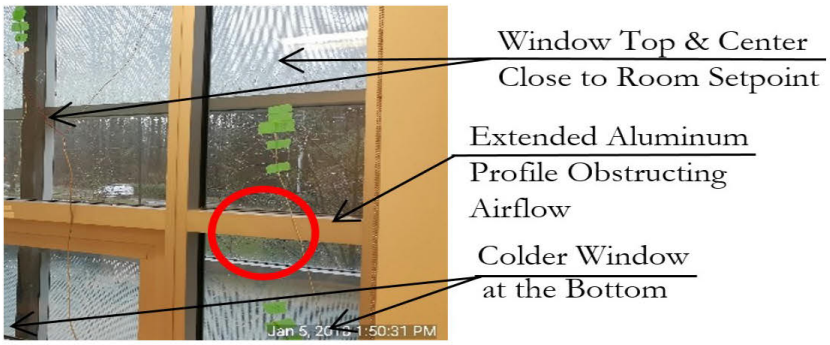

Figure 9.9 - Aluminum Extended Profile Obstructing Airflow at the Bottom Portion of the Window

9.1.5 Room Air Distribution

Figure 9.11 shows air velocity and air temperature distribution, when room setpoint was 20°C (68°F), at possible occupant's location as shown in Figure 9.10. The velocities were within the ASHRAE recommended limit in the occupied zone to avoid the draft. It should be noted that this section presented data only for steady state condition. All measurements were done at the steady state condition with different room setpoints. With the setpoint of 20°C (68°F), the room air is almost uniform and the temperature at a height of 0.6 m (2.0 ft.) can be observed close to the setpoint. Figure 9.12 shows the temperature distribution at 4 different heights with

different room setpoints near the occupant on different days during the experiment. It can be observed that when the setpoint was raised above 21 °C, thermal stratification starts to appear.

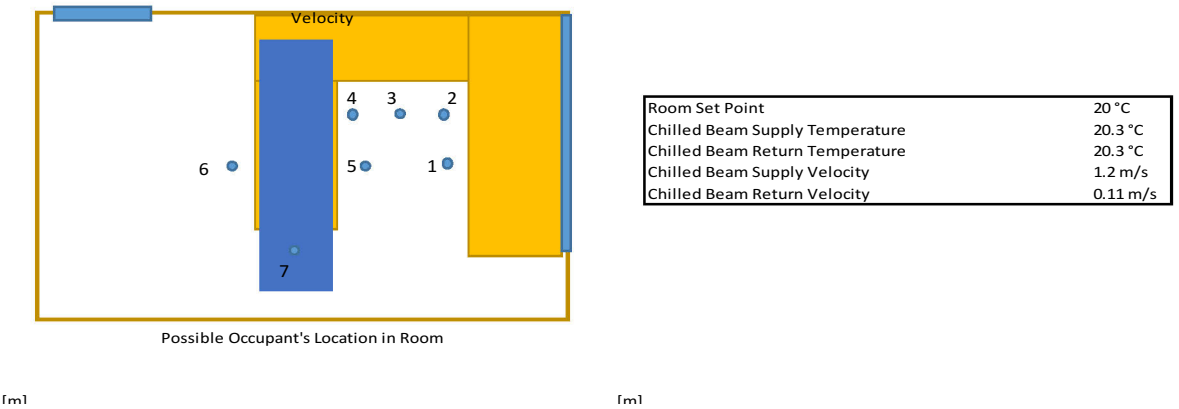

Figure 9.10 - Possible Occupant's Location

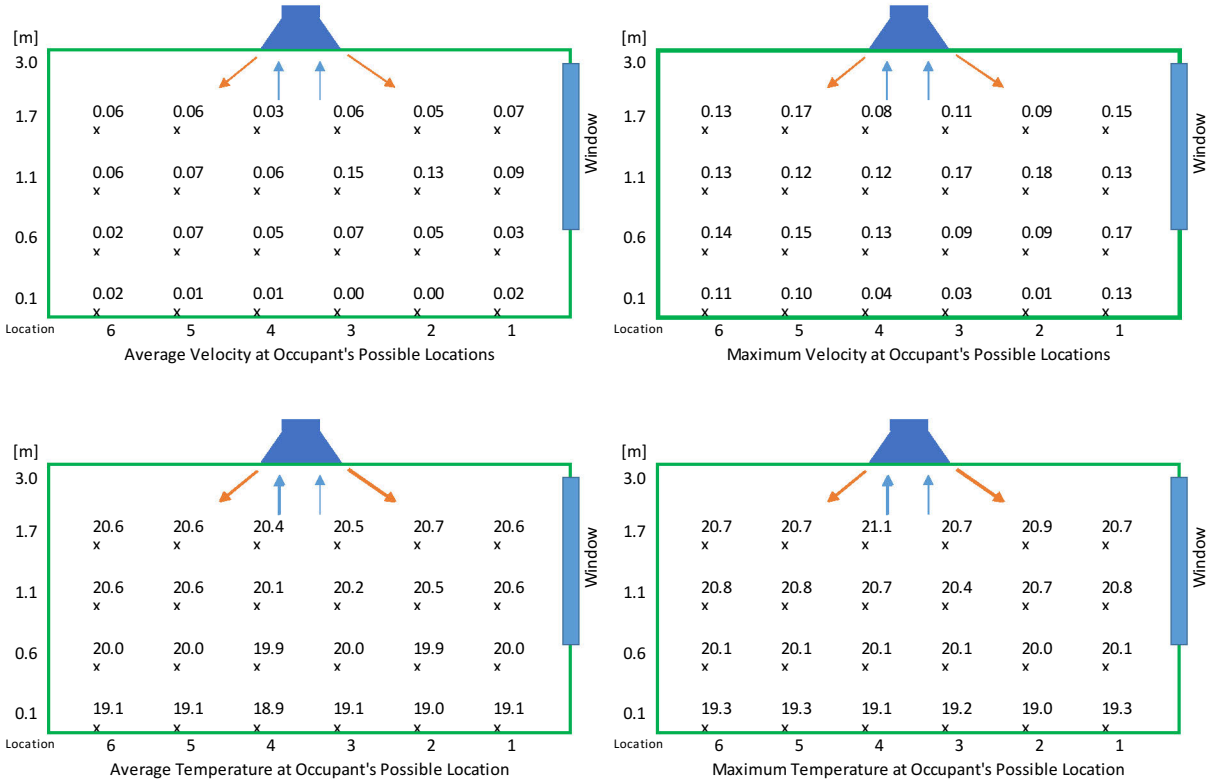

Figure 9.11 - Average / Maximum Air Velocity and Temperature Distribution (at Setpoint 20°C)

The Figure 9.12 shows the air temperature and air velocity at different points in the test room at 4 different heights at different set points.

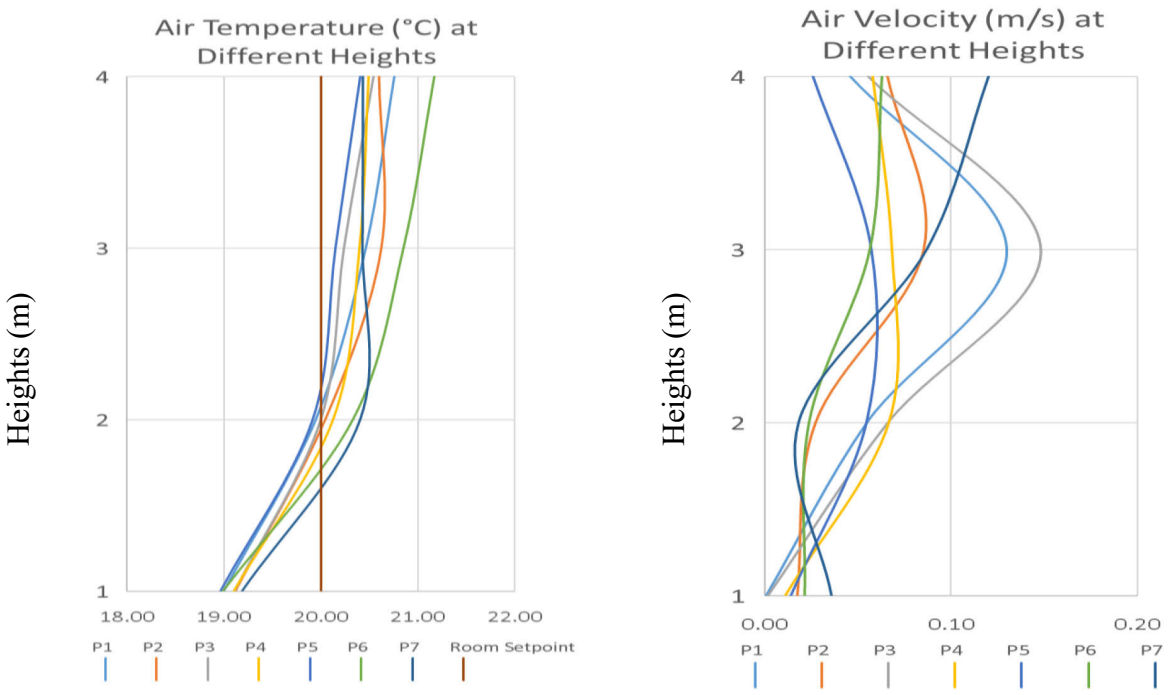

Figure 9.12 - Air Temperatures & Air Velocity at 0.1, 0.6, 1.1 and 1.7 m Heights at 20°C (Heating)

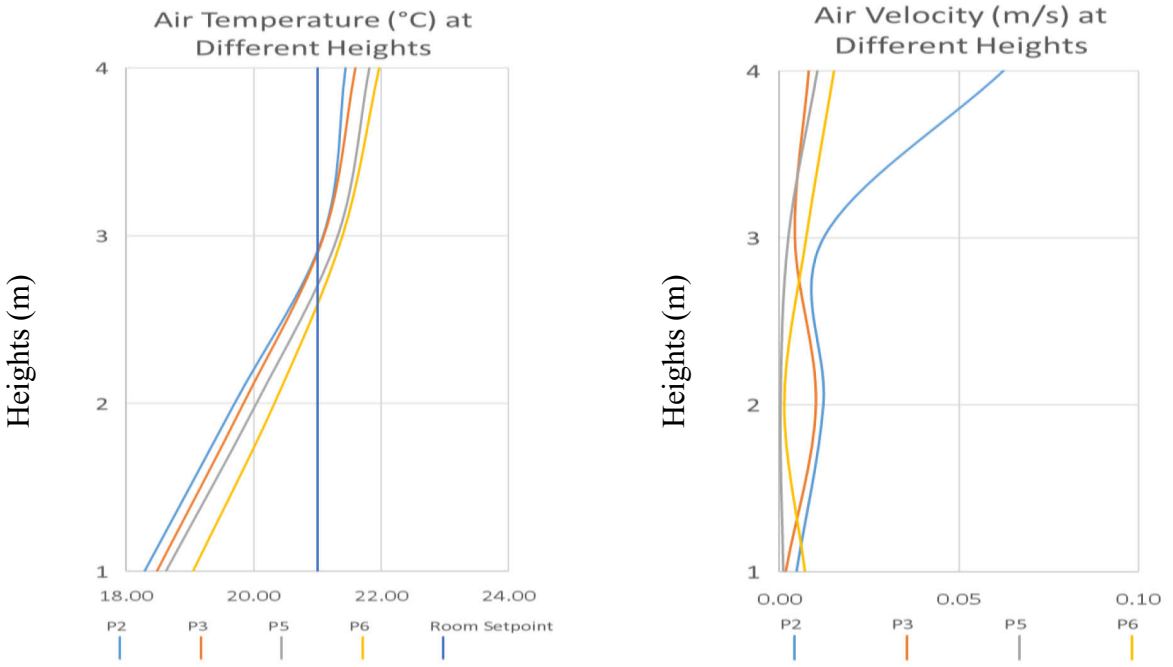

Figure 9.13 - Air Temperatures & Air Velocity at 0.1, 0.6, 1.1 and 1.7 m Heights at 21°C (Heating)

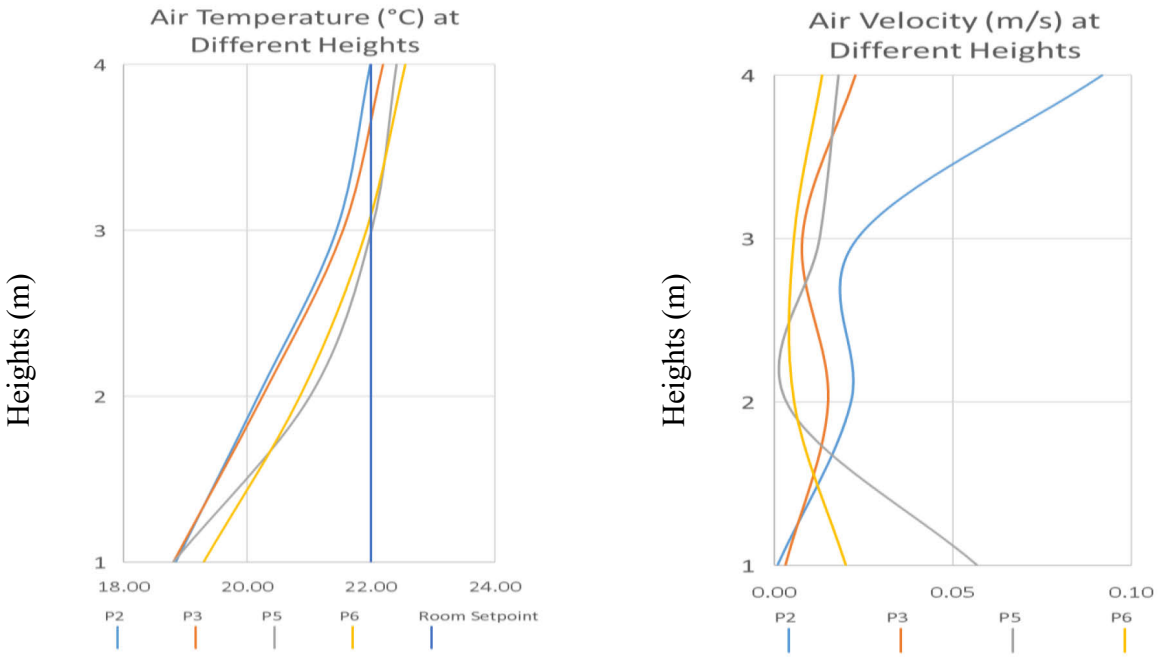

Figure 9.14 - Air Temperatures & Air Velocity at 0.1, 0.6, 1.1 and 1.7 m Heights at 22°C (Heating)

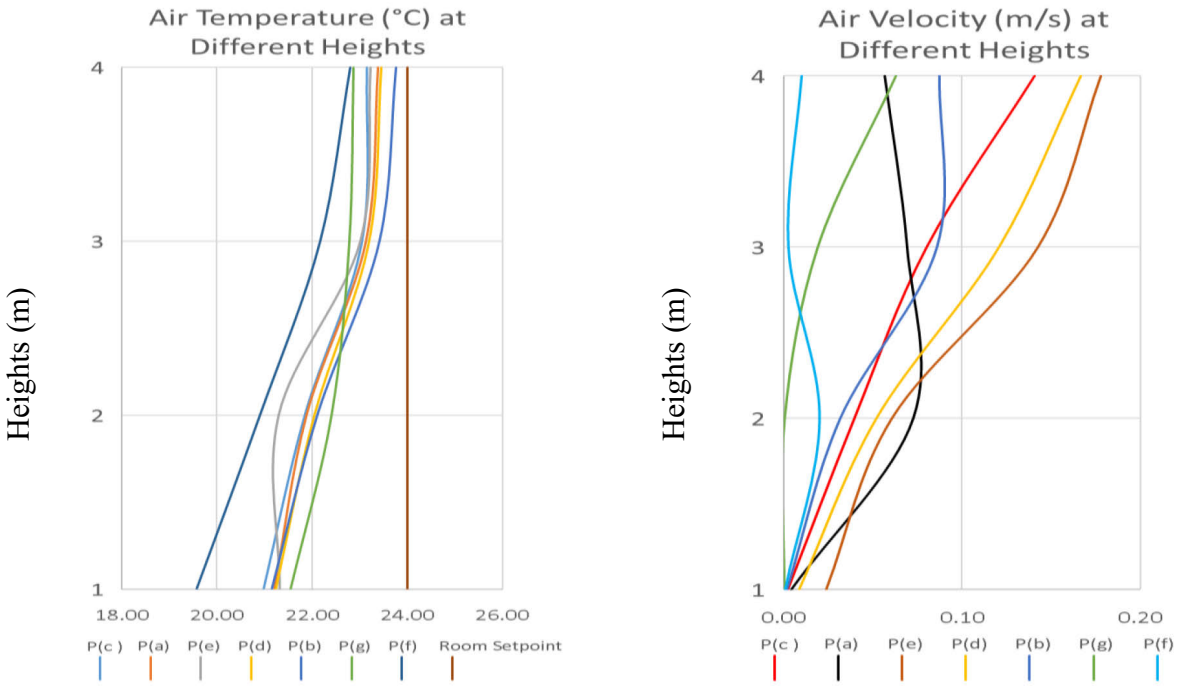

Figure 9.15 - Air Temperatures & Air Velocity at 0.1, 0.6, 1.1 and 1.7 m Heights at 24°C at Window (Heating)

From all the above figures, it can be deduced that the air velocity near occupant starts approaching zero when the temperature is raised from 21°C to 24°C. The velocity can be seen

almost zero for 0.1 m and 0.6 m heights because of stratification in the room. Similarly, the temperature gradient can be observed between 0.1 m and 1.7 m height. The heating operation shows that stratification is likely to occur with Active Beams at higher room setpoint temperatures. This could be visualized in a controlled environment with smoke patterns and require further research. There is a risk of contaminants staying at breathing levels with no air movement at lower levels and therefore active beams must be tested for air change effectiveness in heating. Appendix D shows spatial measurements in the room with higher temperatures.

9.1.6 Operative Temperature

The operative temperature was recorded for different setpoints in the test room at 3 places as shown in Figure 9.16. The graph plotted between room setpoint temperature and room temperature through thermostat as shown in Figure 9.17 shows that the room is not able to achieve temperature above 22 °C when the room setpoint is 22/24 °C. However, the temperature measured by the operative temperature sensors as shown in Figure 9.18, Figure 9.19 and Figure 9.20 shows the opposite, the data was cleaned and is plotted against the room temperature setpoint. It is clearly visible that for a particular temperature setpoint, the span of the room temperature is big which shows that the temperature is varying in nature and further analyses of data show the slow response of beam to achieve the heating setpoint. This raises questions on the location of the thermostat which actually controls the room temperature. Please note that the operative temperature data is for the working weekdays and only for the occupied hours from 8 to 5 pm.

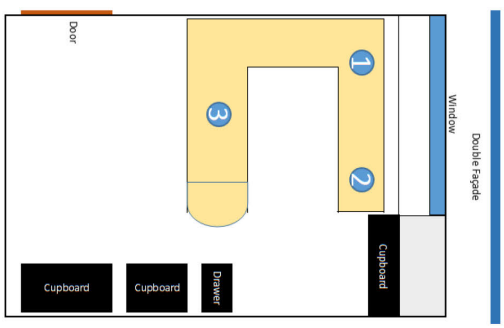

Figure 9.16 – Location of Operative Temperature Measurement (Heating)

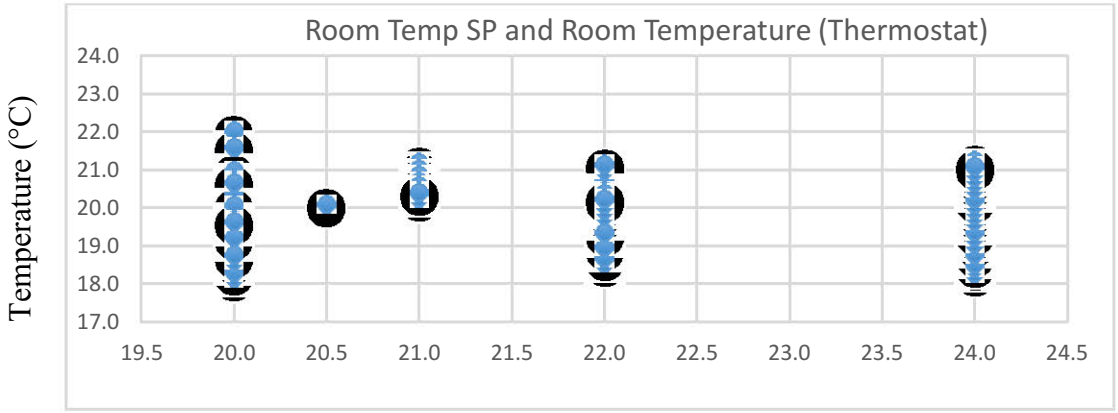

Figure 9.17 - Room Setpoint and Room Temperature (Heating)

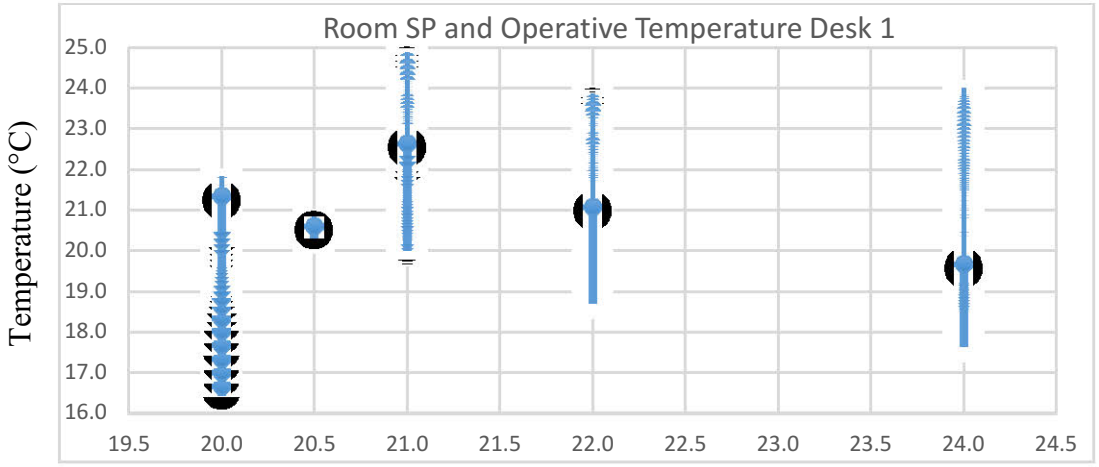

Figure 9.18 - Room Setpoint and Operative Temperature at Desk 1

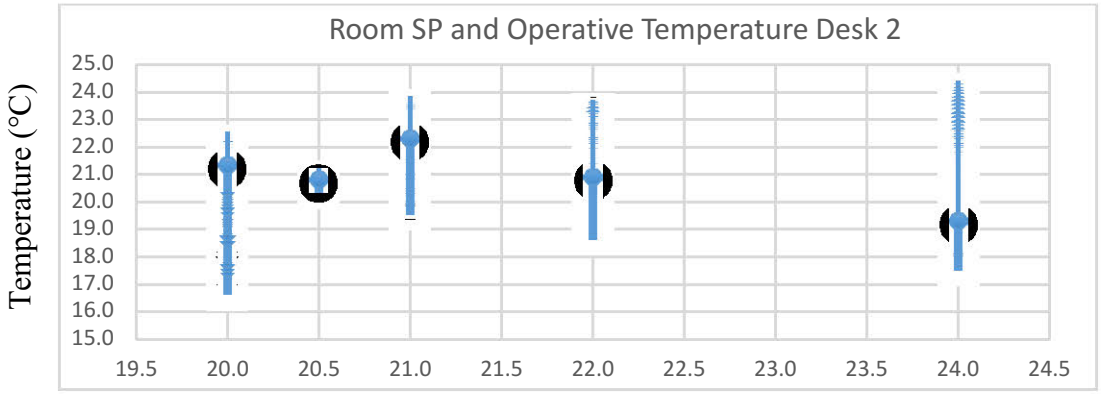

Figure 9.19 - Room Setpoint and Operative Temperature at Desk 2

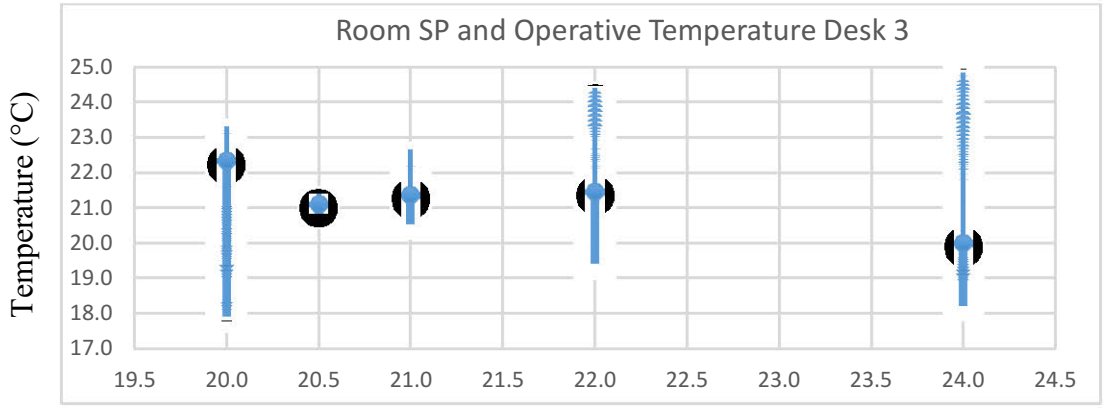

Figure 9.20 - Room Setpoint and Operative Temperature at Desk 3

9.2 Test Room 2 – Cooling Mode

Experiments conducted on Active Chilled Beam in Test Room 2 under cooling mode are discussed in this section. Results are explained with graphs and images.

9.2.1 Discharge Air Velocity

Supply (Discharge) Velocity from both the slots of Active Beam was studied and many observations are noted which are discussed here. Figure 9.21 shows the velocity measure at 3 equidistant points in one slot.

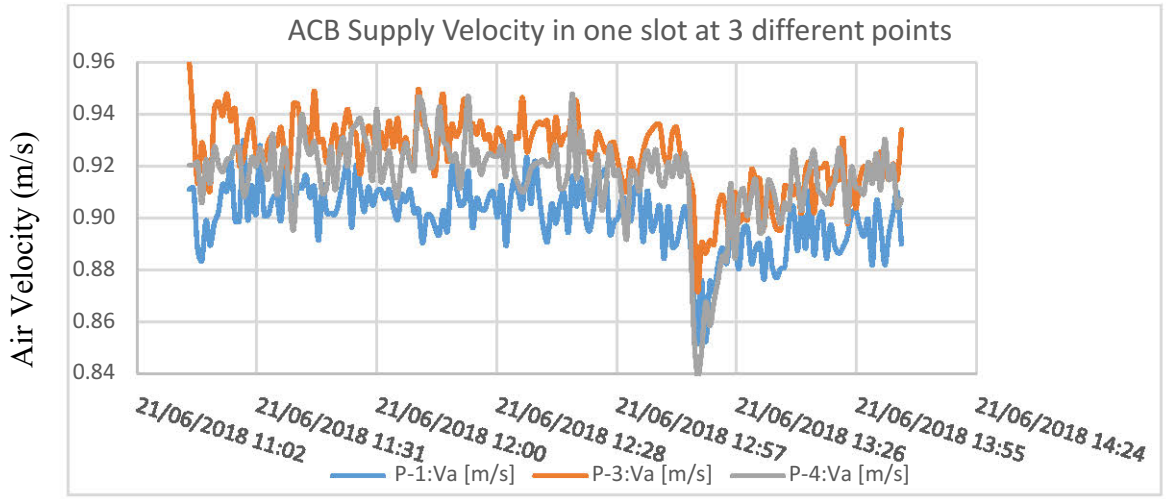

Figure 9.21 - Discharge Air Velocities at One Slot (Cooling)

The graph shows that the velocity is not same at 3 different points which is due to the uneven pressure distribution between nozzles in beam plenum, room thermal load and subsequently the amount of induction takes place at the beam surface. However, the trend of velocities at 3 different points is almost the same. A similar difference was seen at the other slot as shown in Figure 9.23. The average air velocity at each slot was calculated and it was found that the average air velocities are not equal and have a big difference which was found during the heating test as well. The difference in average air velocities measured under cooling mode at the two slots of ACB is shown in Figure 9.24.

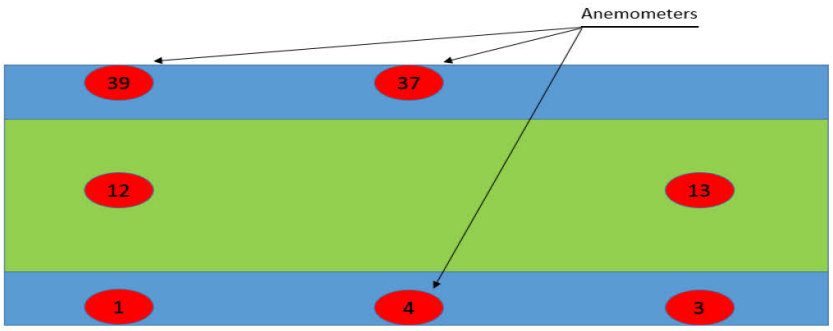

Figure 9.22 - Location of Anemometers at Supply Slots and Induction Surface of ACB

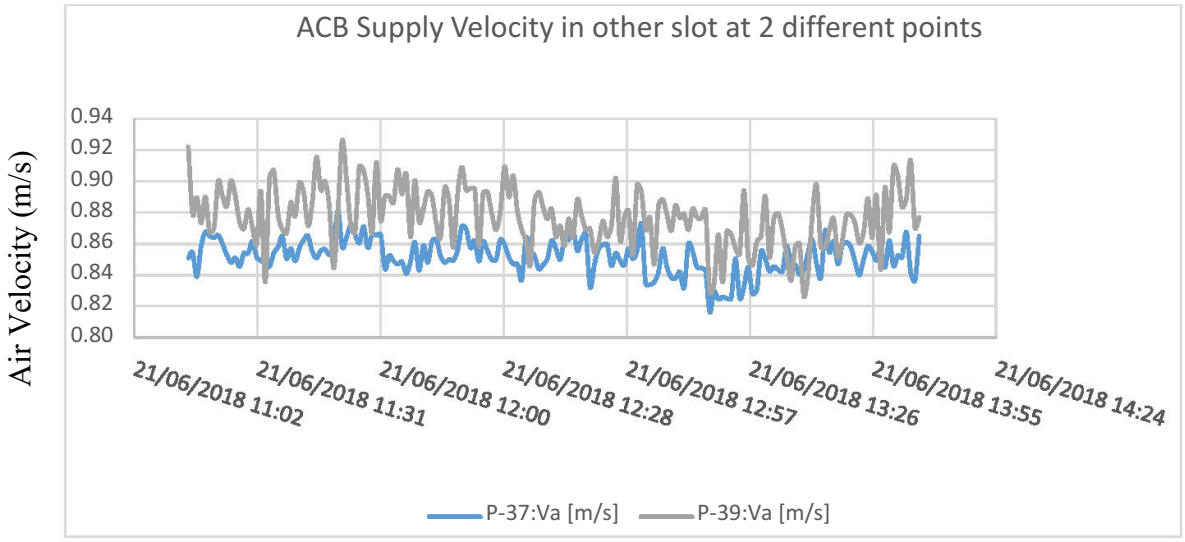

Figure 9.23 - Discharge Air Velocities at the Other Slot (Cooling)

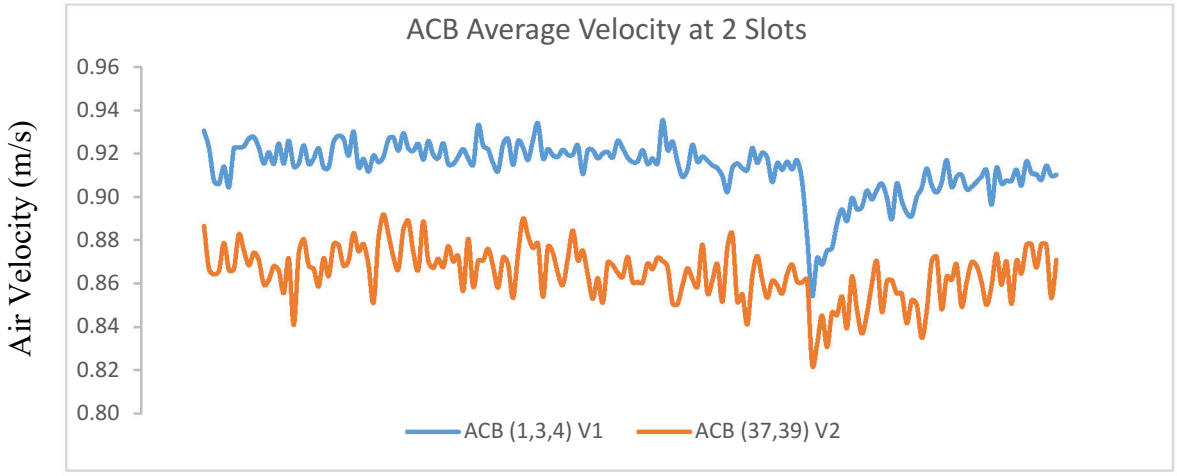

Figure 9.24 - Difference in Average Air Velocities at 2 Slots of ACB (Cooling)

9.2.2 Discharge Air Temperature

The discharge temperatures recorded at the same 3 points as shown in Figure 9.22, were found uniform at the slot. The discharge temperature at slot 1 can be seen in Figure 9.25, the beam was initially in cooling and then the temperature was raised through the occupant, all three temperatures in cooling and after changing the setpoint were found equal which proves proper mixing of primary air and secondary air through coil at one end of the beam.

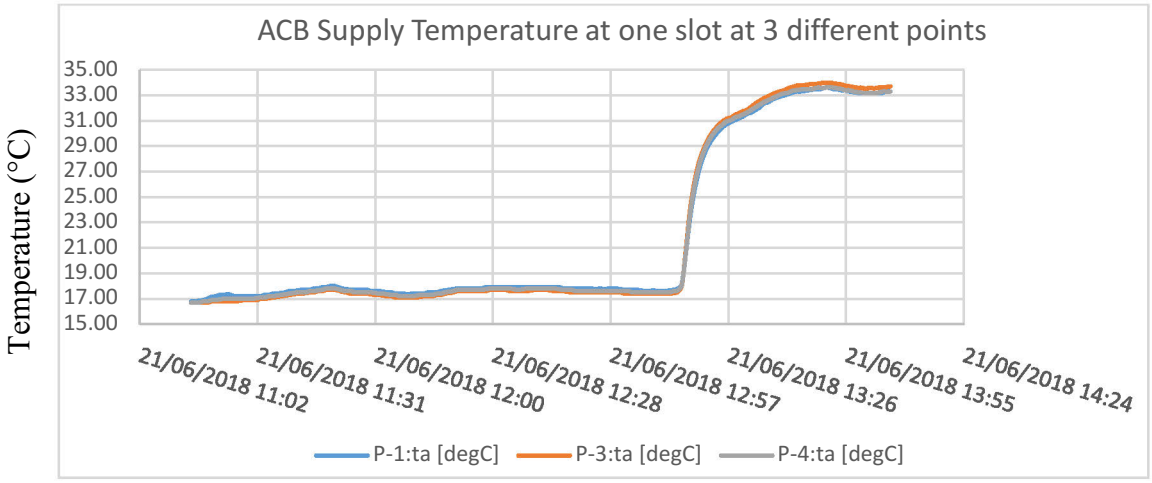

Figure 9.25 - Discharge Temperature at Slot 1 at 3 Different Locations

Discharge air temperatures at the other slot were also found almost equal to each other as shown in Figure 9.26. However, the average temperatures at both the slots were found almost

equal in cooling mode and found unequal whenever the setpoint temperature was raised. The induction air temperature in cooling represents the room temperature while it was found closely following the supply air temperatures in heating which are due to the short circuit and stratification of hot air at higher levels as shown in Figure 9.27 and Figure 9.28.

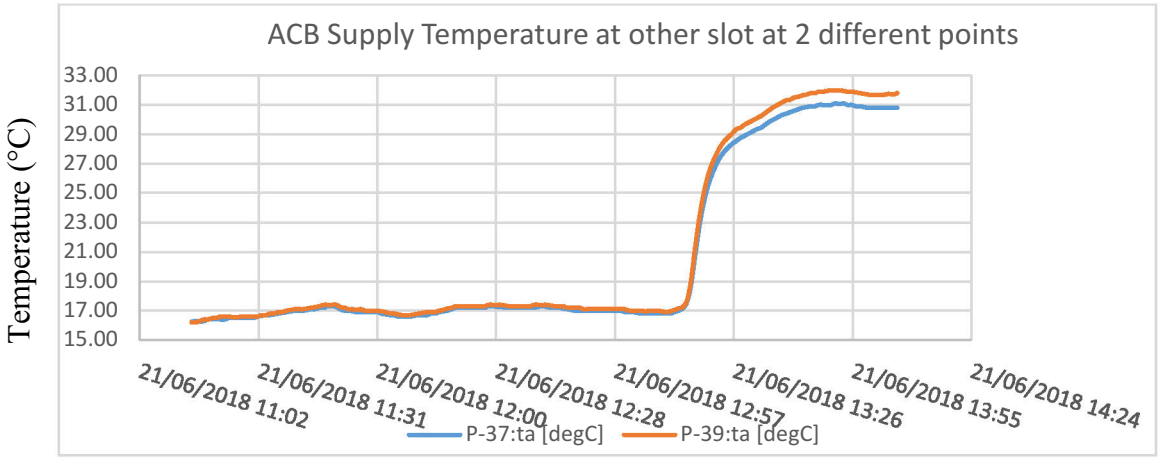

Figure 9.26 - Discharge Temperature at Slot 2 at 2 different locations

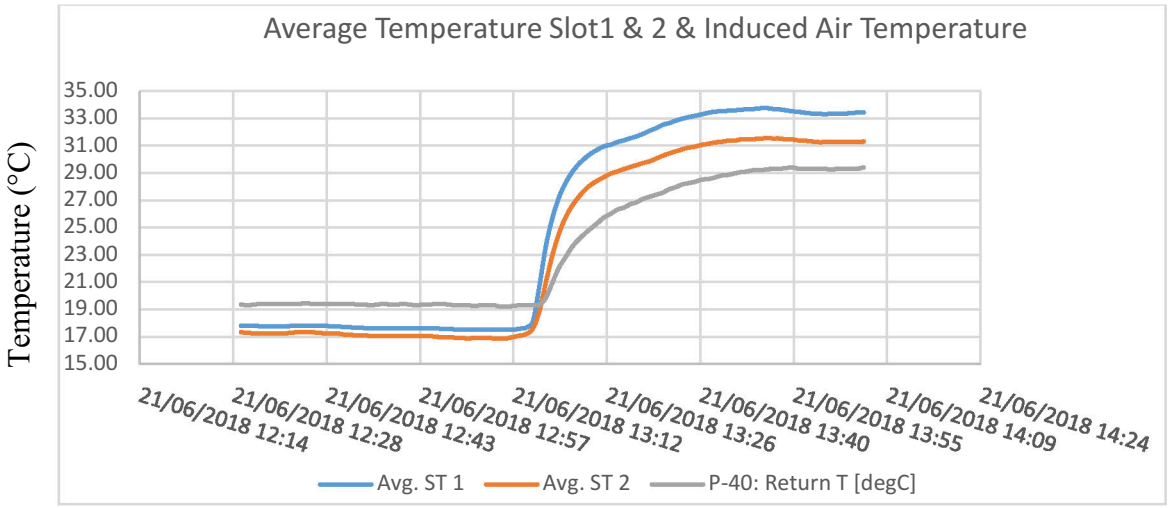

Figure 9.27 - Difference in Discharge Air Temperature & Induced Air Temperature (Cooling)

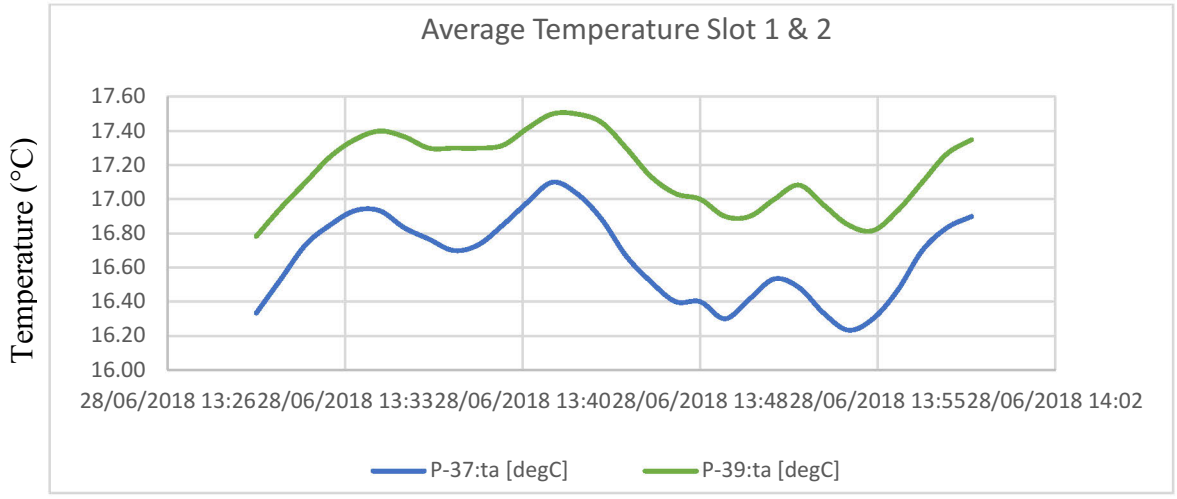

Figure 9.28 - Difference in Discharge Air Temperature (Cooling)

9.2.3 Induced Air Velocity & Temperature

Induced air velocity and the temperature were measured at 2 points (center of the beam) during the cooling experiment under the steady-state condition as shown in Figure 9.29 and Figure 9.30 respectively for a room setpoint temperature of 24°C, the velocity was found nearly equal at both the locations. Few fluctuations were found but due to the limitation of velocity probes during the experiment, the induction phenomenon was not studied in detail. Further study is required in a controlled environment.

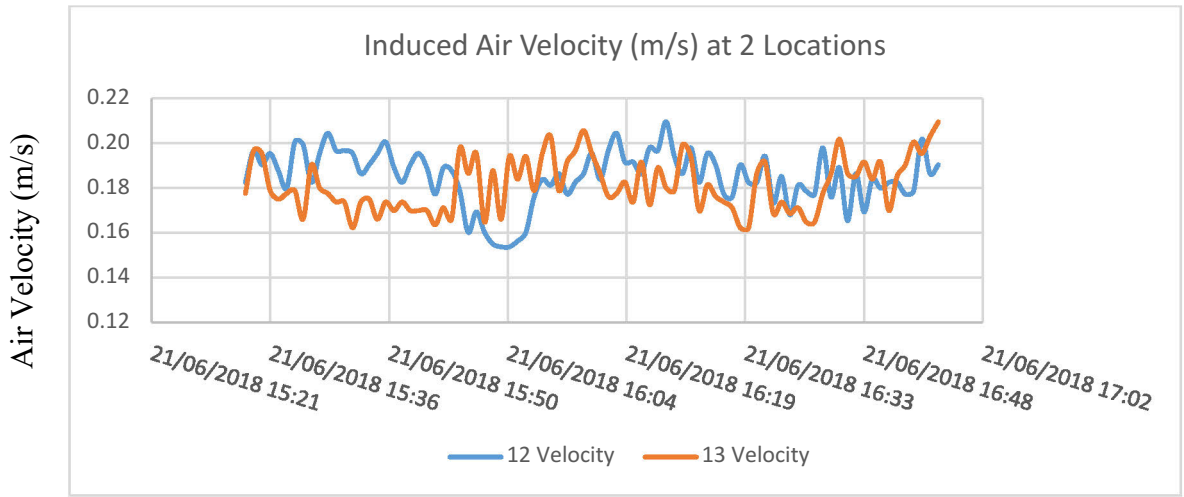

Figure 9.29 - Induced Air Velocity at ACB 1 (Cooling)

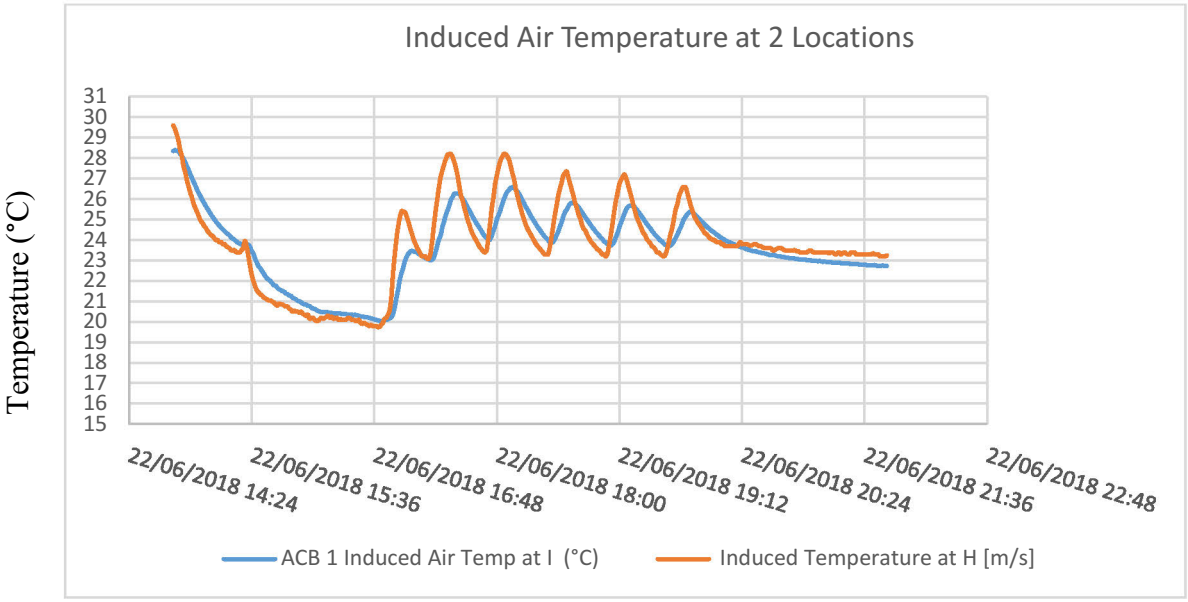

Figure 9.30 - Induced Air Temperature at ACB 1 (Cooling)

9.2.4 Surface Temperature Distribution

Figure 9.31 to Figure 9.37 shows that the surface temperature in cooling mode. The temperature of all surfaces follows the room setpoint temperature when it is varied by the occupant. The setpoint temperature is varied between 20°C to 24°C in cooling mode to test the response of ACB. The test room surfaces are in line with the setpoint temperature within ±1°C. The response of ACB to achieve setpoint as shown in the figures is quick and the steady state response shows the temperature for all the measured points are almost equal. It can be seen in Figure 9.31 that the floor temperature near occupant is higher due to the presence of occupant than the temperature recorded near the guest location in the room. The operative temperature measured near 1 meter of occupant shows that the room operative temperature follows the varying setpoint.

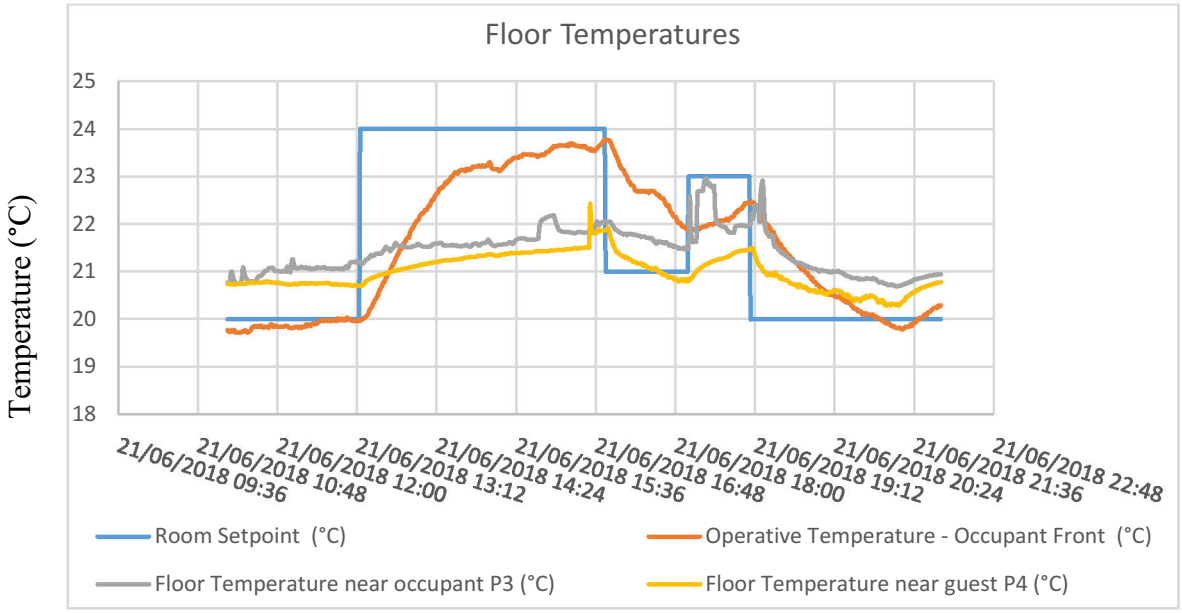

Figure 9.31 - Floor Surface Temperature Measured at 2 Locations (Cooling)

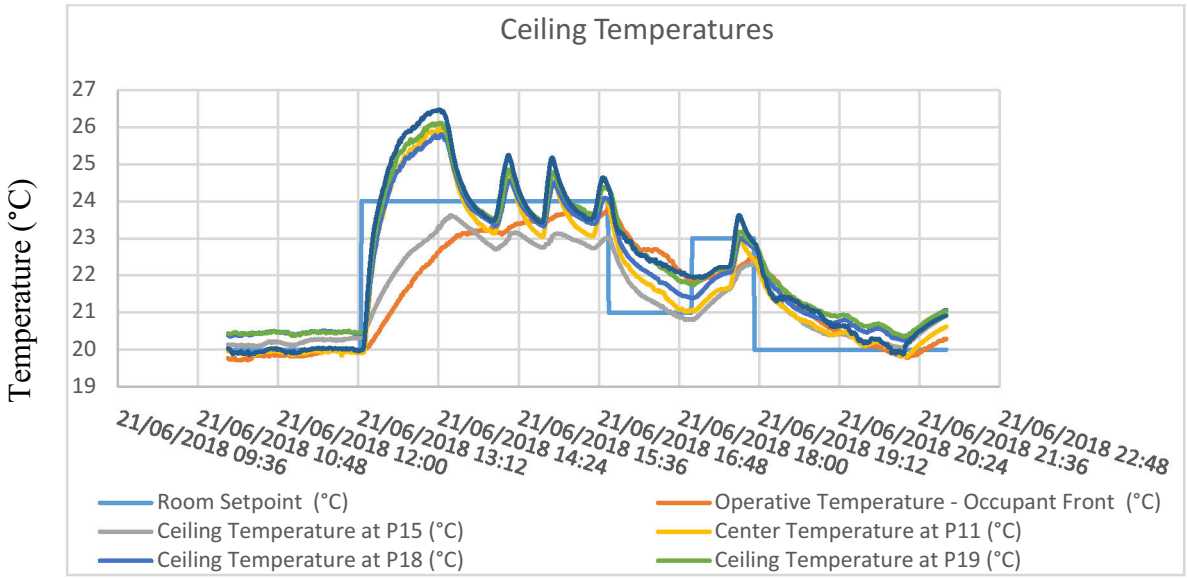

Figure 9.32 - Ceiling Temperatures Measured at 5 Locations (Cooling)

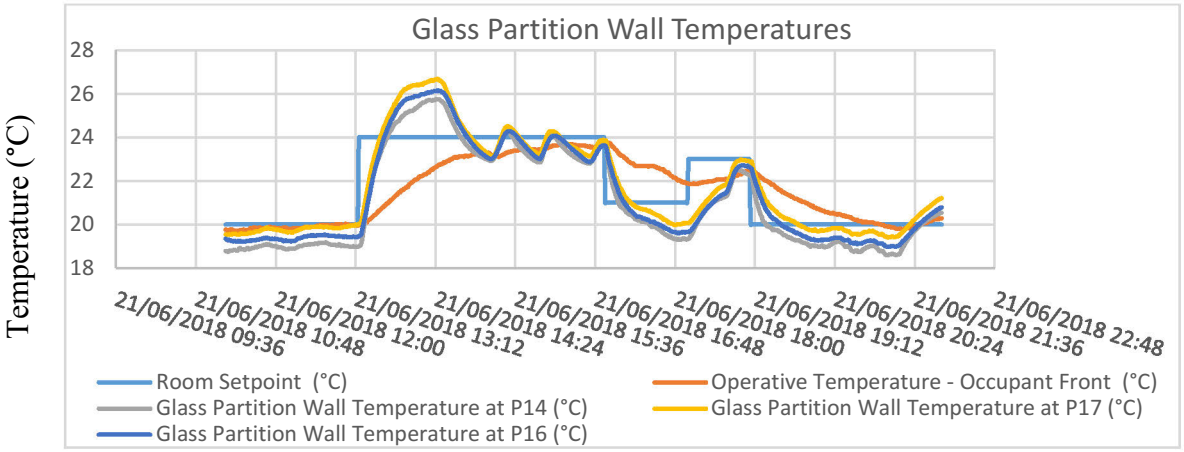

Figure 9.33 - Glass Partition Surface Temperatures Measured at 3 Locations (Cooling)

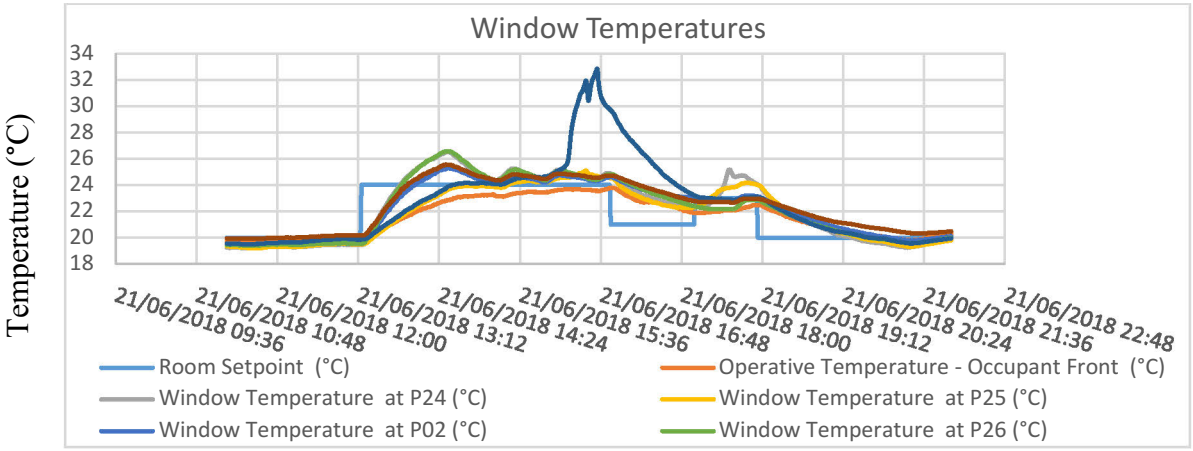

Figure 9.34 - Window Temperatures Measured at 6 Locations (Cooling)

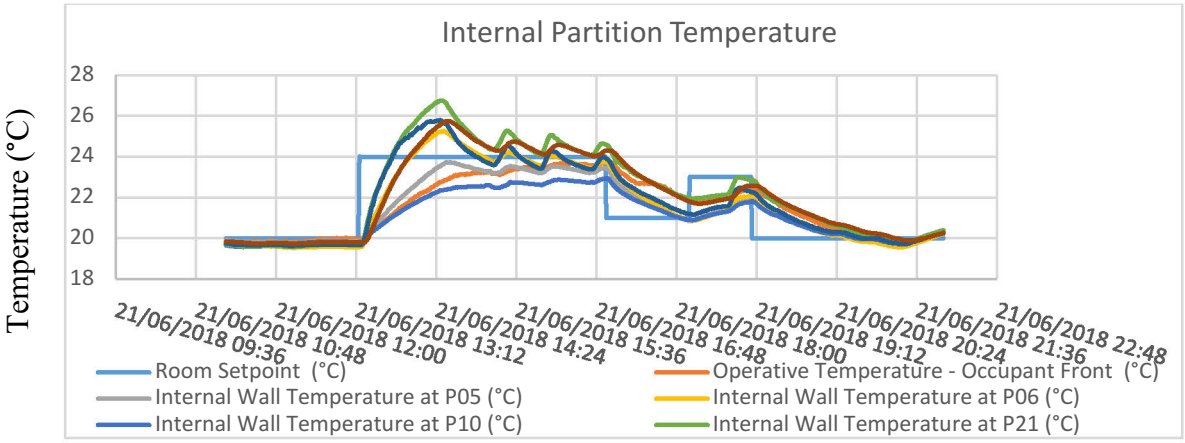

Figure 9.35 - Internal Partition Temperature Measured at 4 Locations (Cooling)

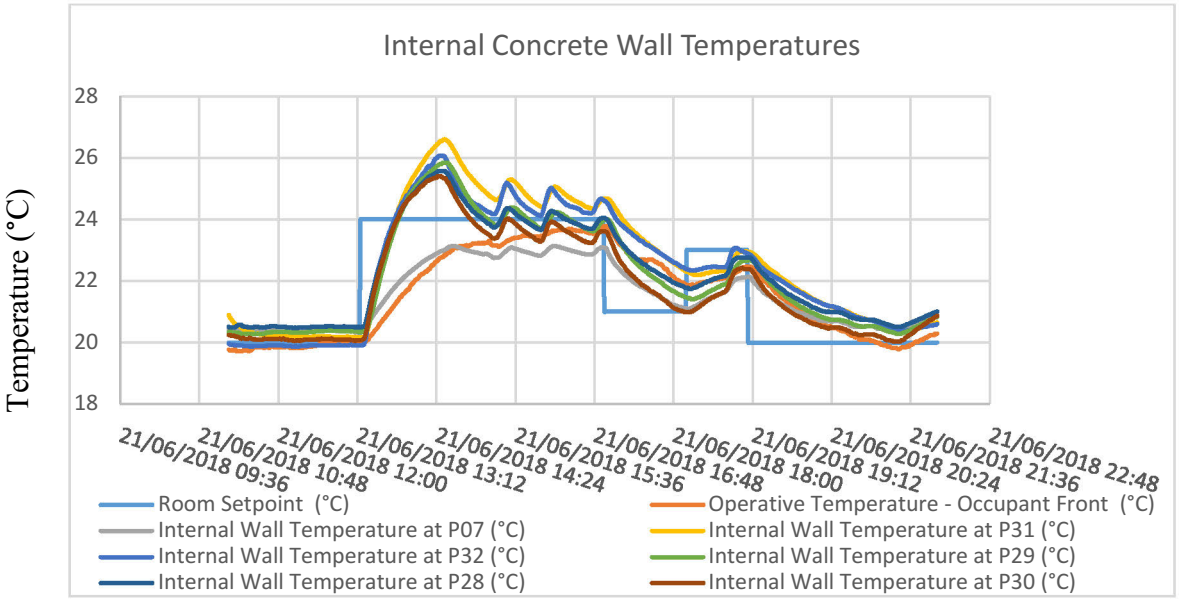

Figure 9.36 - Internal Concrete Wall Temperature Measured at 6 Locations (Cooling)

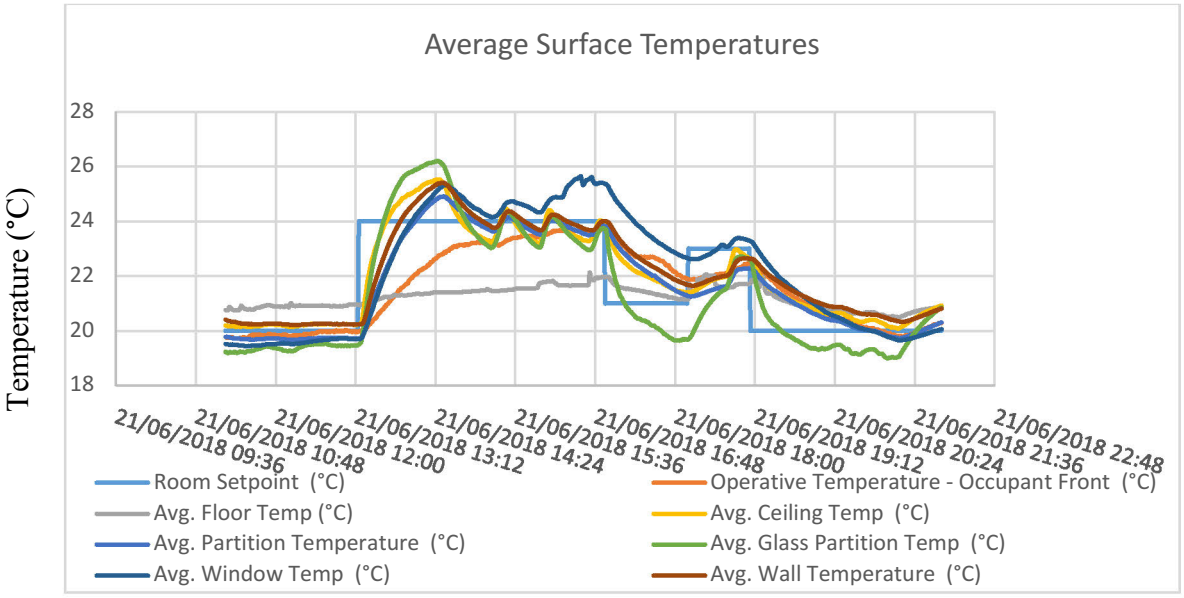

Figure 9.37 - Average Surface Temperatures (Cooling)

9.2.5 Room Air Distribution

Figure 9.38 shows the measurement points where air velocity and air temperature was measured in the Test Room 2. The test room is equipped with 2 units of ACB which can be seen supplying cold air to the room. The setpoint in the room was varied by the occupant and the measurement was recorded at four different heights (0.1 m, 0.6 m, 1.1 m and 1.7 m) at the steady state condition. The velocities were within the ASHRAE recommended limit in the occupied zone to avoid the draft. The air temperature and air velocity recorded for a setpoint temperature of 22°C are presented in Table 9.1 for 3 different sections (planes) at 0.75 m, 1.2 m and 1.6 m. A typical section with measurement point and their location from the wall is shown in Figure 9.38

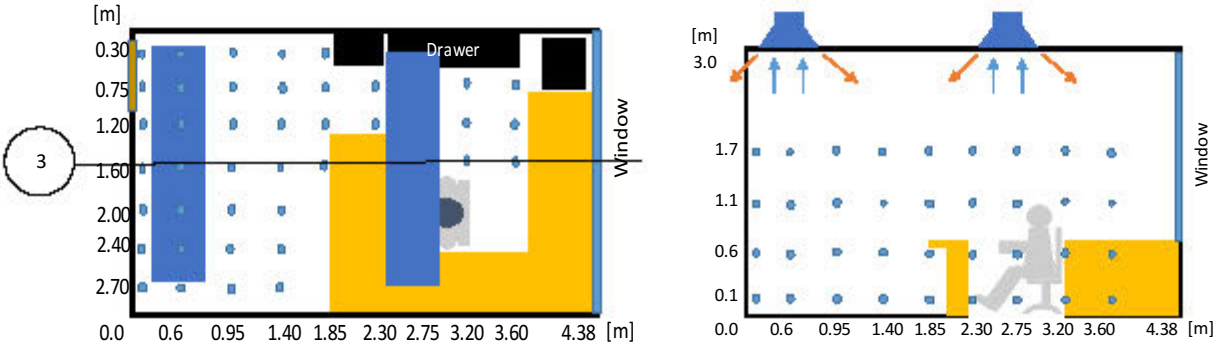

Figure 9.38 - Measurement Points in the Test Room 2 for Room Air Distribution (Cooling)

Figure 9.39 shows the spatial distribution of air temperature and air velocity at room setpoint of 22°C across Section 3. The results for section 1 (0.75 m) and section 2 (1.2 m) are shown in Appendix B for room setpoint 22°C. Other figures with a different set point for 3 sections are also added in Appendix B for the same test room. The spatial distribution shows that the air velocity is lower than the recommended air velocity for a seated person by ASHRAE for thermal comfort near the occupant. The measured values are shown in different ways to visualize the change in velocities and temperature across section 3 which is nearby the occupant at 1.6 m from the wall.

Table 9.1 - Air Velocity and Air Temperature in Cooling at Setpoint Temperature 22°C (Cooling)

Experimental Results (Room Setpoint 22 (°C))										
Plane	Point No	Distance (m)	Air Velocity (m/s)				Air Temperature (°C)			
			Height (m)				Height (m)			
			0.1	0.6	1.1	1.7	0.1	0.6	1.1	1.7
PLANE 1 (0.75 m)	38	0.05	0.10	0.08	0.12	0.19	21.31	21.40	21.39	21.30
	31	0.60	0.12	0.17	0.21	0.22	21.14	21.11	21.08	21.04
	24	0.95	0.19	0.10	0.08	0.08	20.58	20.70	20.73	20.75
	17	1.40	0.09	0.05	0.05	0.08	21.12	21.20	21.24	21.26
	13	1.85	0.06	0.05	0.09	0.04	21.58	21.63	21.62	21.75
	10	2.30	0.12	0.12	0.13	0.13	21.32	21.32	21.24	21.35
	7	2.75	0.05	0.05	0.07	0.12	21.90	22.00	22.00	21.98
	4	3.20	0.05	0.06	0.12	0.14	21.79	21.81	21.93	21.90
	1	3.60	0.06	0.10	0.12	0.10	20.77	20.67	20.89	20.85

Experimental Results (Room Setpoint 22 (°C))										
Plane	Point No	Distance (m)	Air Velocity (m/s)				Air Temperature (°C)			
			Height (m)				Height (m)			
			0.1	0.6	1.1	1.7	0.1	0.6	1.1	1.7
PLANE 2 (1.2 m)	39	0.05	0.08	0.17	0.25	0.27	21.48	21.48	21.40	21.32
	32	0.60	0.12	0.12	0.14	0.25	21.01	20.93	20.96	20.82
	25	0.95	0.14	0.07	0.09	0.21	20.68	20.78	20.83	20.65
	18	1.40	0.05	0.05	0.07	0.09	21.57	21.64	21.66	21.70
	14	1.85	0.08	0.07	0.11	0.07	21.68	21.70	21.66	21.80
	11	2.30	0.13	0.12	0.13	0.08	20.86	20.89	20.92	21.13
	8	2.75	0.07	0.08	0.12	0.13	21.99	22.00	21.93	21.98
	5	3.20	0.09	0.10	0.11	0.14	21.80	21.84	21.97	21.98
	2	3.60	0.07	0.10	0.11	0.12	21.50	21.48	21.90	21.76

Experimental Results (Room Setpoint 22 (°C))										
Plane	Point No	Distance (m)	Air Velocity (m/s)				Air Temperature (°C)			
			Height (m)				Height (m)			
			0.1	0.6	1.1	1.7	0.1	0.6	1.1	1.7
PLANE 3 (1.6 m)	40	0.05	0.10	0.20	0.25	0.29	21.51	21.51	21.50	21.48
	33	0.60	0.15	0.13	0.11	0.12	20.85	20.89	21.00	21.01
	26	0.95	0.15	0.08	0.10	0.12	20.98	21.10	21.18	21.16
	19	1.40	0.09	0.11	0.11	0.05	21.28	21.26	21.35	21.59
	15	1.85	0.09	0.18	0.10	0.07	21.05	20.86	21.20	21.31
	9	2.75	0.08	0.10	0.12	0.14	21.89	21.86	21.85	21.81
	6	3.20	0.10	0.10	0.13	0.14	21.80	21.90	21.99	22.03
	3	3.60	0.08	0.12	0.13	0.14	21.60	21.63	21.78	21.88

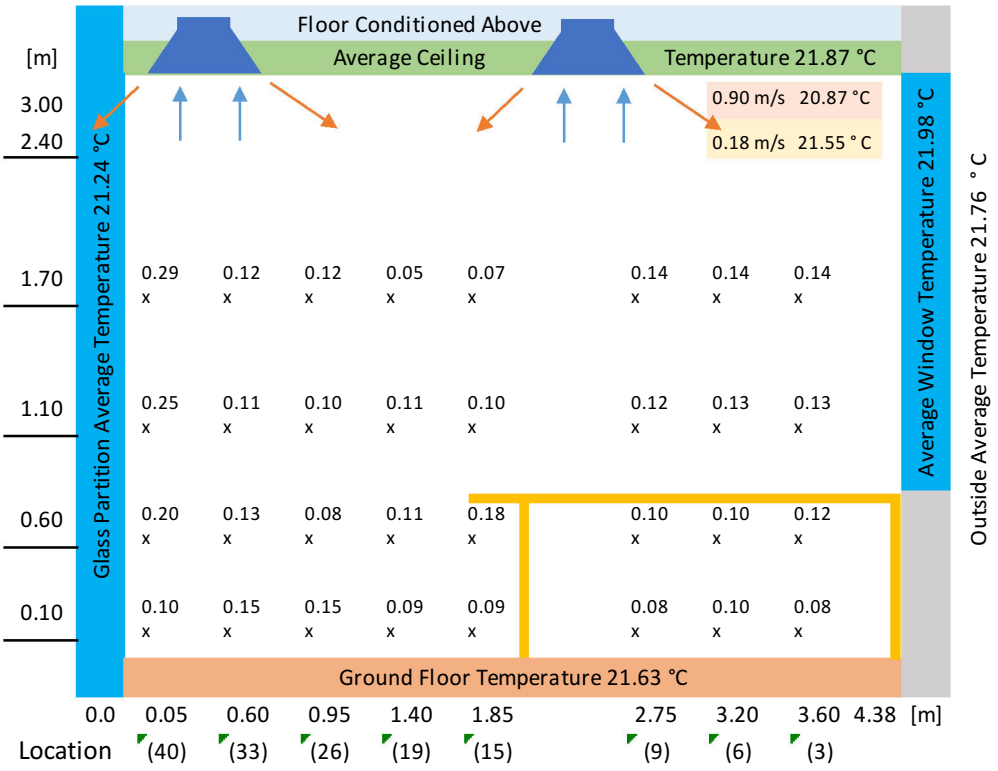

Plane - 3 (1.6 m) - Average Velocity at different heights

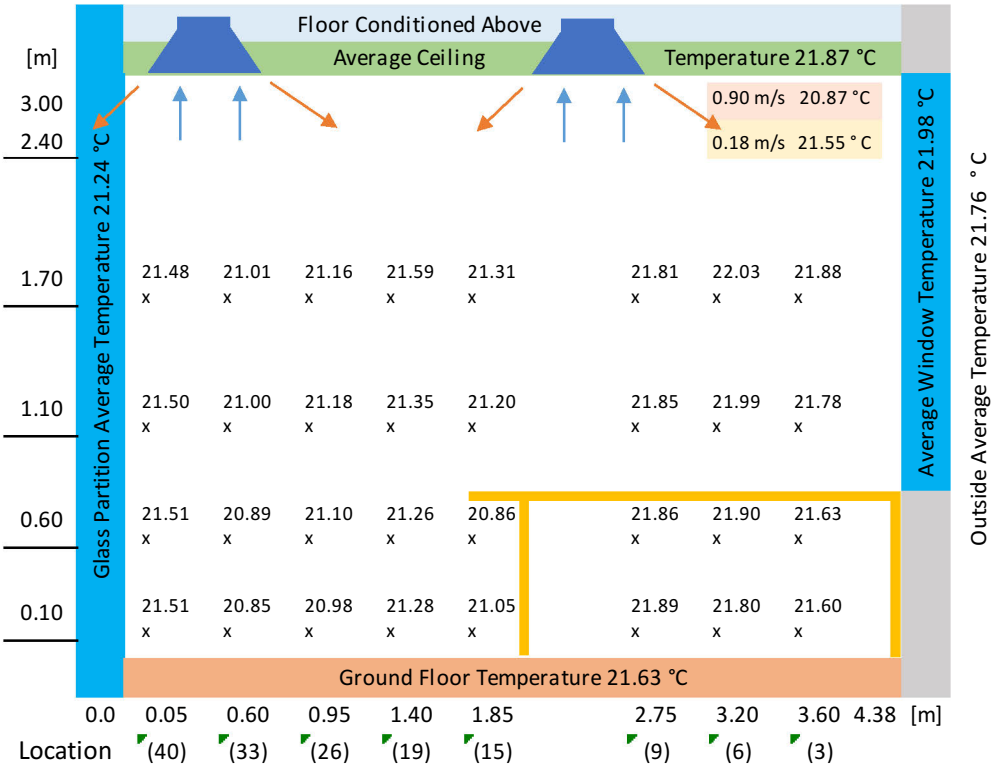

Plane - 3 (1.6 m) - Average Temperature at different heights

Figure 9.39 - Average Air Velocity & Air Temperature at Section 3 (1.6 m) in Cooling

Figure 9.40 shows that the air temperature at occupant location (Point 9 & 6) is equal to the room setpoint, the air temperature near the window (Point 3) and the other end of the room (Point 40 & 33) is lower than the room setpoint due to the downdraft of air. The Active Beam 2 is located near the glass partition which causes the air draft to fall directly down the room resulting in higher velocity near the glass partition (Point 40) as shown in Figure 9.41.

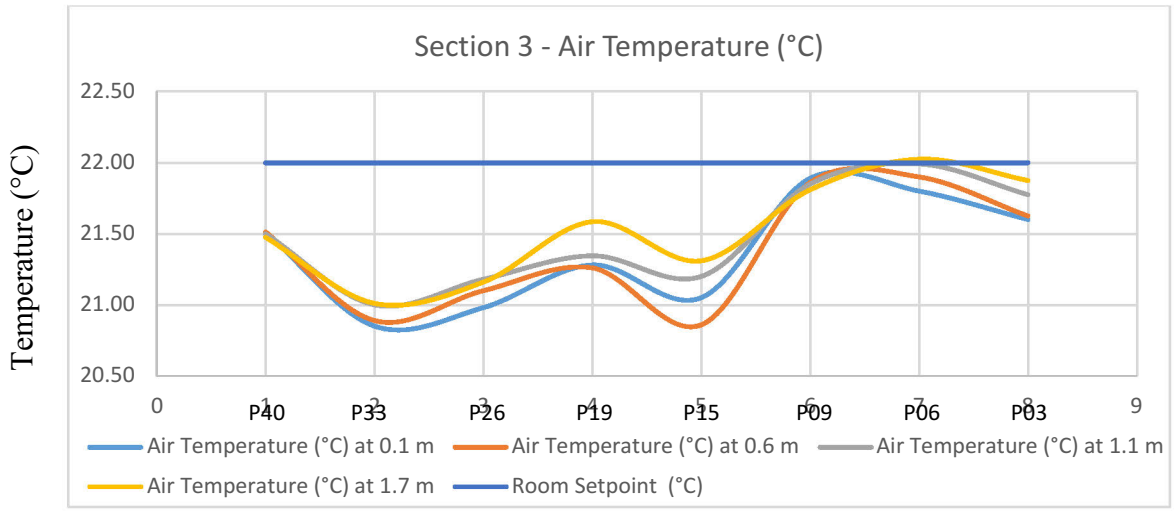

Figure 9.40 - Air Temperature at Section 3 of Test Room 2 (Setpoint 22°C in Cooling)

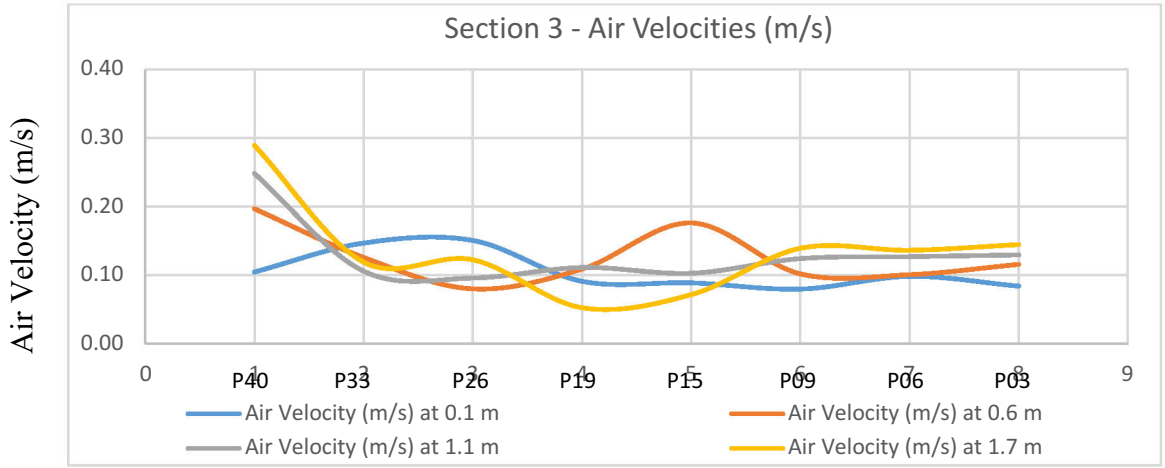

Figure 9.41 - Air Velocity at Section 3 of Test Room 2 (Setpoint 22°C in Cooling)

Figure 9.42 shows the difference between the air temperatures at different heights. The air temperature at all heights at different points is quite uniform in cooling and nearly close to the setpoint. The air velocities as shown in Figure 9.43 were found lower than ASHRAE recommended air velocity for occupied zone accept the few velocities at higher levels near glass partition due to obstruction in the throw. Air velocities and air temperatures at 3 different sections are compared in Figure 9.44. Air temperatures and air velocities at other room setpoint and for different sections are presented in Appendix B.

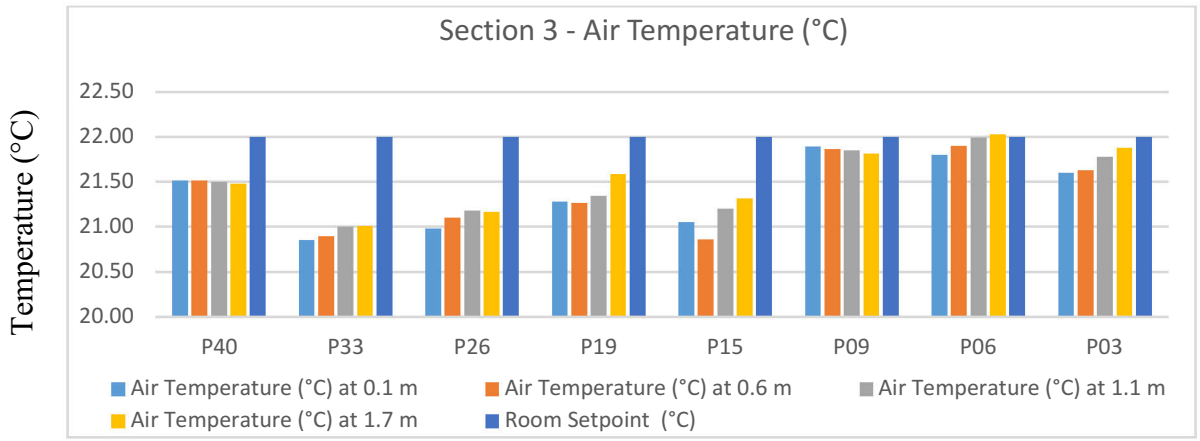

Figure 9.42 - Air Temperature at 4 Different Heights across Section 3 of Test Room 2 (Setpoint 22°C in Cooling)

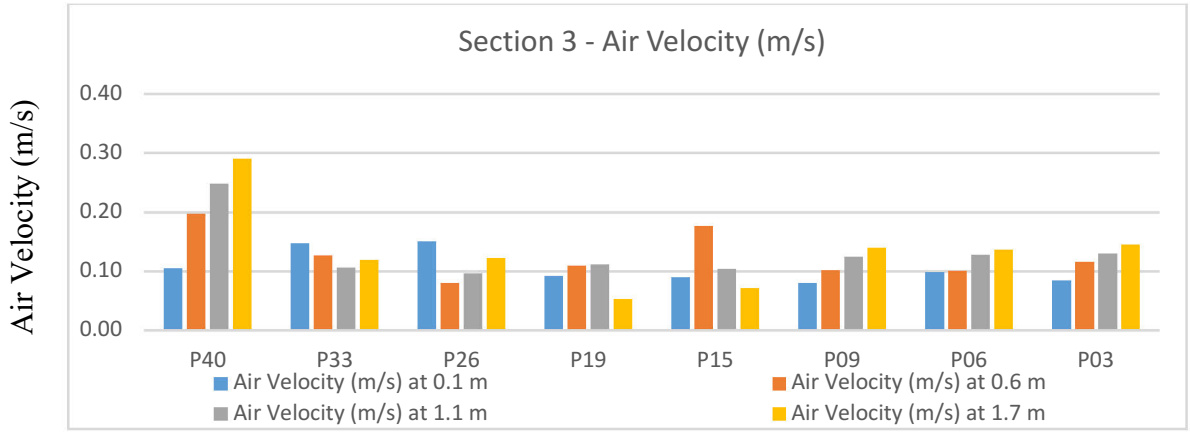

Figure 9.43 - Air Velocity at 4 Different Heights across Section 3 of Test Room 2 (Setpoint 22°C in Cooling)

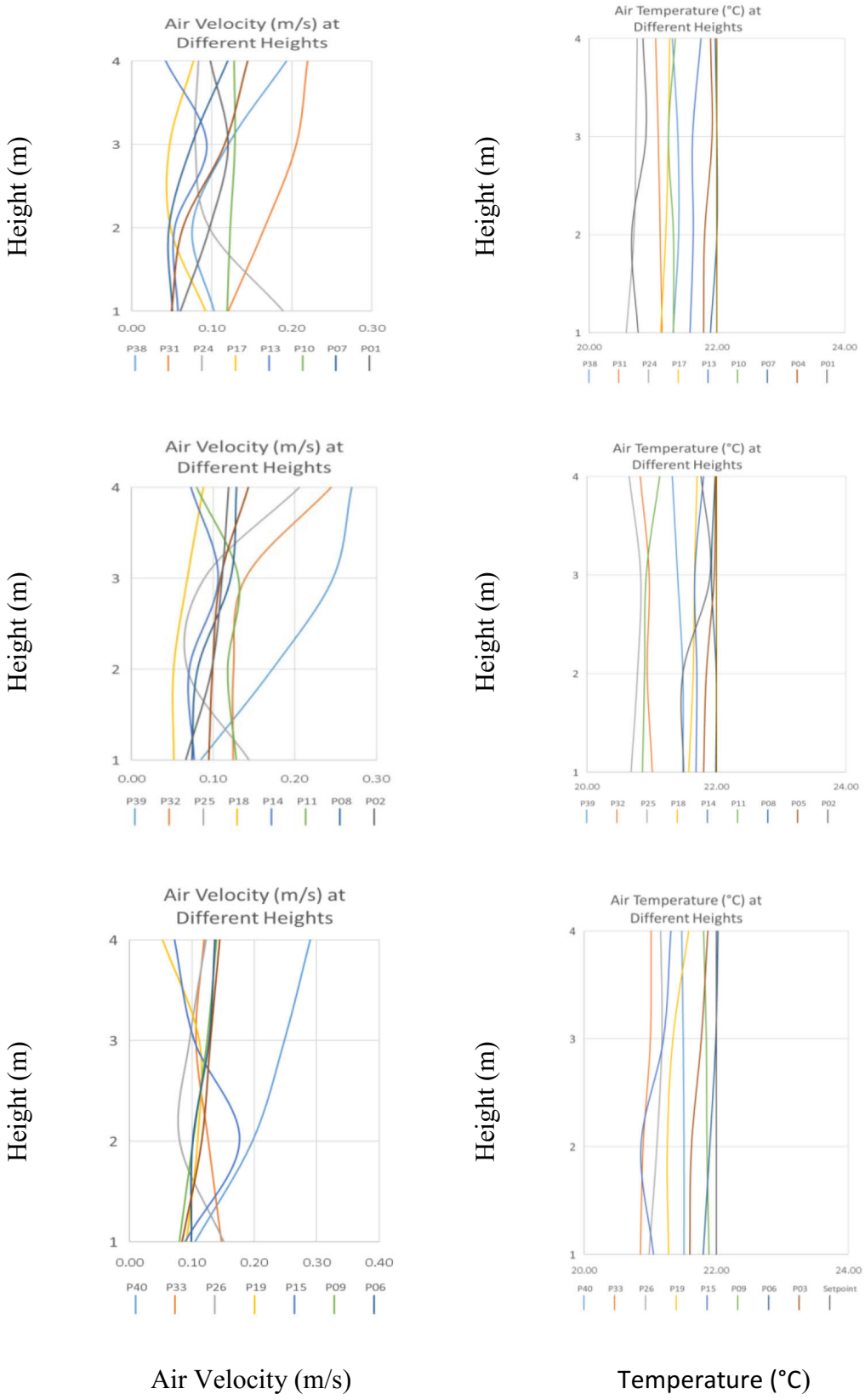

Figure 9.44 - Air Velocities & Temperatures at Section 1, 2 and 3 respectively at SP 22°C

9.2.6 Operative Temperature

The operative temperature was recorded in front of the occupant (1 meter, on desk) for different setpoints in the test room 2. The graph plotted between room setpoint temperature and operative temperature as shown in Figure 9.45 shows that the room achieves the cooling setpoint most of the time. The variation between room setpoint and operative temperature under cooling was small.

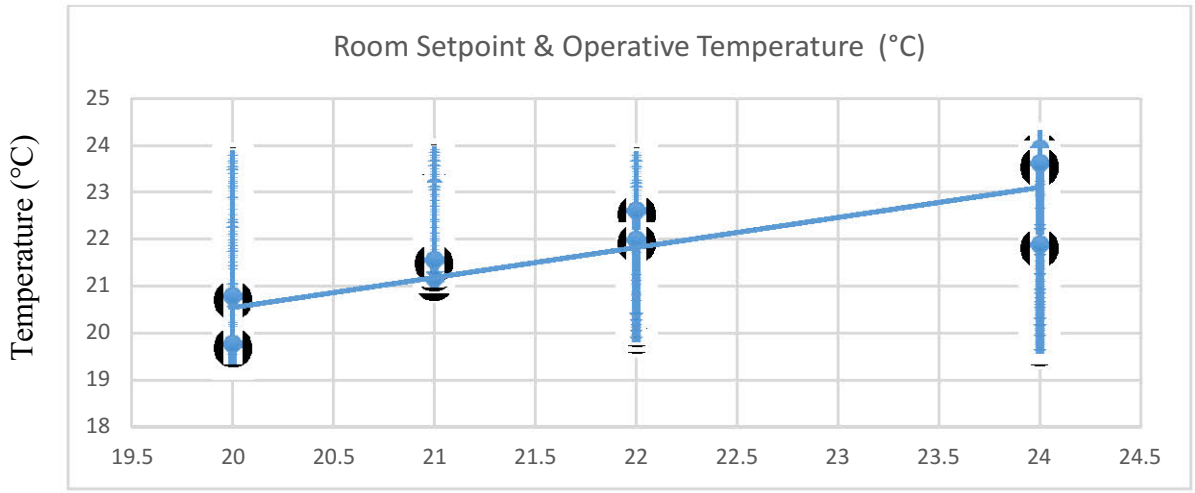

Figure 9.45 - Room Setpoint and Operative Temperature (Near Occupant, In Cooling)

9.3 Air Velocity in Heating and Thermal Stratification

Based on the experiments, smaller air velocities were found in heating operation. This is because of thermal stratification in heating. A thick layer of air is always being stratified near the ceiling. The airflow and temperature recorded at the exhaust grille during the measurement show that the exhaust air temperature is almost the same as hot supply air from the ACB. Thermal stratification was more when the room set point was higher than 21°C, especially, during morning hours when occupant tends to increase the set point being colder in winter. This results in negligible or zero velocity in the occupied zone and all the hot air supplied from the ACB stays up and exhaust out at the same temperature. The average air velocity in heating for a typical day in steady state condition is shown in Figure 9.46. The air velocity at 0.1 m, 0.6 m height is much lower for sitting occupant and was found nearly zero which makes the

air stagnant and full of contaminants. Therefore it is recommended to test the beam for air change effectiveness and indoor air quality in heating mode in a controlled environment.

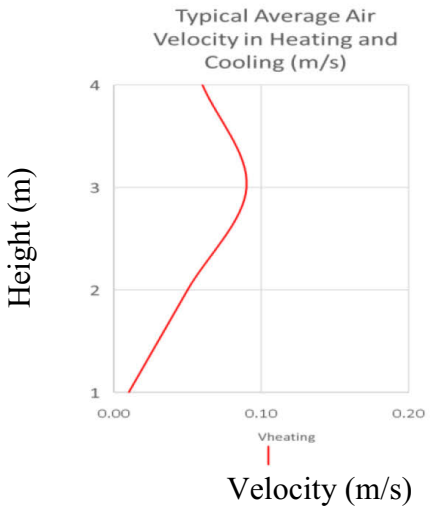

Figure 9.46 - Typical Average Air Velocities in Heating at 0.1, 0.6, 1.1, 1.7 m

9.4 Heat Exchanger – Heating Mode

Based on the temperature difference found during the heating and cooling experiment, the heat exchanger study was conducted to find out the cause of temperature difference at supply slots. The cross section of the heat exchanger is shown in Figure 9.47, it has 12 passes for cooling and 4 passes for heating. As there are only 4 passes of heating and the hot water is routed through inlet ‘w’ to the outlet ‘z’ as explained in heating section during this travel the hot water transfer heat to cooler induced air and becomes warmer by the time it reaches the outlet and therefore a big temperature difference exists in heating. It is to be noticed that 12 passes of cooling are divided into 2 circuits, which is effective in proper distribution of cooling on each section of the ACB, however small temperature difference (0.5°C to 1°C) was found in cooling process as well. The reason for this difference could be the circuit’s arrangements which are shown in Figure 9.47. The circuit on the left has supply inlet to the first pass ‘a’ of the heat exchanger while the second circuit has an inlet to the pass ‘p’ which is located in the middle of the heat exchanger. As explained in the heating section the induced velocity of air due to beam plenum pressure is different on either side of exchanger which also contribute to different heat exchange and thus cause the temperature difference. Ideally, the distribution circuit must be the

same for optimum distribution of chilled water in the heat exchanger to minimize this difference.

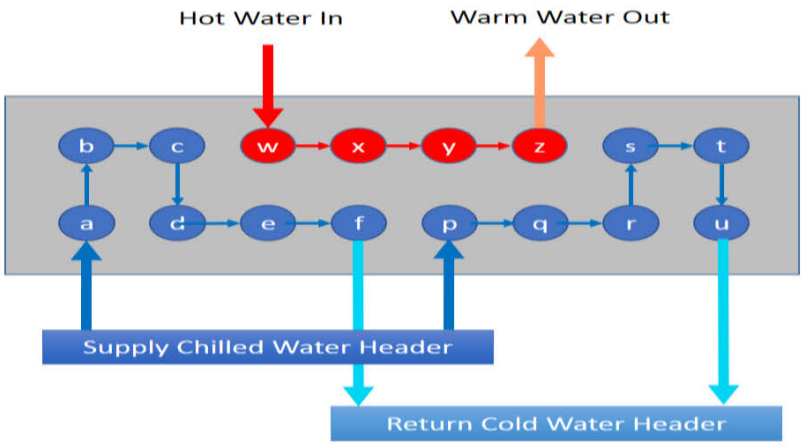

Figure 9.47 - Vertical Cross Section of Heat Exchanger of ACB

The heat exchanger was studied in order to find out the maximum temperature difference during cooling and heating. The heat exchanger (coil) was instrumented with many temperature sensors as shown in Figure 9.48 and Figure 9.49. The air temperature above and below the coil, surface temperature above and below coil was measured along the length and width of the heat exchanger. During the transient analyses of the heat exchanger, it was found that the average temperature drop along the length of Chilled beam heat exchanger is only 1°C which is reduced to 0.3°C while attaining the quasi-steady state as shown in Figure 9.55. However, the width-wise temperature difference is around 5.0°C which causes a big temperature difference in supply jets from ACB as shown in Figure 9.56. The results of these tests are shown in Figure 9.50 to Figure 9.56.

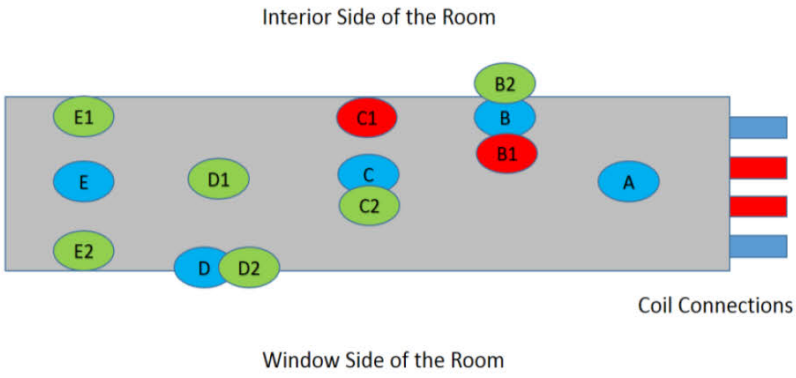

Figure 9.48 - Top View of Heat Exchanger of ACB with Temperature Sensor Location

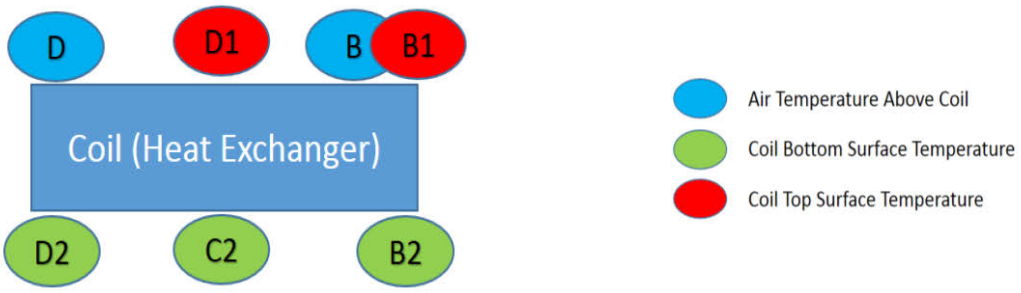

Figure 9.49 - Cross-Section of Heat Exchanger and Temperature Sensor Location

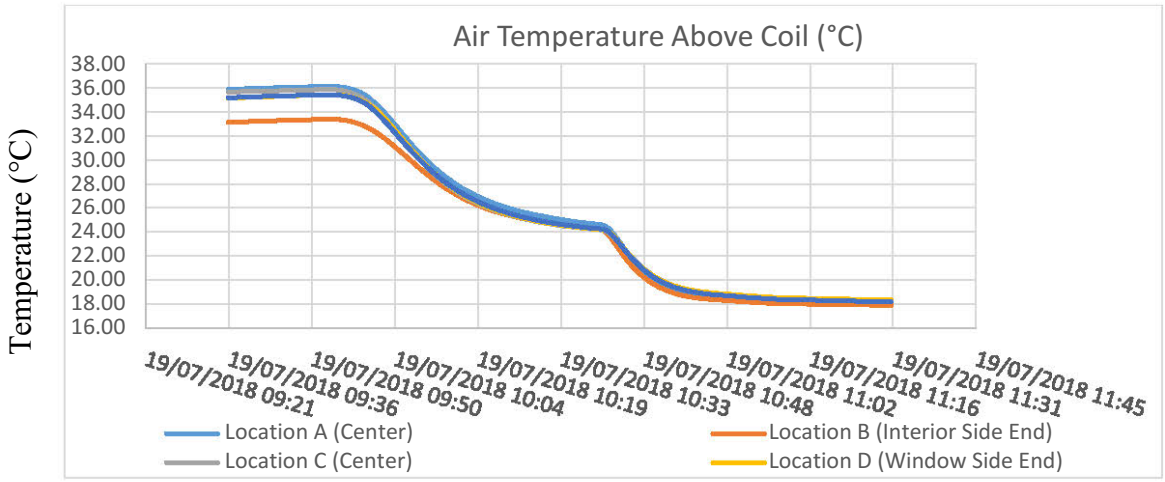

Figure 9.50 - Air Temperature above the Coil at Different Locations (Cooling)

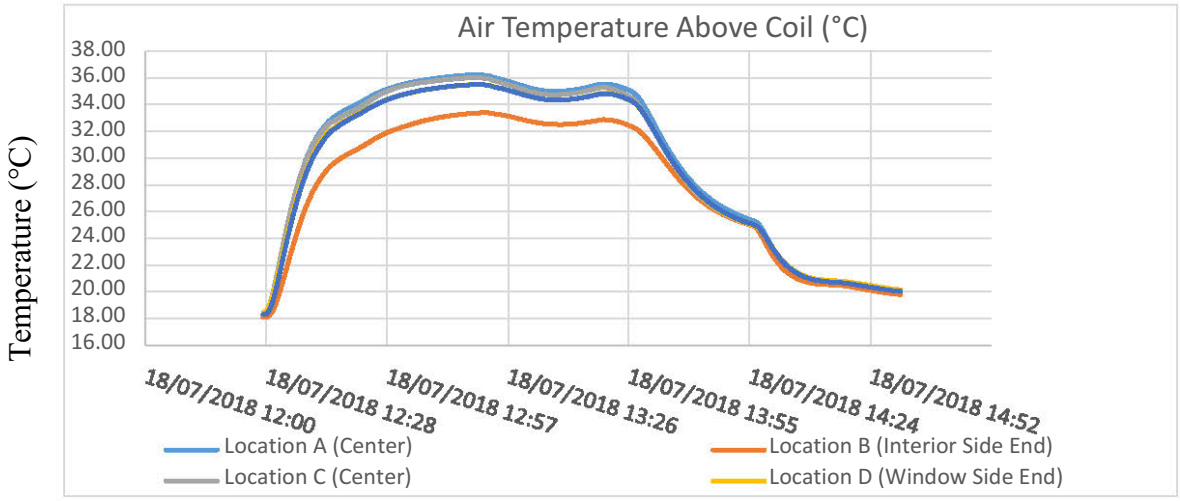

Figure 9.51 - Air Temperature above the Coil at Different Locations (Heating)

The Figure 9.52 shows that the temperature of the side end near the hot water outlet pass is always lower on different dates. The air temperature difference is more than 2.5°C during the heating period. Similarly, the surface temperature of the coil has approximately 4.5°C difference between middle to the end section of the coil as shown in Figure 9.56.

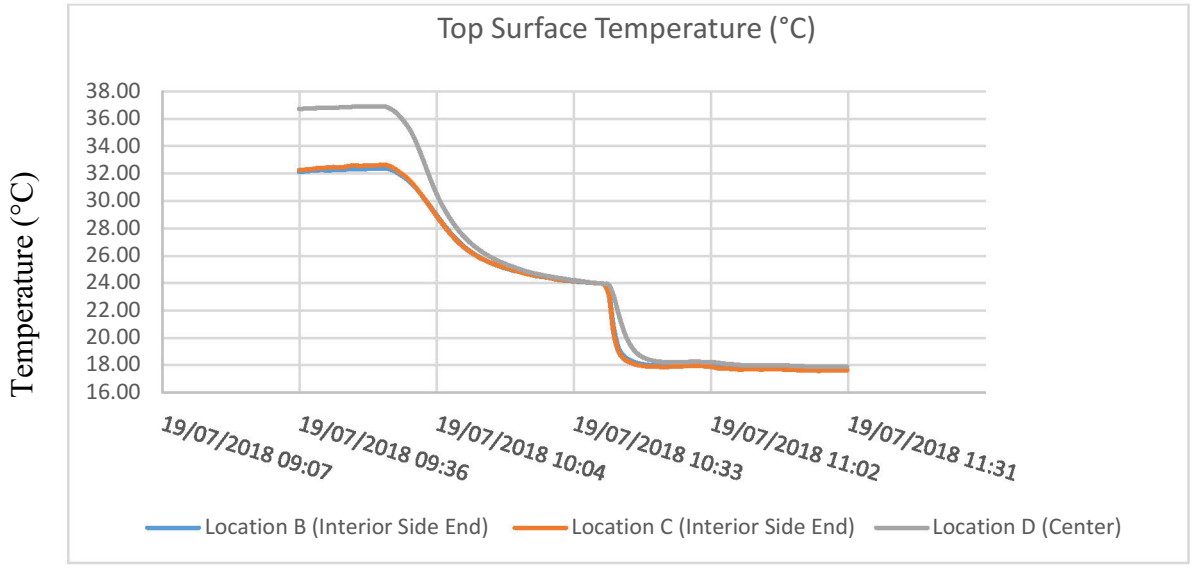

Figure 9.52 - Difference between Top Center & End Surface Temperature of the Coil (Cooling)

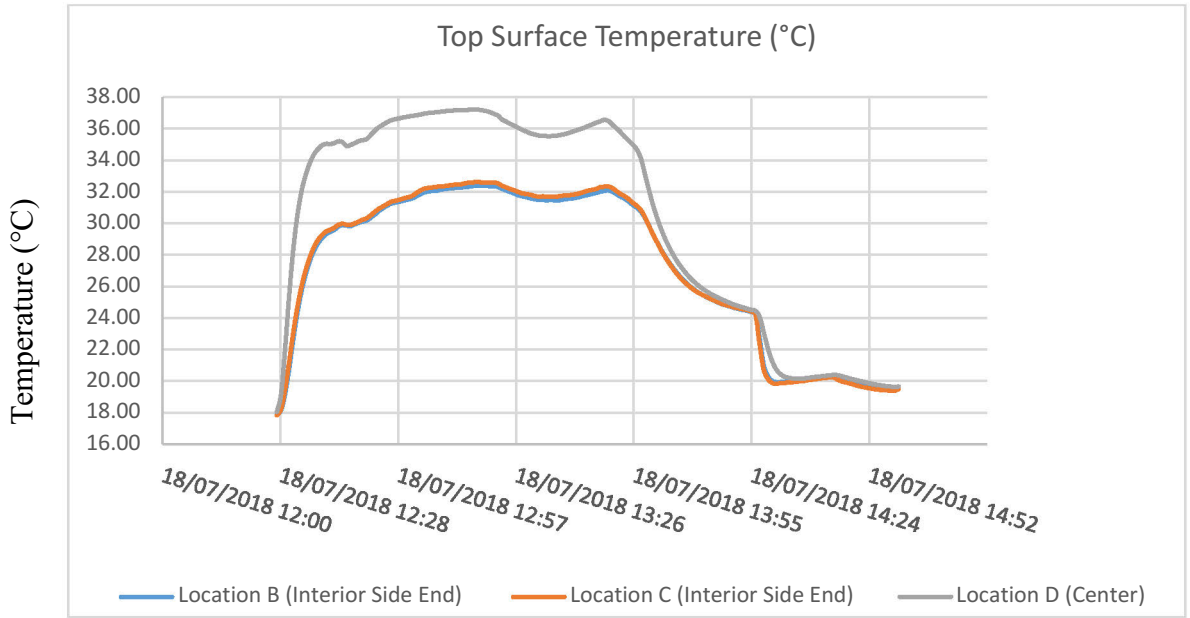

Figure 9.53 - Difference between Top Center & End Surface Temperature of the Coil (Heating)

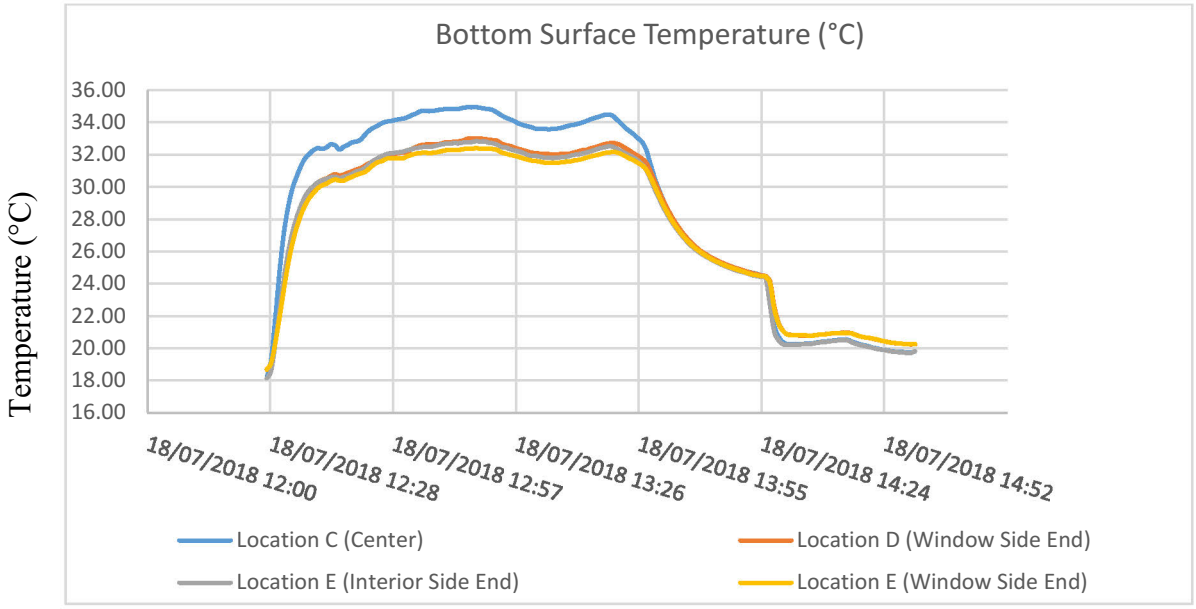

Figure 9.54 - Difference in Bottom Surface Temperature of the Heat Exchanger (Heating)

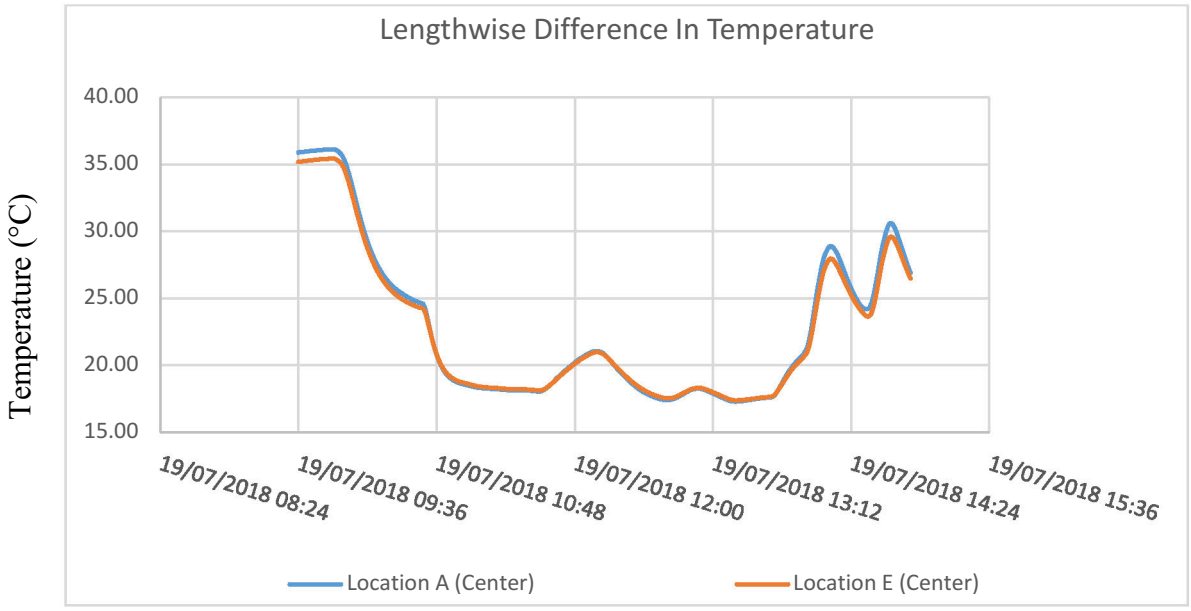

Figure 9.55 - Lengthwise Difference in Air Temperature of the Heat Exchanger

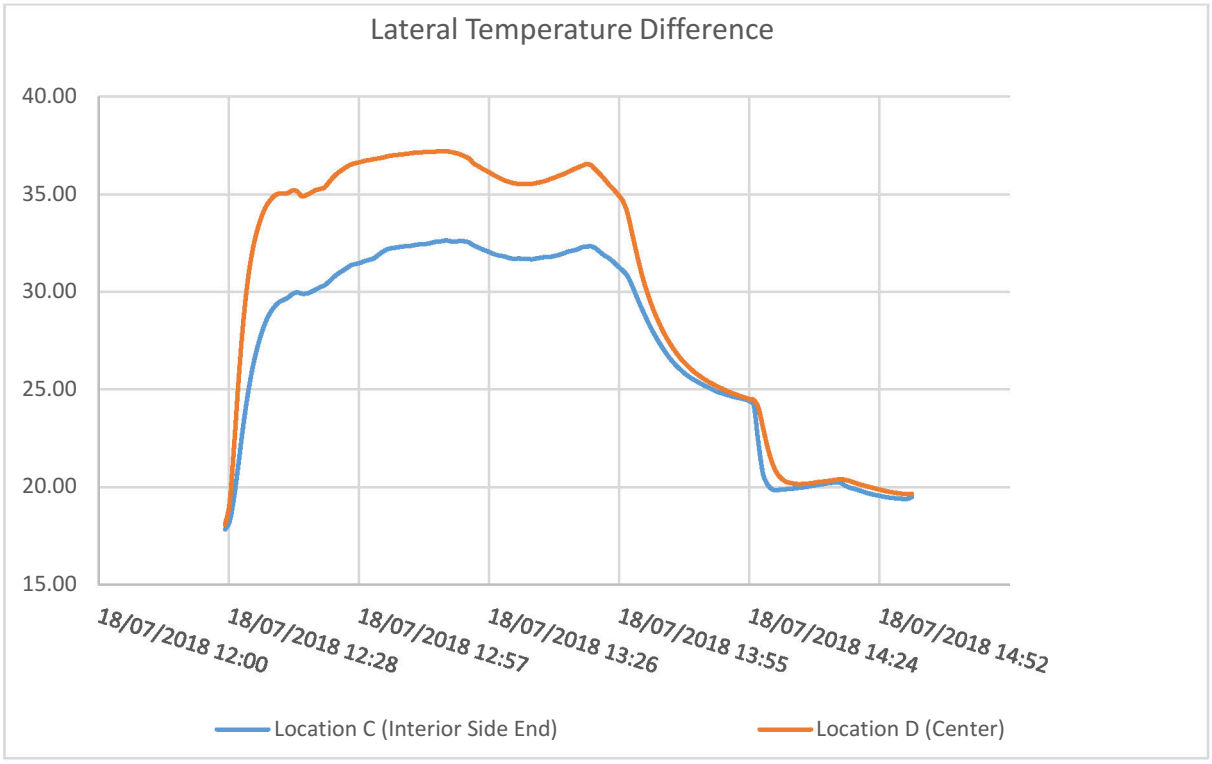

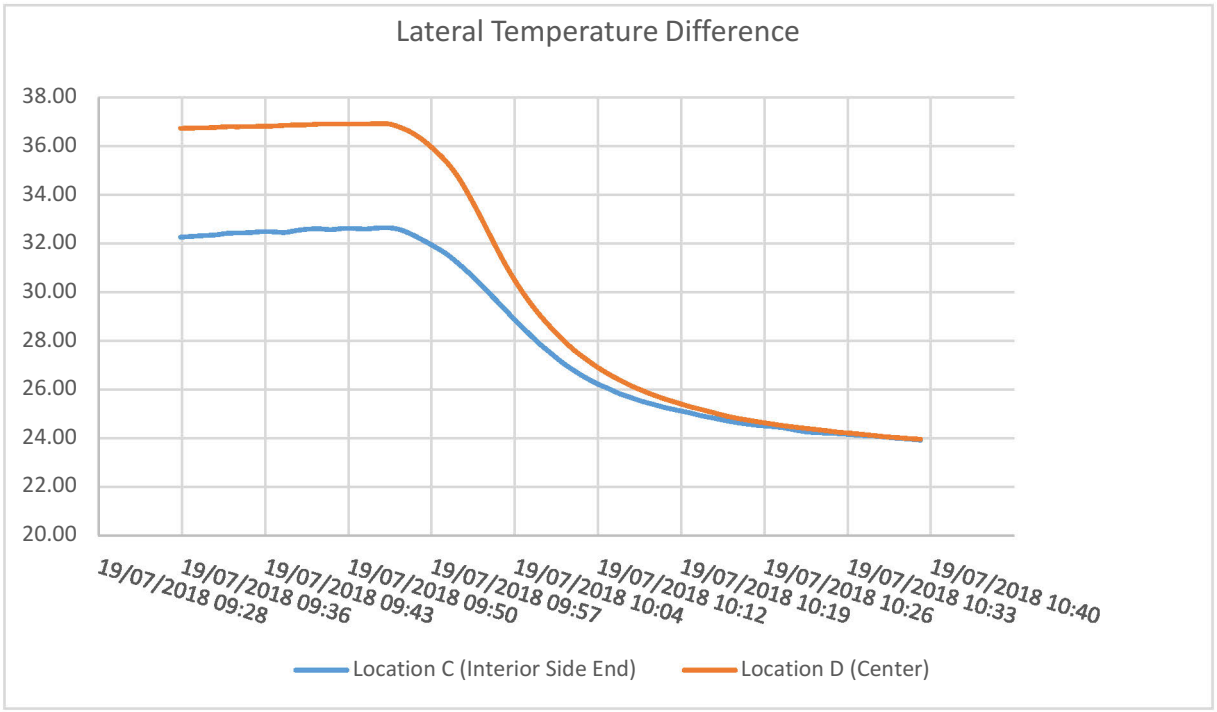

Figure 9.56 - Widthwise Temperature Difference of Heat Exchanger (Heating)

9.5 CFD Model

This section describes the results achieved from CFD modelling of ACB under heating and cooling, coupled with test rooms and the challenges faced during ACB modelling and assumptions made to simplify the geometry. The beam was equipped with 186 nozzles i.e. 93 nozzles of approx. 3.5 mm diameter in each side. Initially, efforts were made to model the actual geometry of the chilled beam inside the office to study temperature and air distribution for the office, however, many issues were found as explained below.

Issues with CFD Model of ACB

Complexity of Beam Structure

Active Chilled Beam has quite complex geometry as shown in Figure 9.57 due the addition of heat exchanger and high-velocity nozzles. The size of the beam and the size of nozzles are quite smaller as compared to the room dimensions which required high-density mesh and elements (elements more than 100,000,000 when coupled with the room) to correctly mesh each and every nozzle with the room which increases computational cost, time and intensity.

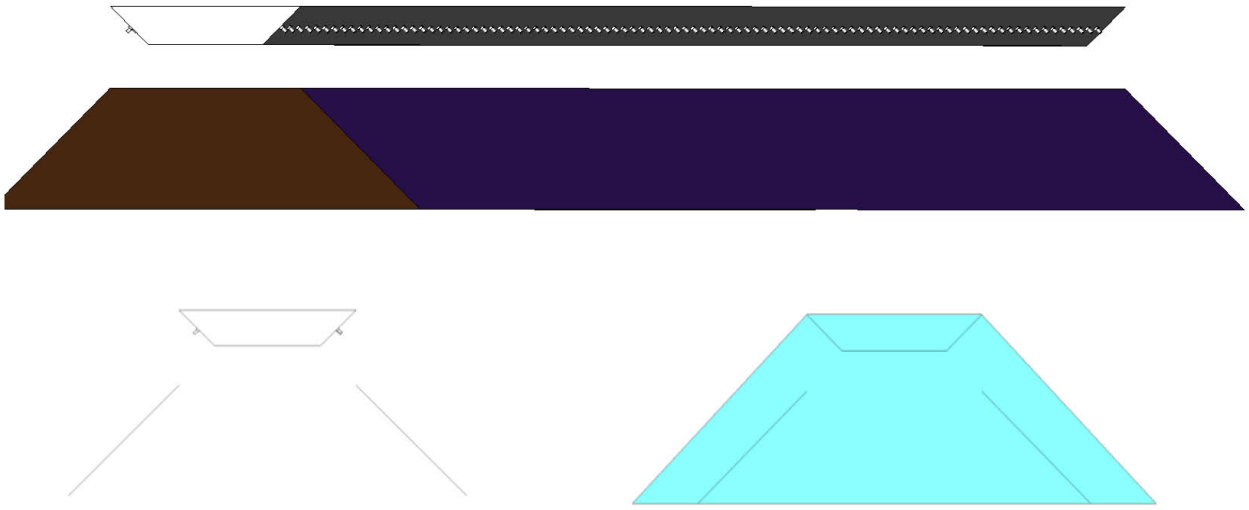

Figure 9.57 - Active Chilled Beam Complex Geometry Model in CFD

Simplified Model Approach

Although, Computational fluid dynamics (CFD) is gaining popularity as an analytical tool for indoor environment design and to improve knowledge and prediction of HVAC systems. Unfortunately, the major drawback as discussed earlier is modelling the complete beam with very tiny nozzles into the room which is much smaller compared to room size. To study the flow pattern through the nozzles to the room and further room air flow by the whole beam requires extensive mesh which proportionally increases the computation cost and most of the time resulted in inaccurate solution during the study. Therefore, a simplified beam modelling approach has been adopted in the study.

This strategy was adopted by Jelena in her paper where she confirmed that the requirements for modeling the flow inside an air terminal unit such as diffusers or ACB to predict the outflow characteristics are much different and incompatible with the requirements for modeling the corresponding room airflow [45]. Therefore, 2 different models are made in the study.

1. A small slice of ACB model without room to study the flow patterns inside the beam.

2. Simplified beam model coupled with the test rooms to study the room air flow distribution.

A simplified model of ACB was made with panels available in scStream (panels are '0' thickness flat surfaces modeled as "Condition Region"). The beam consisted of 2 supply slots and one big induction surface as shown in Figure 9.58. The mass flow inlet condition was specified at a certain discharge angle from supply slots which includes both the primary and secondary airflow assuming at the same temperature after mixing well in the mixing air plenum. The total mass flow rate and temperatures were obtained from the field experiments based on equation 9.2. Induction surface was also given a mass flow outlet boundary condition based on the average induction velocity measured from the field experiment. It is to be noted that as ACB works on induction, and the pressure drop across the beam induction surface and discharge slot is huge which results in low velocity at the induction surface. Any additional pressure drop by any measuring device to measure the discharge flow rate would give the incorrect value. Therefore, the total supply flowrate from ACB cannot be measured by any method like flow hood or any other device like anemometers ad the velocity profile is varying

across the length and width of the open slot. The same is recommended by the manufacturers as below.

Note
Do not attempt to read the total discharge airflow rate using a hood or any other device that adds down-stream pressure to the beam, as it will reduce the amount of induction and give false readings.
The total air flow (primary + induced) cannot be measured.

If Q_I is Induced mass flowrate, A_I is the induction surface area of the ACB and induced velocity measured from the experiment is V_I, then Q_I can be calculated as below

$$Q_I = A_I \times V_I \quad 9.1$$

If primary airflow is Q_P then the total mass flow rate (Q_T) from the ACB is given as

$$Q_T = Q_P + Q_I \quad 9.2$$

The primary air volume can be calculated based on measured static pressure difference (ΔP) between the ACB primary air plenum and the room which is given by

$$Qp = K\sqrt{\Delta P} \quad 9.3$$

where K is constant and is given by the manufacturer of the beam based on the length of ACB and type of nozzle, the study has a beam of 8' length and with Z nozzle type, from the manufacturer catalog in Appendix A, the constant K is found to be 67.

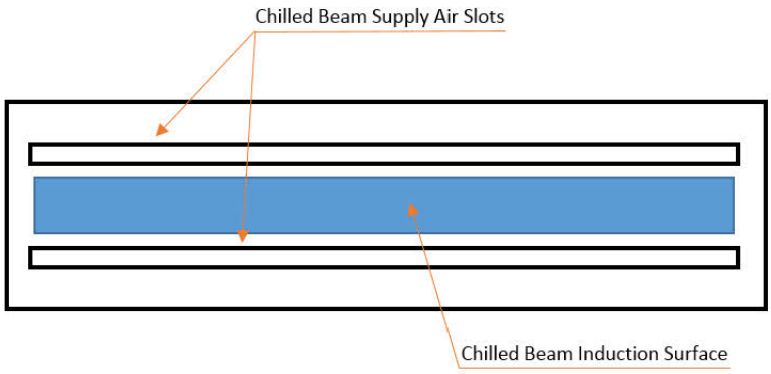

Figure 9.58 - Active Chilled Beam Flat Panel Model

Beam Model

The Figure 9.59 shows a slice of beam 54 mm wide (cross section) of a beam with 2 nozzles only, the primary air is injected from the nozzle on each side of the beam in the supply slot. The beam is open at the bottom, the two extreme sides are supply slots (outlet) and the middle section is induced surface (typically house a heat exchanger and is covered with a perforated sheet metal to induced air. The nozzle diameter and beam plenum pressure are designed to have a high-velocity primary injected into the slot which induces room air through induction surface. The higher the air velocity (or primary airflow rate), higher the induction. The same phenomenon can be seen in Figure 9.60. The airspeed is high at the nozzle but as air travels in such a wide space and due to the mixing of induced air with the primary air, the velocity of mixed air drops drastically. Higher induction near nozzle can be seen because of higher air velocity, as the velocity reduces the amount of induced air reduces as well while travel. Most of the air goes out by the supply slot, however, a small about of air constructs a vortex which further helps in the induction of room air.

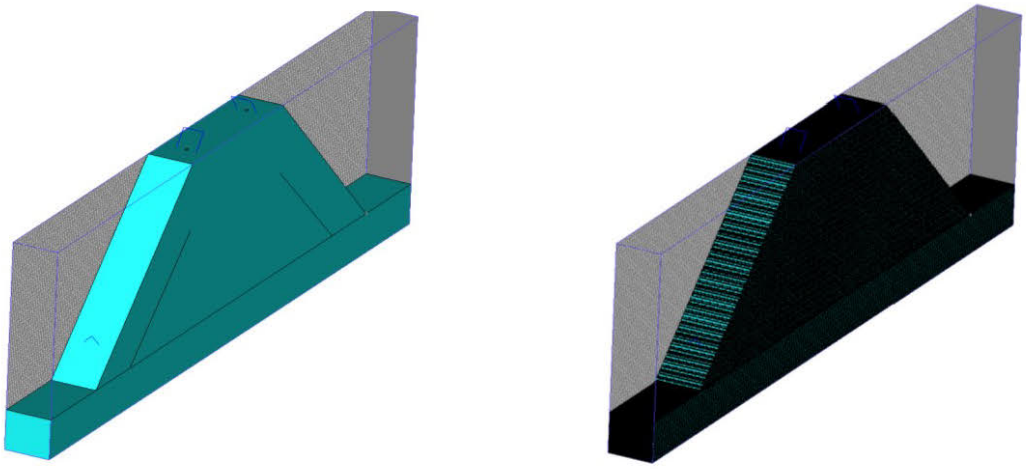

Figure 9.59 - Section of ACB with One Nozzle on Each Side

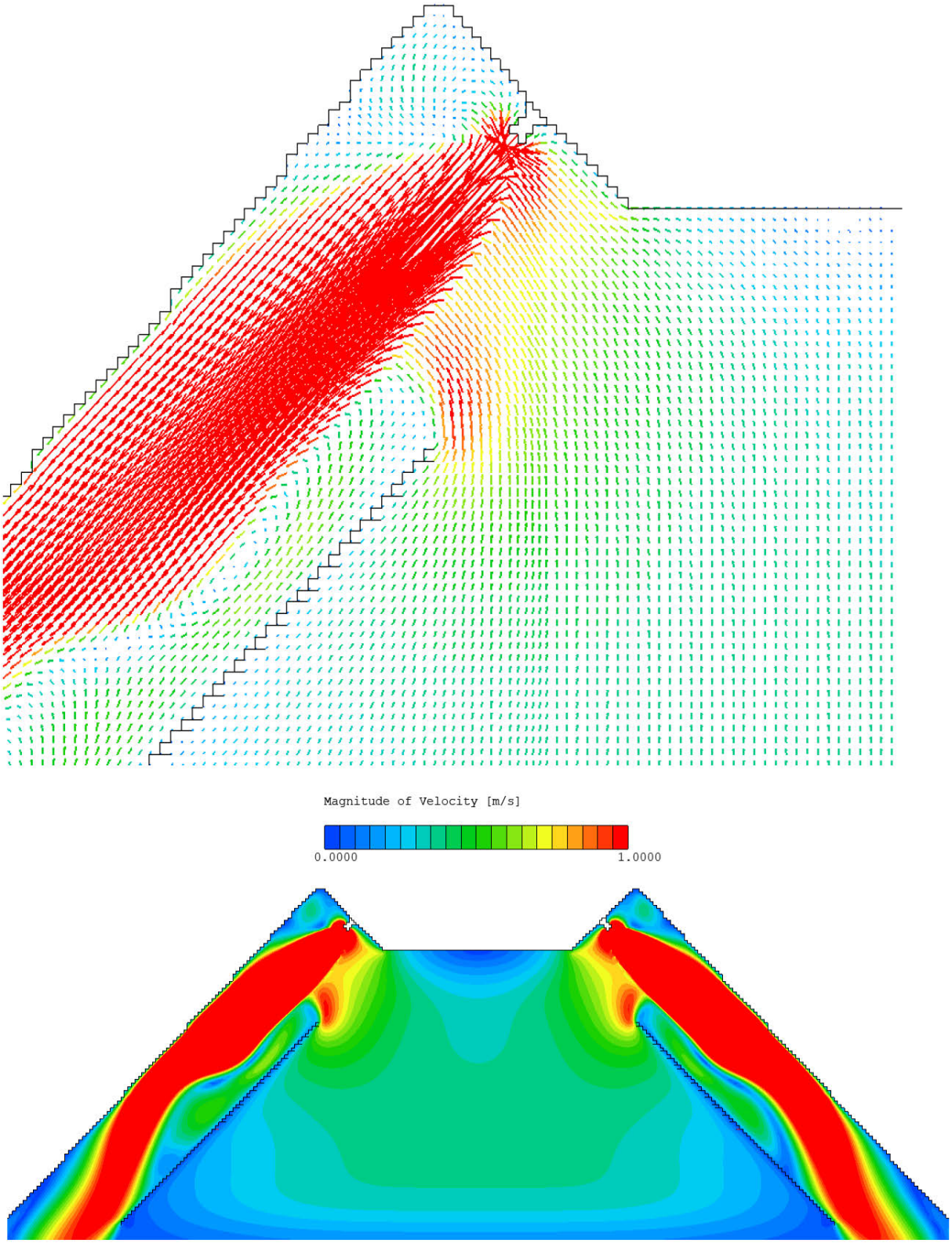

Figure 9.60 - Velocity Profile inside an ACB

Discharge Angle of Mixed Air

Discharge angle of Active Chilled Beam is the angle at which the mixture of primary and secondary air leaves the slot of the beam. The angle is very important to obtain the throw of the supply jet and “Coanda Effect” so that the outlet airflow can travel touching to the ceiling and the walls and enable proper mixing of room air to provide heating and cooling. If the discharge angle is not appropriate which could result in a direct throw of air in the occupied area, no Coanda effect, and non-uniform mixing of the air. It is difficult to obtain the angle of the discharged air from the beam slot and therefore smoke patterns are used to approximately guess the discharge angle or PIV measurements are done to calculate the discharge angle correctly. The angle of discharge is not published by the manufacturers but it is really important for the effective performance of beam and to model the airflow from the beams. Figure 9.61 to Figure 9.63 shows the effect on velocity profile (room airflow) with various discharge angle. At 60° angle, the Coanda effect totally vanishes and the ACB throw directly in the occupied zone as shown in Figure 9.63

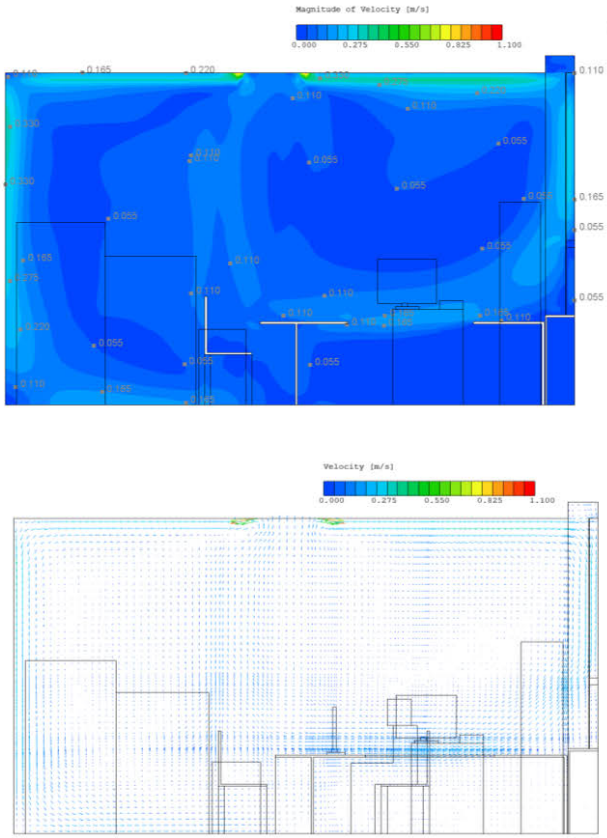

Figure 9.61 - Velocity Contour and Velocity Vectors at 26° Discharge Angle

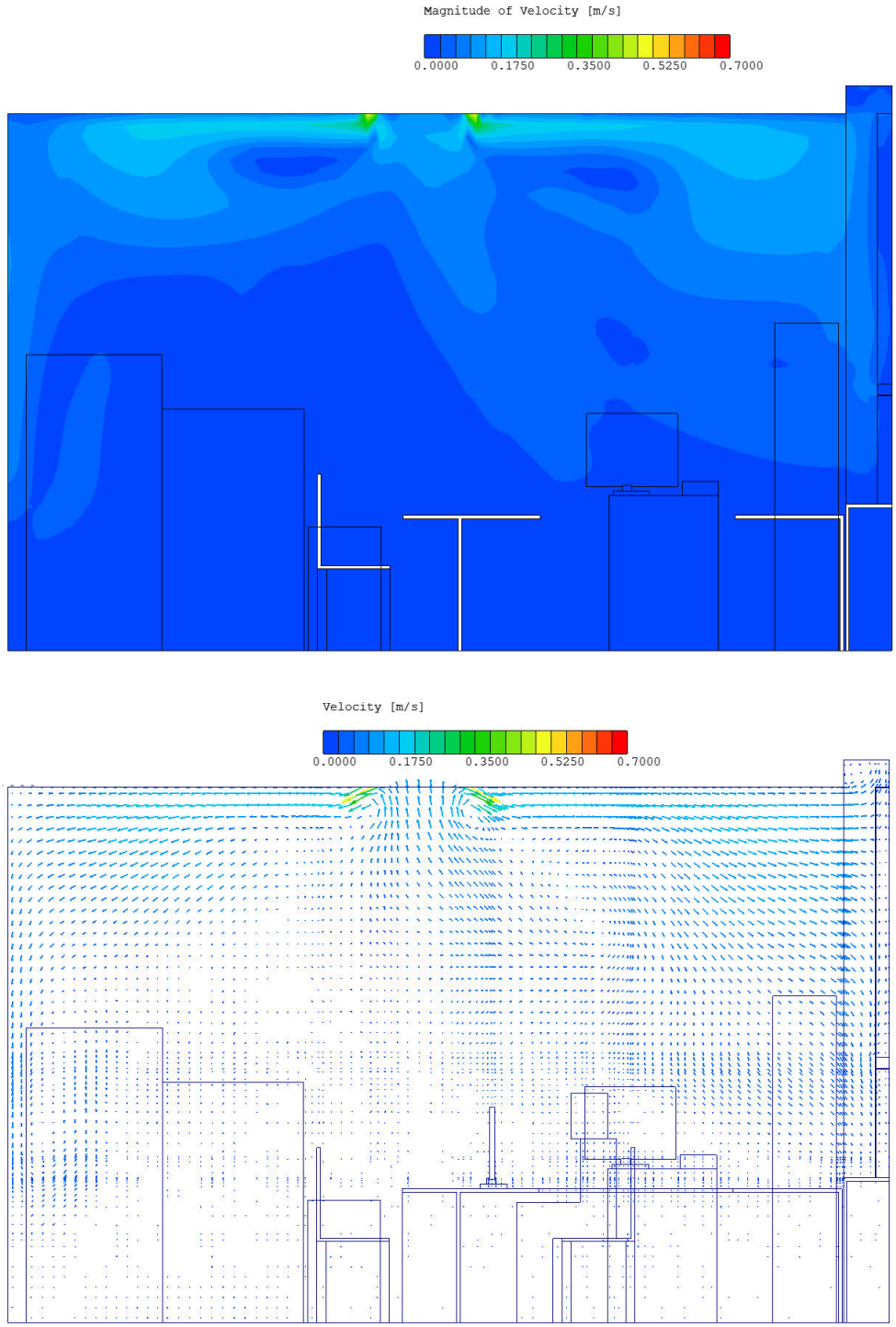

Figure 9.62 - Velocity Contour and Velocity Vectors at 45° Discharge Angle

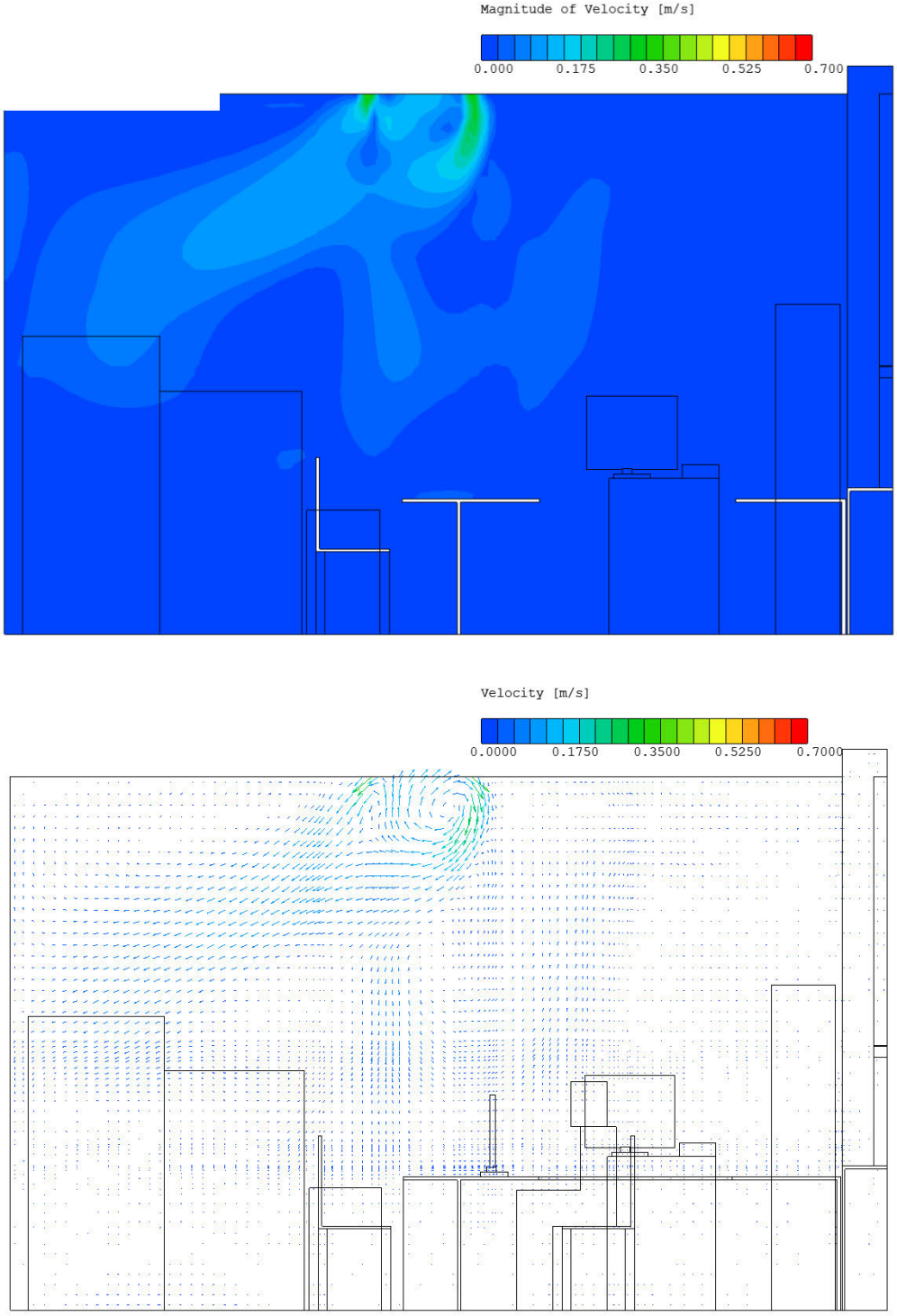

Figure 9.63 - Velocity Contour and Velocity Vectors at 60° Discharge Angle

Induction phenomenon

The key design feature of Active Chilled Beam is its induction process, ACB is supplied with primary air which induces airflow from the room, and mixed air is then supplied back to the room which enhances air change per hour and ensures proper mixing of air. To correctly simulate the induction velocity at the induction surface, the pressure loss at the induction surface is required to be specified. The pressure difference (loss) between the room and the heat exchanger was difficult to measure with the limitation of available instruments. If pressure loss is not specified correctly, it results in higher induction velocity as induced air flows without resistance. The biggest challenge in the CFD model was to set up such a condition. Further, most of the previous studies had considered the induction surface at '0' (zero) pressure condition, ignoring the pressure loss at the induction surface and not simulating the induction phenomenon in their model. The '0' pressure case could be used when the room is symmetrical and has no heat load in the room or symmetrical heat load in the room. However, when there is a heat load in the room and especially if the heat load is asymmetric the '0' pressure condition should not be used at beam induction surface because the asymmetric heat load increases the thermal plumes and air velocity above the heat load and therefore induction velocity increases above higher heat load area, which results in equal reduction in velocity at the other 0 pressure condition. This effect was tested with the experimental results and induction flowrate was found higher in the CFD model in the high heat load zone. Therefore, it is advisable to use manufacturer data in absence of field/experimental data to model a beam to assign a boundary condition at the induction surface. Manufacturer provides Induction Ratio (IR) of the beam which can be used to set the boundary condition (velocity condition or mass flowrate condition) and further analyses could be completed to select the beam for any space.

9.5.1 CFD Model of Test Room 1 (Under Heating)

CFD model of Test Room 1 is shown in Figure 9.64. The model was given boundary conditions as described earlier in Chapter 8 based on experimental data. The analyses were done for room setpoint of 20°C and 24°C and the results are shown in Figure 9.65 to Figure 9.74. Figure 9.65 clearly shows the difference in temperature in the room and thermal stratification. Although CFD predicted higher air velocities in the room than the experimental values, Figure 9.68 shows that the air velocity is still much lower in all areas. For room setpoint 24°C, a larger difference in temperature is seen as shown in Figure 9.71 and air velocity much lesser and close to zero in all areas as shown in Figure 9.74.

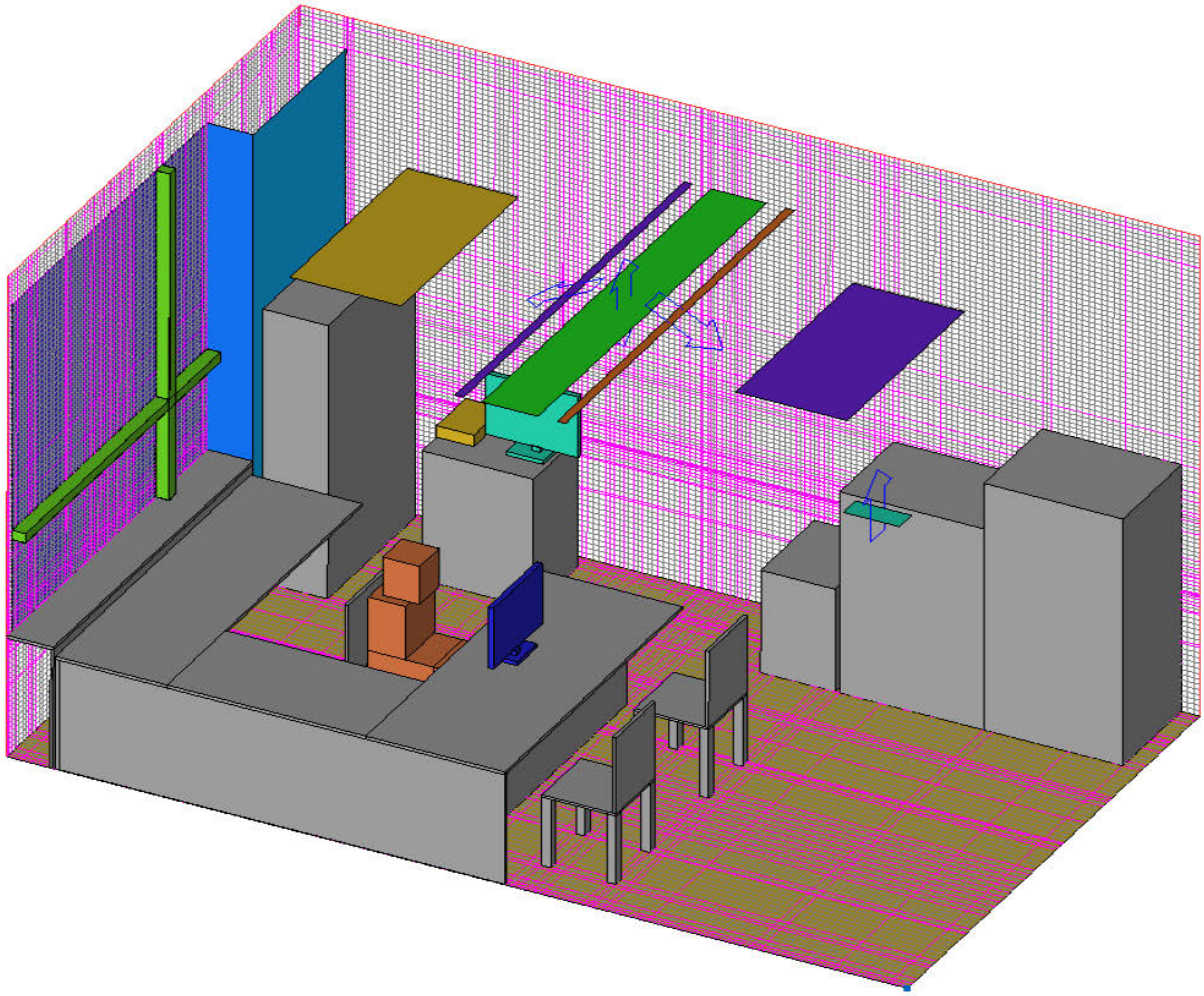

Figure 9.64 - CFD Model of Test Room 1 (Heating)

CFD Results at Room Setpoint 20°C (Heating)

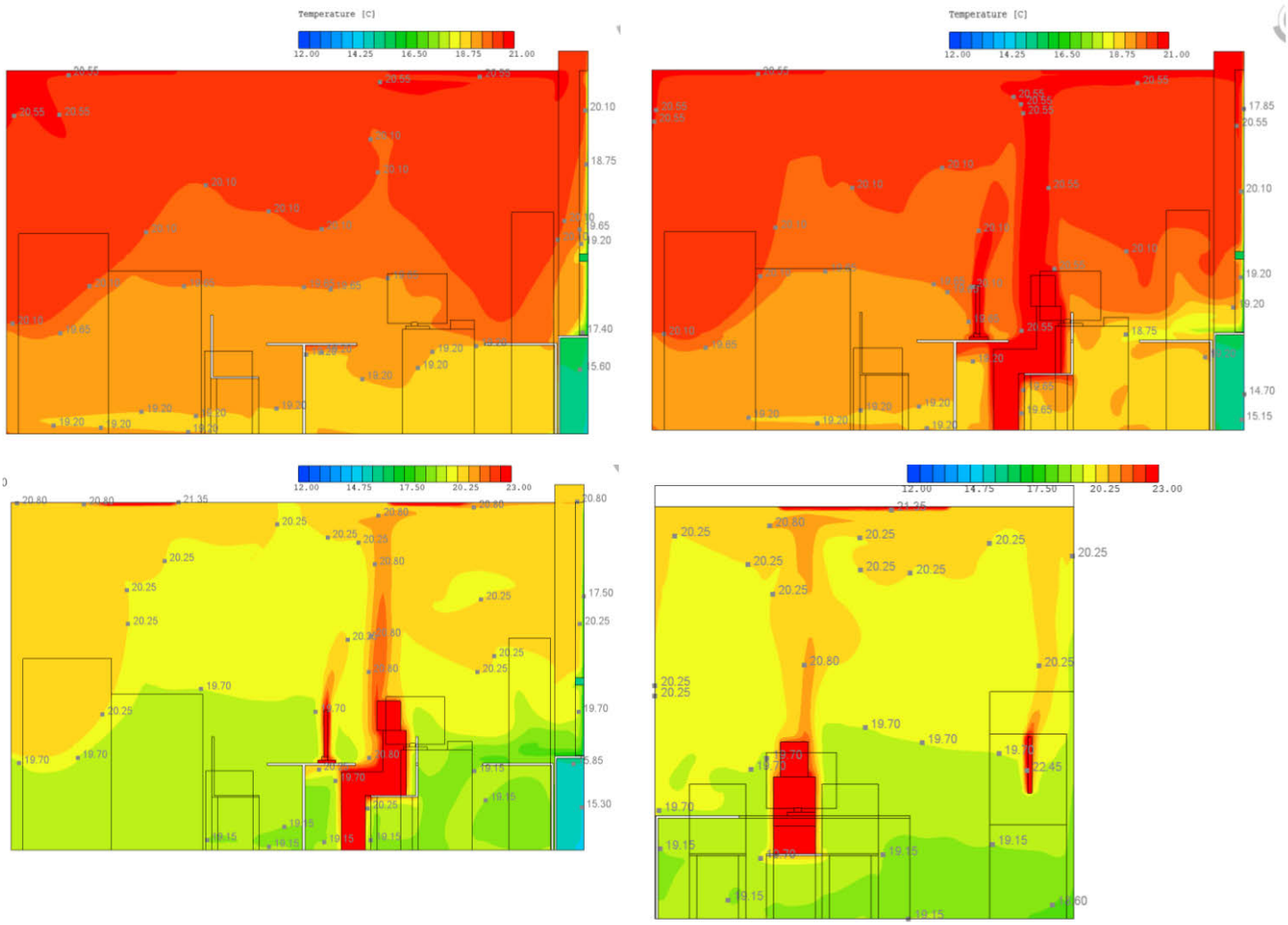

Figure 9.65 - Temperature Contour Plot at Different Room Sections at Setpoint 20 °C (Heating)

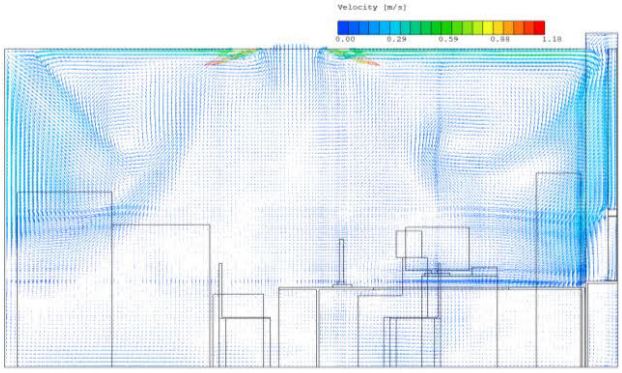

Figure 9.66 - Velocity Vector Plot at 20°C (Heating)

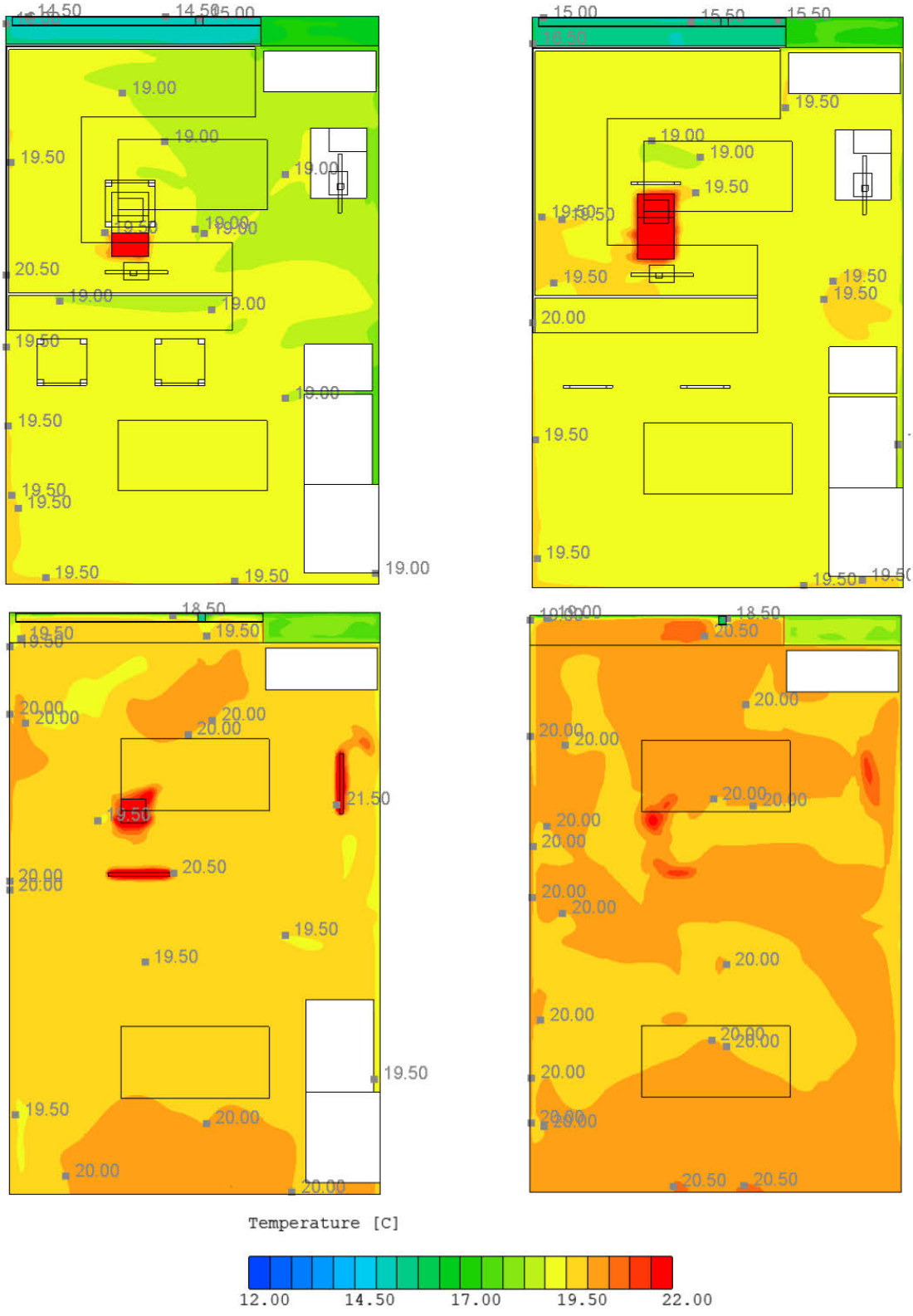

Figure 9.67 - Temperature Contour Plot at Room Height 0.1 m, 0.6 m, 1.1 m and 1.7 m at 20°C (Heating)

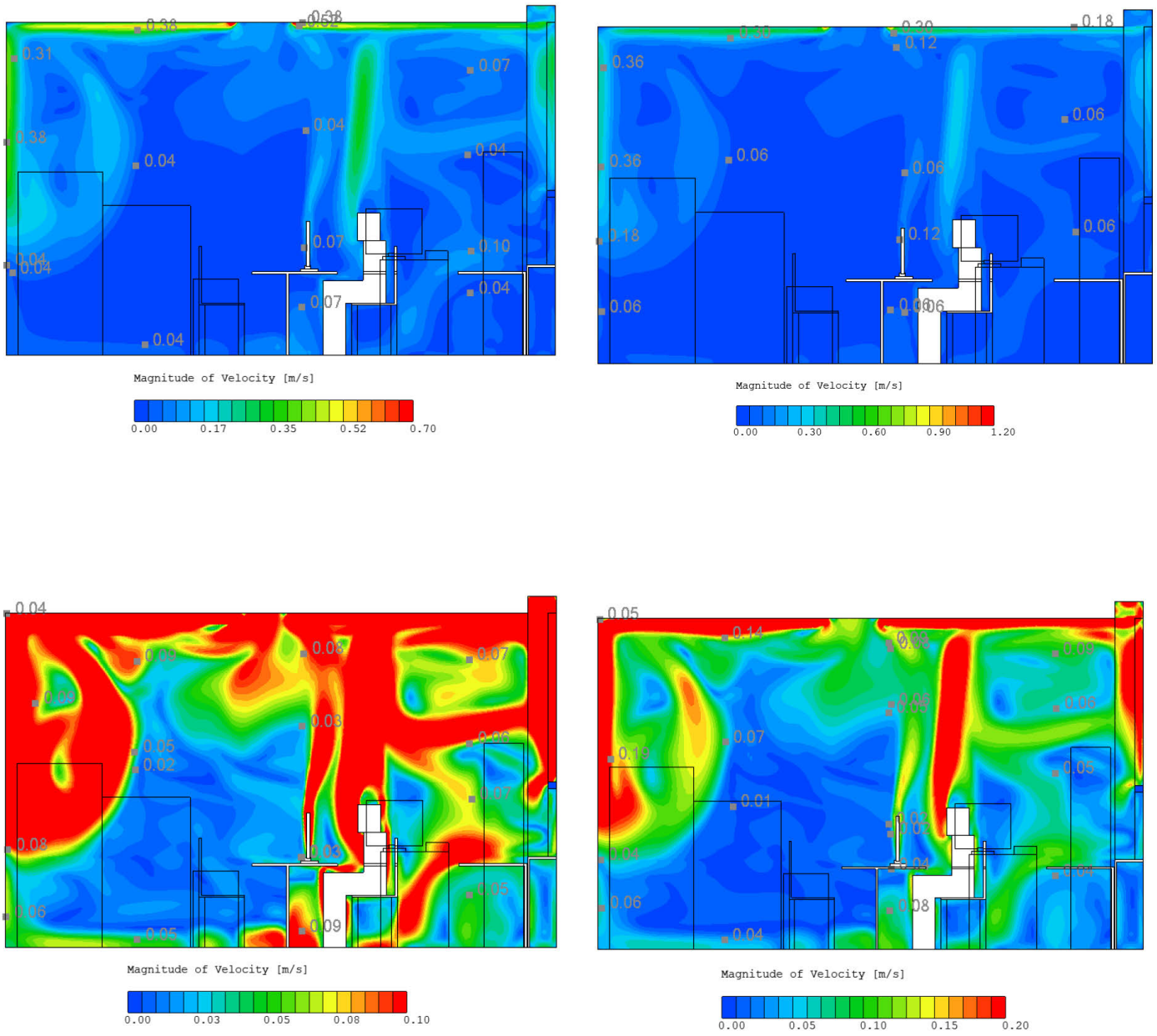

Figure 9.68 - Velocity Contour Plot – Room Sections - at Different Range of Velocity at 20°C (Heating)

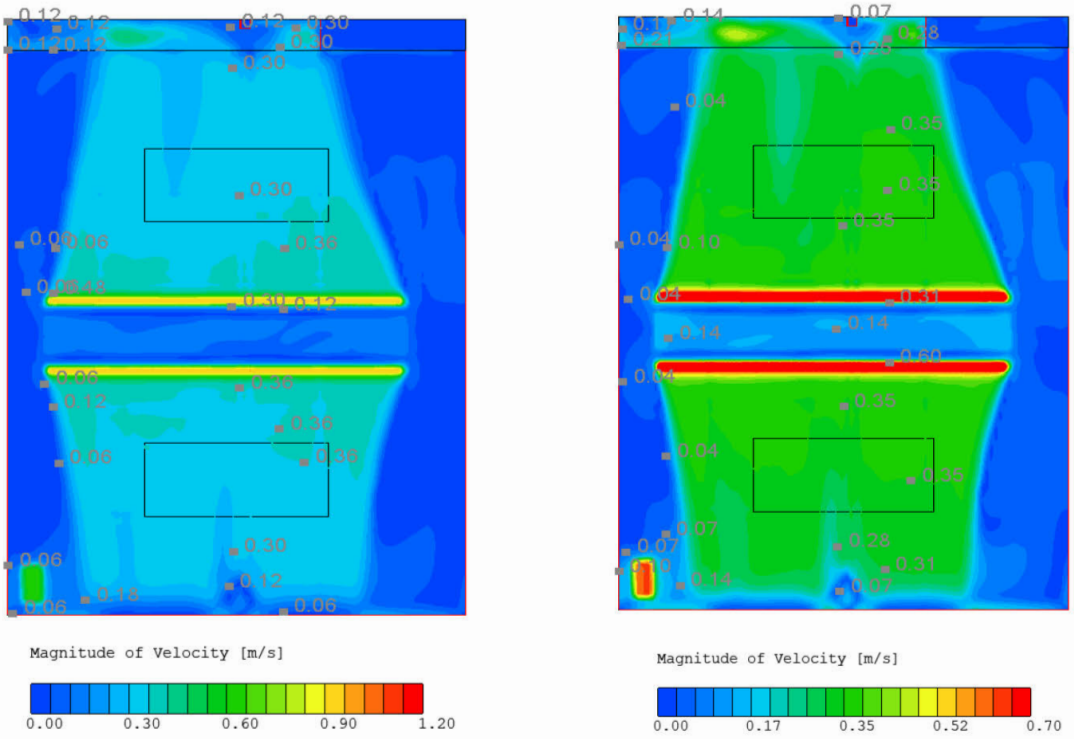

Figure 9.69 - Velocity Contour Plot at 2.945 m Height at 20°C (Heating)

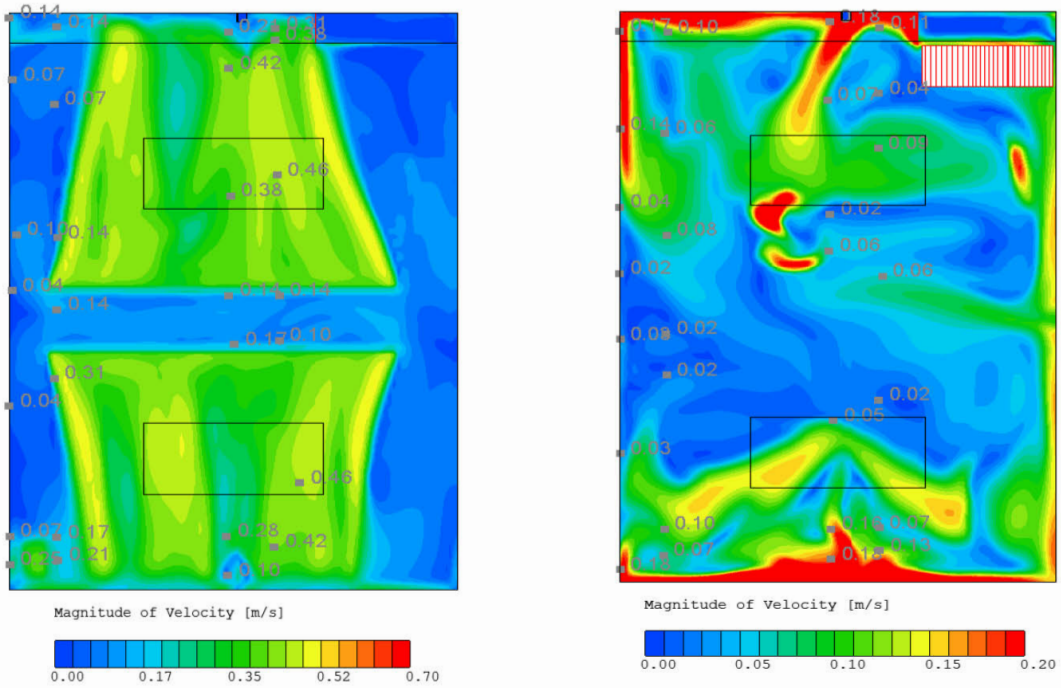

Figure 9.70 - Velocity Contour Plot at 2.9 m Height (Left) and 1.8 m Height (Right) at 20°C (Heating)

Table 9.2 - Temperature and Velocity Comparison of Experiment and CFD Model at 20°C (Heating)

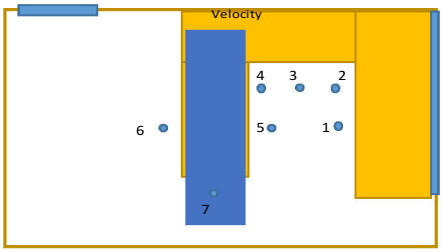

Possible Occupant's Location in Room

Room Set Point	20 °C
Chilled Beam Supply Temperature	20.3 °C
Chilled Beam Return Temperature	20.3 °C
Chilled Beam Supply Velocity	1.2 m/s
Chilled Beam Return Velocity	0.11 m/s

[m] [m]

Experimental Result								
Point No	Air Velocity (m/s)				Air Temperature (°C)			
	Height (m)				Height (m)			
	0.1	0.6	1.1	1.7	0.1	0.6	1.1	1.7
1	0.02	0.03	0.09	0.07	19.1	20.0	20.6	20.6
2	0.00	0.05	0.13	0.05	19.0	19.9	20.5	20.7
3	0.00	0.07	0.15	0.06	19.1	20.0	20.2	20.5
4	0.01	0.05	0.06	0.03	18.9	19.9	20.1	20.4
5	0.01	0.07	0.07	0.06	19.1	20.0	20.6	20.6
6	0.02	0.02	0.06	0.06	19.1	20.0	20.6	20.6
	CFD Model Result							
Point No	Air Velocity (m/s)				Air Temperature (°C)			
	Height (m)				Height (m)			
	0.1	0.6	1.1	1.7	0.1	0.6	1.1	1.7
1	0.04	0.02	0.06	0.10	18.8	19.1	20.2	20.3
2	0.02	0.04	0.03	0.07	19.2	19.2	19.6	20.1
3	0.02	0.03	0.01	0.03	19.1	19.2	19.7	19.9
4	0.03	0.07	0.02	0.03	19.4	19.6	19.7	19.9
5	0.07	0.02	0.02	0.02	19.1	19.1	19.6	19.9
6	0.05	0.01	0.01	0.02	19.1	19.4	19.5	19.9
	Absolute Error							
Point No	Air Velocity (m/s)				Air Temperature (°C)			
	Height (m)				Height (m)			
	0.1	0.6	1.1	1.7	0.1	0.6	1.1	1.7
1	0.02	0.01	0.03	0.03	0.30	0.90	0.40	0.30
2	0.02	0.01	0.10	0.02	0.20	0.70	0.90	0.60
3	0.02	0.04	0.14	0.03	0.00	0.80	0.50	0.60
4	0.02	0.02	0.04	0.00	0.50	0.30	0.40	0.50
5	0.06	0.05	0.05	0.04	0.00	0.90	1.00	0.70
6	0.03	0.01	0.05	0.04	0.00	0.60	1.10	0.70
	% Error							
Point No	Air Velocity (m/s)				Air Temperature (°C)			
	Height (m)				Height (m)			
	0.1	0.6	1.1	1.7	0.1	0.6	1.1	1.7
1	100.0	33.3	33.3	42.9	1.6	4.5	1.9	1.5
2	-	20.0	76.9	40.0	1.1	3.5	4.4	2.9
3	-	57.1	96.0	50.0	0.0	4.0	2.5	2.9
4	200.0	40.0	66.7	0.0	2.6	1.5	2.0	2.5
5	600.0	71.4	71.4	66.7	0.0	4.5	4.9	3.4
6	150.0	50.0	85.0	71.7	0.0	3.0	5.3	3.4

CFD Results for Room Set Point 24°C (Heating)

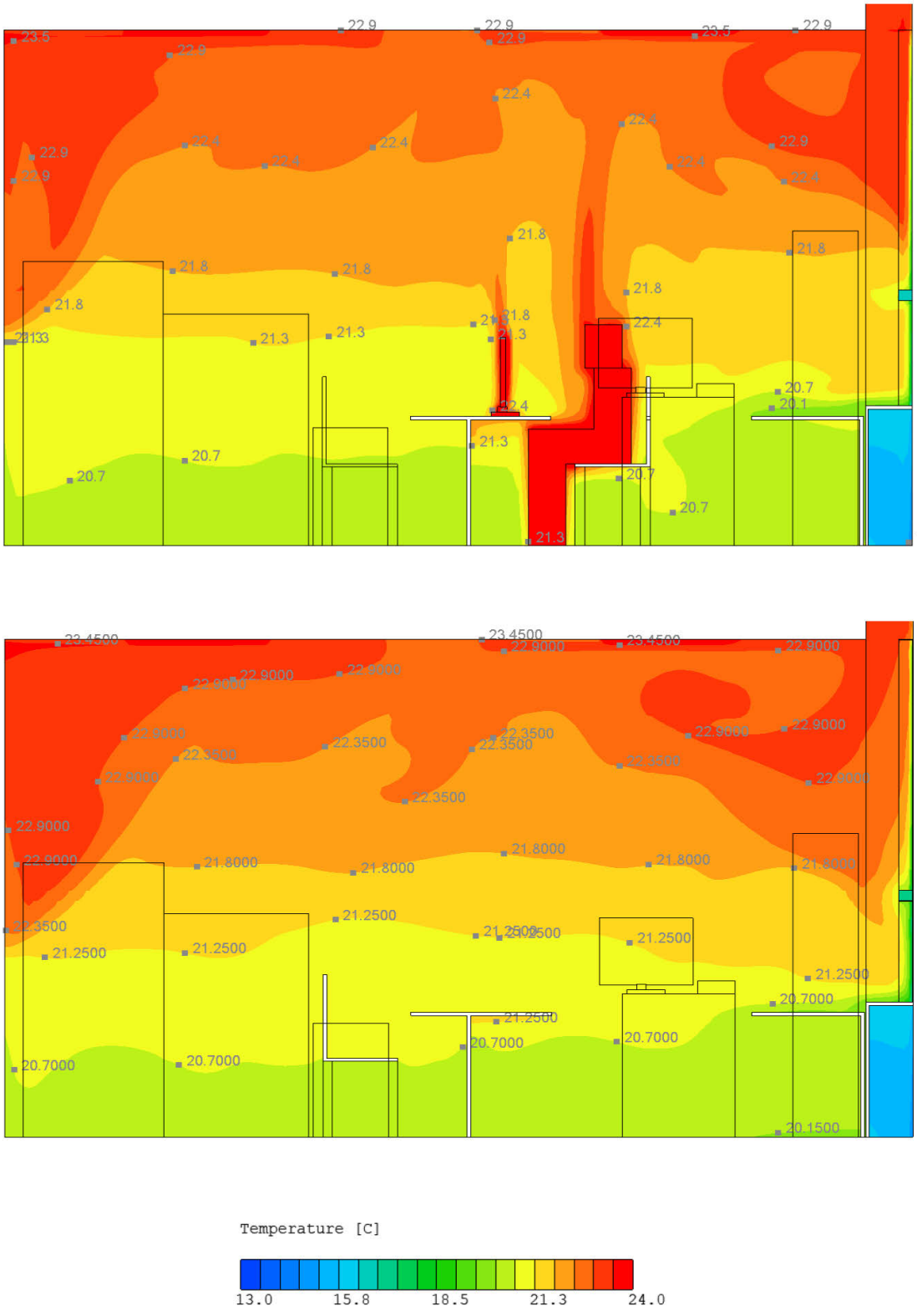

Figure 9.71 - Temperature Contour Plot - Different Room Sections at Setpoint 24°C (Heating)

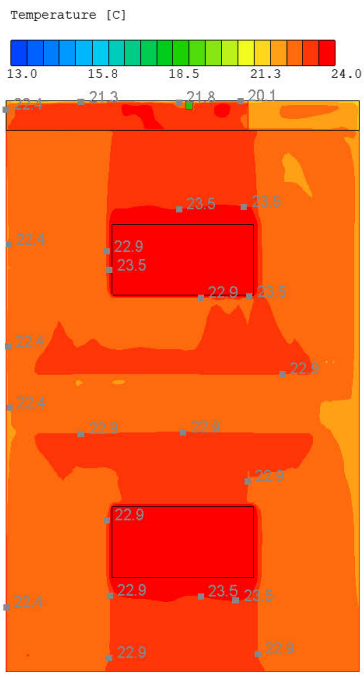

At 2.945 m Height

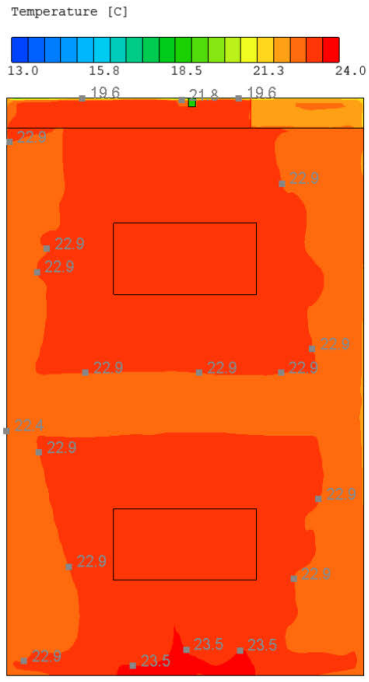

At 2.90 m Height

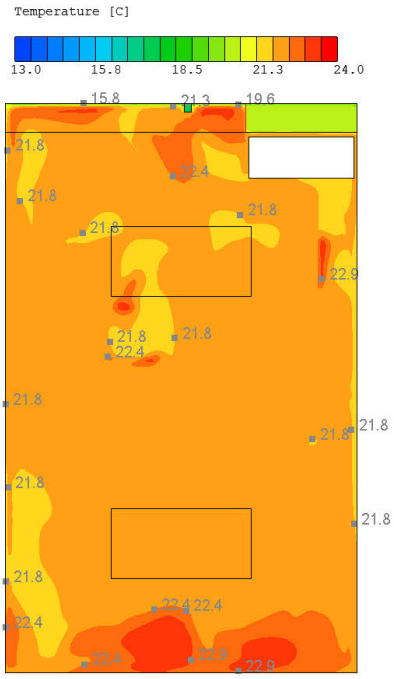

At 1.70 m Height

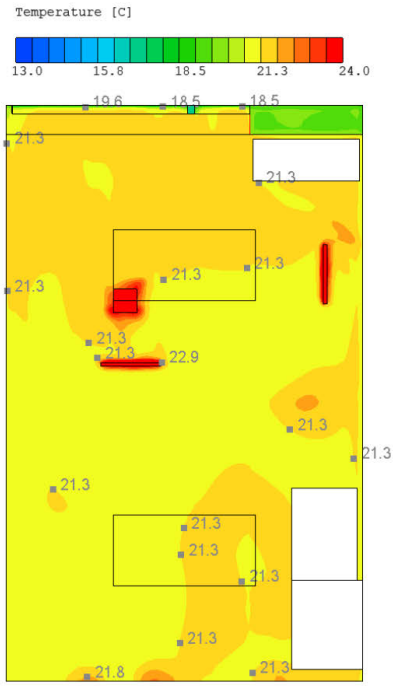

At 1.1 m Height

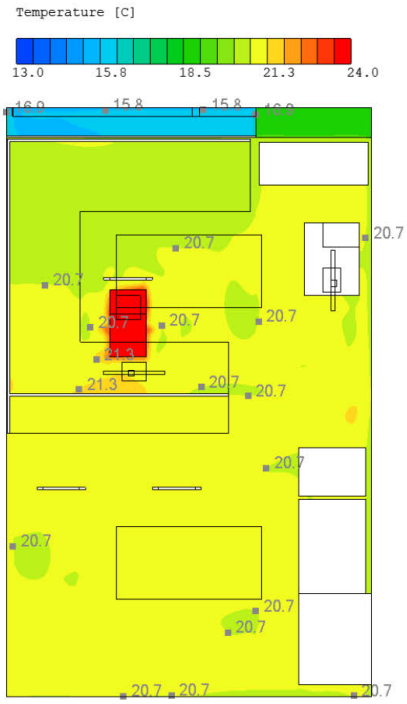

At 0.6 m Height

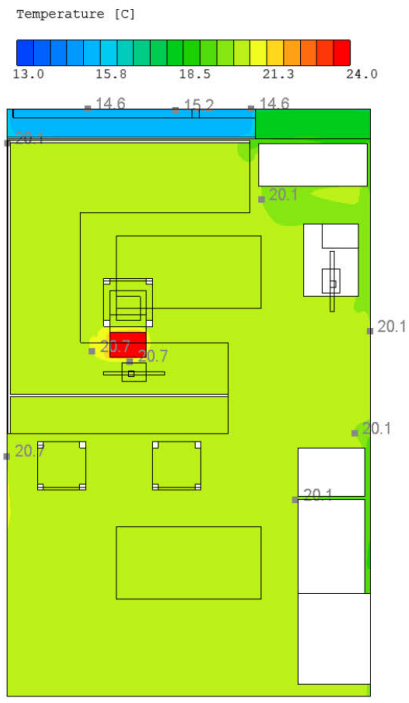

At 0.1 m Height

Figure 9.72 - Temperature Contour Plot at Different Room Heights at SP 24°C (Heating)

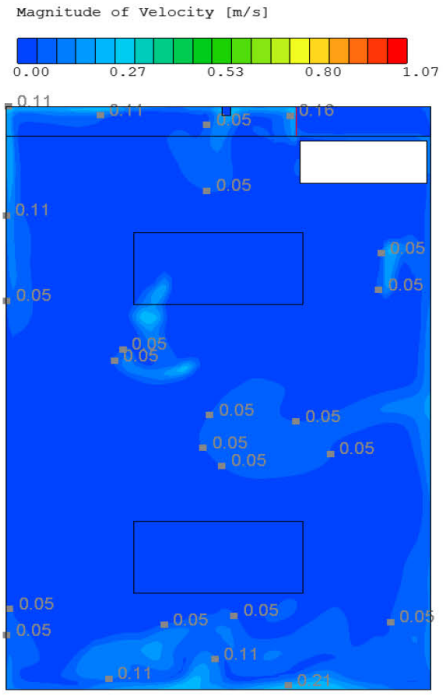

At 1.7 m Height

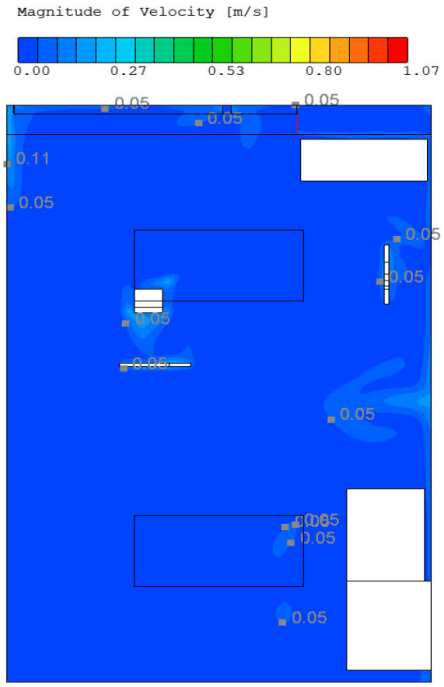

At 1.1 m Height

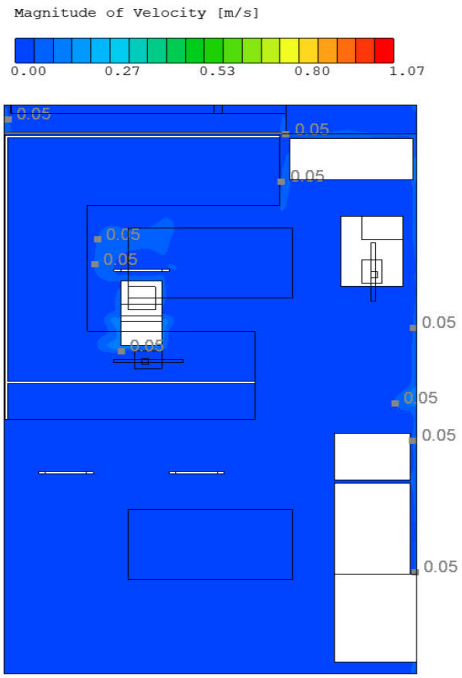

At 0.6 m Height

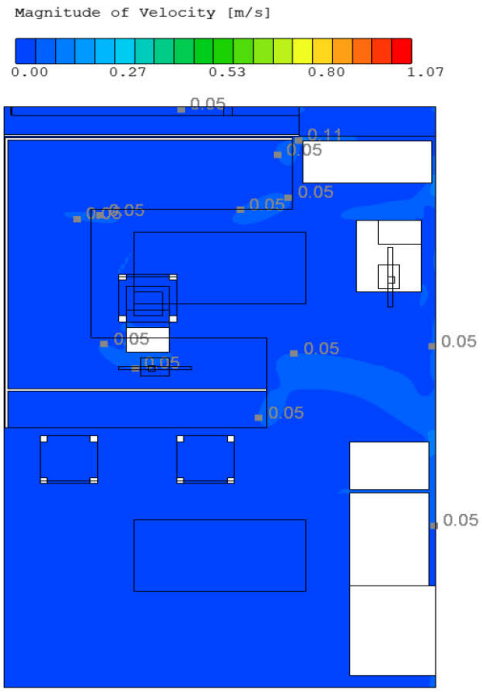

At 0.1 m Height

Figure 9.73 - Velocity Contour Plot at Different Room Heights at SP 24°C (Heating)

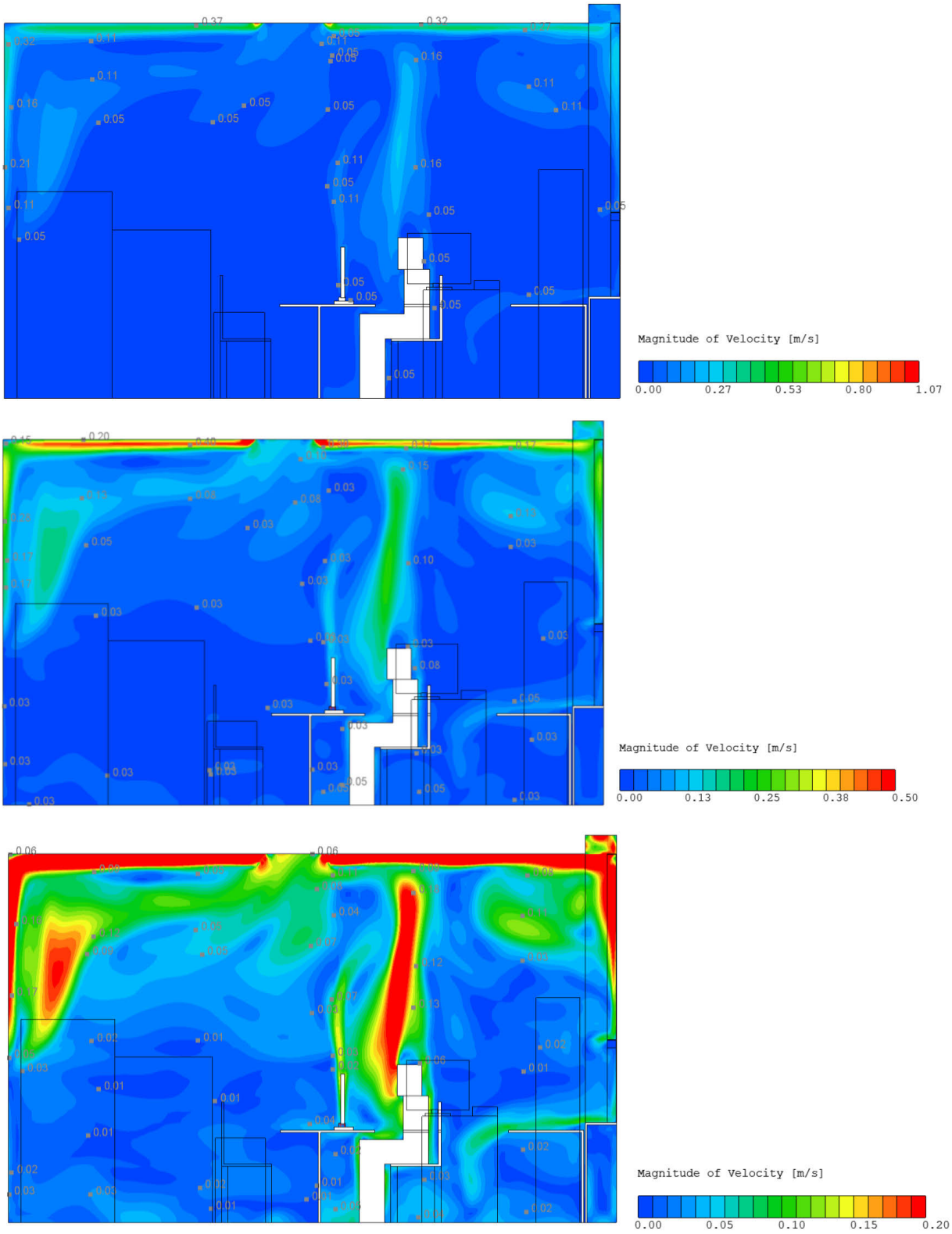

Figure 9.74 - Velocity Contour Plot at Different Room Sections at SP 24°C (Heating)

Table 9.3 - Temperature & Velocity Comparison of Experiment and CFD Model at 24°C

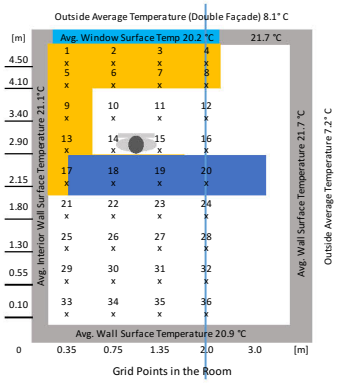

Experimental Result								
Point No	Air Velocity (m/s)				Air Temperature (°C)			
	Height (m)				Height (m)			
	0.1	0.6	1.1	1.7	0.1	0.6	1.1	1.7
36	0.00	0.01	0.07	0.11	20.1	21.2	22.2	22.8
32	0.00	0.00	0.01	0.07	19.8	20.9	22.1	22.7
28	0.00	0.00	0.01	0.06	19.8	21.1	22.2	22.6
24	0.00	0.00	0.00	0.07	19.9	21.3	22.1	22.6
20	0.01	0.01	0.02	0.06	20.3	21.5	22.2	22.6
16	0.01	0.00	0.02	0.02	19.3	20.8	21.8	22.3
12	0.02	0.02	0.02	0.02	19.3	20.8	21.8	22.3
8	0.05	0.05	0.08	0.06	20.7	22.3	22.9	23.1
4	0.02	0.07	0.13	0.17	20.4	20.6	22.4	22.5
	CFD Model Result							
Point No	Air Velocity (m/s)				Air Temperature (°C)			
	Height (m)				Height (m)			
	0.1	0.6	1.1	1.7	0.1	0.6	1.1	1.7
36	0.02	0.01	0.01	0.07	20.5	20.7	21.1	22.9
32	0.03	0.02	0.06	0.03	20.5	20.7	21.3	21.9
28	0.02	0.01	0.06	0.02	20.6	20.7	21.3	22.1
24	0.05	0.01	0.03	0.06	20.5	20.7	21.3	22.0
20	0.05	0.01	0.02	0.07	20.4	20.7	21.1	22.3
16	0.04	0.03	0.02	0.02	20.3	20.7	21.1	22.0
12	0.02	0.01	0.02	0.03	20.4	20.8	21.2	21.8
8	0.04	0.01	0.02	0.08	20.9	21.5	21.9	22.7
4	0.11	0.02	0.04	0.08	19.9	21.7	22.4	22.9
	Absolute Error							
Point No	Air Velocity (m/s)				Air Temperature (°C)			
	Height (m)				Height (m)			
	0.1	0.6	1.1	1.7	0.1	0.6	1.1	1.7
36	0.02	0.00	0.06	0.04	0.38	0.47	1.11	0.12
32	0.03	0.02	0.05	0.04	0.71	0.21	0.82	0.77
28	0.02	0.01	0.05	0.04	0.79	0.38	0.88	0.48
24	0.05	0.01	0.03	0.01	0.56	0.59	0.83	0.63
20	0.04	0.00	0.00	0.01	0.12	0.77	1.07	0.34
16	0.03	0.03	0.00	0.00	1.00	0.08	0.72	0.29
12	0.00	0.01	0.00	0.01	1.05	0.05	0.59	0.46
8	0.01	0.04	0.06	0.02	0.24	0.83	0.98	0.43
4	0.09	0.05	0.09	0.09	0.47	1.14	0.01	0.42
	% Error							
Point No	Air Velocity (m/s)				Air Temperature (°C)			
	Height (m)				Height (m)			
	0.1	0.6	1.1	1.7	0.1	0.6	1.1	1.7
36		24.0	89.3	33.4	1.9	2.2	5.0	0.5
32				63.0	3.6	1.0	3.7	3.4
28				68.1	4.0	1.8	4.0	2.1
24				19.0	2.8	2.7	3.8	2.8
20	386.6	20.4	16.7	12.0	0.6	3.6	4.8	1.5
16	298.0		15.2	13.5	5.2	0.4	3.3	1.3
12	21.8	64.1	0.4	42.0	5.5	0.2	2.7	2.0
8	26.1	80.6	77.2	25.4	1.2	3.7	4.3	1.9
4	462.7	71.8	70.8	50.2	2.3	5.5	0.1	1.9

Table 9.4 - Temperature & Velocity Comparison of Experiment and CFD Model at 24°C (Section 2 - Heating)

Experimental Result (Section 2)								
Point No	Air Velocity (m/s)				Air Temperature (°C)			
	Height (m)				Height (m)			
	0.1	0.6	1.1	1.7	0.1	0.6	1.1	1.7
35	0.00	0.01	0.07	0.13	20.2	21.1	22.3	22.9
31	0.00	0.00	0.01	0.04	19.8	21.0	22.1	22.9
27	0.02	0.02	0.00	0.01	19.8	21.0	22.1	22.8
23	0.01	0.00	0.00	0.01	19.8	21.0	22.0	22.5
15	0.01	0.01	0.01	0.02	19.3	20.8	21.9	22.2
11	0.00	0.00	0.01	0.01	19.4	20.8	21.8	22.2
7	0.01	0.05	0.09	0.05	20.7	22.0	22.7	22.7
3	0.01	0.05	0.13	0.16	20.4	21.1	22.3	22.4
	CFD Model Result							
Point No	Air Velocity (m/s)				Air Temperature (°C)			
	Height (m)				Height (m)			
	0.1	0.6	1.1	1.7	0.1	0.6	1.1	1.7
35	0.01	0.01	0.03	0.22	20.6	20.9	21.5	23.2
31	0.02	0.01	0.02	0.09	20.6	20.8	21.2	22.4
27	0.03	0.02	0.01	0.03	20.5	20.8	21.2	21.9
23	0.02	0.01	0.01	0.04	20.5	20.8	21.1	22.0
15	0.03	0.03	0.04	0.02	20.3	20.7	21.2	21.6
11	0.03	0.03	0.02	0.04	20.3	20.7	21.3	21.8
7	0.03	0.01	0.07	0.07	20.7	21.5	22.2	23.0
3	0.03	0.04	0.04	0.14	19.9	21.6	22.4	23.0
	Absolute Error							
Point No	Air Velocity (m/s)				Air Temperature (°C)			
	Height (m)				Height (m)			
	0.1	0.6	1.1	1.7	0.1	0.6	1.1	1.7
35	0.01	0.00	0.04	0.09	20.5	20.7	21.1	22.9
31	0.02	0.01	0.01	0.05	20.5	20.7	21.3	21.9
27	0.01	0.00	0.01	0.02	20.6	20.7	21.3	22.1
23	0.01	0.01	0.01	0.03	20.5	20.7	21.3	22.0
15	0.02	0.02	0.03	0.00	20.3	20.7	21.1	22.0
11	0.03	0.03	0.01	0.03	20.4	20.8	21.2	21.8
7	0.02	0.04	0.02	0.02	20.9	21.5	21.9	22.7
3	0.02	0.01	0.09	0.02	19.9	21.7	22.4	22.9
	% Error							
Point No	Air Velocity (m/s)				Air Temperature (°C)			
	Height (m)				Height (m)			
	0.1	0.6	1.1	1.7	0.1	0.6	1.1	1.7
35		32.3	52.7	68.4	2.0	1.1	3.4	1.2
31			143.2	124.7	4.0	1.0	4.3	2.1
27	52.0	10.6		244.2	3.8	1.1	4.2	3.9
23	67.9			326.8	3.6	1.1	3.9	2.3
15	197.2	232.4	250.7	15.8	5.1	0.4	3.4	2.7
11			136.6	271.8	4.7	0.4	2.5	1.7
7	200.0	79.4	24.4	42.5	0.2	2.2	2.1	1.1
3	200.0	22.9	65.4	12.9	2.6	2.5	0.5	2.8

9.5.2 CFD Model of Test Room 2 (Under Cooling)

CFD model of Test Room 2 is shown in Figure 9.75. The model was given boundary conditions as described earlier in Chapter 8 based on experimental data. The analysis was done for room setpoint of 22°C and results are shown in Figure 9.76 to Figure 9.81. Figure 9.76 clearly shows that the temperature are uniform all across the room and at all heights in the occupied zone. The air velocity are well below ASHRAE recommended velocity in occupied zone as shown in Figure 9.77.

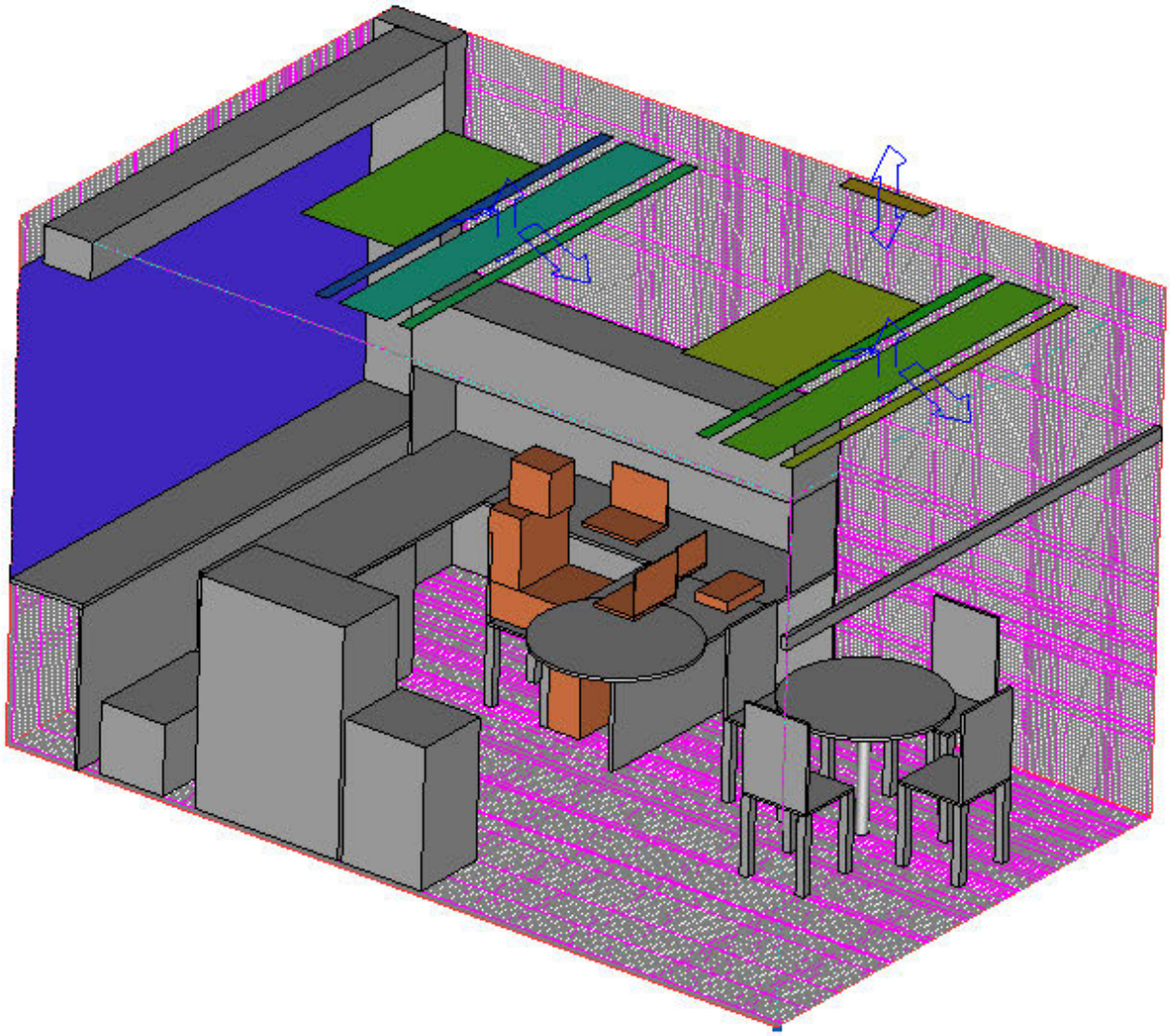

Figure 9.75 - CFD Model of Test Room 2

CFD Results for Room Setpoint 22°C (Cooling)

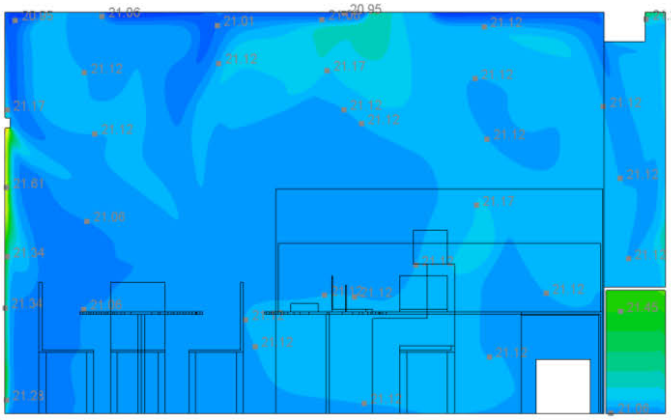

Section 1 (X = 0.75 m)

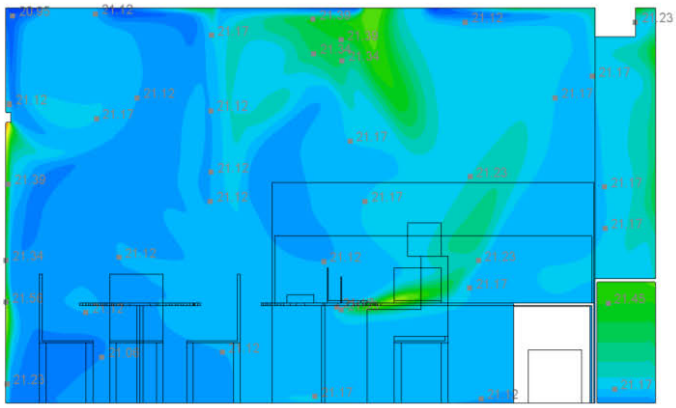

Section 2 (X= 1.2 m)

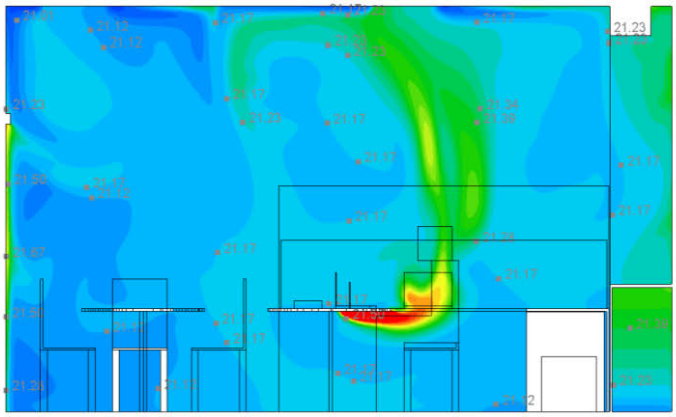

Section 3 (X = 1.6 m)

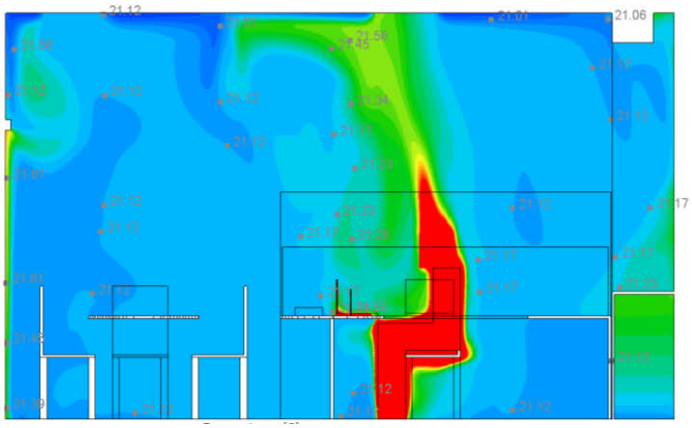

Section 4 (X = 2.2 m)

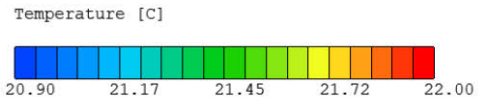

Figure 9.76 - Temperature Contour Plot at Room Setpoint 22 °C

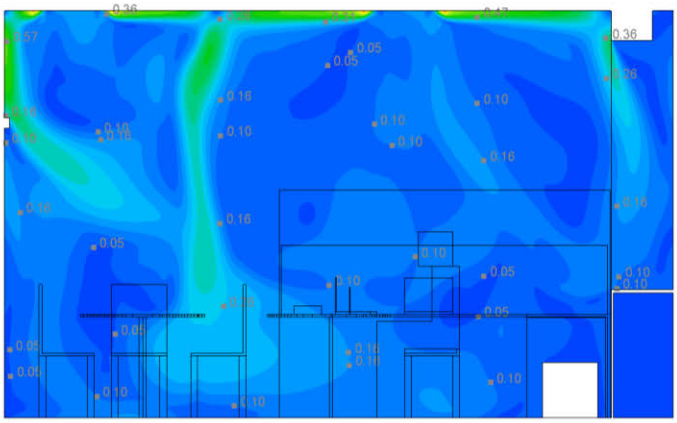

Section 1 (X = 0.75 m)

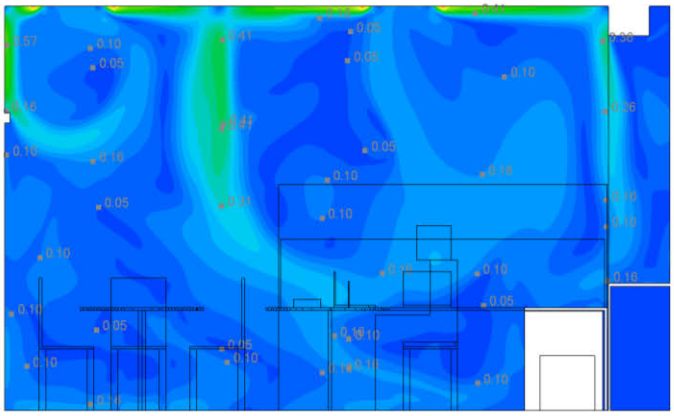

Section 2 (X= 1.2 m)

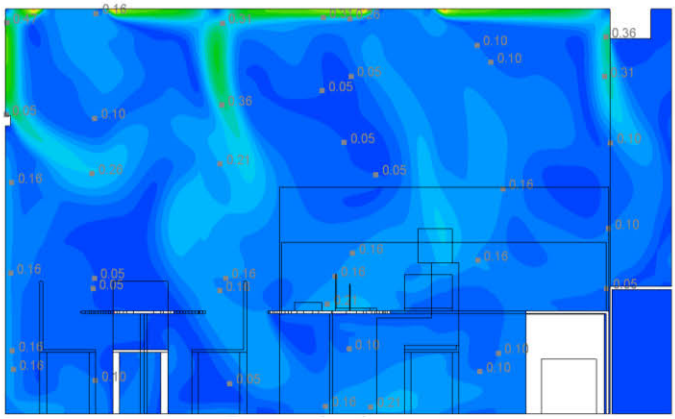

Section 3 (X = 1.6 m)

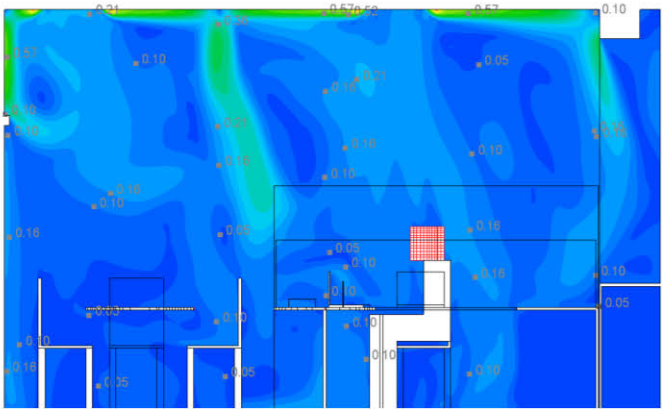

Section 4 (X = 2.2 m)

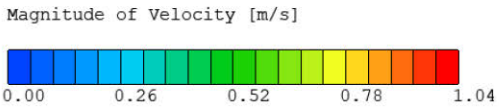

Figure 9.77 - Velocity Contour Plot at Room Setpoint 22 °C

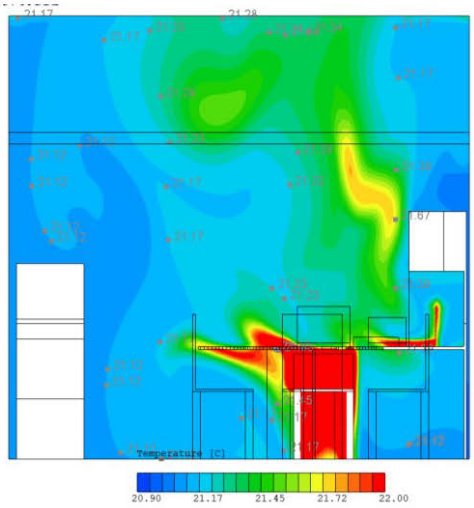

Section Y at 2.91 m

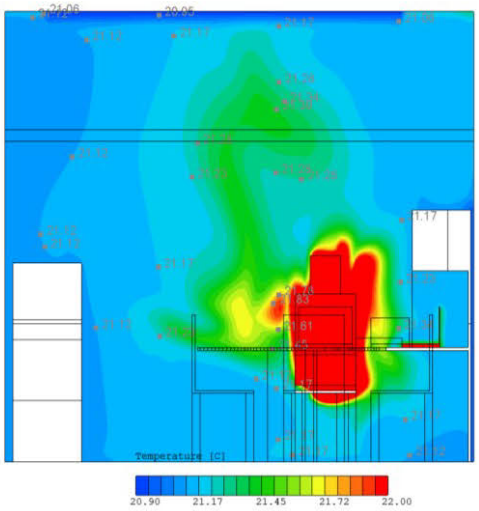

Section Y at 3.2 m

Figure 9.78 - Temperature Contour Plot at the Occupant in Y Direction

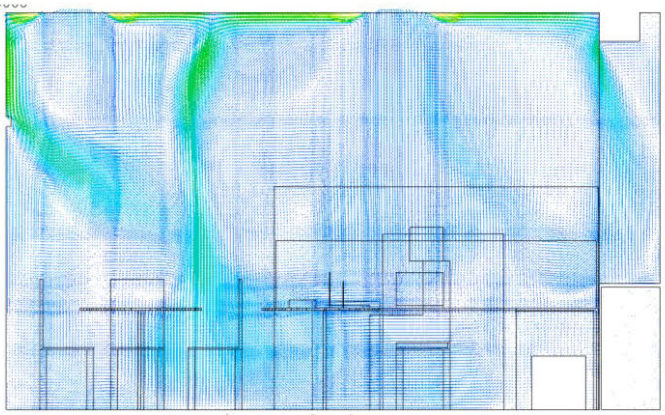

Section 1 (X = 0.75 m)

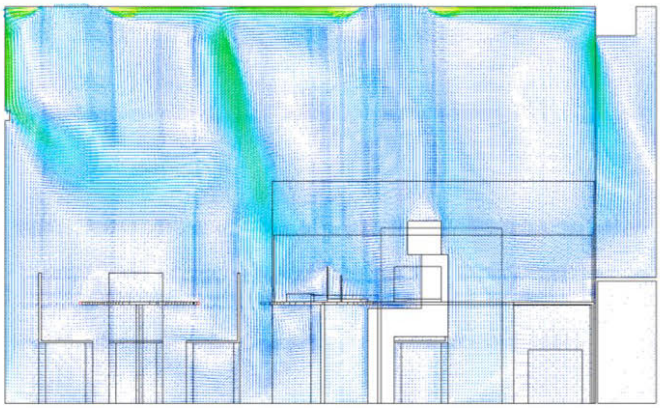

Section 4 (X= 2.2 m)

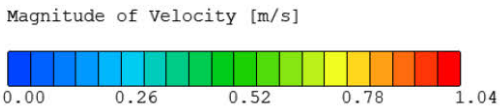

Figure 9.79 - Velocity Vector Plot at Section 1 and 4

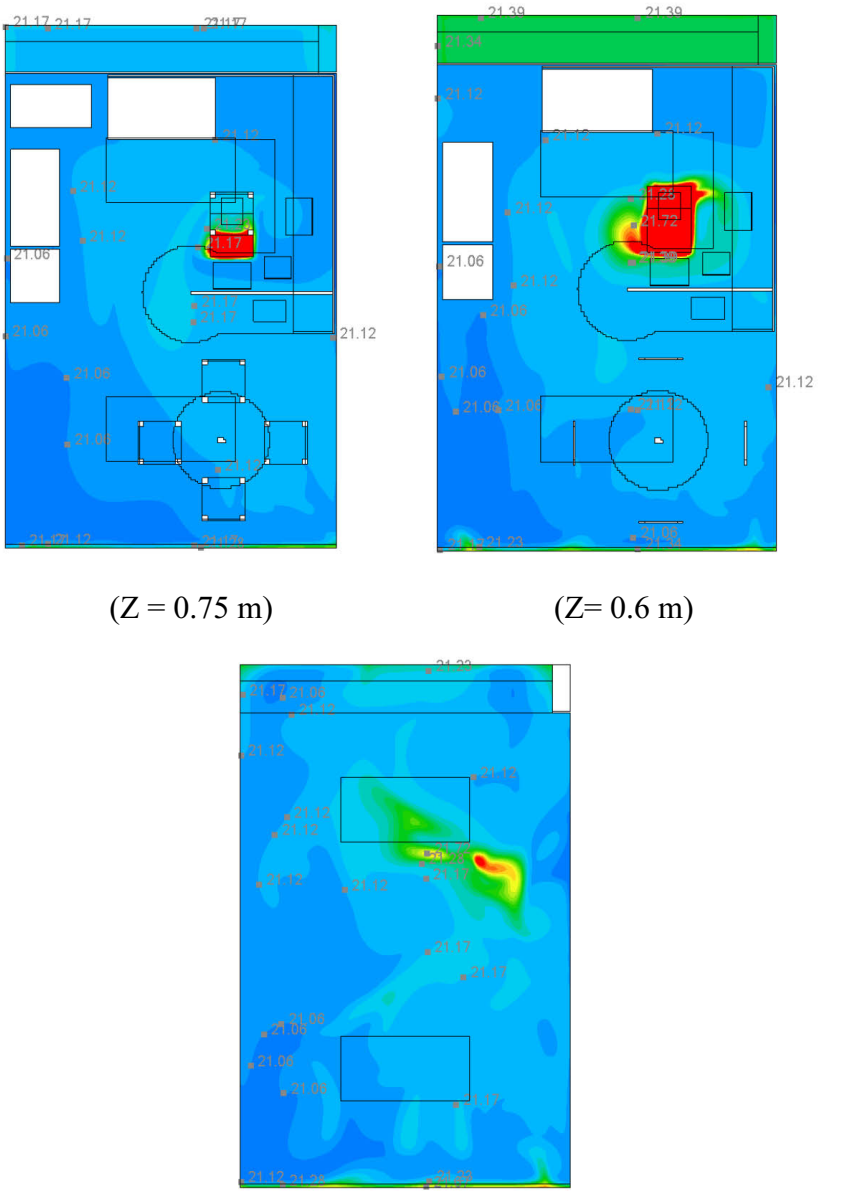

Figure 9.80 - Temperature Plot at Different Heights in the Room

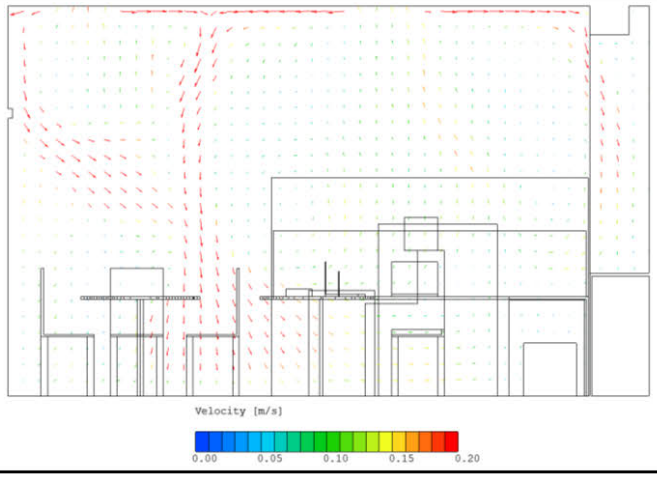

Section 1 (X = 0.75 m)

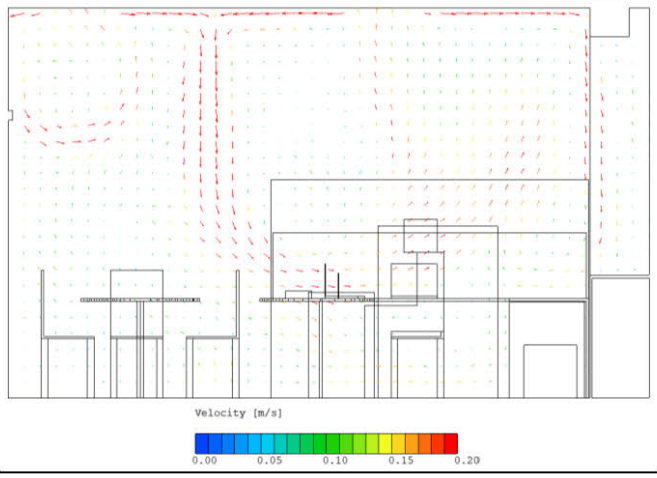

Section 2 (X = 1.2 m)

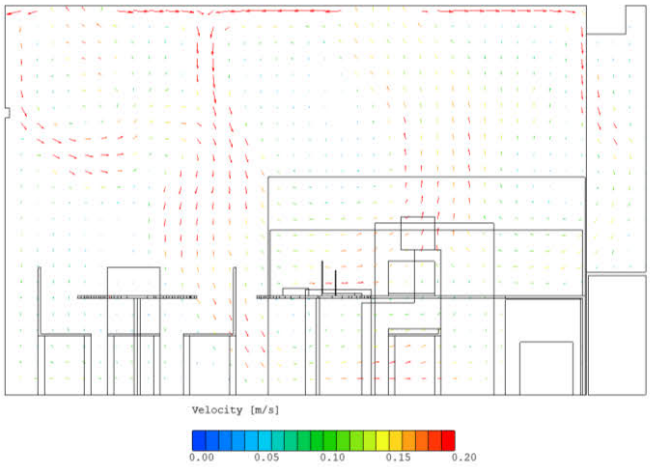

Section 3 (X = 1.6 m)

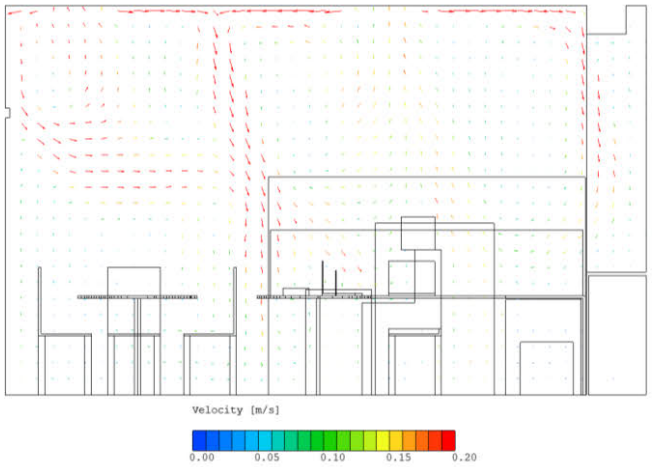

Section 4 (X = 2.2 m)

Figure 9.81 - Velocity Vectors Higher Than 0.2 m/s at 4 Different Sections in Occupied Zone

Table 9.5 - Air Characteristics Comparison of Experiment and CFD Model (Section 1)

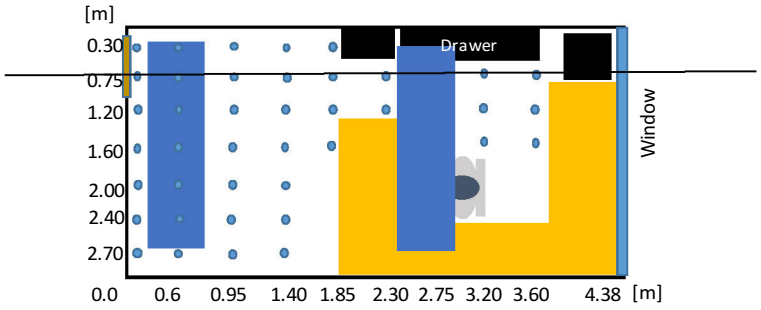

Experimental Results (Room Setpoint 22 (°C))									
Plane/ Section	Point No	Distance (m)	Air Velocity (m/s) Height (m)				Air Temperature (°C) Height (m)			
			0.1	0.6	1.1	1.7	0.1	0.6	1.1	1.7
Section 1 (0.75 m)	24	0.95	0.19	0.10	0.08	0.08	20.58	20.70	20.73	20.75
	17	1.40	0.09	0.05	0.05	0.08	21.12	21.20	21.24	21.26
	13	1.85	0.06	0.05	0.09	0.04	21.58	21.63	21.62	21.75
	10	2.30	0.12	0.12	0.13	0.13	21.32	21.32	21.24	21.35
	7	2.75	0.05	0.05	0.07	0.12	21.90	22.00	22.00	21.98
	4	3.20	0.05	0.06	0.12	0.14	21.79	21.81	21.93	21.90
	1	3.60	0.06	0.10	0.12	0.10	20.77	20.67	20.89	20.85
CFD Results (Room Setpoint 22 (°C))										
Plane/ Section	Point No	Distance (m)	Air Velocity (m/s) Height (m)				Air Temperature (°C) Height (m)			
			0.1	0.6	1.1	1.7	0.1	0.6	1.1	1.7
Section 1 (0.75 m)	24	0.95	0.12	0.12	0.11	0.09	21.23	21.20	21.21	21.26
	17	1.40	0.13	0.15	0.09	0.05	21.22	21.20	21.21	21.26
	13	1.85	0.14	0.15	0.07	0.07	21.20	21.19	21.20	21.25
	10	2.30	0.14	0.13	0.06	0.07	21.19	21.19	21.20	21.24
	7	2.75	0.12	0.10	0.09	0.11	21.19	21.18	21.19	21.22
	4	3.20	0.06	0.08	0.09	0.13	21.18	21.17	21.17	21.16
	1	3.60	0.06	0.08	0.09	0.13	21.18	21.17	21.17	21.16
Absolute Error										
Plane/ Section	Point No	Distance (m)	Air Velocity (m/s) Height (m)				Air Temperature (°C) Height (m)			
			0.1	0.6	1.1	1.7	0.1	0.6	1.1	1.7
Section 1 (0.75 m)	24	0.95	0.06	0.01	0.01	0.03	0.66	0.51	0.48	0.49
	17	1.40	0.03	0.07	0.06	0.01	0.11	0.00	0.03	0.00
	13	1.85	0.07	0.10	0.00	0.01	0.36	0.43	0.41	0.49
	10	2.30	0.02	0.03	0.06	0.06	0.12	0.13	0.04	0.10
	7	2.75	0.09	0.08	0.01	0.05	0.71	0.81	0.80	0.74
	4	3.20	0.07	0.04	0.03	0.03	0.60	0.63	0.74	0.68
	1	3.60	0.00	0.02	0.03	0.03	0.41	0.50	0.28	0.31
Percentage Error										
Plane/ Section	Point No	Distance (m)	Air Velocity (m/s) Height (m)				Air Temperature (°C) Height (m)			
			0.1	0.6	1.1	1.7	0.1	0.6	1.1	1.7
Section 1 (0.75 m)	24	0.95	51.31	7.48	14.68	52.86	3.10	2.42	2.26	2.31
	17	1.40	24.82	59.49	53.61	11.10	0.51	0.02	0.15	0.02
	13	1.85	53.46	66.02	1.36	20.86	1.72	2.05	1.92	2.32
	10	2.30	15.66	20.76	89.39	91.20	0.55	0.61	0.17	0.46
	7	2.75	63.67	60.78	13.86	60.90	3.33	3.83	3.79	3.48
	4	3.20	56.56	42.79	31.44	31.14	2.85	2.96	3.47	3.21
	1	3.60	0.72	23.72	33.42	24.83	1.92	2.38	1.32	1.46

Table 9.6 - Air Characteristics Comparison of Experiment and CFD Model (Section 2)

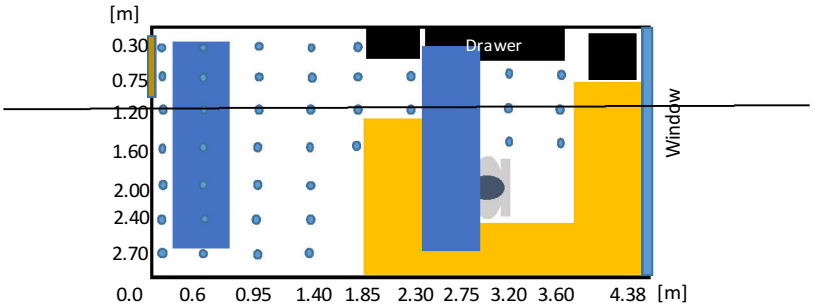

Experimental Results (Room Setpoint 22 (°C))									
Plane/ Section	Point No	Distance (m)	Air Velocity (m/s) Height (m)				Air Temperature (°C) Height (m)			
			0.1	0.6	1.1	1.7	0.1	0.6	1.1	1.7
Section 2 (1.2 m)	25	0.95	0.14	0.07	0.09	0.21	20.68	20.78	20.83	20.65
	18	1.40	0.05	0.05	0.07	0.09	21.57	21.64	21.66	21.7
	14	1.85	0.08	0.07	0.11	0.07	21.68	21.7	21.66	21.8
	11	2.30	0.13	0.12	0.13	0.08	20.86	20.89	20.92	21.13
	8	2.75	0.07	0.08	0.12	0.13	21.99	22	21.93	21.98
	5	3.20	0.09	0.1	0.11	0.14	21.8	21.84	21.97	21.98
	2	3.60	0.07	0.1	0.11	0.12	21.5	21.48	21.9	21.76
CFD Results (Room Setpoint 22 (°C))										
Plane/ Section	Point No	Distance (m)	Air Velocity (m/s) Height (m)				Air Temperature (°C) Height (m)			
			0.1	0.6	1.1	1.7	0.1	0.6	1.1	1.7
Section 2 (1.2 m)	25	0.95	0.08	0.09	0.09	0.07	21.26	21.28	21.25	21.23
	18	1.40	0.12	0.10	0.04	0.11	21.27	21.31	21.30	21.24
	14	1.85	0.12	0.12	0.06	0.11	21.26	21.33	21.35	21.43
	11	2.30	0.12	0.11	0.09	0.08	21.25	21.32	21.38	21.30
	8	2.75	0.10	0.10	0.07	0.08	21.23	21.27	21.27	21.25
	5	3.20	0.09	0.12	0.11	0.20	21.21	21.23	21.23	21.22
	2	3.60	0.06	0.14	0.17	0.23	21.20	21.19	21.19	21.16
Absolute Error										
Plane/ Section	Point No	Distance (m)	Air Velocity (m/s) Height (m)				Air Temperature (°C) Height (m)			
			0.1	0.6	1.1	1.7	0.1	0.6	1.1	1.7
Section 2 (1.2 m)	25	0.95	0.06	0.02	0.00	0.14	0.58	0.50	0.42	0.58
	18	1.40	0.07	0.05	0.03	0.02	0.30	0.33	0.36	0.46
	14	1.85	0.04	0.05	0.05	0.04	0.42	0.37	0.31	0.37
	11	2.30	0.01	0.01	0.04	0.00	0.39	0.43	0.46	0.17
	8	2.75	0.03	0.02	0.05	0.05	0.76	0.73	0.66	0.73
	5	3.20	0.00	0.02	0.00	0.06	0.59	0.61	0.74	0.76
	2	3.60	0.01	0.04	0.06	0.11	0.30	0.29	0.71	0.60
Percentage Error										
Plane/ Section	Point No	Distance (m)	Air Velocity (m/s) Height (m)				Air Temperature (°C) Height (m)			
			0.1	0.6	1.1	1.7	0.1	0.6	1.1	1.7
Section 2 (1.2 m)	25	0.95	69.14	26.29	1.41	195.38	2.75	2.34	1.96	2.72
	18	1.40	58.06	50.45	63.83	14.35	1.43	1.54	1.71	2.15
	14	1.85	34.80	39.28	77.69	38.83	1.97	1.73	1.44	1.72
	11	2.30	12.79	9.40	52.20	3.23	1.83	2.01	2.14	0.79
	8	2.75	32.28	19.46	74.74	61.19	3.59	3.44	3.12	3.42
	5	3.20	0.71	17.03	0.67	30.71	2.79	2.88	3.49	3.58
	2	3.60	24.99	30.81	36.29	47.73	1.44	1.35	3.33	2.84

Table 9.7 - Air Characteristics Comparison of Experiment and CFD Model (Section 3)

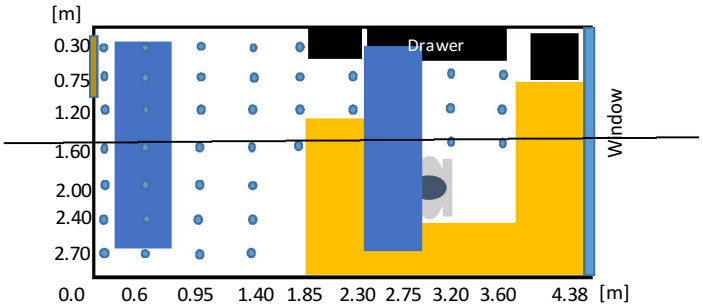

Experimental Results (Room Setpoint 22 (°C))									
Plane/ Section	Point No	Distance (m)	Air Velocity (m/s) Height (m)				Air Temperature (°C) Height (m)			
			0.1	0.6	1.1	1.7	0.1	0.6	1.1	1.7
Section 3 (1.6 m)	26	0.95	0.15	0.08	0.1	0.12	20.98	21.1	21.18	21.16
	19	1.4	0.09	0.11	0.11	0.05	21.28	21.26	21.35	21.59
	15	1.85	0.09	0.18	0.1	0.07	21.05	20.86	21.2	21.31
	9	2.75	0.08	0.1	0.12	0.14	21.89	21.86	21.85	21.81
	6	3.2	0.1	0.1	0.13	0.14	21.8	21.9	21.99	22.03
	3	3.6	0.08	0.12	0.13	0.14	21.6	21.63	21.78	21.88
CFD Results (Room Setpoint 22 (°C))										
Plane/ Section	Point No	Distance (m)	Air Velocity (m/s) Height (m)				Air Temperature (°C) Height (m)			
			0.1	0.6	1.1	1.7	0.1	0.6	1.1	1.7
Section 3 (1.6 m)	26	0.95	0.06	0.09	0.11	0.18	21.22	21.34	21.24	21.24
	19	1.4	0.09	0.05	0.03	0.09	21.22	21.37	21.33	21.28
	15	1.85	0.09	0.03	0.08	0.15	21.22	21.36	21.45	21.52
	9	2.75	0.09	0.03	0.15	0.10	21.25	21.49	21.46	21.27
	6	3.2	0.09	0.06	0.18	0.22	21.24	21.40	21.40	21.18
	3	3.6	0.07	0.15	0.18	0.17	21.21	21.25	21.21	21.14
Absolute Error										
Plane/ Section	Point No	Distance (m)	Air Velocity (m/s) Height (m)				Air Temperature (°C) Height (m)			
			0.1	0.6	1.1	1.7	0.1	0.6	1.1	1.7
Section 3 (1.6 m)	26	0.95	0.09	0.01	0.01	0.06	0.24	0.24	0.06	0.08
	19	1.4	0.00	0.06	0.08	0.04	0.06	0.11	0.02	0.31
	15	1.85	0.00	0.15	0.02	0.08	0.17	0.50	0.25	0.21
	9	2.75	0.01	0.07	0.03	0.04	0.64	0.37	0.39	0.54
	6	3.2	0.01	0.04	0.05	0.08	0.56	0.50	0.59	0.85
	3	3.6	0.01	0.03	0.05	0.03	0.39	0.38	0.57	0.74
Percentage Error										
Plane/ Section	Point No	Distance (m)	Air Velocity (m/s) Height (m)				Air Temperature (°C) Height (m)			
			0.1	0.6	1.1	1.7	0.1	0.6	1.1	1.7
Section 3 (1.6 m)	26	0.95	161.77	7.59	12.93	31.51	1.15	1.13	0.30	0.36
	19	1.4	1.97	121.23	254.30	41.50	0.27	0.53	0.09	1.45
	15	1.85	4.01	446.96	18.30	53.19	0.78	2.35	1.18	0.95
	9	2.75	9.68	293.72	18.76	46.25	3.00	1.74	1.81	2.56
	6	3.2	11.38	53.97	27.73	35.86	2.66	2.32	2.75	4.01
	3	3.6	14.11	17.58	26.72	16.12	1.83	1.79	2.67	3.50

9.6 Ventilation Effectiveness in Heating and Cooling

Age of Air

Age of air near the occupant is shown in the Figure 9.82 and Figure 9.83 in heating and cooling respectively. The scale range (0 to 2) is kept similar for both the simulations to compare the age of air in cooling and heating. The low value (blue color indicates that the age is small and red color shows the old age of the air. As it is already shown that the CFD model predicted higher velocity in the space and with that air velocity the age of air is quite higher in heating which shows that most of the air is stagnant in the occupied zone near the occupant in heating mode which is also proved by the experimental data which shows 'zero' air velocity near occupant in heating mode. Although the age of air does not confirm anything about the contaminants or indoor air quality but it shows that the fresh air is only at the top portion of the room and much of the air is old and stagnant. While the Figure 9.83 with the same scale does not show any stagnant air and the value of age of air is relatively lower in cooling as compared to heating. Therefore, CFD is a useful tool in predicting the age of air while designing beam for a space.

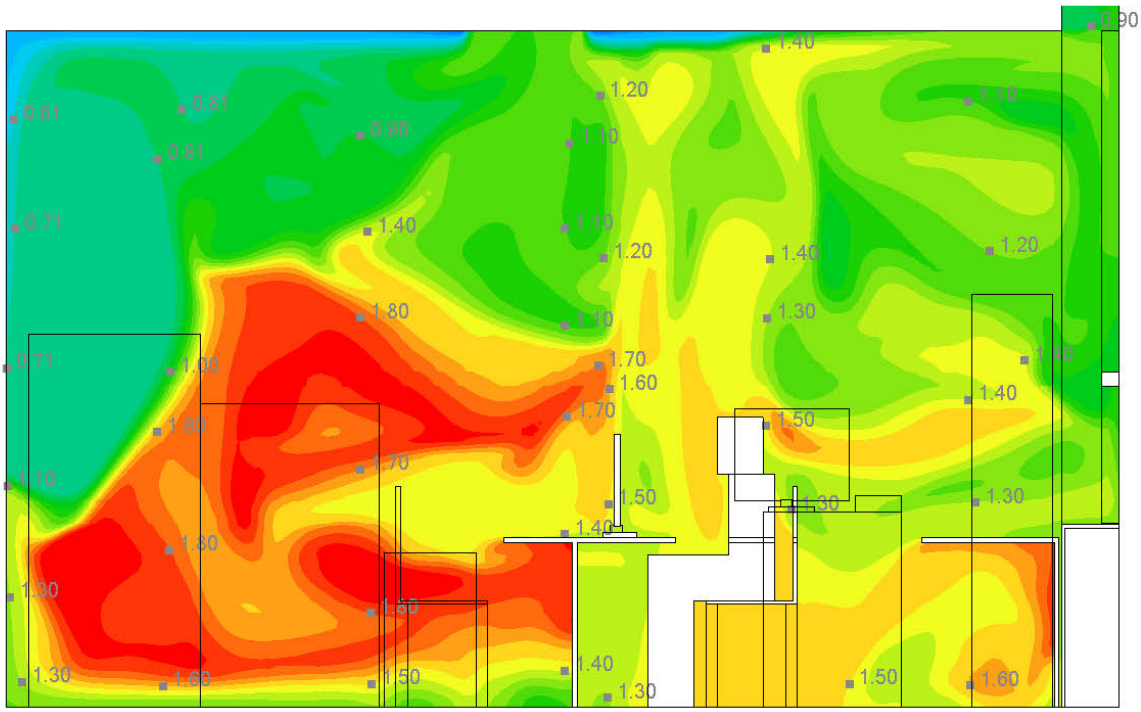

Figure 9.82 - Age of Air at Test Room 1 (Heating)

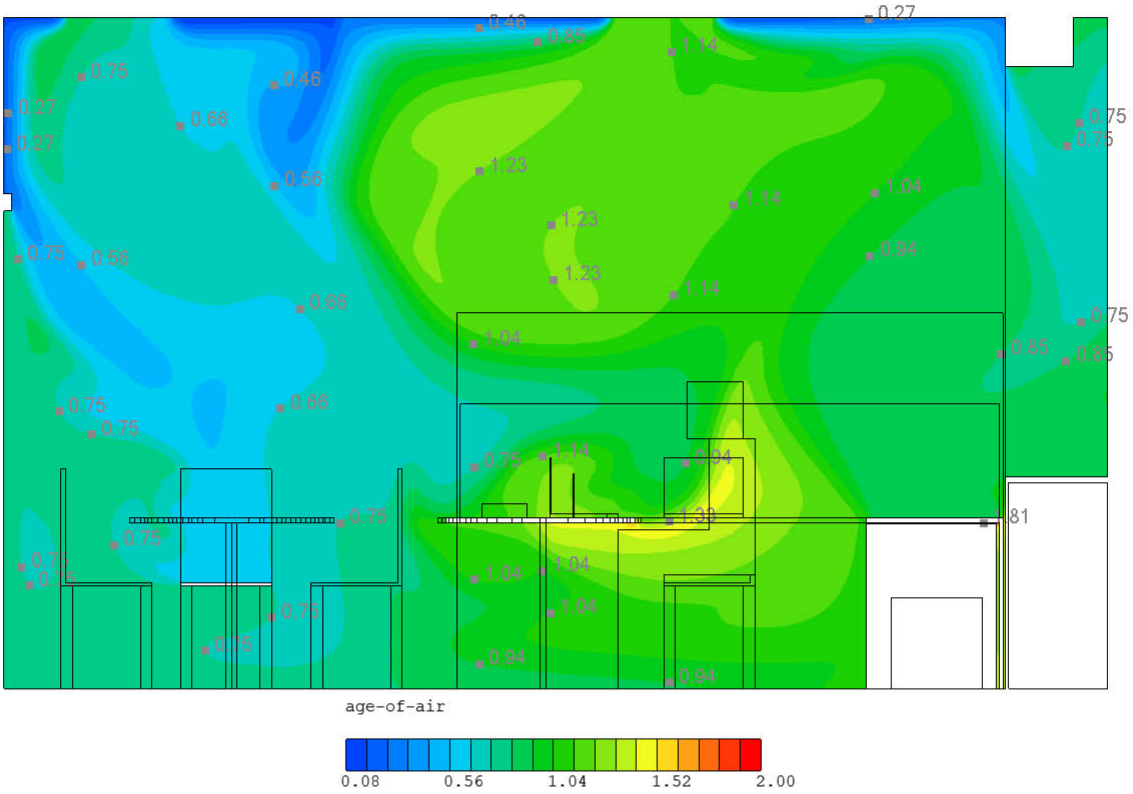

Figure 9.83 - Age of Air at Test Room 2 (Cooling)

Remainder of Air (Residual Lifetime of Air)

Figure 9.84 and Figure 9.85 shows the residual lifetime of air. The scale range (0 to 2) is kept similar to compare cooling and heating CFD simulations. Zero (blue color) means a smaller life of air and that will be exhausted soon. The air with red color has a large life and it will take longer for that air to be exhausted from the room. It is clearly visible that the residual lifetime of air is high in heating which implies that the air will take more time to exhaust out as compared to the air in cooling. The comparison is shown with the same scale and the remainder of air is much less in cooling mode.

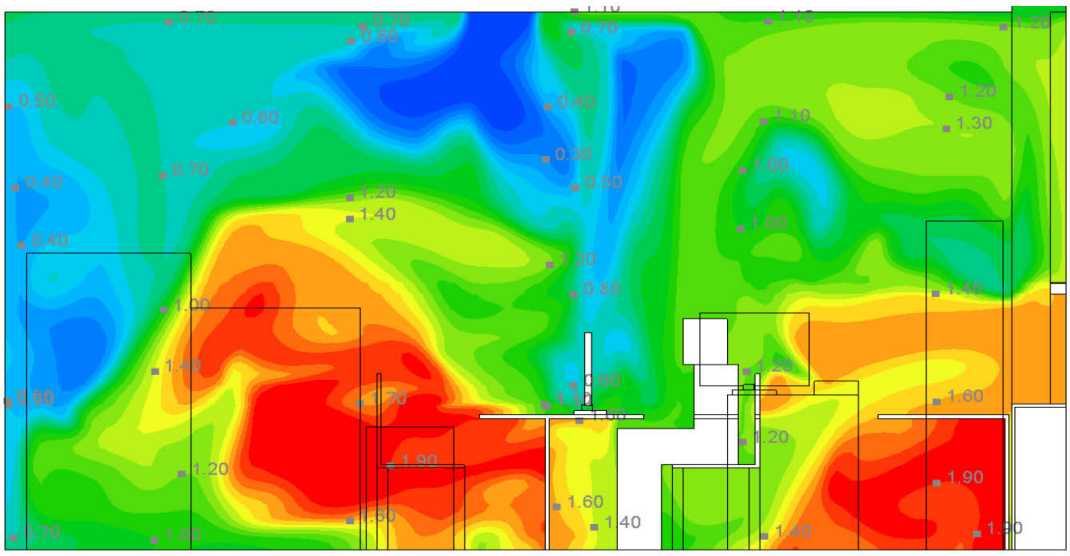

Figure 9.84 - Residual Lifetime of Air at Test Room 1 (Heating)

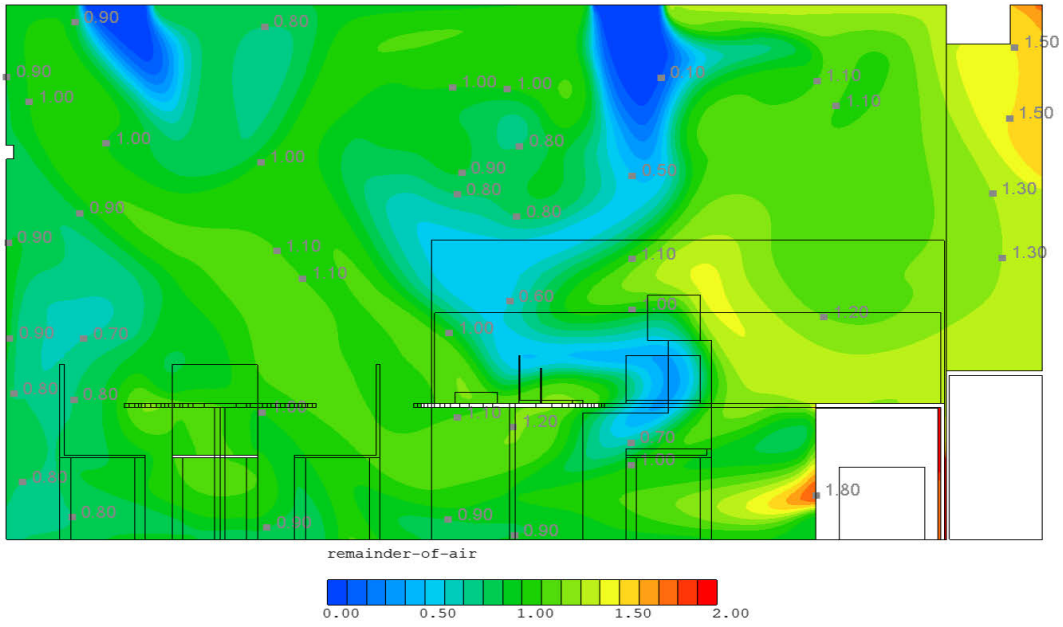

Figure 9.85 - Residual Lifetime of Air at Test Room 2 (Cooling)

Contribution Ratio of Supply Opening

Figure 9.86 shows the contribution ratio of supply openings in the room in cooling and heating. The contribution ratio also depends on the location of the supply opening/exhaust. As Test Room 2 has 2 units of ACB, the contribution ratio is much lesser than in heating by each slot. The scale of contribution ratio is shown from 0 to 1. Zero (blue) means the area which is not contributed by the supply and red means, the area which is contributed by the supply opening.

The figure shows that the contribution ratio of supply is approximately 0.75 near the occupant in heating and CHBS1 & CHBS2 cater to a larger area while the others slots in cooling ACB1_S1 and ACB1_S2 contribute to the much lesser area. Similarly, the contribution of exhaust grille in the room can be seen in Figure 9.87 and contribution ratio of induction surface of ACB can be seen in Figure 9.88 and Figure 9.89. The location of exhaust grille is also an important factor to contribute for easy exhaust of old age air which is clearly visible.

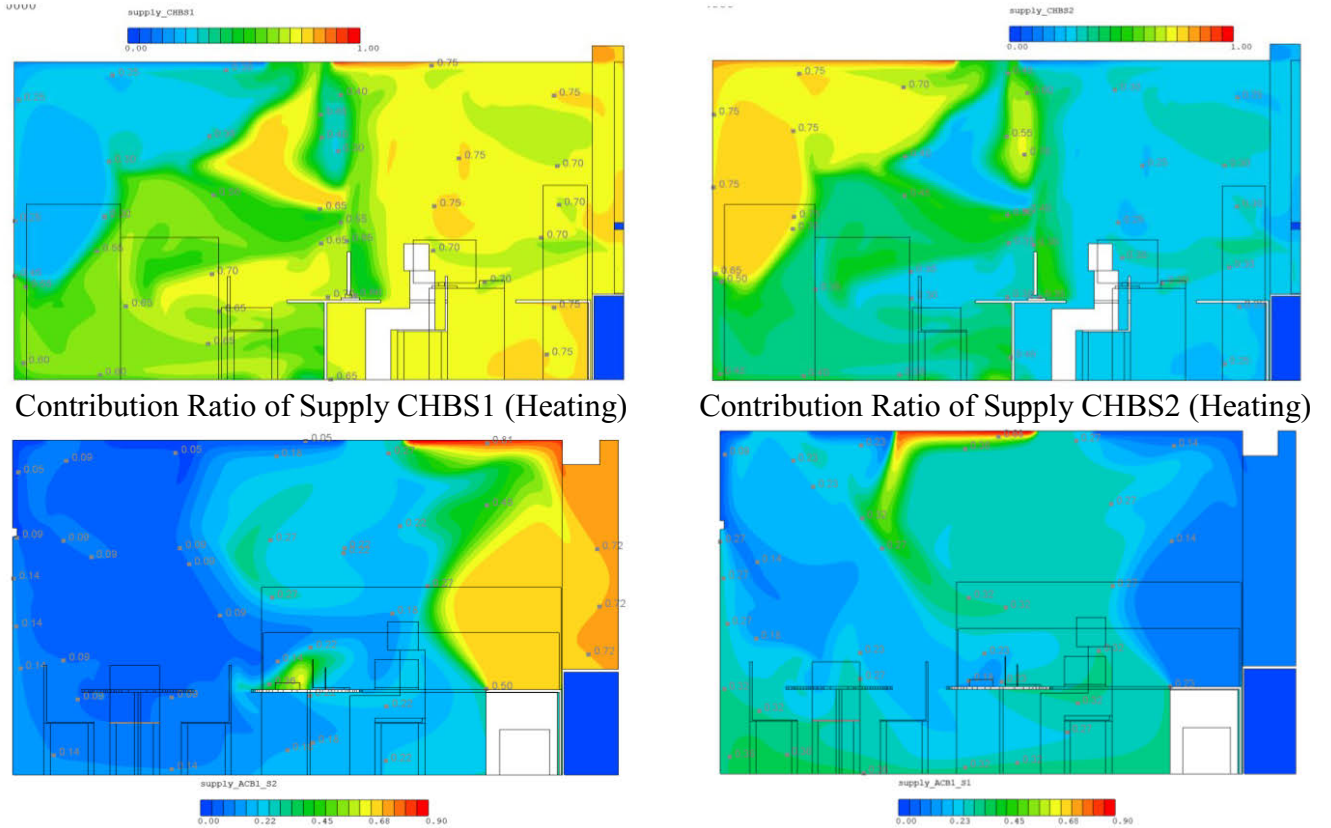

Contribution Ratio of Supply CHBS1 (Heating)

Contribution Ratio of Supply CHBS2 (Heating)

Contribution Ratio of Supply ACB1_S2 (Cooling)

Contribution Ratio of Supply ACB1_S1 (Cooling)

Figure 9.86 - Contribution Ratio of Supply Openings in Heating and Cooling

Exhaust Grille as shown in Figure 9.87 in Test Room 1 is at the end of the room close to the wall while in Test Room 2 it is in the center of the room close to the wall. The effect of exhaust grille could be seen with their contribution effect. One thing is to be noted that the exhaust airflow rate in Test Room 2 is nearly double that of Test Room 1. To test whether the exhaust contribution depends mostly on based on volume flow rate or location of exhaust opening, the location of exhaust openings in both the calibrated model without changing their exhaust flow

rate and the results were found interesting. The Exhaust at Test Room 1, when located to the center of the room shows higher contribution while the exhaust at Test Room 2 shows lower than the actual case. Therefore, the location of exhaust opening plays a vital role in Indoor Air Quality of room and through CFD simulations such design decision can be easily made.

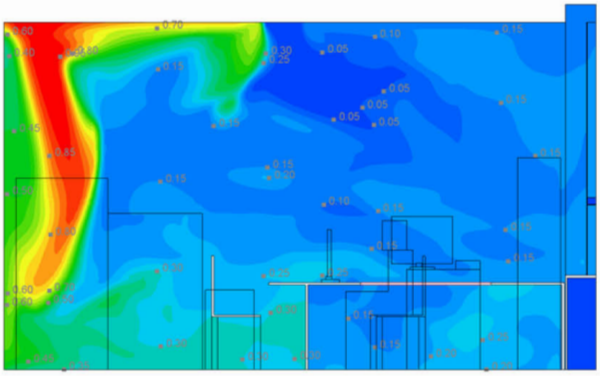

Exhaust Opening in Test Room 1 (End)

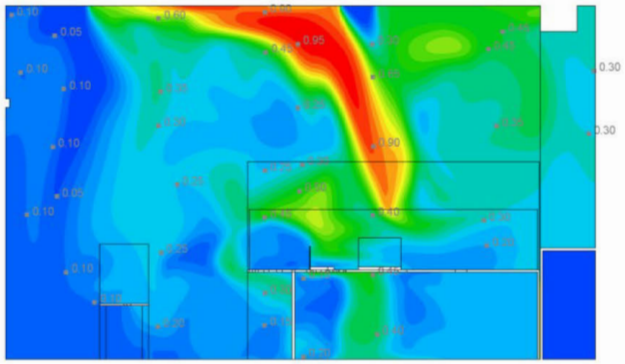

Exhaust Opening in Test Room 2 (Center)

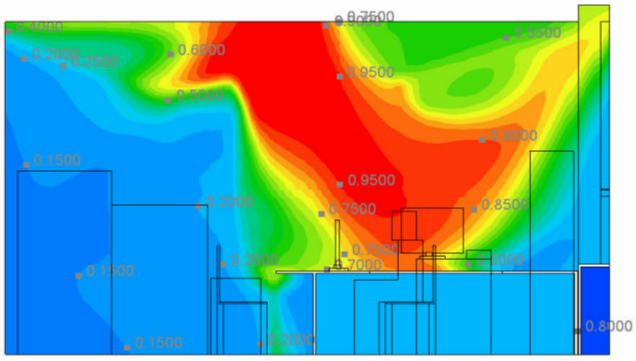

Test Room 1 – Exhaust Relocated to Center

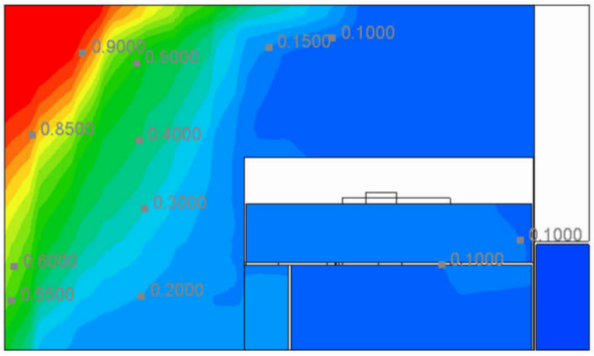

Test Room 2 – Exhaust Relocated to the End

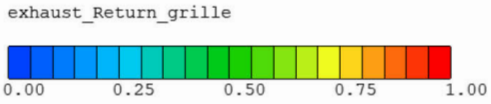

Figure 9.87 - Contribution Ratio of Exhaust Grille

Similarly, the contribution ratio of induction surface could be seen in Figure 9.88 and Figure 9.89 in heating and cooling respectively.

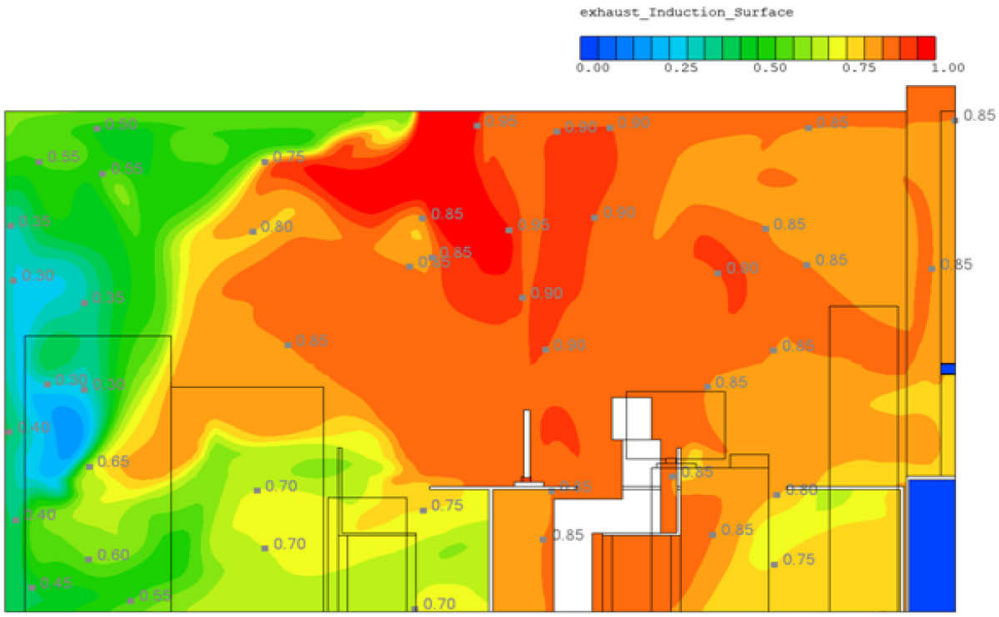

Figure 9.88 - Contribution Ratio of Induction Surface (Heating)

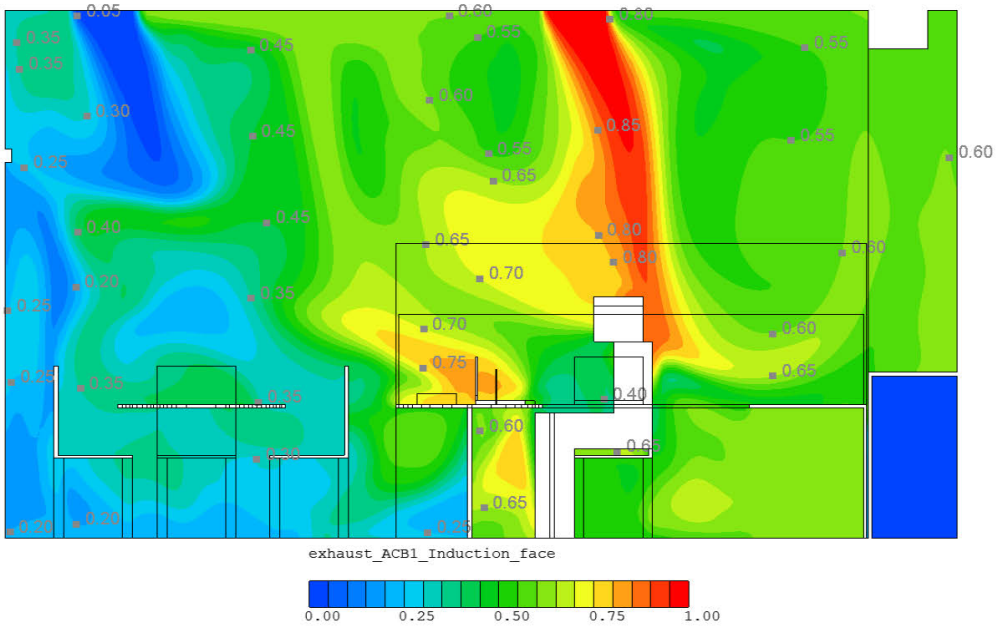

Figure 9.89 - Contribution Ratio of Induction Surface (Cooling)

10. CONCLUSIONS

The intent of this research was to assess the performance of ACB by obtaining field data and developing numerical models of ACB coupled with the rooms to appreciate the real factors that affect the performance of ACB in the heating and cooling operation, for the benefit of manufacturers and designers.

The major conclusions of this study are mentioned below:

1) The temperature distribution in the office (test room) under cooling mode was found uniform and close to the room setpoint across the room and at different heights, which shows that ACB performs really well in the cooling mode of operation.

2) The temperature distribution in the office under heating mode was not found uniform with a temperature difference at all heights during the experiment. The non-uniformity of temperature increases when the room setpoint was raised beyond 21°C, the temperature difference more than 3°C between head and ankle for a standing person and around 2.5°C for a seated person was found.

3) The air velocity in cooling mode was found well below the ASHRAE recommended velocity of 0.2 m/s in the occupied zone. Air movement was also noticed at all the heights and all measurement points in the room in cooling which proves ACB is effective in ventilating the room with the primary air.

4) The air velocity was found negligible, close to zero and zero at many points in the heating mode of operation which shows that air is stagnant in the occupied zone because of thermal stratification. The air quality must be checked in a controlled environment under heating mode and ACB must be tested for air change effectiveness.

5) CFD modelling of the whole beam was found challenging to simulate the induction phenomenon because of the complex geometry of beam with tiny nozzles, heat exchanger and perforated plate in the induction path.

6) The CFD model with a simplified beam was validated by the boundary conditions recorded in the experiment. Significant agreement was achieved between the CFD

simulation and experimental values.

7) The average percentage error between measured and simulated air temperature in space varied from 0% to 5% with an absolute error of 1°C.

8) The CFD model predicted higher air velocities throughout the room. An average percentage error for air velocities in the order of 250% was found at the 0.1 m height and isolated occurrences of errors in excess of 600% with an absolute error of 0.08 m/s.

9) The difference in velocities could be due to the assumptions made like no leakage from the room and modelling of ACB through simple slots (flat panels) with fixed face uniform velocities which is not exactly the same when the room air in actual is delivered through nozzles and velocity and temperature of air is not constant all along the slots with difference in temperature and velocity in either slot as well, therefore, resulted in significant error.

10) Ventilation efficiency was simulated through CFD model by indices like the age of air and the residual lifetime of air which further proved that the age of air in heating is higher than in cooling and air stagnant zone was clearly visible in the contours.

The minor conclusions and ACB specific conclusions are below:

1) Coanda effect with larger throw was seen in both heating and cooling mode which helps in proper air distribution and prevent direct throw of cold and hot air in the occupied zone.

2) The discharge velocity and discharge temperature from ACB slots are not equal in cooling and heating operation which affect the room temperature and airflow distribution.

3) The effect was more prominent in heating operation where the difference in slots temperature was more than 3°C due to the design and placement of the heating coil. The effect of temperature distribution in heating can cause one side of the area warmer as compared to the other side of the room and therefore it requires further research in a controlled environment.

11. FURTHER WORK

The results reported in this research correspond to 2 single person office, which can be considered representative of many similar offices in this high-performance building. Other factors affecting the performance of ACB have been observed, such as the proximity of light fittings to ACB which disturb the Coanda effect, the location of ceiling return grille relative to ACB, partition walls layout etc.

The results reported in this study are mainly recorded in an uncontrolled environment which needs to be verified in a controlled laboratory environment. The results are also influenced by the design of ACB by a particular manufacturer and therefore the results are not generalized for all types of ACB or ACB from a different manufacturer.

Experiments in the same offices in winter and summer were not conducted because of limitation in the availability of office in a running building and therefore the results in cooling and heating are not comparable. The experiments must be conducted in the same office for the complimentary season to compare the results whenever the offices are available. CFD simulation is also limited based on the software available during the study.

More studies are required to assess the performance of ACB in heating mode. The performance must be assessed in terms of indoor air quality, air change effectiveness, thermal stratification and energy efficiency under heating mode. Comparison of ACB under heating mode must be done with standard ceiling diffuser with above-mentioned parameters.

REFERENCES

[1] ASHRAE Standard Committee, ASHRAE Handbook: Fundamentals 2013, ASHRAE Inc, Atlanta, USA, 2013.

[2] D. P. Wyon, "Individual microclimate control: required range, probable benefits and current feasibility," in 7th International Conference on Indoor Air Quality and Climate (Indoor Air), 1996, pp. 1067-1072.

[3] U.S. Energy Information Administration | Annual Energy Outlook 2014, https://www.eia.gov/outlooks/aeo/pdf/0383(2014).pdf

[4] Carrier, Induction beams, available from: http://www.carrier.com.

[5] ACEEE emerging technologies report, Active chilled beam cooling with DOAS, 2009.

[6] Thomas Gibson and Mindy Espinosa, "Chilled Beams: What They Are, Why You Should Use Them," https://www.achrnews.com/articles/123293-chilled-beams-what-they-are-why-you-should-use-them.

[7] B.S. Setty, "Application issues for chilled beam technologies," ASHRAE Transactions, 117 (2011) 494-501.

[8] K. Loudermilk, "Designing Chilled Beams for Thermal Comfort," ASHRAE Journal. 2009 p. 58-64.

[9] Darren Alexander and Mike, "Design Considerations for Active Chilled Beams," ASHRAE Journal. Sep. 2008 p. 50-58.

[10] HVACR Nation_2010_11_SW.pdf www.airah.org.au

[11] Dadanco, Active chilled beams, available from: http://dadanco.com/.

[12] K. Loudermilk, and D. Alexander, "Efficient space humidity control with active chilled beam systems," ASHRAE Journal, 54 (1) (2012) 28-38.

[13] A. Livchak, and C. Lowell, "Don't turn active beams into expensive diffusers," ASHRAE Journal, 54 (4) (2012) 52-60.

[14] A. Livtchak, P. Horttanainen, G. Yankov, and V. Artemov, "The Effect of Room Thermal Environment on the Performance of Cooled Beams,". CLIMA Brussels Technical Session 3 1997 pp231 253

[15] R. Kosonen, "An analysis of a flexibility chilled beam system in hot and humid climate," in 8th International Symposium on Heating, Ventilation and Air Conditioning, 2013, pp. 227-234.

[16] P. Filipsson, A. Truschel, J. Graslund, and J.O. Dalenback, "Induction ratio of active chilled beams- Measurement methods and influencing parameters."

[17] M. Ruponen, and J. A.Tinker, "A novel method to measure the air entrainment ratio of an active chilled beam," International Journal of Ventilation, 7 (2009) 299-308.

[18] C. Chen, W. Cai, Y. Wang, and C. Lin, "Further study on the heat exchanger circuitry arrangement for an active chilled beam terminal unit," Energy Build. 103 (2015) 352–364,

[19] Z. Guan, and C. Wen, "Numerical investigation of geometry parameters for designing efficient terminal units in active chilled beam," in IEEE 9th Conference on Industrial Electronics and Applications (ICIEA), 2014, pp. 1114-1118.

[20] Z. Guan and C. Wen, "Geometric optimization on active chilled beam terminal unit to achieve high entrainment efficiency."

[21] K. Roth, J. Dieckmann, R. Zogg, J. Brodrick, "Chilled beam cooling," ASHRAE J. 49 (2007) 84.

[22] Jérôme Le Dréau, ”Energy Flow and Thermal Comfort in Buildings Comparison of Radiant and Air-based Heating & Cooling Systems,” 2014 River Publishers

[23] Aleksejs Prozuments, "Testing the use of an active chilled beam technology in a hospital ward mock-up," REHVA Journal / 04/2015

[24] J. L. Dréau, P. Heiselberg and R. L. Jensen, "A full-scale experimental set up for assessing the energy performance of radiant wall and active chilled beam for cooling buildings." Building Simulation (2014) 39-50

[25] J. L. Dréau and P. Heiselberg, "Sensitivity analysis of the thermal performance of radiant and convective terminals for cooling buildings," Energy and Buildings 82 (2014) 482–491

[26] P. Mustakallio, Z. Bolashikov, K. Kostov, A. Melikov and R. Kosonen, "Thermal environment in simulated offices with convective and radiant cooling systems under cooling (summer) mode of operation." Building and Environment (2016) 82-91

[27] K. N. Rhee, M. S. Shin and S. H. Choi, "Thermal uniformity in an open plan room with an active chilled beam system and conventional air distribution systems."

[28] A. Melikov, B. Yordanova, L. Bozkhov, V. Zboril, and R. Kosonen, “Impact of the airflow interaction on occupants’ thermal comfort in rooms with active chilled beams,” The 6th International Conference on Indoor Air Quality, Ventilation & Energy Conservation in Buildings IAQVEC (2007), Sendai, Japan.

[29] ASHRAE Standard Committee, ASHRAE Standard 55-2004, Thermal environmental conditions for human occupancy, ASHRAE Inc, Atlanta, USA, (2004).

[30] G. Cao, M. Sivukari, J. Kurnitski, M. Ruponen, and O. Seppänen, "Particle Image Velocimetry (PIV) application in the measurement of indoor air distribution by an active chilled beam," Building and Environment, 45 (2010) 1932-1940.

[31] G. Cao, M. Sivukari, J. Kurnitski, and M. Ruponen, "PIV measurement of the attached plane jet velocity field at a high turbulence intensity level in a room," International Journal of Heat and Fluid Flow, 31 (2010) 897-908.

[32] G. Cao, M. Ruponen, R. Paavilainen, and J. Kurnitski, "Modelling and simulation of the near-wall velocity of a turbulent ceiling attached plane jet after its impingement with the corner," Building and Environment, 46 (2011) 489-500G.

[33] G. Cao, M. Ruponen, and J. Kurnitski, "Experimental investigation of the velocity distribution of the attached plane jet after impingement with the corner in a high room," Energy and Buildings, 42 (2010) 935-944.

[34] G. Cao, J. Kurnitski, P. Mustakallio, and O. Seppänen, "Active chilled beam wall jet prediction by the free convection model," International Journal of Ventilation, 7 (2008) 169-178.

[35] G. Cao, J. Kurnitski, M. Ruponen, P. Mustakallio, and O. Seppänen, "Plane-air-jet corner zone modelling in a room ventilated by an active chilled beam," International Journal of Ventilation, 7 (2009) 287-297.

[36] H. Koskela, H. Häggblom, R. Kosonen, and M. Ruponen, "Air distribution in office environment with asymmetric workstation layout using chilled beams," Building and Environment, 45 (2010) 1923-1931.

[37] H. Koskela, H. Häggblom, R. Kosonen, and M. Ruponen, "Flow pattern and thermal comfort in office environment with active chilled beams," HVAC & R Research, 18 (2012) 723-736.

[38] R. Kosonen, A. Melikov, B. Yordanova, and L. Bozkhov, "Impact of heat load distribution and strength on airflow pattern in rooms with exposed chilled beams,"

[39] R. Kosonen, M. Virta, and A. Melikov, "The impact of thermal loads on indoor airflow," 2018

[40] J. True, V. Zboril, R. Kosonen, and A. Melikov, "Consideration for minimizing draught discomfort in rooms with active chilled beams," Proceedings of Clima (2007) Wellbeing Indoors.

[41] R. Kosonen, P. Saarinen, H. Koskela, and A. Hole, "Impact of heat load location and strength on air flow pattern with a passive chilled beam system," International Conference on Building Energy and Environment COBEE2008, Vol.42 (1), 34-42.

[42] Nygaard L, Uth SC., "Task Ambient Environment - Chilled Beam", Technical University of Denmark, 2014.

[43] Q. Chen, Z. Zhang, W. Zuo, "Computational Fluid Dynamics for Indoor Environment Modeling: Past, Present and Future", Presented at The 6th International Indoor Air Quality, Ventilation and Energy Conservation in Buildings Conference (IAQVEC 2007), Sendai, Japan.

[44] H.E. Feustel, J. Dieris, "A Survey on Air Flow Models for Multizone Structures, Energy and Buildings", 18 (1992) 79-100.

[45] J. Srebric, Q. Chen, Simplified Numerical Models for Complex Air Supply Diffusers, HVAC&R Research, 8 (3) (2002) 277-294.

[46] Karimi, Abdullah, "Design Optimization of Active Chilled Beam for an Office Space using Large Eddy Simulation". (2018).

[47] G. Cammarata, and G. Petrone, "A numerical investigation on active chilled beams for indoor air conditioning," COSMOL Conference, (2008), Hannover.

[48] Qingyan Chen & J. Srebric, "A Procedure for Verification, Validation, and Reporting of Indoor Environment CFD Analyses," HVAC&R Research, (2002), 8:2, 201-216

[49] J. Srebric, and Q. Chen, “An example of verification, validation, and reporting of indoor environment CFD analyses,” ASHRAE Transactions, (2002),108 (2), 185-194.

[50] J. Abanto, D. Barrero, M. Reggio, and B. Ozell, “Airflow modeling in a computer room,” Building and Environment, (2004), 39, 1393-1402.

[51] L. Zhu, R. Li, and D. Yuan, “Numerical analysis of a cold air distribution system,” HVAC Technologies for Energy Efficiency, (2006) Vol.IV-2-3.

[52] D. Müller, C. Kandzia, R. Kosonen, A. K. Melikov and P. V. Nielsen, "Mixing Ventilation. Guide on mixing air distribution design," REHVA guide book. Federation of European Heating, Ventilation and Air Conditioning Associations, 2013.

[53] S. Gilani, H. Montazeri, B. Blocken, "CFD simulation of stratified indoor environ ment in displacement ventilation: Validation and sensitivity analysis," Building & Environment, September 2015

[54] Sasan Sadrizadeh and Sture Holmberg, "Evaluation of various turbulence models for indoor airflow prediction: a comparison study with experimental data," 2006.

[55] Z. Zhang, W. Zhang, Z. Zhai, and Q. Chen, “Evaluation of various turbulence models in predicting airflow and turbulence in enclosed environments by CFD: Part-2: comparison with experimental data from literature,” HVAC & R Research, (2007) Vol.13 Issue (6)

[56] L. Pérez-Lombard, J. Ortiz, C. Pout, "A review on buildings energy consumption information," Energy Build 2008; 40:394–8. doi: 10.1016/j.enbuild.2007.03.007.

[57] D. P. Wyon, "The effects of indoor air quality on performance and productivity. Indoor Air," 2004;14 Suppl 7:92–101. doi:10.1111/j.1600-0668.2004.00278.x.

[58] H. B. Awbi, “Ventilation of Buildings”, Spon Press, 2th edition, 2003.

[59] P. Mustakallio, T. Moilanen, M. Ruponen, R. Kosonen, K. Hagström, "Development of CFD model for a cooled beam – Importance of product specific boundary conditions", Halton Oy.

[60] Wu, Bingjie; Cai, Wenjian; Wang, Qinguo; Chen, Can; Lin, Chen; and Chen, Haoran, "The Air Distribution Around Nozzles Based On Active Chilled Beam System". International High-Performance Buildings Conference. 2016. Paper 173.

[61] https://www.troxuk.co.uk/chilled-beams-and-multi-service-chilled-beams/multi-service-chilled-beams-(mscb)-63d6b7289c65af72

[62] Basics of CFD Analysis, ScStream Manual Version 13, Software Cradle Co. Ltd.

APPENDIX A – ROOM AIR DISTRIBUTION – HEATING

This section shows graphically the experimental measurement at different room setpoint temperature and the air temperature and air velocity recorded at 4 different heights including the supply velocity and induction (return) velocity at the ACB during the heating season. (January 2018).

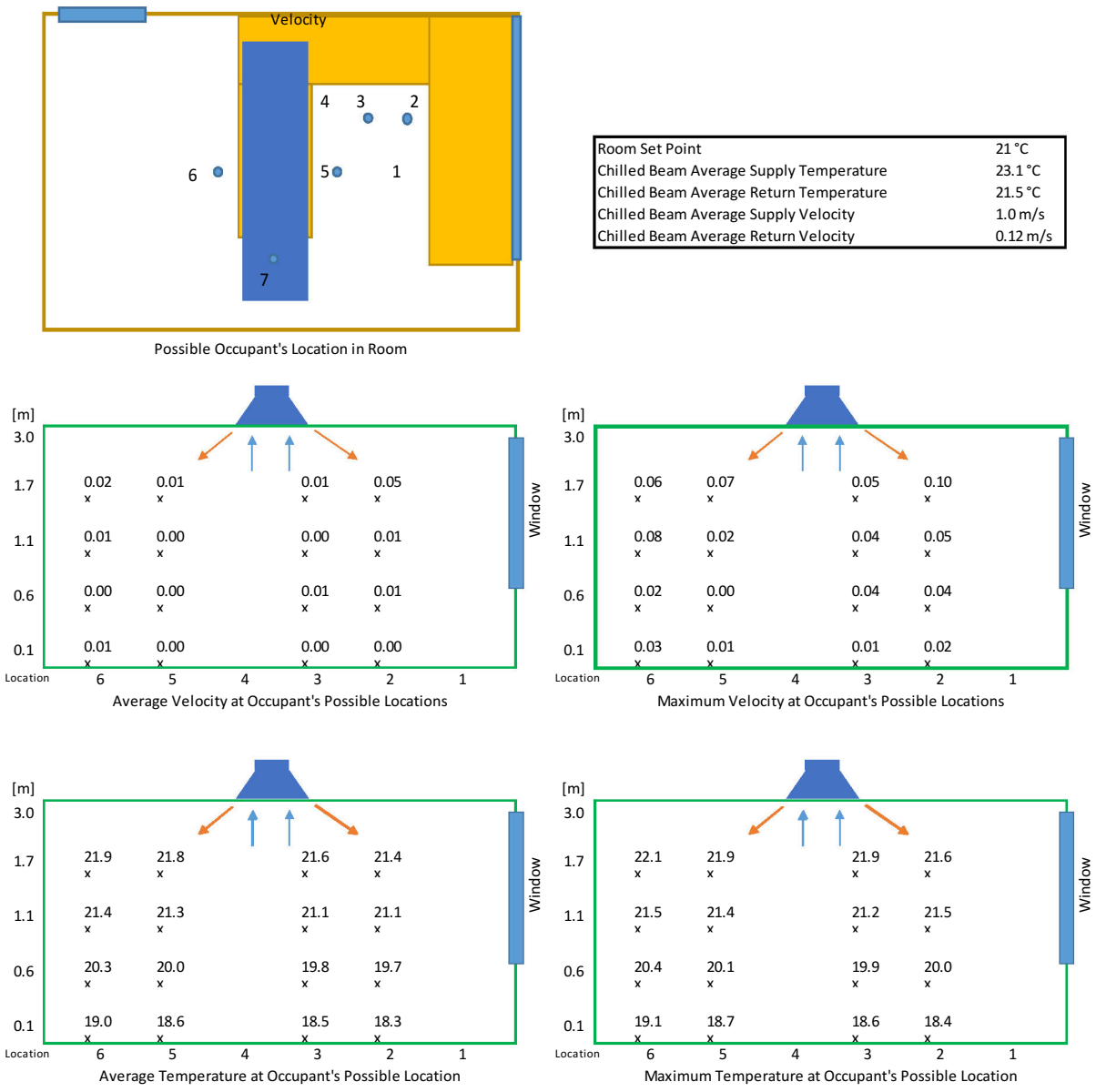

Figure A.1 - Air Temperature and Velocity Distribution at Room Setpoint 21 (°C)

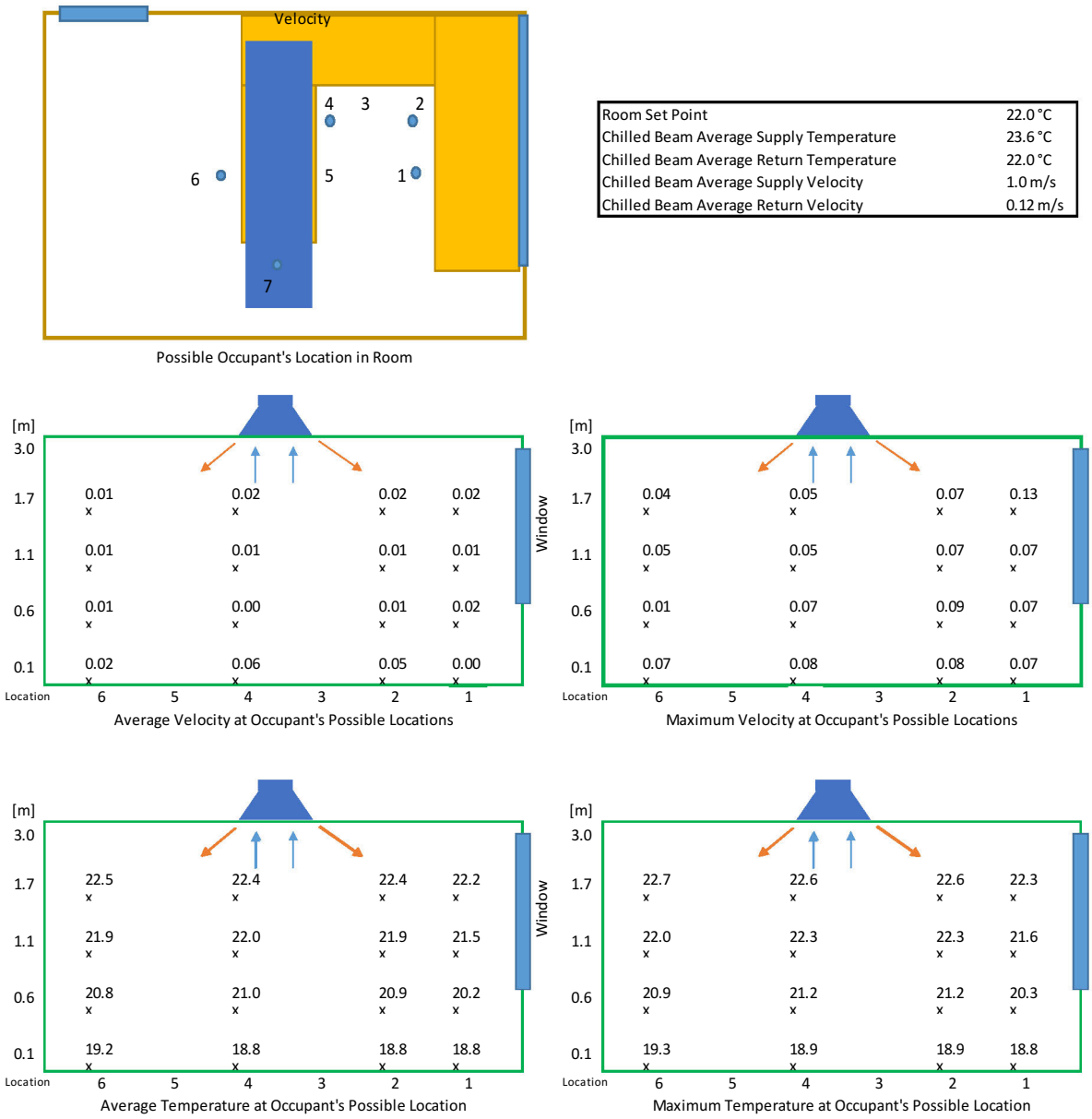

Figure A.2 - Air Temperature and Velocity Distribution at Room Setpoint 22 (°C)

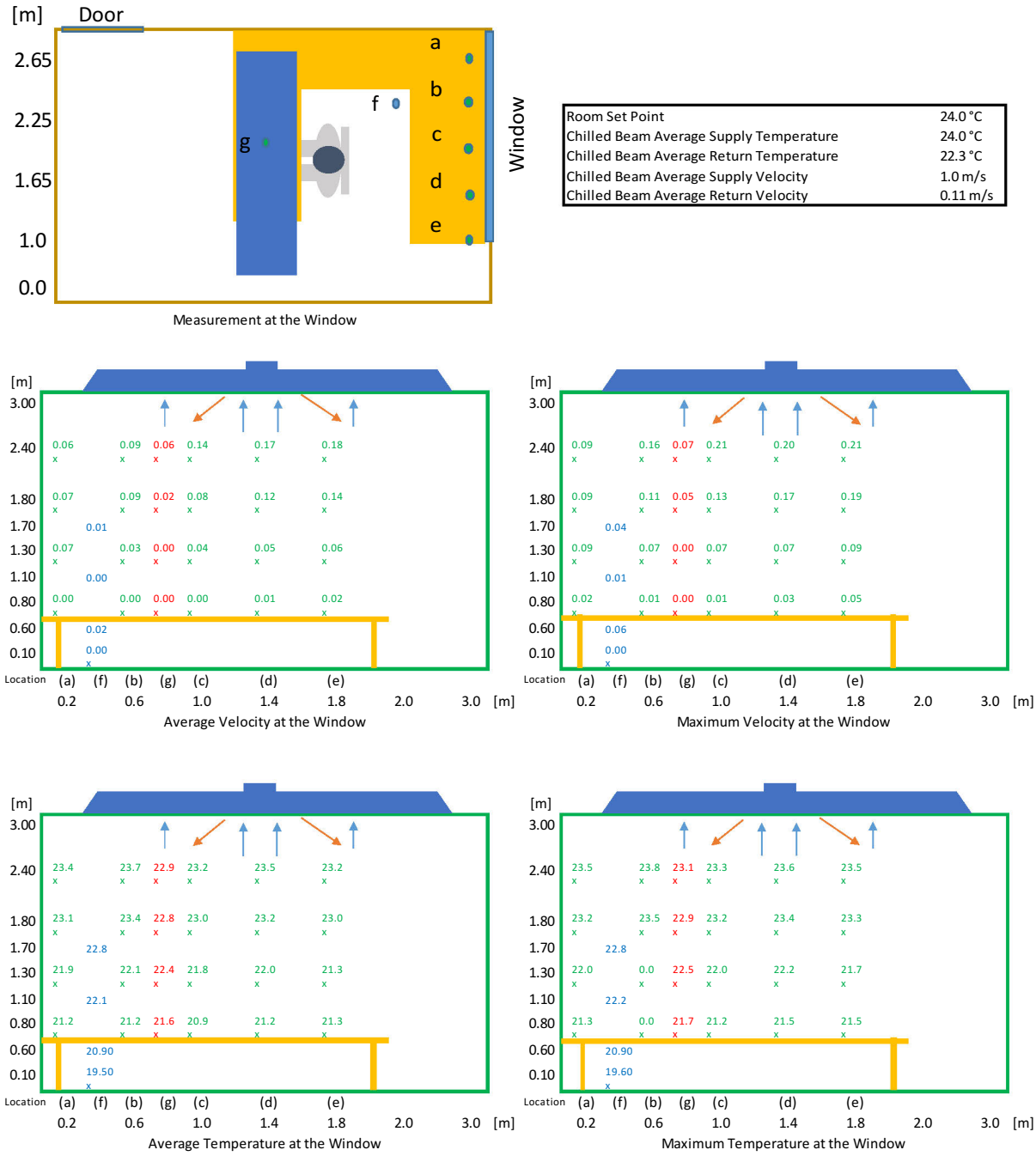

Figure A.3 - Air Temperature and Velocity Distribution at the Window with Room SP 24 (°C)

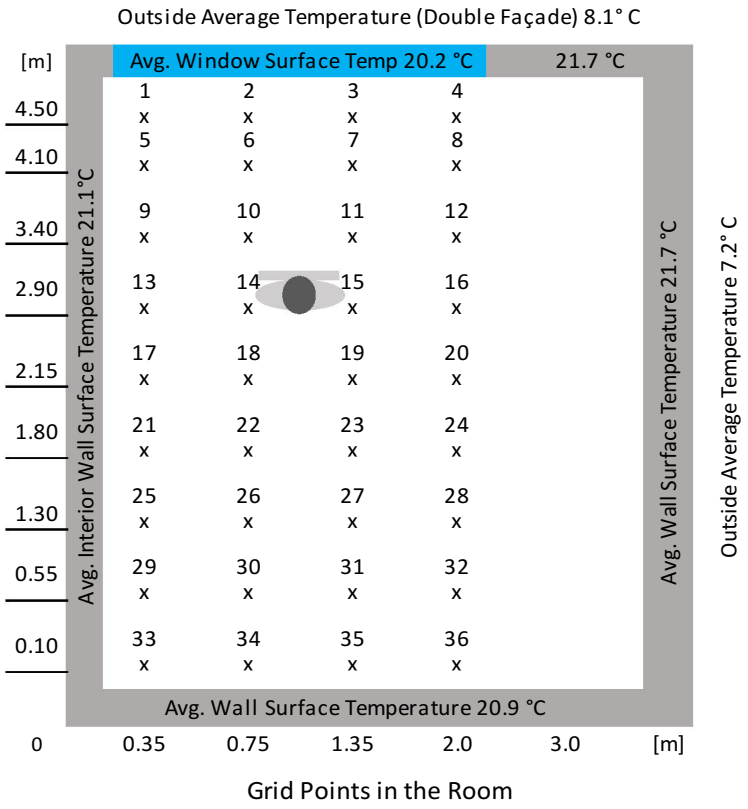

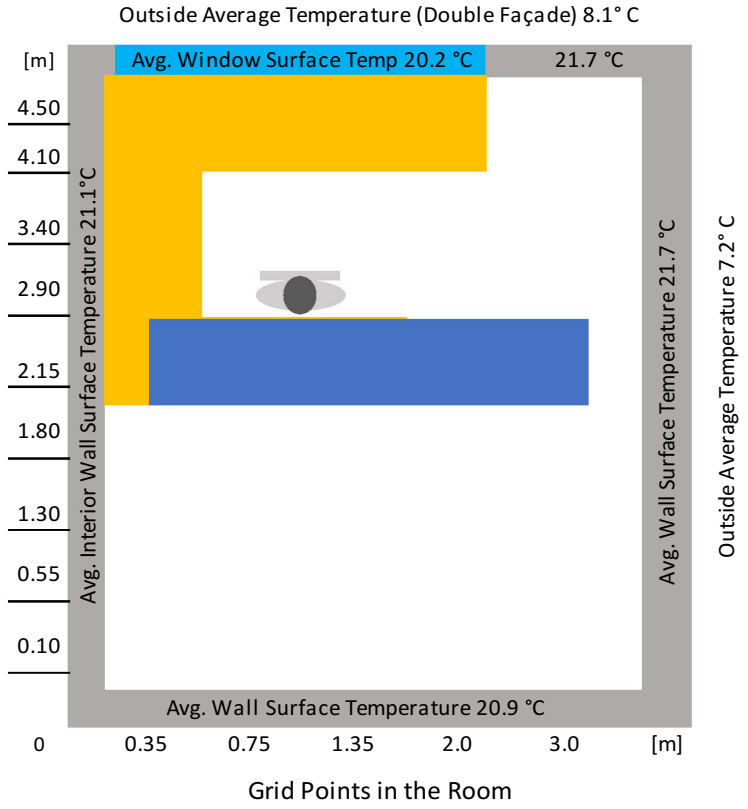

Figure A.4 - Grid Points in the Test Room 1 for Measurement of Air Temperature and Velocity

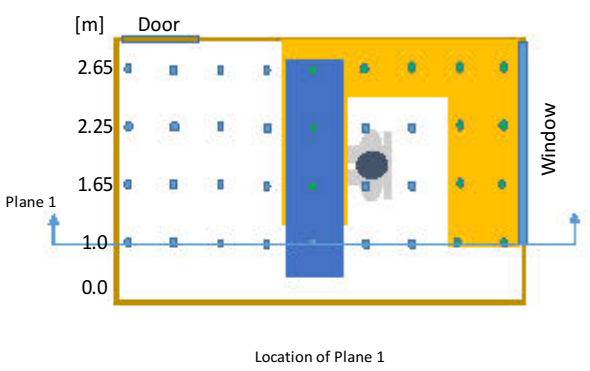

Location of Plane 1

Room Set Point	24 °C
Chilled Beam Supply Temperature	23.5 °C
Chilled Beam Return Temperature	22.0 °C
Chilled Beam Supply Velocity	1.0 m/s
Chilled Beam Return Velocity	0.12 m/s

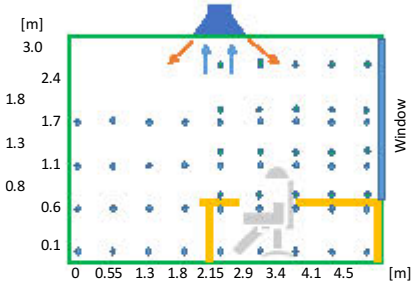

Measuring Points in the Room

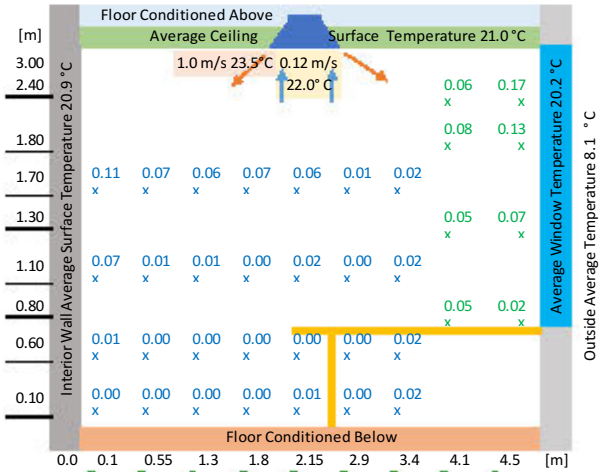

Plane 1 - Average Velocity at different heights

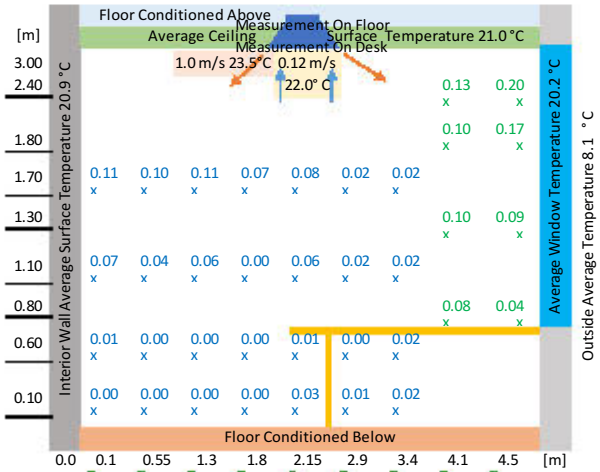

Plane 1 - Maximum Velocity at different heights

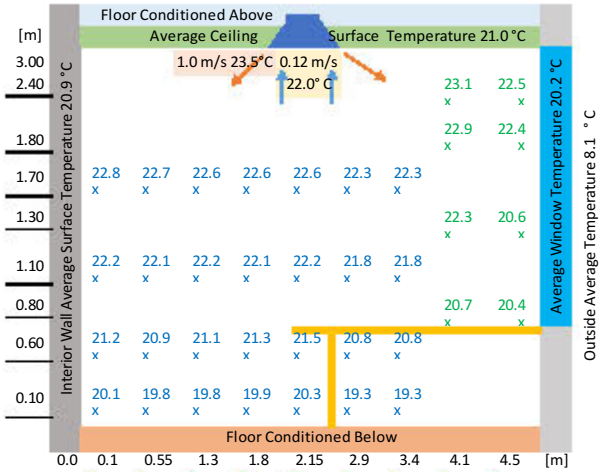

Plane 1 - Average Temperture at different heights

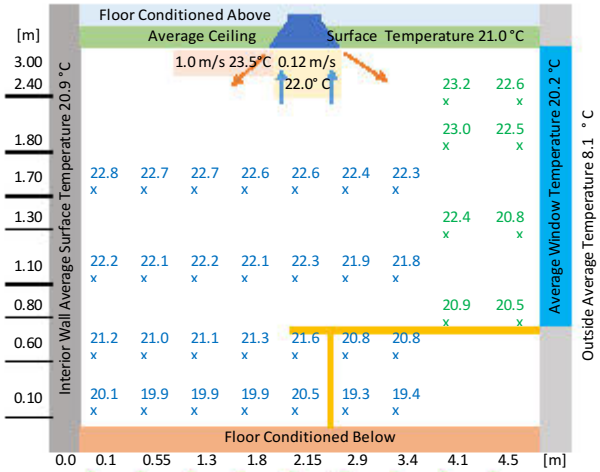

Plane 1 - Maximum Temperture at different heights

Figure A.5 - Section 1 – Air Temperature and Air Velocity at Room SP 24 (°C)

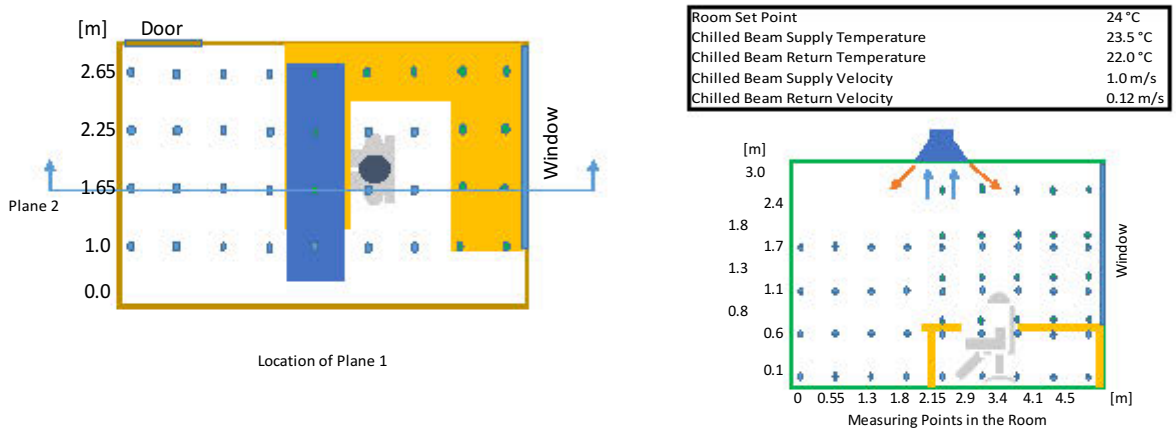

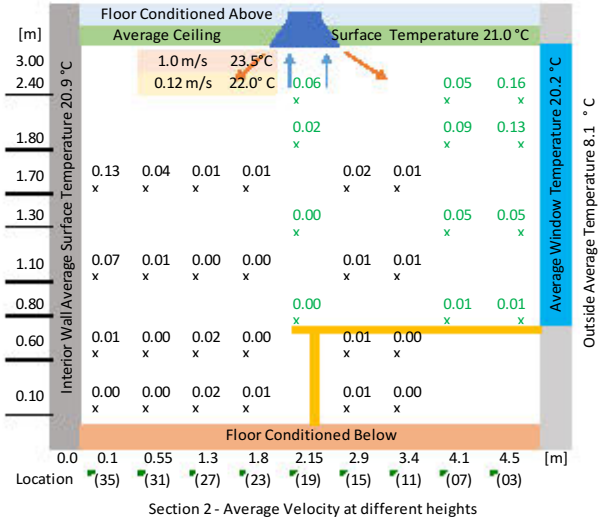

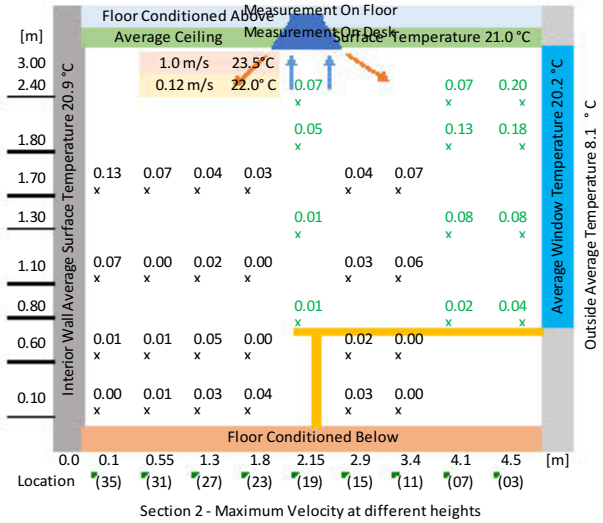

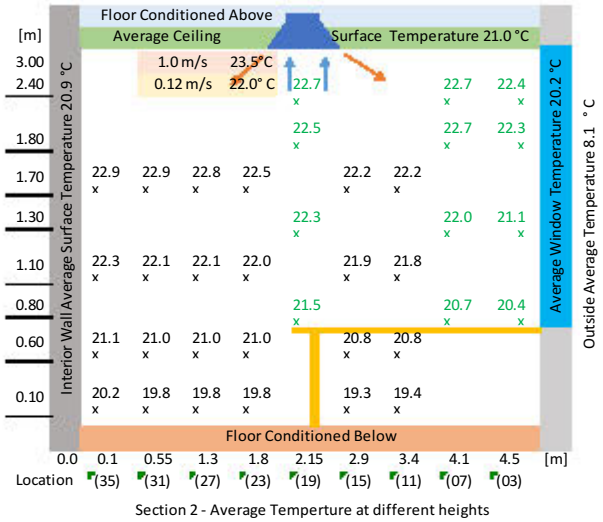

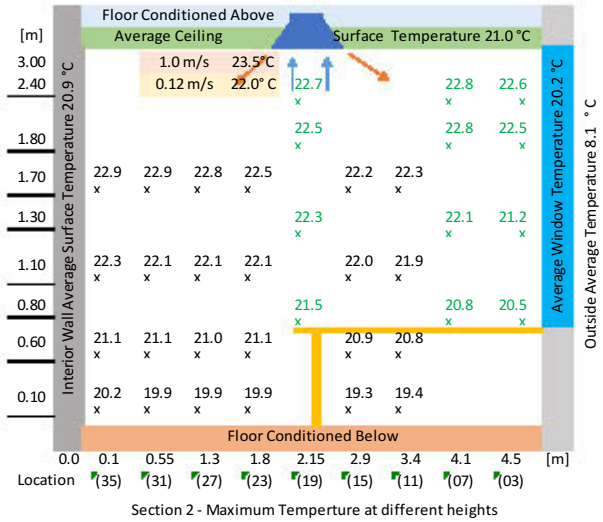

Figure A.6 - Section 2 – Air Temperature and Air Velocity at Room SP 24 (°C)

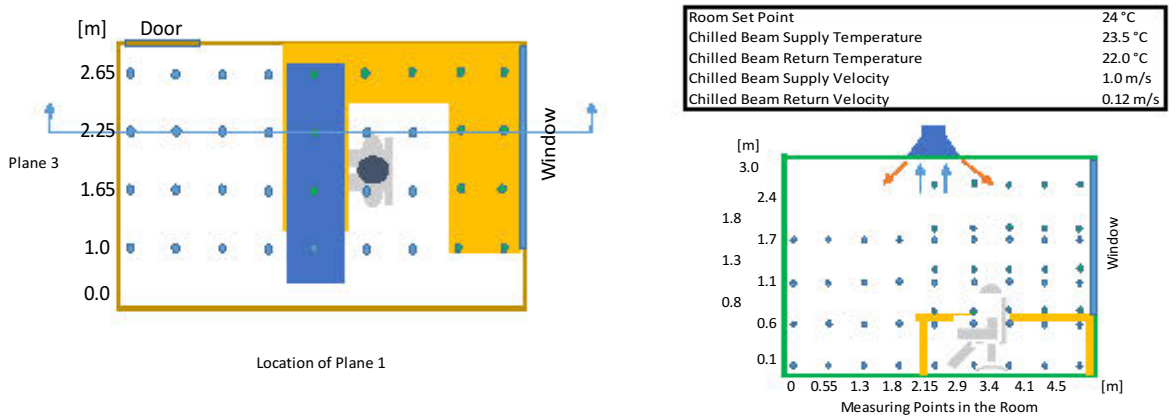

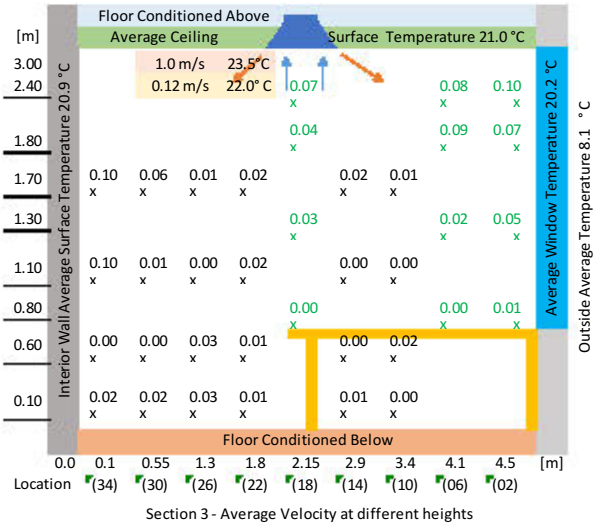

Section 3 - Average Velocity at different heights

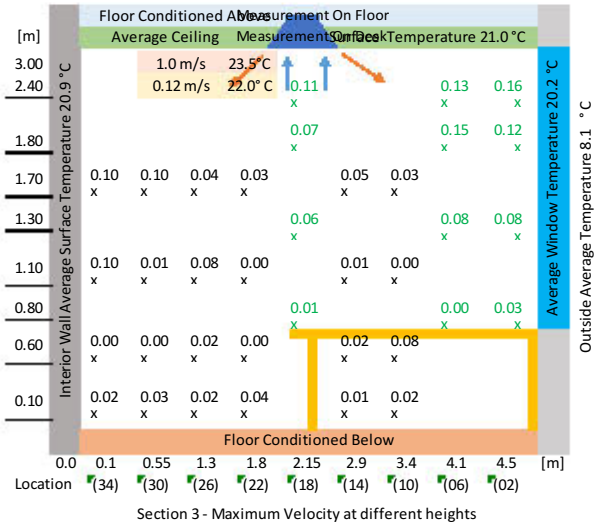

Section 3 - Maximum Velocity at different heights

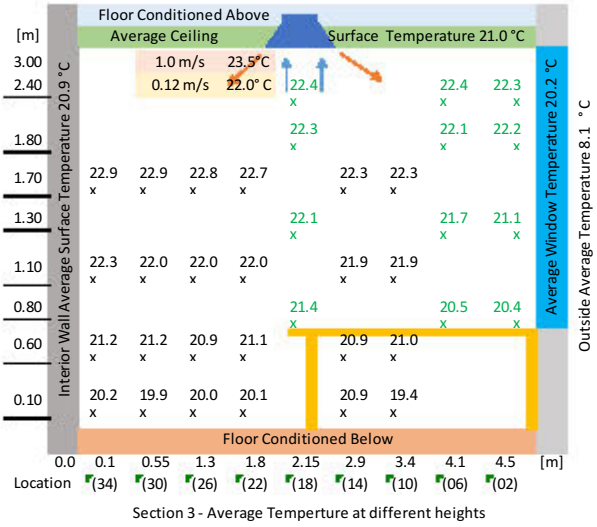

Section 3 - Average Temperture at different heights

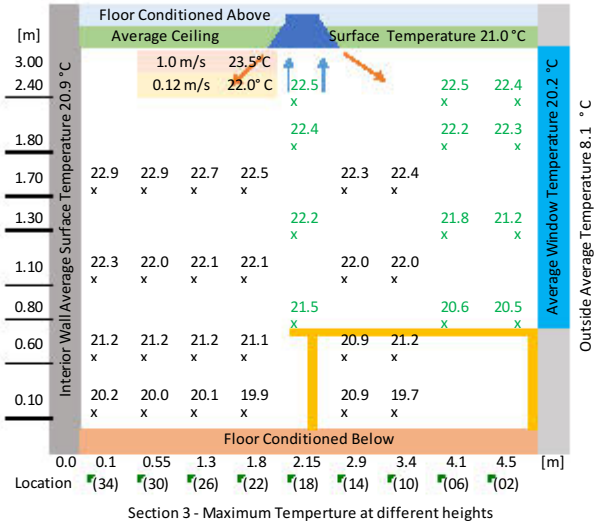

Section 3 - Maximum Temperture at different heights

Figure A.7 - Section 3 – Air Temperature and Air Velocity at Room SP 24 (°C)

APPENDIX B – ROOM AIR DISTRIBUTION – COOLING

This section shows graphically the experimental measurement at different room setpoint temperature and the air temperature and air velocity recorded at 4 different heights including the supply velocity and induction (return) velocity at the ACB during cooling season. (June/July, 2018).

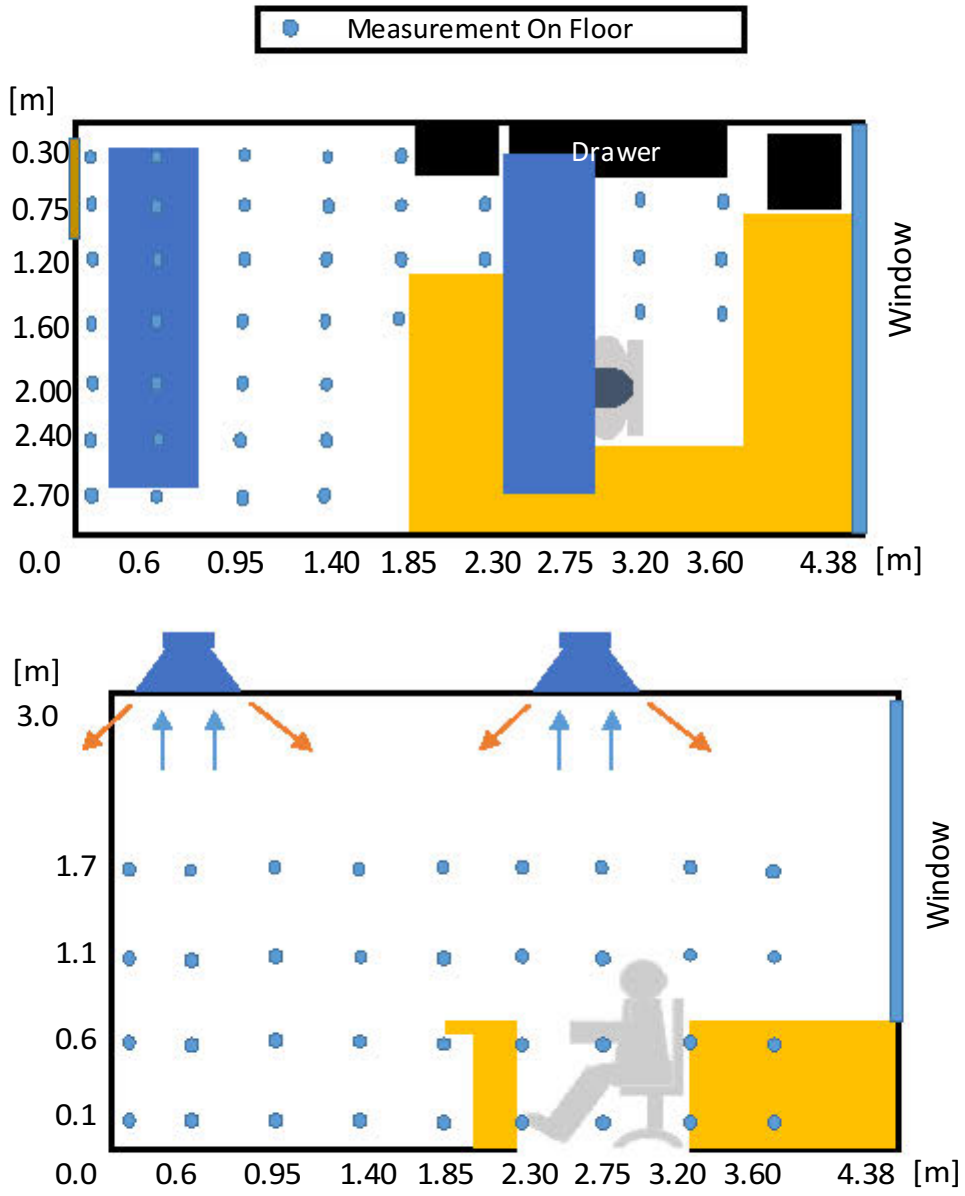

Figure B.1 - Grid Points in the Test Room 2 for Measurement of Air Temperature & Velocity

Room Setpoint 22°C

Table B.1 - Air Velocity and Air Temperature in Cooling at Setpoint 22°C (Cooling)

Experimental Results (Room Setpoint 22 (°C))										
Plane	Point No	Distance (m)	Air Velocity (m/s)				Air Temperature (°C)			
			Height (m)				Height (m)			
			0.1	0.6	1.1	1.7	0.1	0.6	1.1	1.7
PLANE 1 (0.75 m)	38	0.05	0.10	0.08	0.12	0.19	21.31	21.40	21.39	21.30
	31	0.60	0.12	0.17	0.21	0.22	21.14	21.11	21.08	21.04
	24	0.95	0.19	0.10	0.08	0.08	20.58	20.70	20.73	20.75
	17	1.40	0.09	0.05	0.05	0.08	21.12	21.20	21.24	21.26
	13	1.85	0.06	0.05	0.09	0.04	21.58	21.63	21.62	21.75
	10	2.30	0.12	0.12	0.13	0.13	21.32	21.32	21.24	21.35
	7	2.75	0.05	0.05	0.07	0.12	21.90	22.00	22.00	21.98
	4	3.20	0.05	0.06	0.12	0.14	21.79	21.81	21.93	21.90
	1	3.60	0.06	0.10	0.12	0.10	20.77	20.67	20.89	20.85

Experimental Results (Room Setpoint 22 (°C))										
Plane	Point No	Distance (m)	Air Velocity (m/s)				Air Temperature (°C)			
			Height (m)				Height (m)			
			0.1	0.6	1.1	1.7	0.1	0.6	1.1	1.7
PLANE 2 (1.2 m)	39	0.05	0.08	0.17	0.25	0.27	21.48	21.48	21.40	21.32
	32	0.60	0.12	0.12	0.14	0.25	21.01	20.93	20.96	20.82
	25	0.95	0.14	0.07	0.09	0.21	20.68	20.78	20.83	20.65
	18	1.40	0.05	0.05	0.07	0.09	21.57	21.64	21.66	21.70
	14	1.85	0.08	0.07	0.11	0.07	21.68	21.70	21.66	21.80
	11	2.30	0.13	0.12	0.13	0.08	20.86	20.89	20.92	21.13
	8	2.75	0.07	0.08	0.12	0.13	21.99	22.00	21.93	21.98
	5	3.20	0.09	0.10	0.11	0.14	21.80	21.84	21.97	21.98
	2	3.60	0.07	0.10	0.11	0.12	21.50	21.48	21.90	21.76

Experimental Results (Room Setpoint 22 (°C))										
Plane	Point No	Distance (m)	Air Velocity (m/s)				Air Temperature (°C)			
			Height (m)				Height (m)			
			0.1	0.6	1.1	1.7	0.1	0.6	1.1	1.7
PLANE 3 (1.6 m)	40	0.05	0.10	0.20	0.25	0.29	21.51	21.51	21.50	21.48
	33	0.60	0.15	0.13	0.11	0.12	20.85	20.89	21.00	21.01
	26	0.95	0.15	0.08	0.10	0.12	20.98	21.10	21.18	21.16
	19	1.40	0.09	0.11	0.11	0.05	21.28	21.26	21.35	21.59
	15	1.85	0.09	0.18	0.10	0.07	21.05	20.86	21.20	21.31
	9	2.75	0.08	0.10	0.12	0.14	21.89	21.86	21.85	21.81
	6	3.20	0.10	0.10	0.13	0.14	21.80	21.90	21.99	22.03
	3	3.60	0.08	0.12	0.13	0.14	21.60	21.63	21.78	21.88

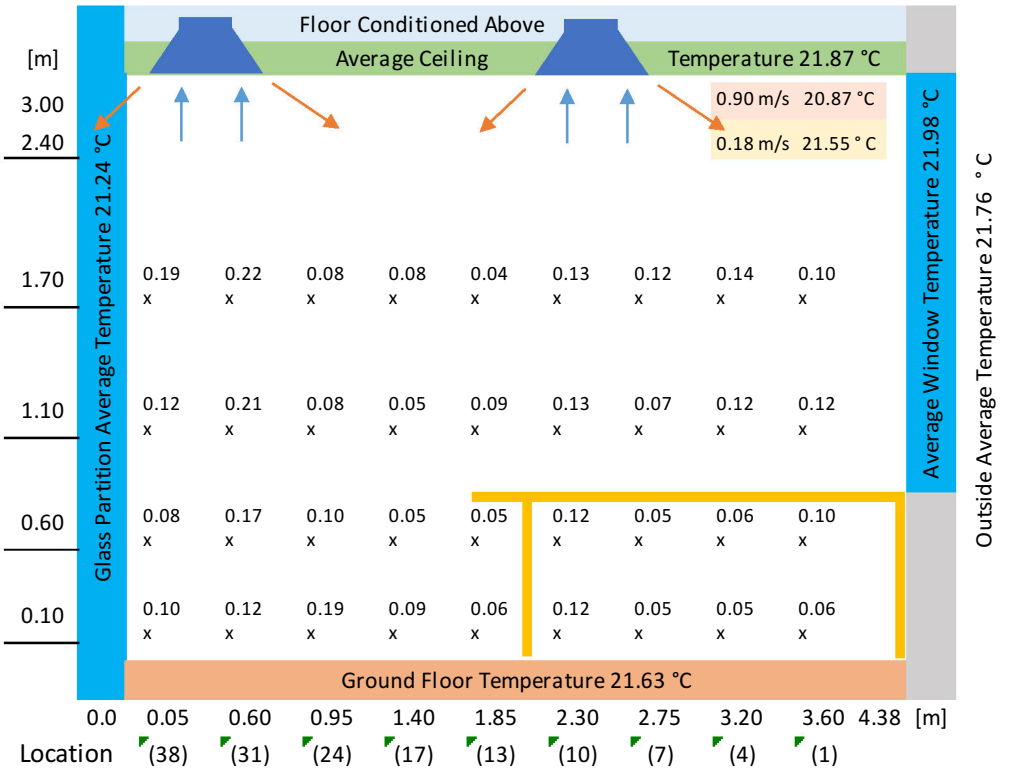

Plane - 1 (0.75 m) - Average Velocity at different heights

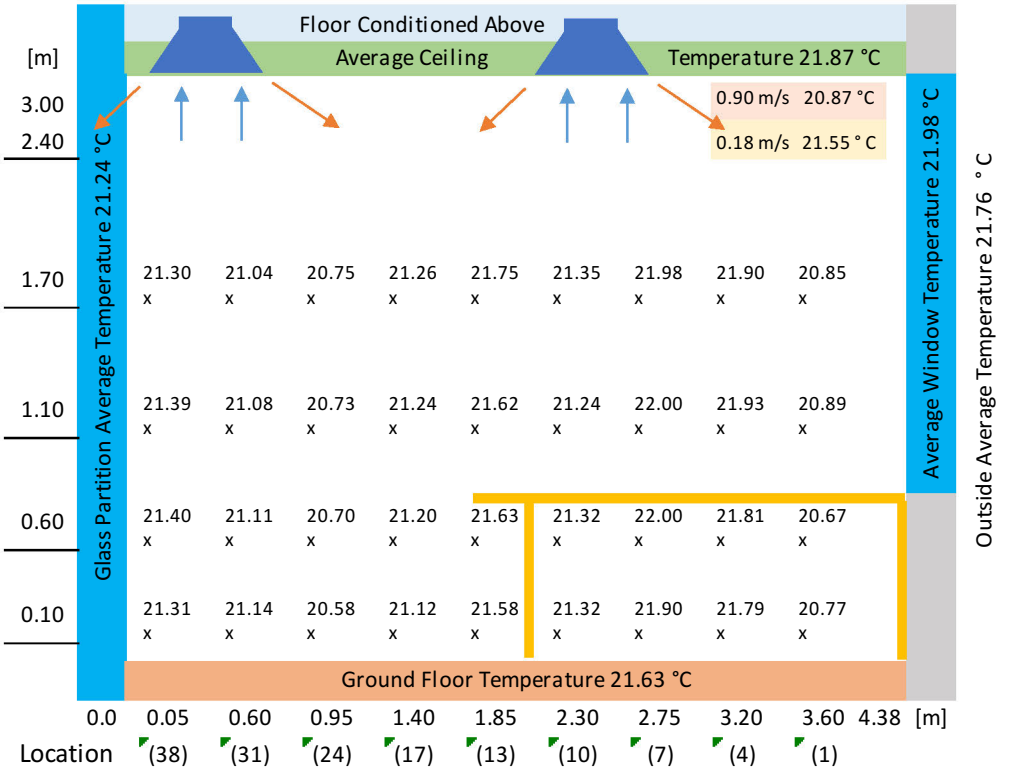

Plane - 1 (0.75 m) - Average Temperature at different heights

Figure B.2 - Average Air Velocity & Air Temperature at Section 1 (0.75 m) in Cooling

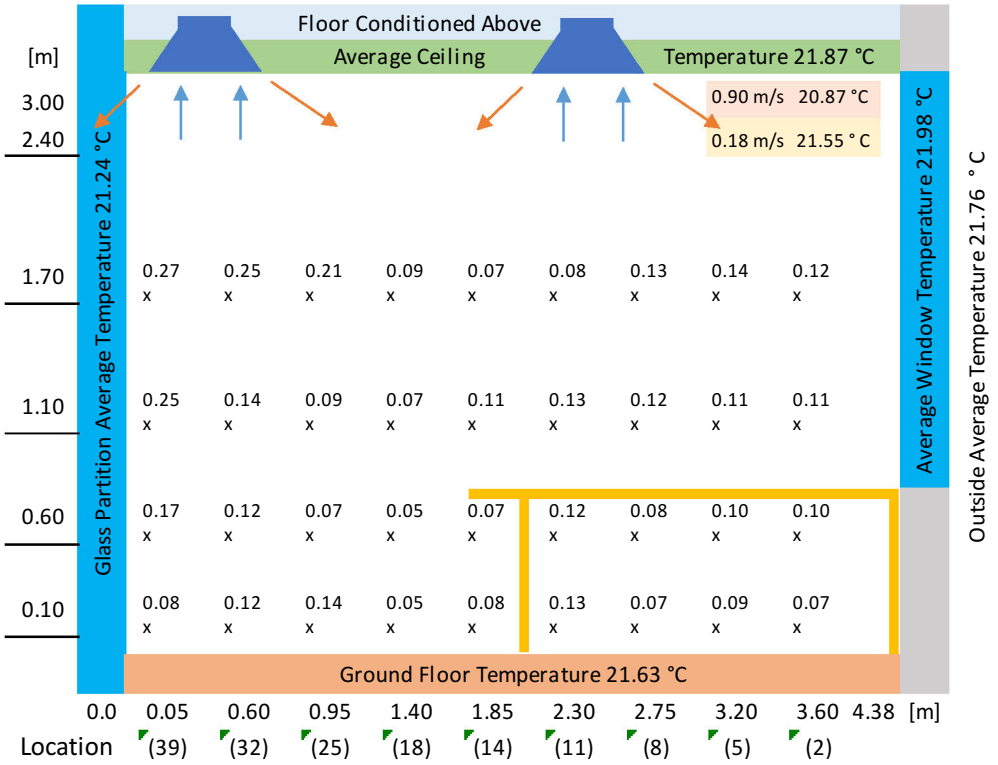

Plane - 2 (1.2 m) - Average Velocity at different heights

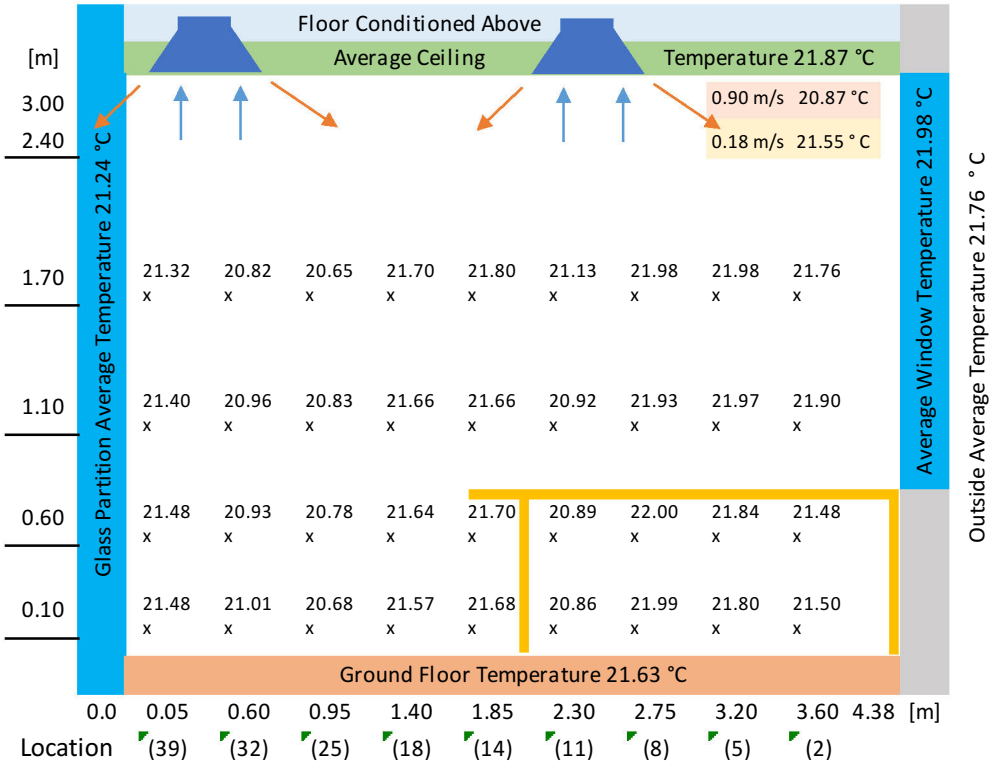

Plane - 2 (1.2 m) - Average Temperature at different heights

Figure B.3 - Average Air Velocity & Air Temperature at Section 2 (1.2 m) in Cooling

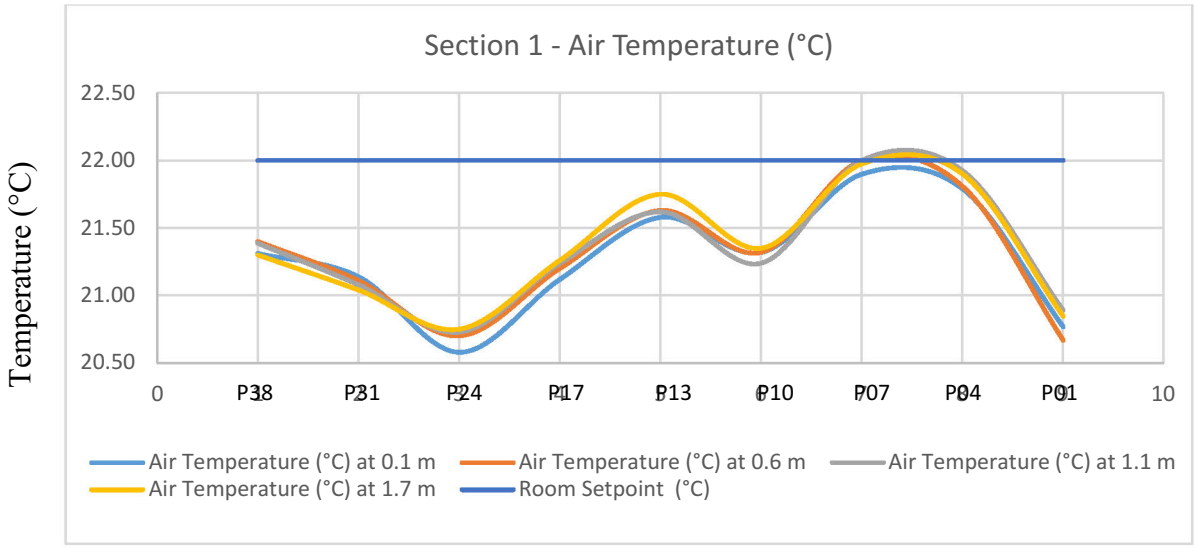

Figure B.4 - Air Temperature at Section 1 of Test Room 2 (Setpoint 22°C in Cooling)

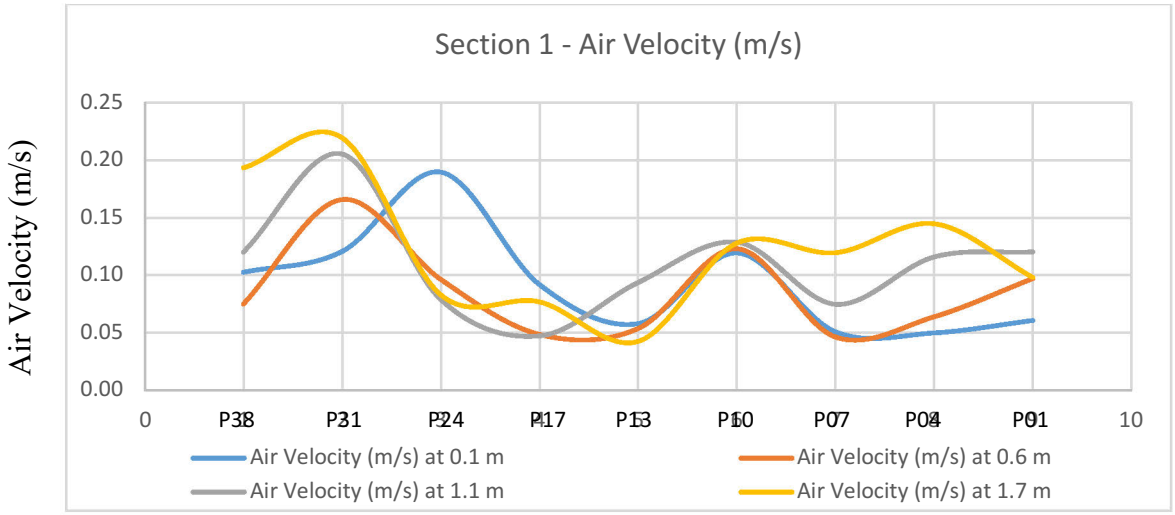

Figure B.5 - Air Velocities at Section 1 of Test Room 2 (Setpoint 22°C in Cooling)

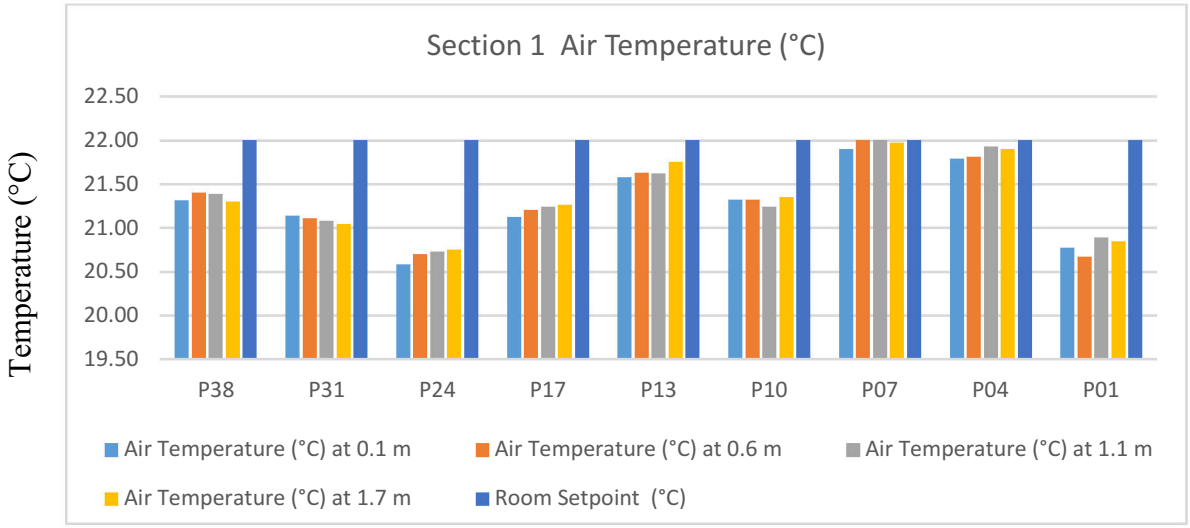

Figure B.6 - Air Temperatures at 4 Different Heights and Room Setpoint (Section 1 @22°C)

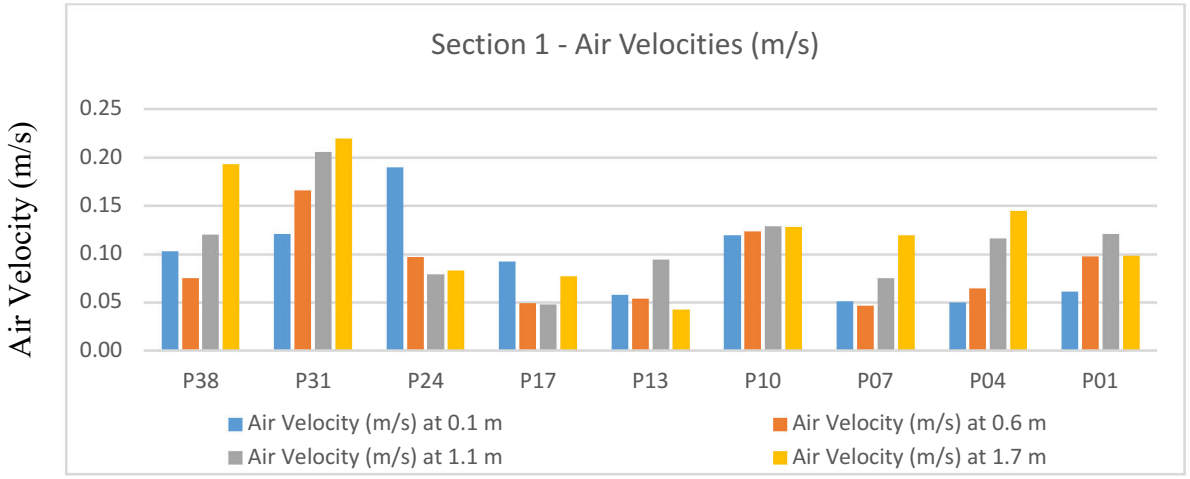

Figure B.7 - Air Velocities at 4 Different Heights and Room Setpoint (Section 1 @22°C)

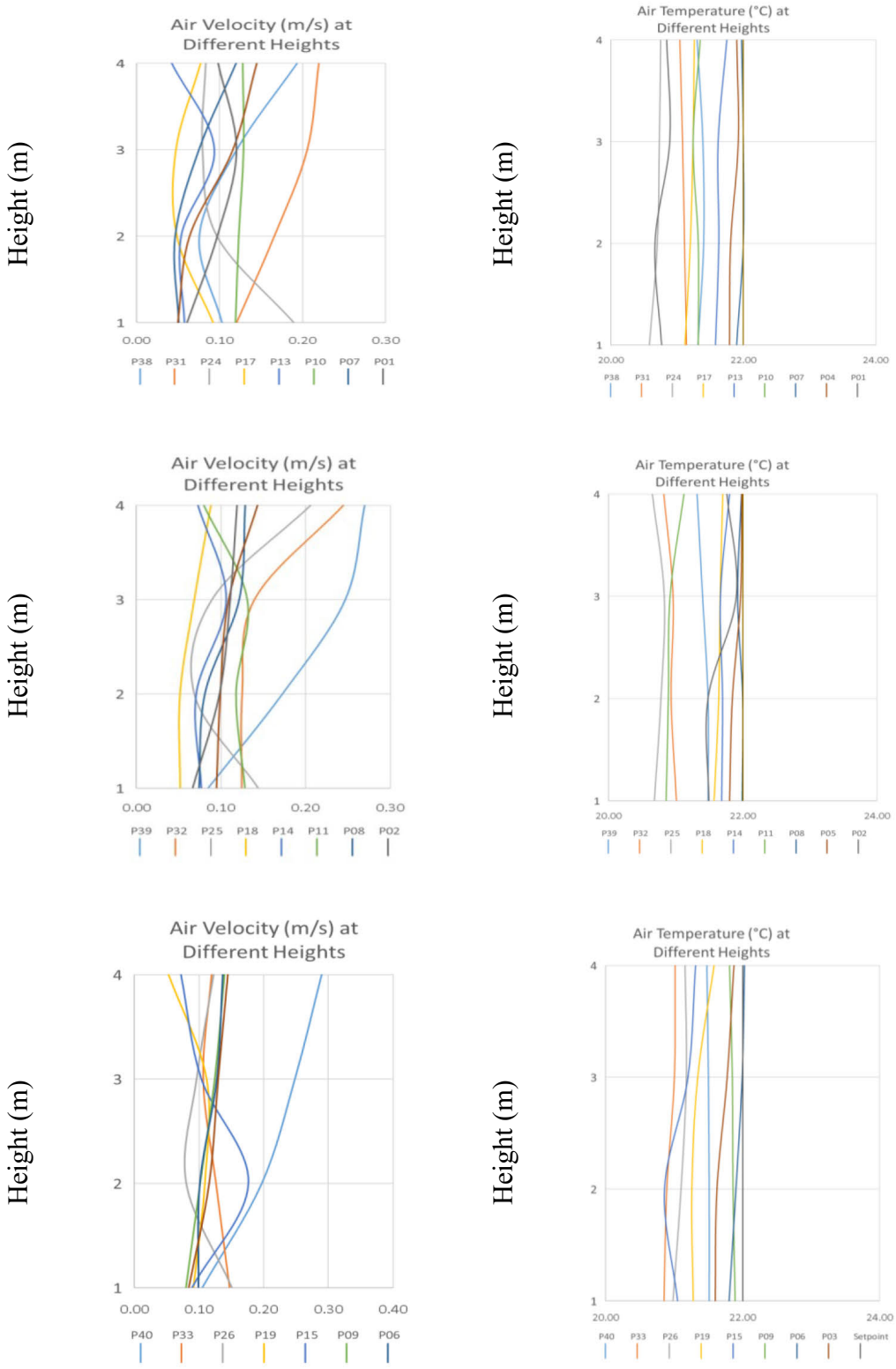

Figure B.8 - Air Velocities & Temperatures at Section 1, 2 and 3 respectively at SP 22°C

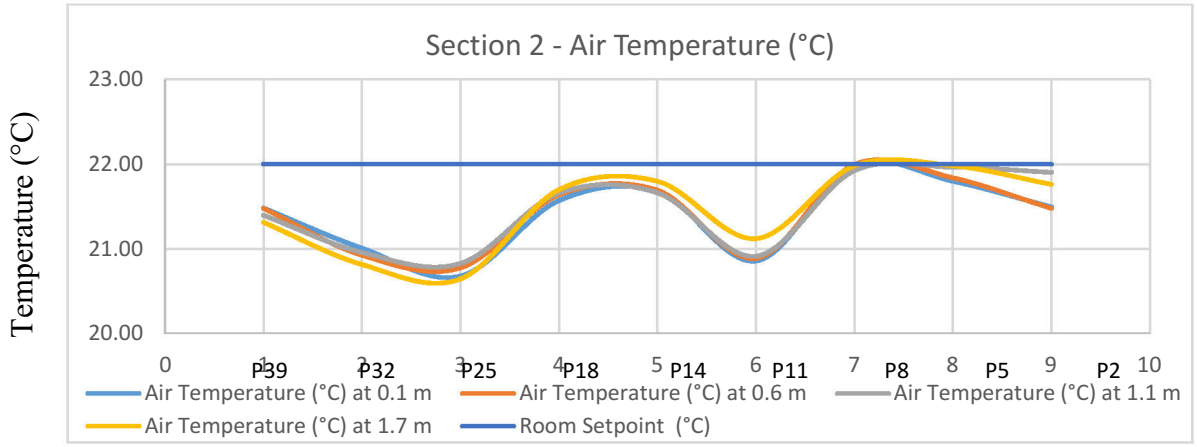

Figure B.9 - Air Temperature at Section 2 of Test Room 2 (Setpoint 22°C in Cooling)

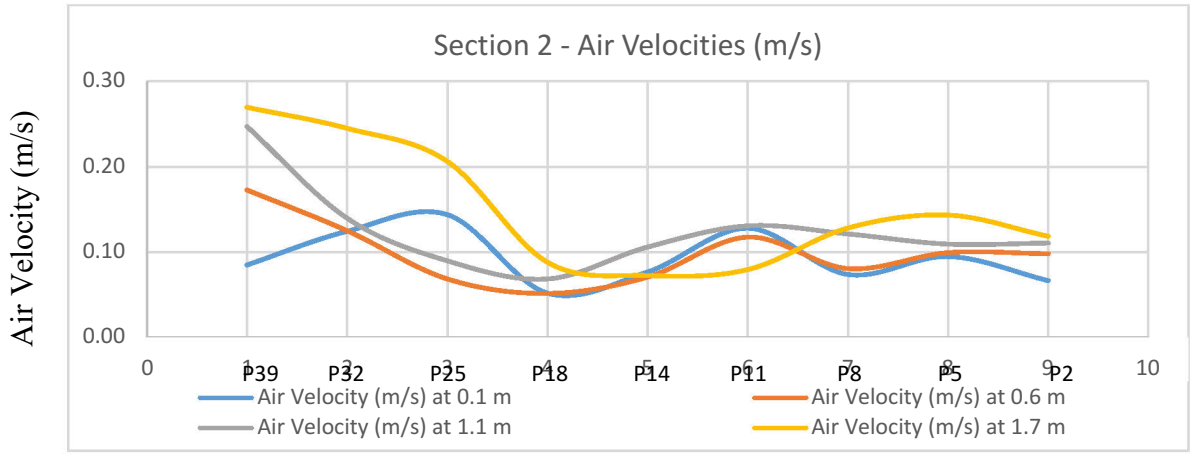

Figure B.10 - Air Velocity at Section 2 of Test Room 2 (Setpoint 22°C in Cooling)

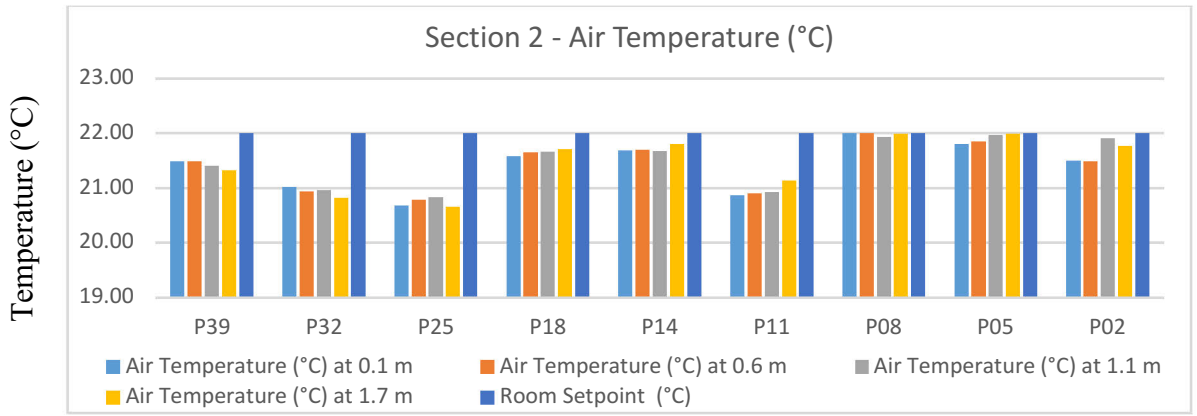

Figure B.11 - Air Temperature at 4 Different Heights across Section 2 of Test Room 2 (Setpoint 22°C in Cooling)

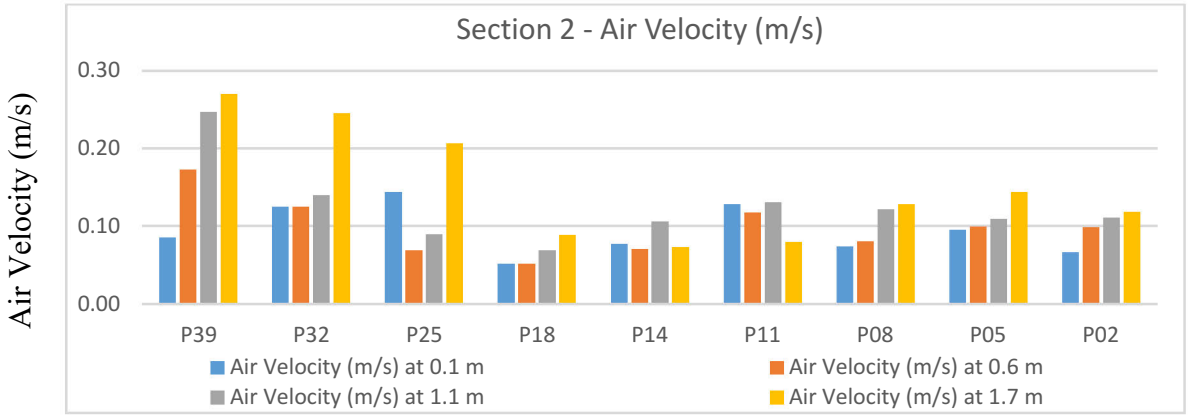

Figure B.12 - Air Velocity at 4 Different Heights across Section 2 of Test Room 2 (Setpoint 22°C in Cooling)

Room Setpoint 24°C

Table B.2 - Air Velocity and Air Temperature in Cooling at Setpoint 24°C (Cooling)

Experimental Results (Room Setpoint 24 (°C))										
Section / Plane	Point No	Distance (m)	Air Velocity (m/s)				Air Temperature (°C)			
			Height (m)				Height (m)			
			0.1	0.6	1.1	1.7	0.1	0.6	1.1	1.7
Section 1 (0.75 m)	38	0.05	0.12	0.19	0.25	0.24	22.95	23.00	22.97	22.88
	31	0.60	0.01	0.02	0.09	0.09	23.28	23.98	24.57	24.98
	24	0.95	0.08	0.10	0.09	0.18	23.63	23.99	24.20	24.19
	17	1.40	0.09	0.07	0.09	0.07	23.24	23.39	23.45	23.58
	13	1.85	0.01	0.02	0.06	0.08	22.93	23.78	24.55	24.99
	10	2.30	0.03	0.07	0.13	0.09	22.85	23.28	23.35	23.46
	7	2.75	0.00	0.03	0.05	0.08	22.68	23.75	24.41	24.73
	4	3.20	0.01	0.02	0.05	0.06	22.62	23.28	23.50	23.62
	1	3.60	0.04	0.05	0.09	0.15	22.19	23.73	24.48	24.29

Experimental Results (Room Setpoint 24 (°C))										
Section / Plane	Point No	Distance (m)	Air Velocity (m/s)				Air Temperature (°C)			
			Height (m)				Height (m)			
			0.1	0.6	1.1	1.7	0.1	0.6	1.1	1.7
Section 2 (1.2 m)	39	0.05	0.11	0.23	0.27	0.28	22.87	22.85	22.82	22.70
	32	0.60	0.06	0.08	0.11	0.16	23.47	24.27	24.75	24.97
	25	0.95	0.09	0.06	0.09	0.20	23.51	23.69	23.73	23.54
	18	1.40	0.08	0.07	0.09	0.06	23.08	23.20	23.22	23.40
	14	1.85	0.01	0.07	0.09	0.10	23.07	23.68	24.02	24.01
	11	2.30	0.04	0.06	0.07	0.06	22.88	23.23	23.42	23.58
	8	2.75	0.01	0.05	0.09	0.12	22.70	23.56	23.98	24.09
	5	3.20	0.01	0.01	0.02	0.07	22.63	23.49	24.07	24.69
	2	3.60	0.00	0.05	0.10	0.10	22.45	23.42	24.10	23.88

Experimental Results (Room Setpoint 24 (°C))										
Section / Plane	Point No	Distance (m)	Air Velocity (m/s)				Air Temperature (°C)			
			Height (m)				Height (m)			
			0.1	0.6	1.1	1.7	0.1	0.6	1.1	1.7
Section 3 (1.6 m)	40	0.05	0.10	0.23	0.28	0.28	22.80	22.80	22.78	22.72
	33	0.60	0.12	0.09	0.13	0.11	23.80	24.10	24.27	24.38
	26	0.95	0.10	0.07	0.09	0.14	23.18	23.37	23.45	23.37
	19	1.40	0.10	0.09	0.12	0.08	22.88	23.01	23.04	23.28
	15	1.85	0.07	0.08	0.11	0.07	23.08	23.38	23.60	23.71
	9	2.75	0.02	0.06	0.11	0.12	22.78	23.40	23.62	23.69
	6	3.20	0.01	0.01	0.01	0.03	22.60	23.63	24.59	25.16
	3	3.60	0.00	0.07	0.11	0.10	22.55	23.15	23.56	23.62

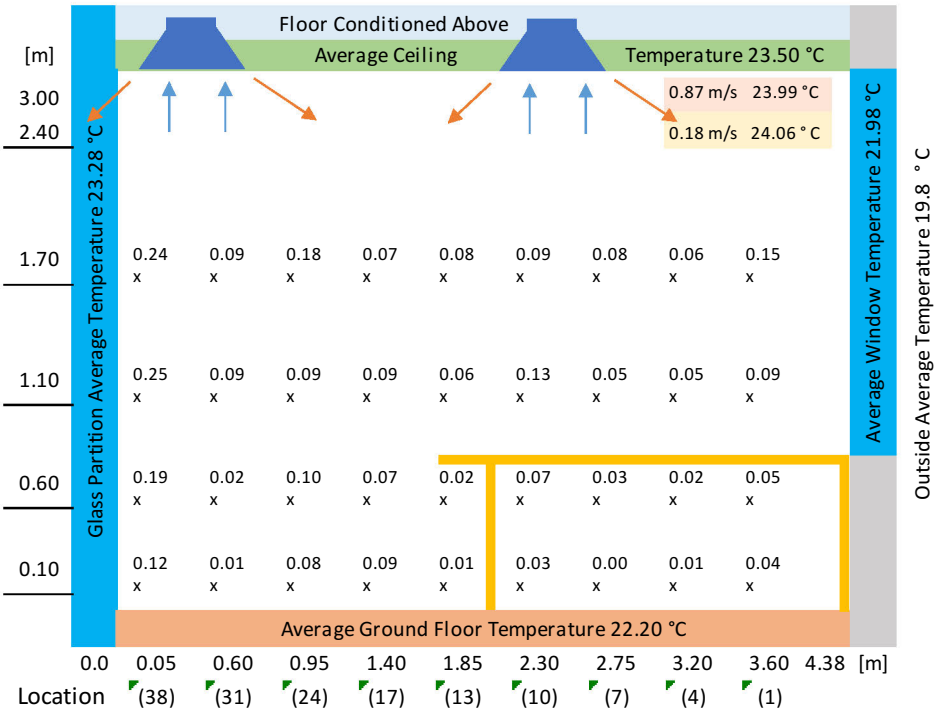

Plane - 1 (0.75 m) - Average Velocity at different heights

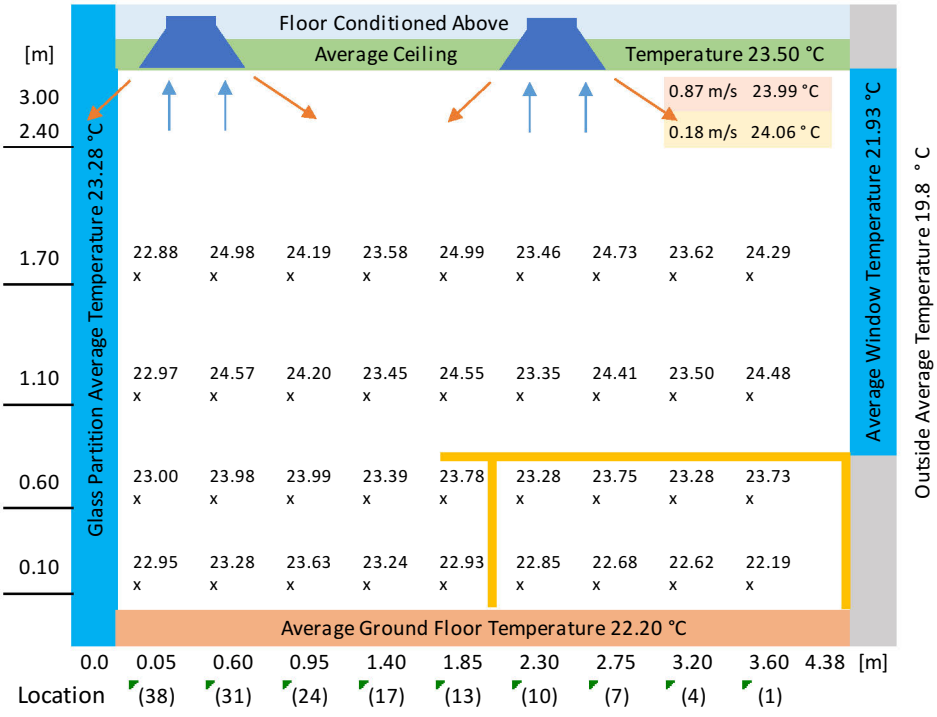

Plane - 1 (0.75 m) - Average Temperature at different heights

Figure B.13 - Spatial Distribution of Air Temperature and Velocity at Room SP Setpoint 24 (°C) (Section 1)

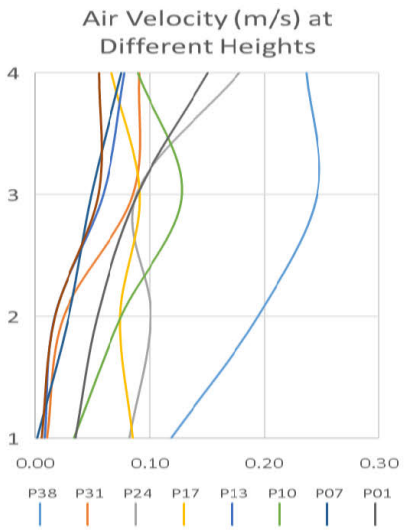

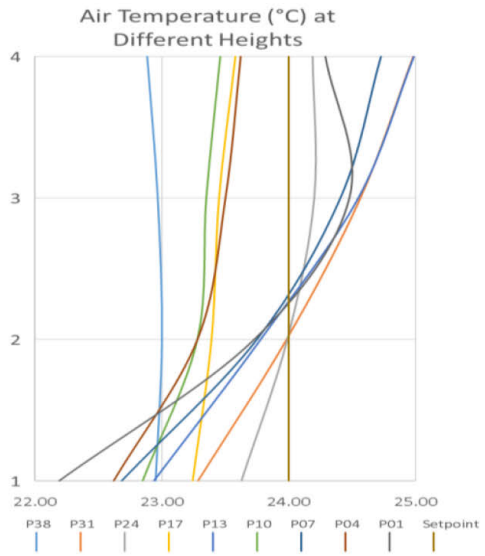

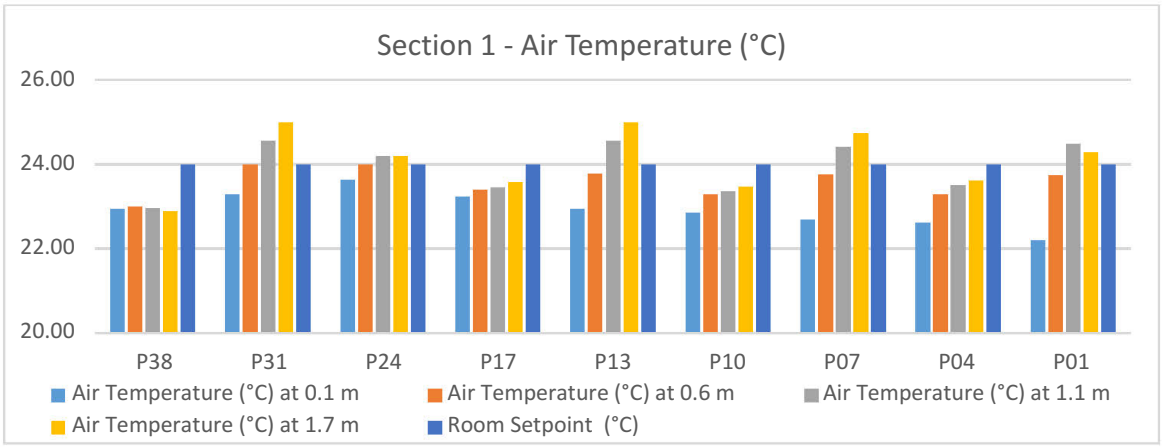

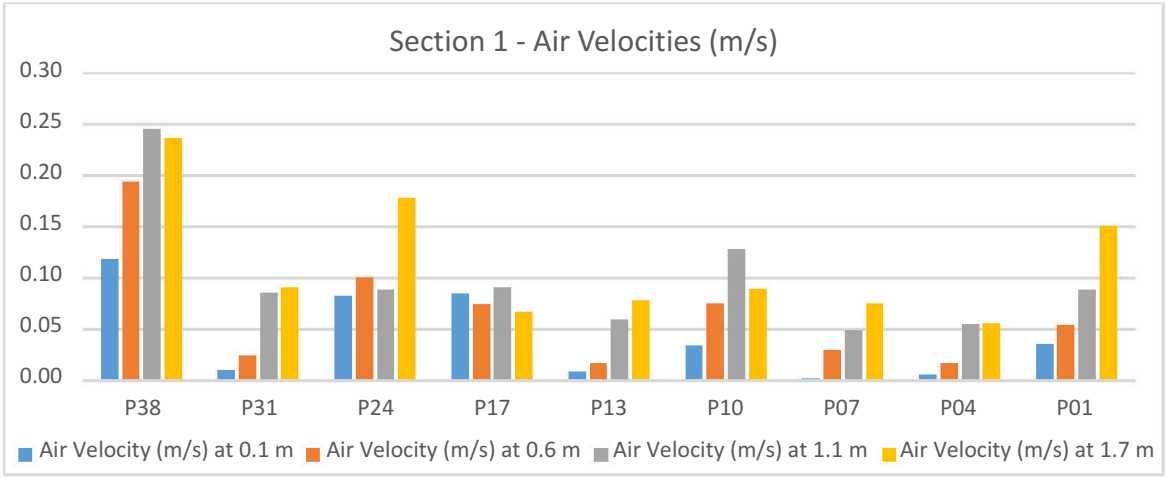

Figure B.14 - Section 1 – Graphs for Air Velocity and Temperature at 4 Different Heights SP 24(°C)

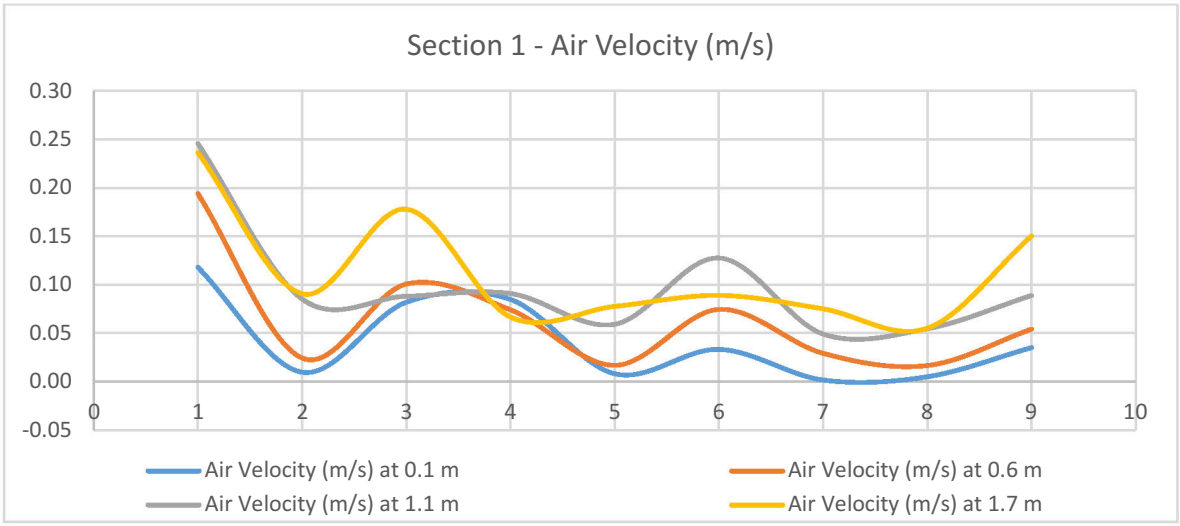

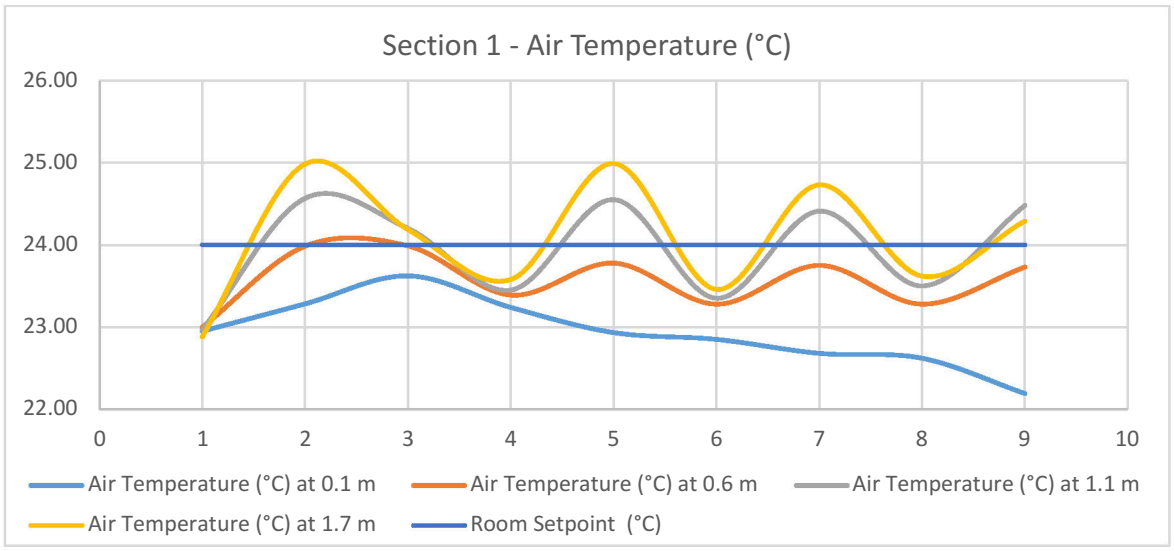

Figure B.15 - Section 1 – Graphs for Air Velocity and Temperature at SP 24(°C)

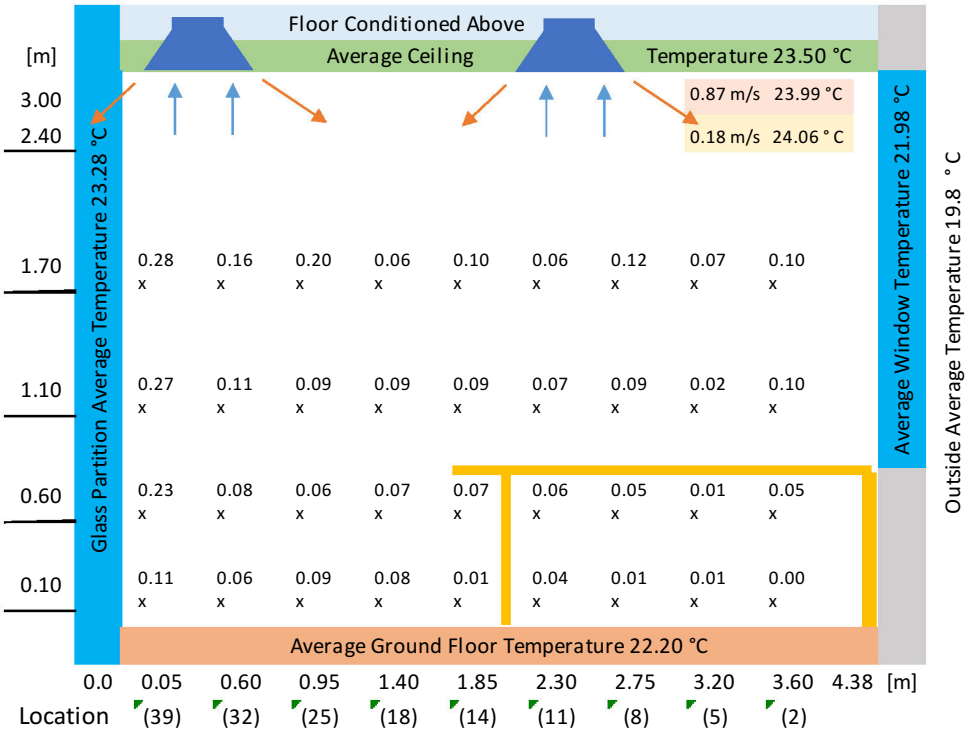

Plane - 2 (1.2 m) - Average Velocity at different heights

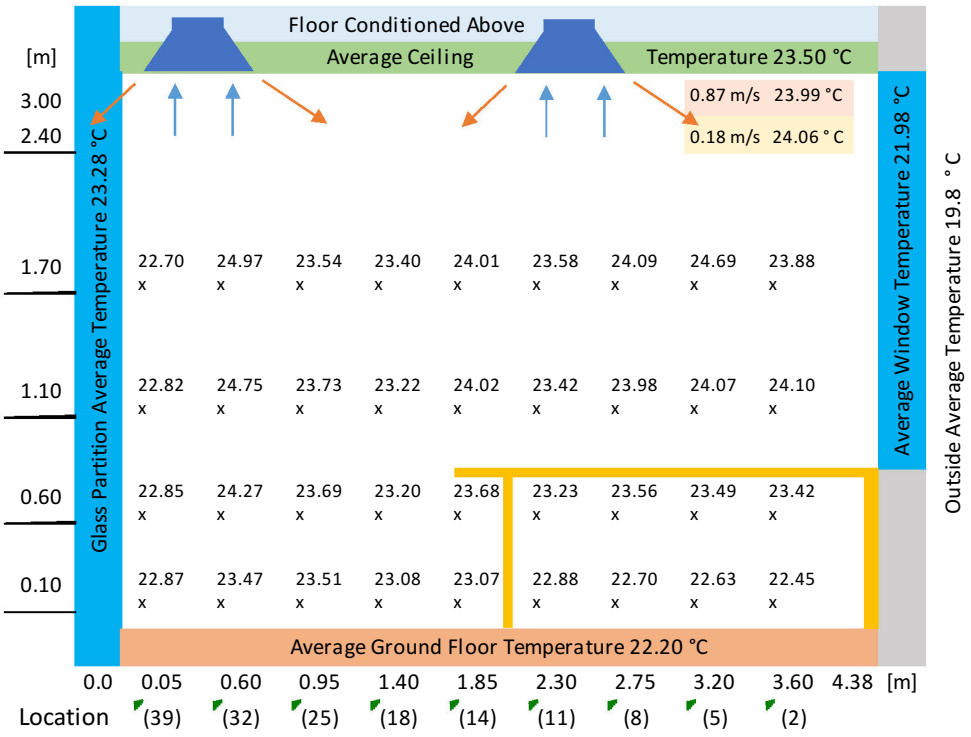

Plane - 2 (1.2 m) - Average Temperature at different heights

Figure B.16 - Spatial Distribution of Air Temperature and Velocity at Room SP Setpoint 24 (°C) (Section 2)

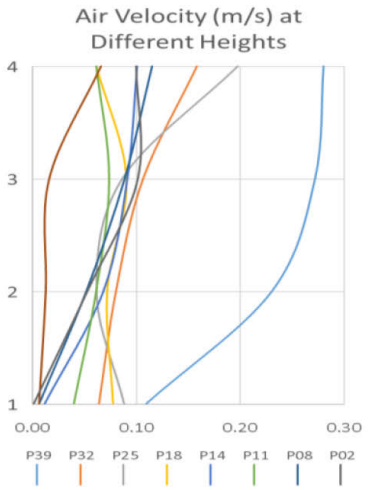

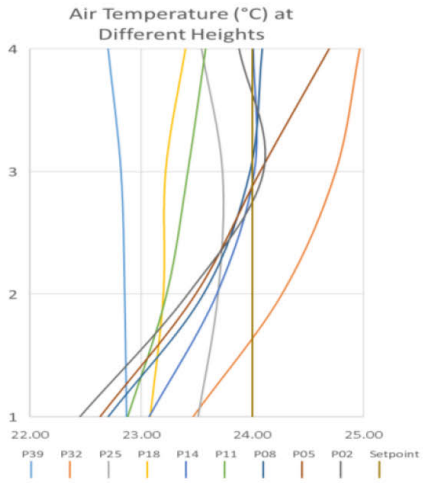

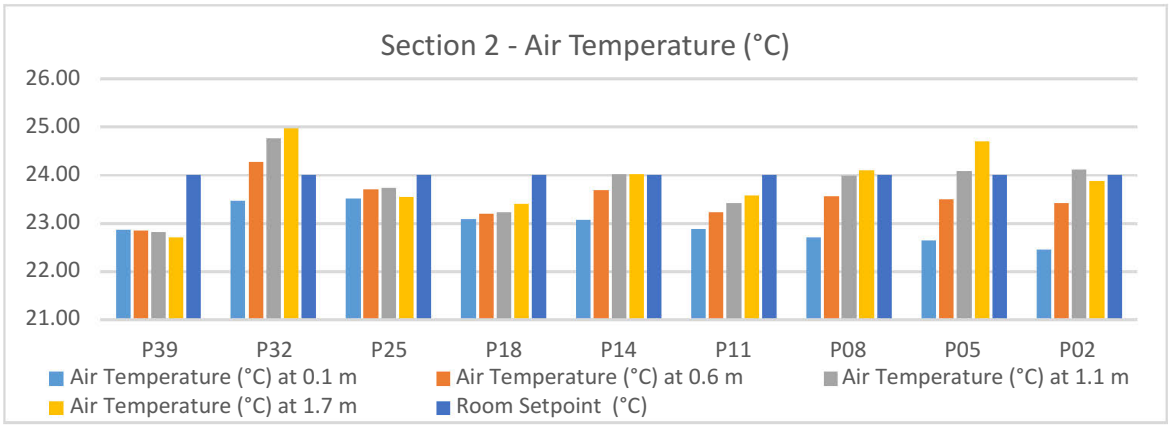

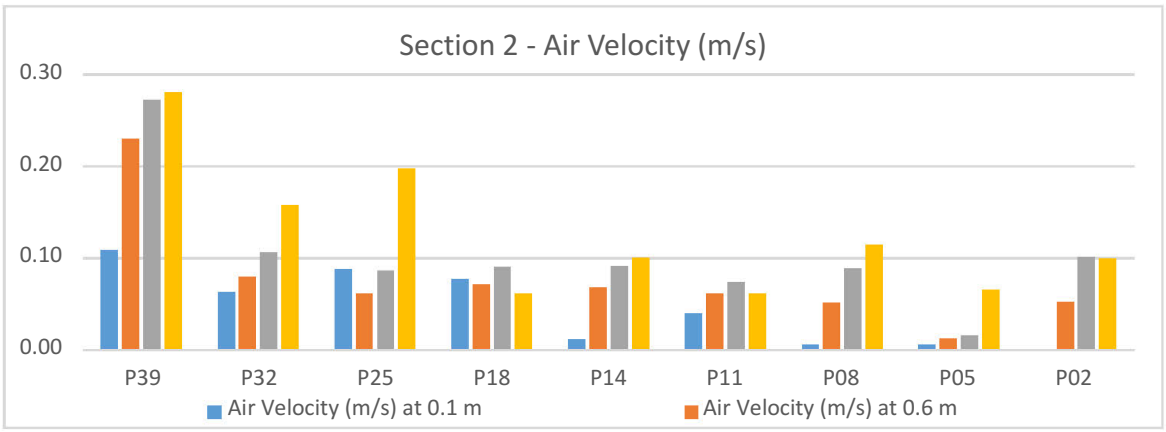

Figure B.17 - Section 2 – Graphs for Air Velocity and Temperature at 4 Different Heights SP 24(°C)

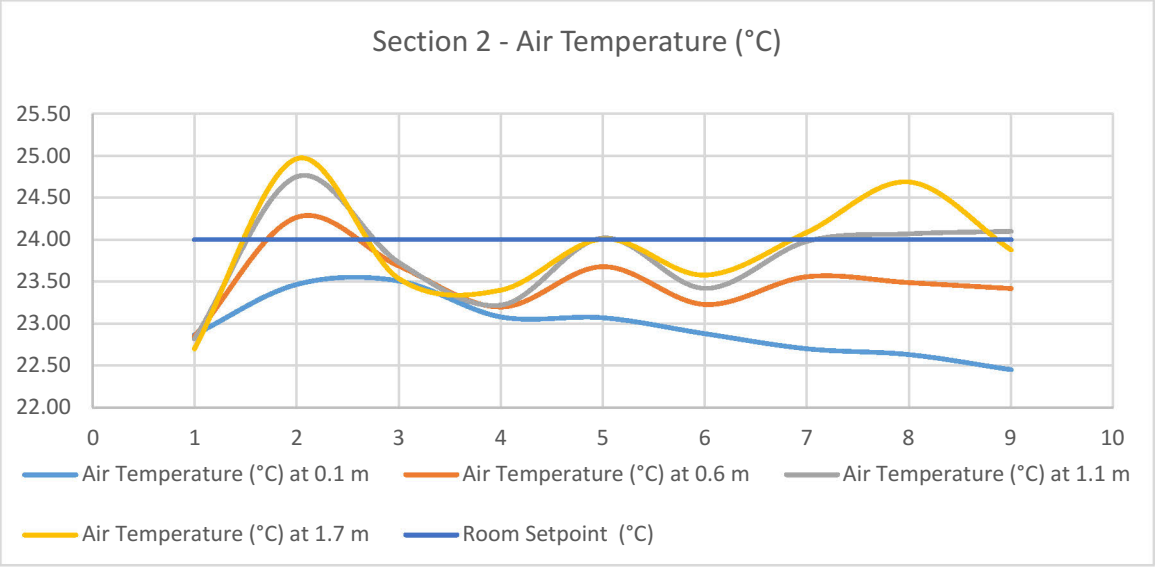

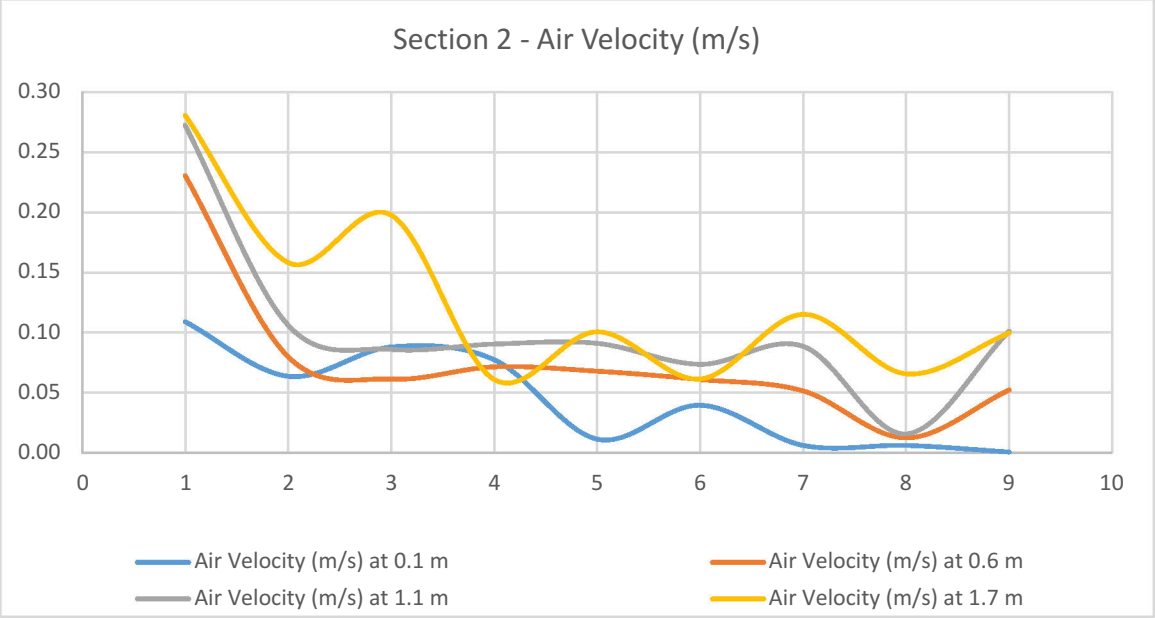

Figure B.18 - Section 2 – Graphs for Air Velocity and Temperature at SP 24(°C)

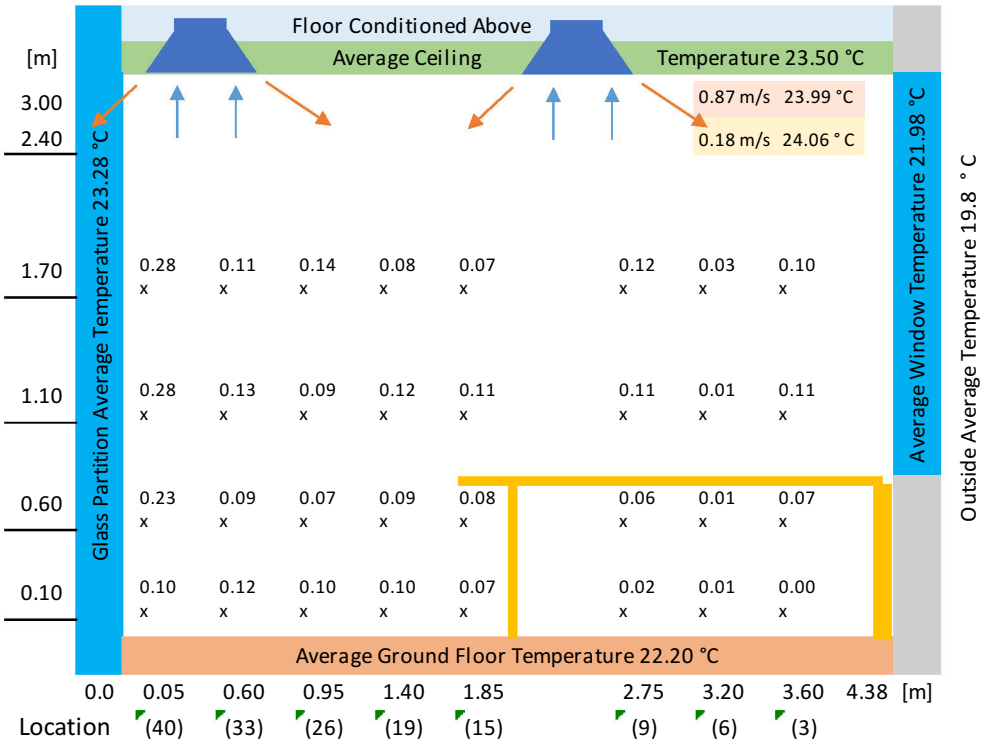

Plane - 3 (1.6 m) - Average Velocity at different heights

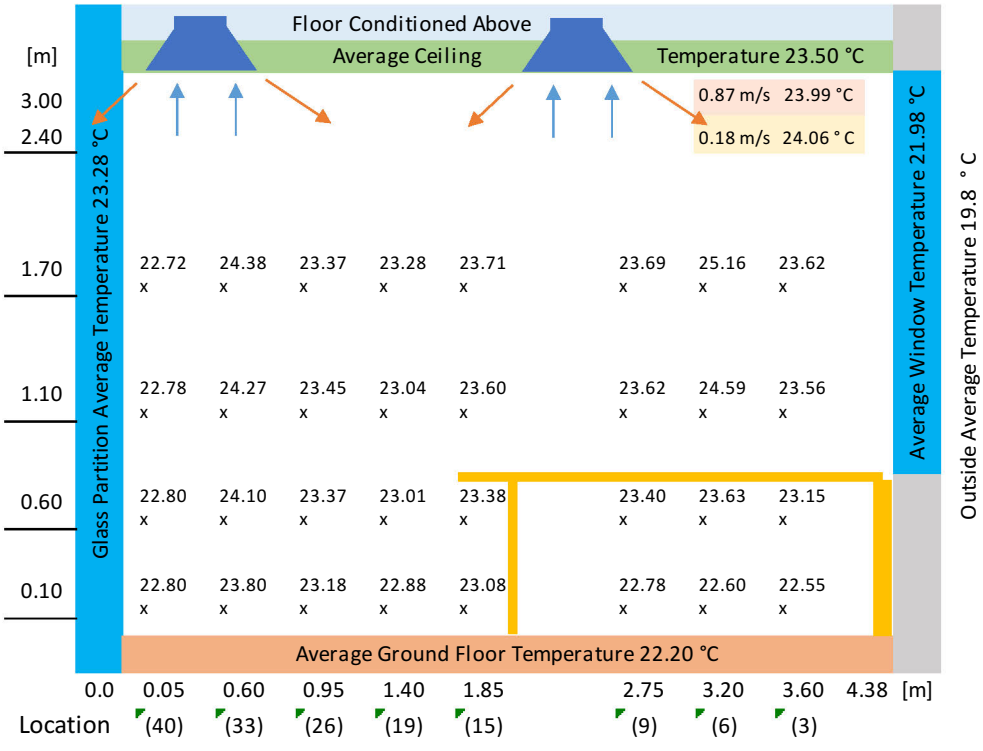

Plane - 3 (1.6 m) - Average Temperature at different heights

Figure B.19 - Spatial Distribution of Air Temperature and Velocity at Room SP Setpoint 24 (°C) (Section 3)

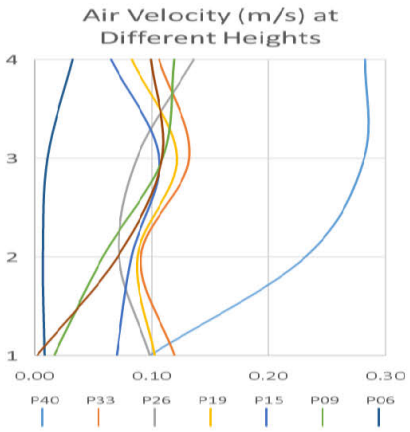

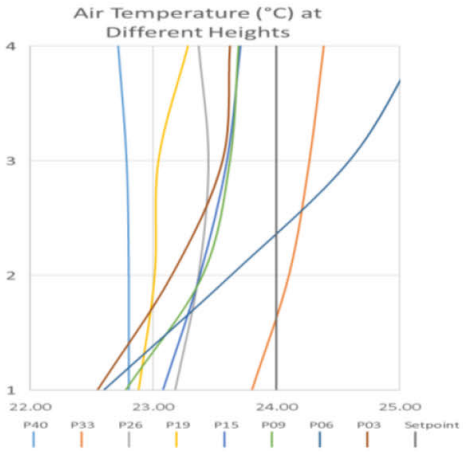

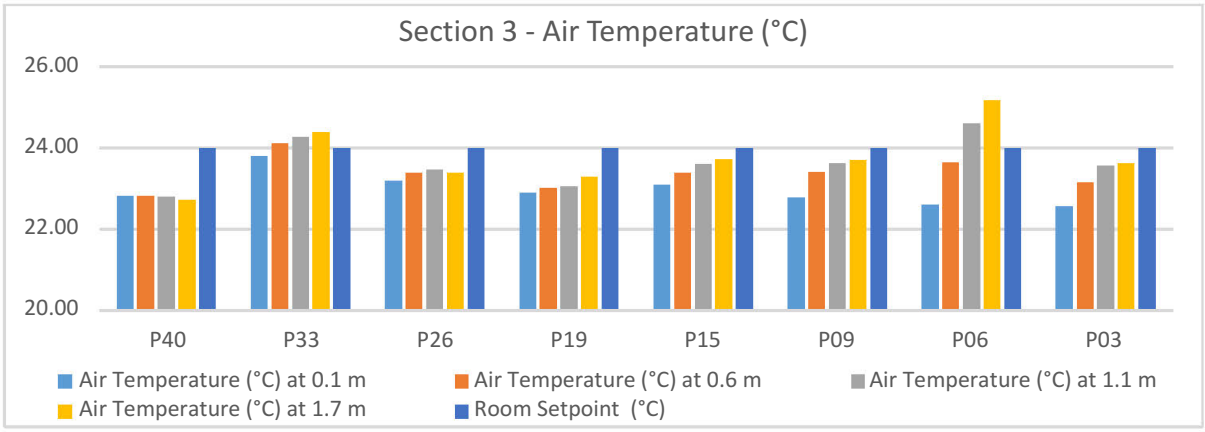

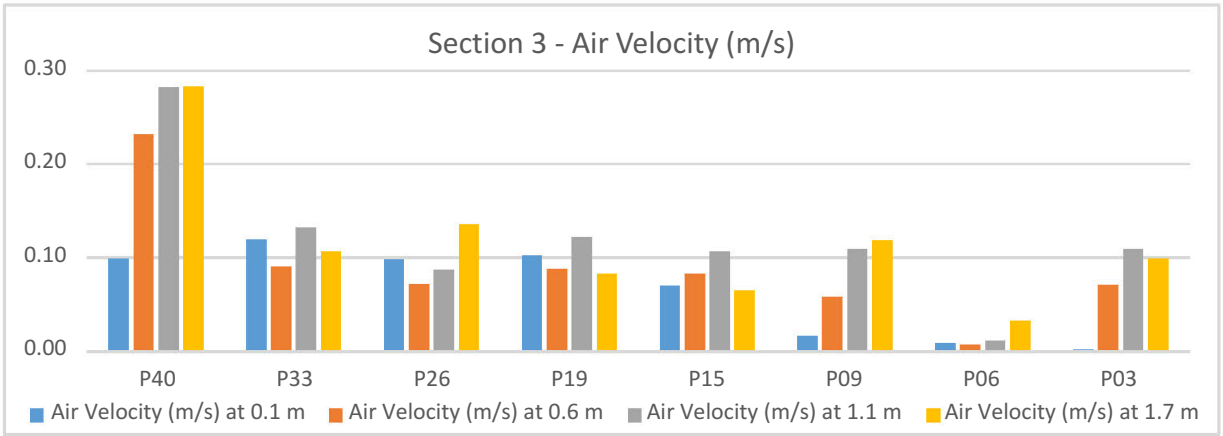

Figure B.20 - Section 3 – Graphs for Air Velocity and Temperature at 4 Different Heights at SP 24(°C)

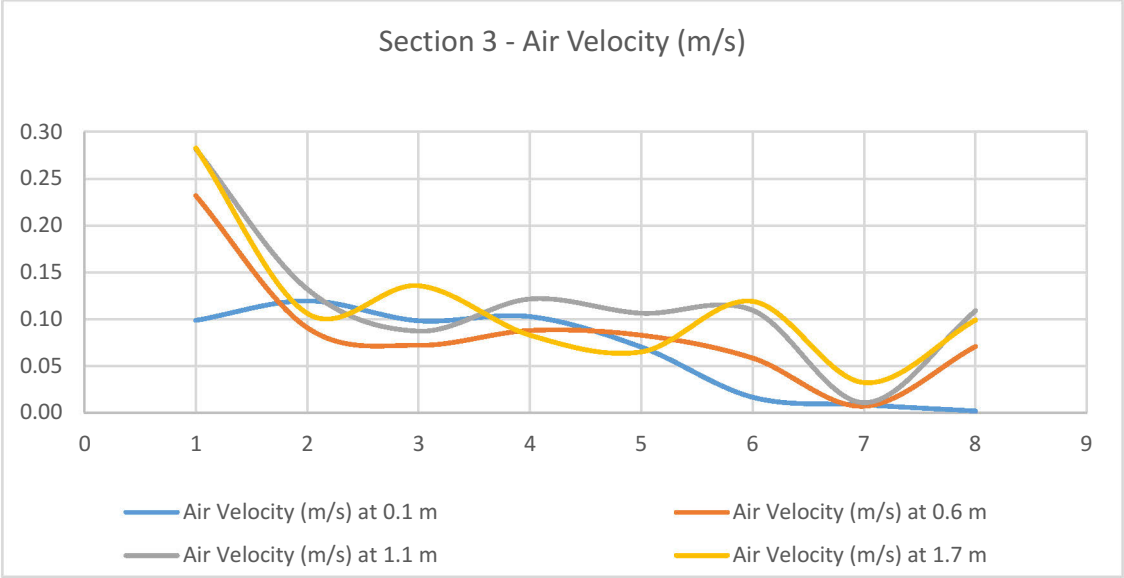

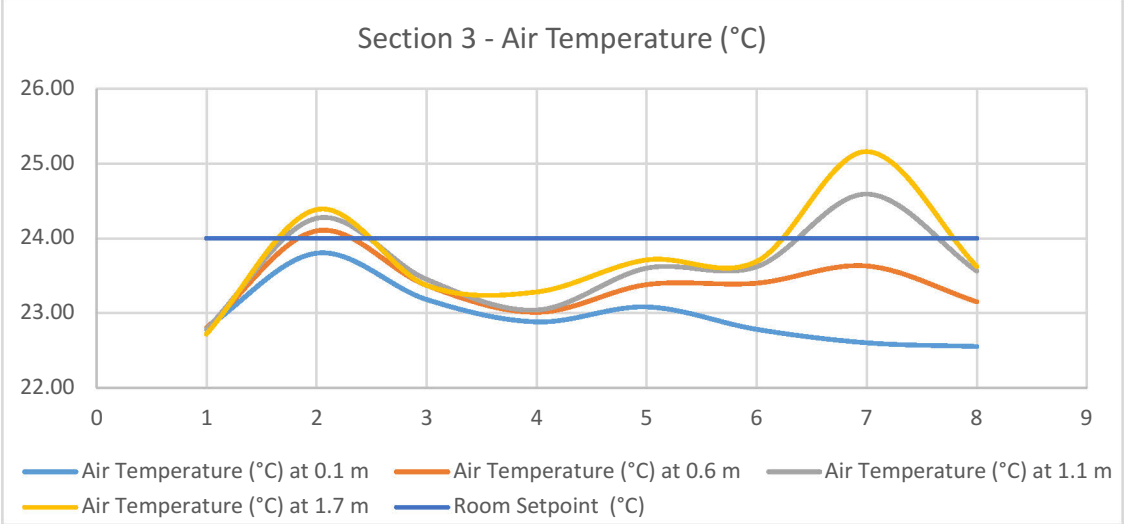

Figure B.21 - Section 3 – Graphs for Air Velocity and Temperature at SP 24(°C)

Room Setpoint 20°C

Table B.3 - Air Velocity and Air Temperature in Cooling at Setpoint 24°C (Cooling)

Experimental Results (Room Setpoint 20 (°C))											
Section / Plane	Point No	Distance (m)	Air Velocity (m/s)					Air Temperature (°C)				
			Height (m)					Height (m)				
			0.1	0.6	1.1	1.7	1.95	0.1	0.6	1.1	1.7	1.95
Section 1 (0.75 m)	38	0.05	0.12	0.12	0.17	0.19	0.14	18.93	18.93	18.84	18.7	18.79
	31	0.6	0.15	0.11	0.11	0.19	0.17	18.19	18.35	18.4	18.35	18.4
	24	0.95	0.18	0.12	0.11	0.17	0.14	17.92	18.2	18.22	18.17	18.18
	17	1.4	0.14	0.1	0.09	0.11	0.1	18.65	18.8	18.93	18.95	18.95
	13	1.85	0.12	0.11	0.11	0.09	0.1	18.83	18.87	18.9	19.02	18.98
	10	2.3	0.12	0.14	0.17	0.16	0.18	19.21	19.15	18.94	18.98	18.93
	7	2.75	0.1	0.09	0.15	0.16	0.16	19.14	19.19	19.19	19.21	19.15
	4	3.2	0.09	0.14	0.18	0.15	0.18	19.31	19.16	19.35	19.46	19.39
	1	3.6	0.05	0.11	0.13	0.08	0.09	19.54	19.52	19.64	19.65	19.59
Experimental Results (Room Setpoint 20 (°C))												
Section / Plane	Point No	Distance (m)	Air Velocity (m/s)					Air Temperature (°C)				
			Height (m)					Height (m)				
			0.1	0.6	1.1	1.7	1.95	0.1	0.6	1.1	1.7	1.95
Section 2 (1.2 m)	39	0.05	0.11	0.15	0.23	0.25	0.21	18.95	18.81	18.68	18.45	18.58
	32	0.6	0.12	0.16	0.15	0.27	0.26	18.41	18.45	18.49	18.34	18.43
	25	0.95	0.17	0.11	0.07	0.17	0.12	17.76	18.09	18.21	18.03	18.14
	18	1.4	0.11	0.08	0.1	0.1	0.07	18.67	18.78	18.82	18.92	18.99
	14	1.85	0.13	0.09	0.13	0.09	0.09	18.8	18.86	18.84	19.03	19.01
	11	2.3	0.12	0.11	0.14	0.13	0.11	18.98	18.9	18.9	18.99	18.93
	8	2.75	0.13	0.11	0.15	0.16	0.16	19.04	19.07	19.02	19.11	19.04
	5	3.2	0.11	0.13	0.2	0.16	0.16	19.16	19.16	19.22	19.39	19.33
	2	3.6	0.1	0.15	0.15	0.11	0.1	19.35	19.27	19.55	19.68	19.64
Experimental Results (Room Setpoint 20 (°C))												
ction / Pla	Point No	Distance (m)	Air Velocity (m/s)					Air Temperature (°C)				
			Height (m)					Height (m)				
			0.1	0.6	1.1	1.7	1.95	0.1	0.6	1.1	1.7	1.95
Section 3 (1.6 m)	40	0.05	0.09	0.25	0.31	0.33	0.3	19	18.68	18.54	18.28	18.38
	33	0.6	0.13	0.15	0.12	0.26	0.17	18.71	18.68	18.8	18.7	18.76
	26	0.95	0.08	0.08	0.08	0.21	0.23	17.92	18.1	18.27	17.82	17.88
	19	1.4	0.11	0.12	0.14	0.12	0.09	18.62	18.67	18.75	18.87	18.92
	15	1.85	0.1	0.15	0.1	0.11	0.09	18.8	18.73	18.9	19.03	19.01
	9	2.75	0.06	0.09	0.13	0.15	0.17	19.46	19.46	19.28	19.1	19.07
	6	3.2	0.19	0.15	0.18	0.16	0.18	19	19.14	19.25	19.3	19.26
	3	3.6	0.17	0.2	0.2	0.1	0.11	19.16	19.04	19.31	19.62	19.57

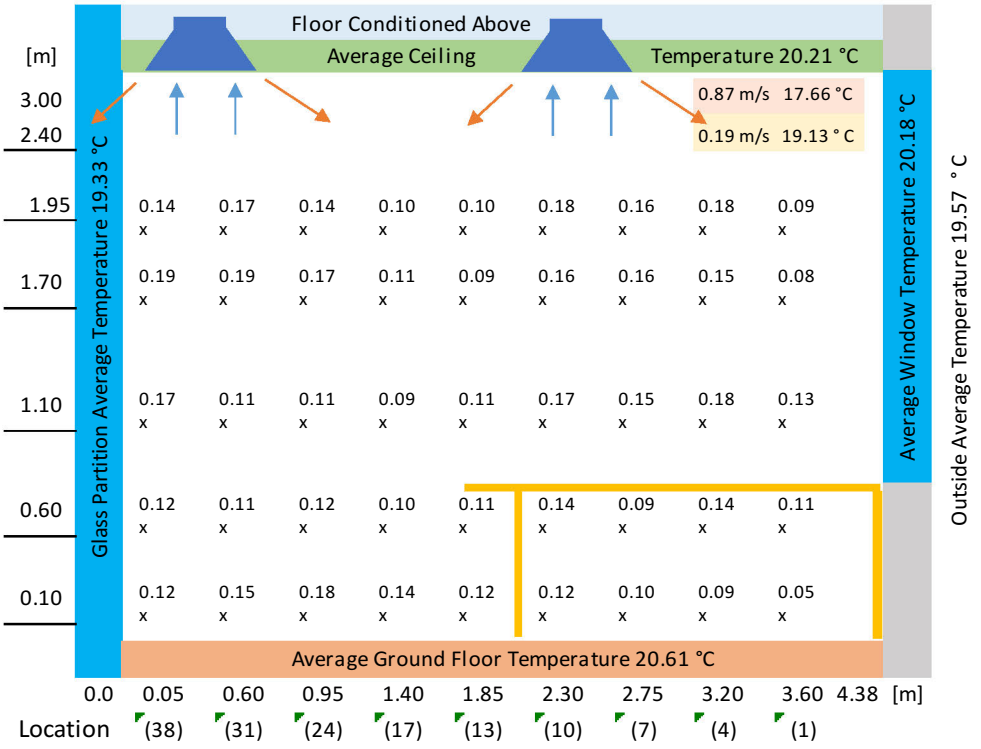

Plane - 1 (0.75 m) - Average Velocity at different heights

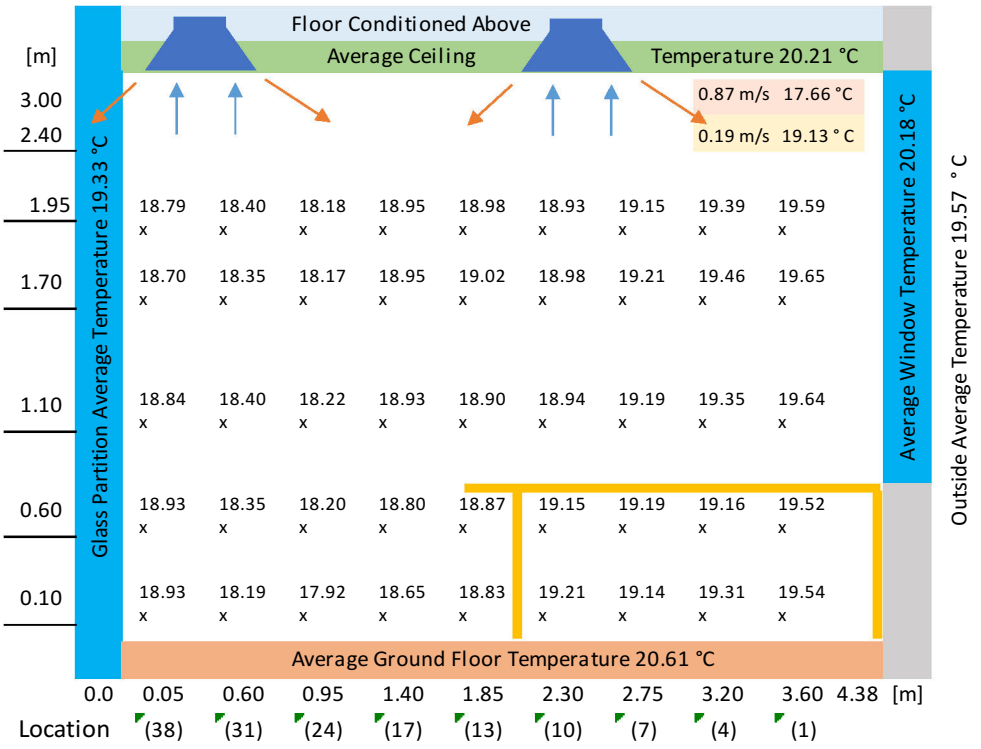

Plane - 1 (0.75 m) - Average Temperature at different heights

Figure B.22 - Spatial Distribution of Air Temperature and Velocity at Room SP Setpoint 20 (°C) (Section 1)

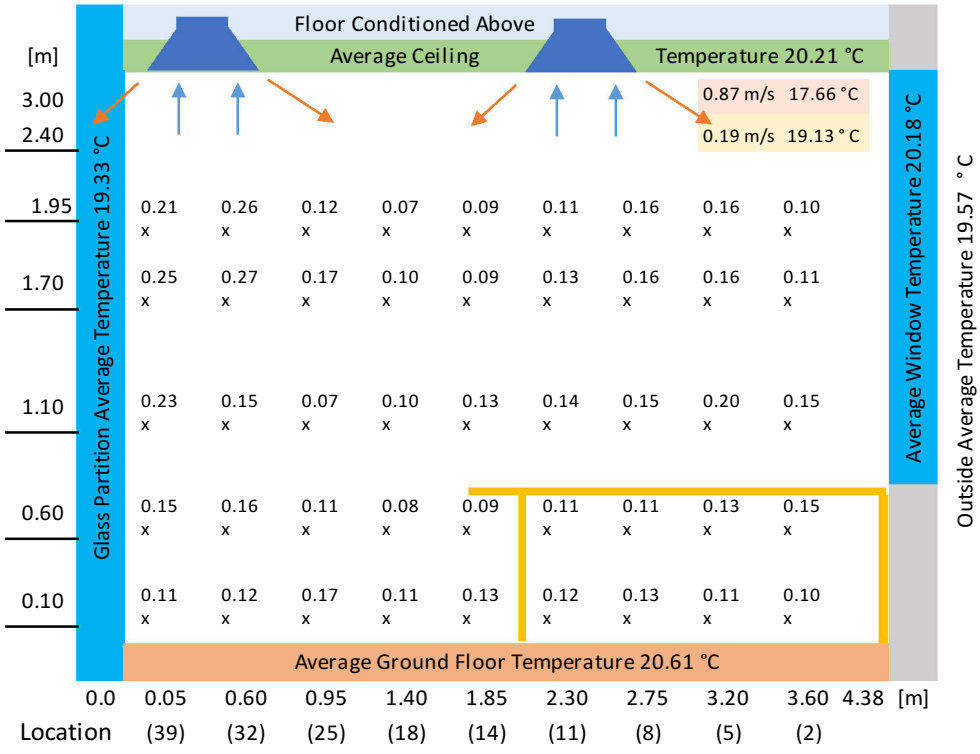

Plane - 2 (1.2 m) - Average Velocity at different heights

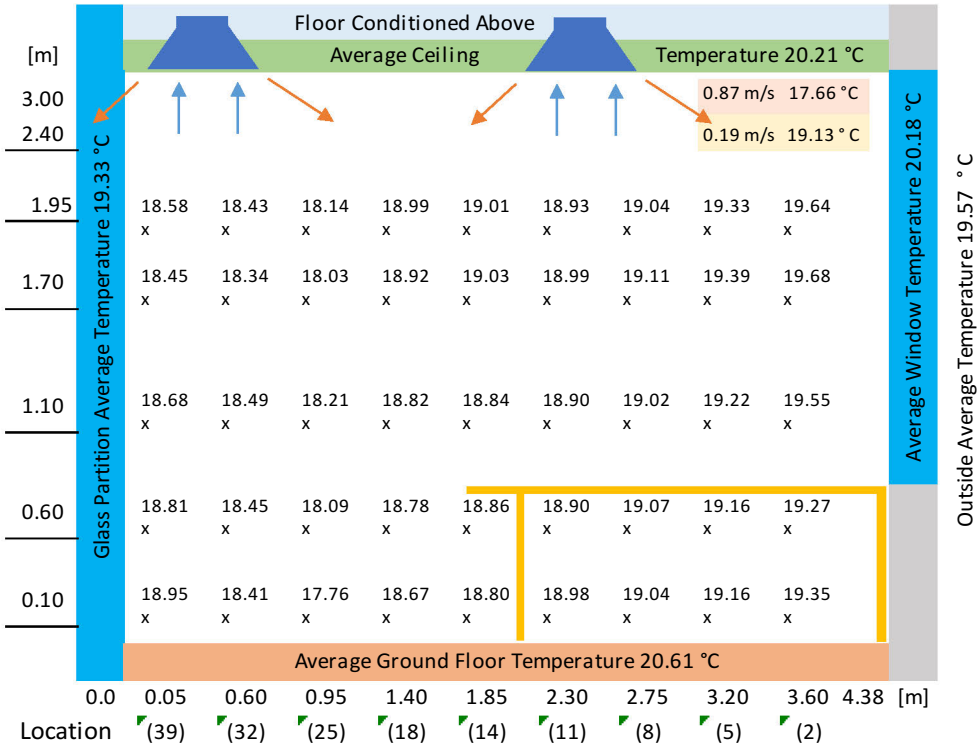

Plane - 2 (1.2 m) - Average Temperature at different heights

Figure B.23 - Spatial Distribution of Air Temperature and Velocity at Room SP Setpoint 20 (°C) (Section 2)

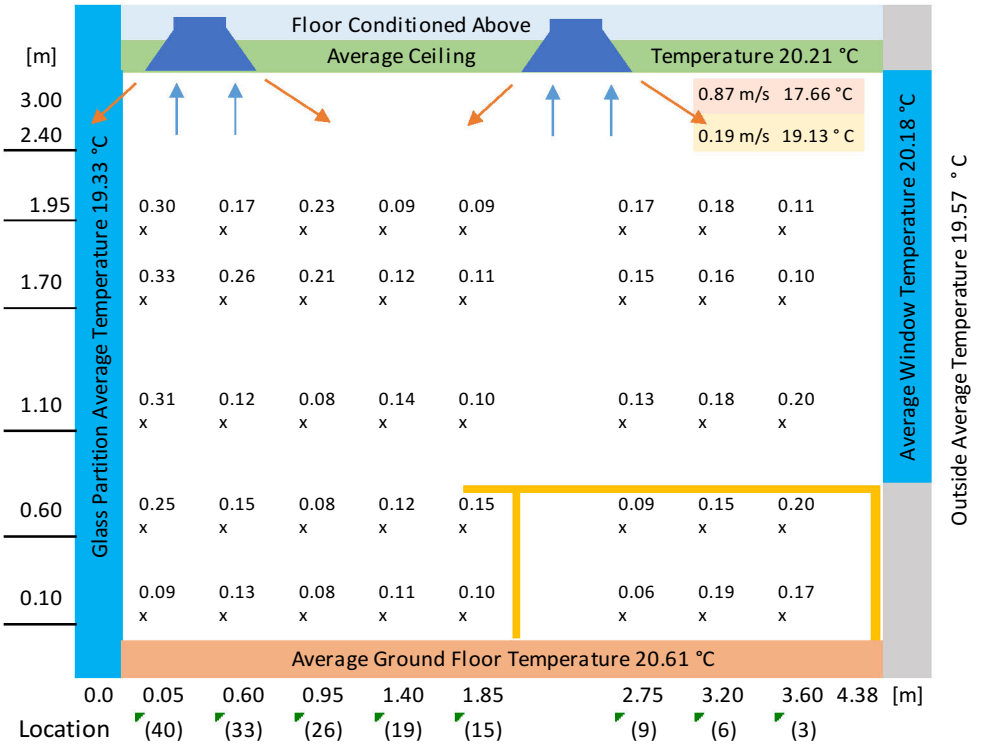

Plane - 3 (1.6 m) - Average Velocity at different heights

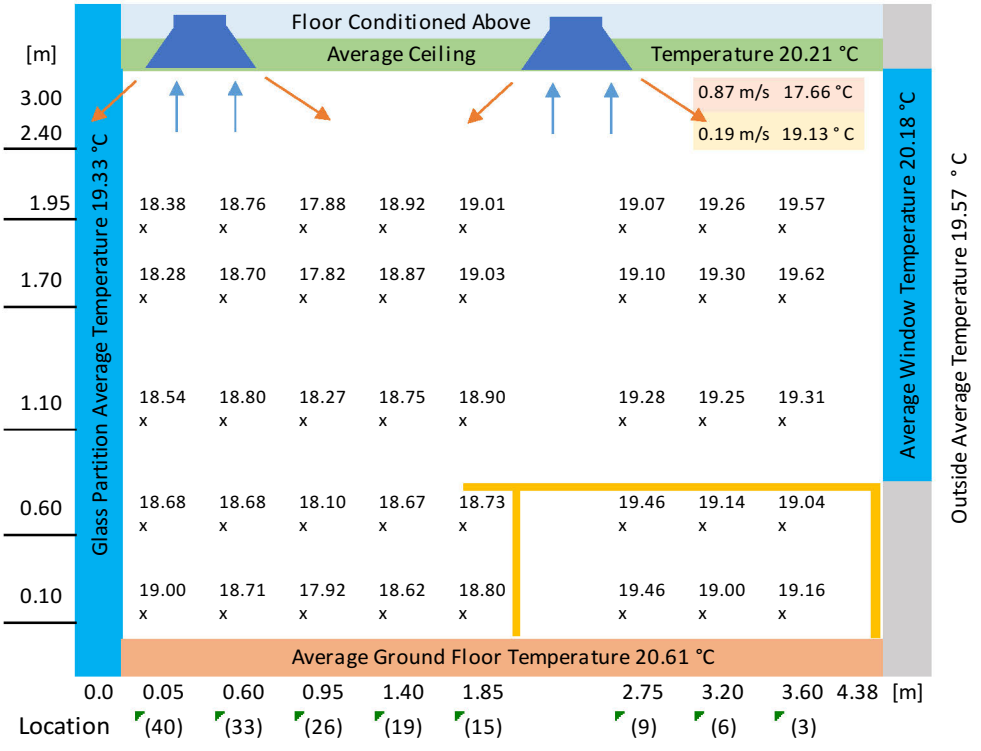

Plane - 3 (1.6 m) - Average Temperature at different heights

Figure B.24 - Spatial Distribution of Air Temperature and Velocity at Room SP Setpoint 20 (°C) (Section 3)

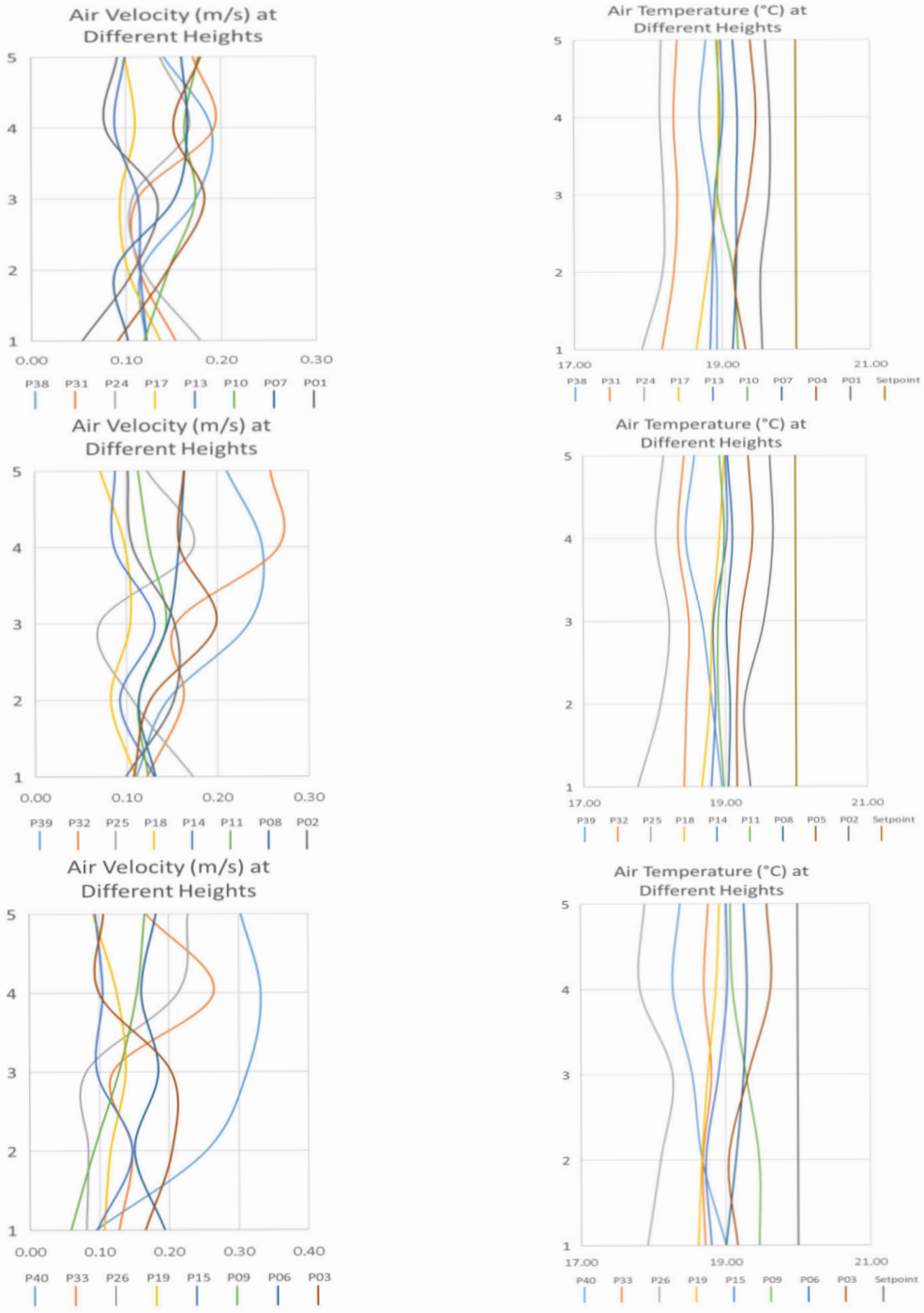

Figure B.25 - Section 1, 2 and 3 – Graphs for Air Velocity and Temperature at SP 20(°C)

APPENDIX C – ACB DETAILS (TROX)

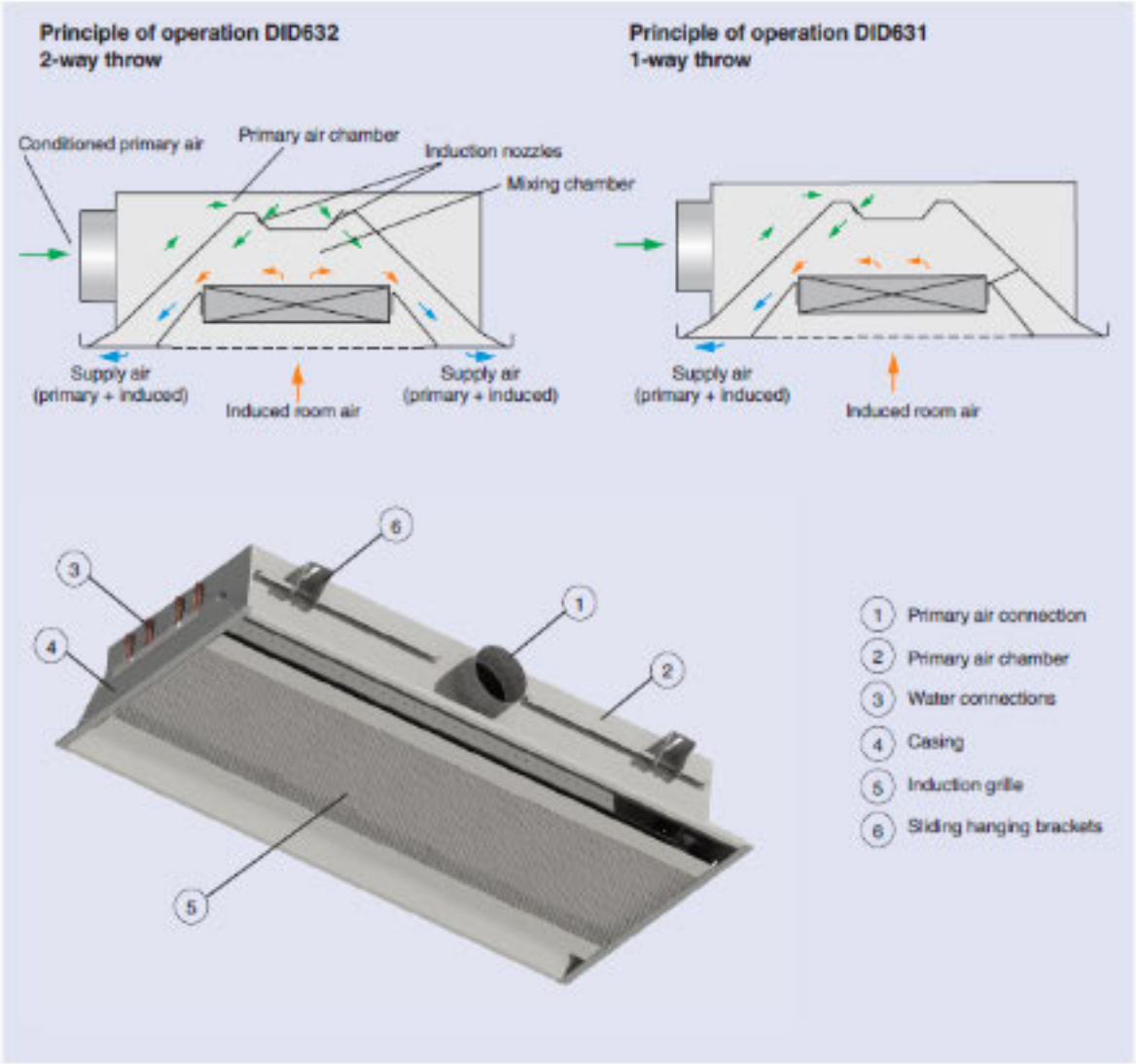

Characteristics

- Primary airflow range from 25 to 360 cfm
- For mounting heights of 8 to 15 ft
- Flush ceiling installation
- Side (standard) or top-entry primary air connection
- Lengths of 4, 5, 6, 7, 8, 9 and 10ft (other lengths on request)
- Integrates into most ceiling systems
- Nozzles in six sizes to optimize induction (see table below)
- Heat exchangers for two- or four-pipe systems
- Supply-return-air combination available (cost option)
- Maximum operating pressure: 250 psi
- Maximum operating temperature: 165˚F - 200˚F (other operating pressures and temperatures upon request)

Construction features

- Primary air connections suitable for circular connecting ducts
- 4 or 6 sliding hanging brackets (dependent on beam length) for on-site installation
- Water connections on the top near either end
- Induction grille can can be reversed in the field so that grille opens in the direction providing the easiest access to coil

Materials

- Casing, nozzle plate, hanging rails and primary air connection made of powder-coated steel
- Hanging brackets made of galvanized steel
- Perforated induction grille (option LR) made from powder-coated steel
- Linear bar induction grille (option GL) made from aluminum (cost option)
- Heat exchanger made of copper tubes and formed aluminum fins
- Heat exchanger natural finish (standard) or flat black (cost option)
- Visible surfaces powder-coated white (RAL 9010) as standard or alternative RAL color as cost option

Standard construction with 4-pipe heat exchanger
Side-entry, Type 0 Border

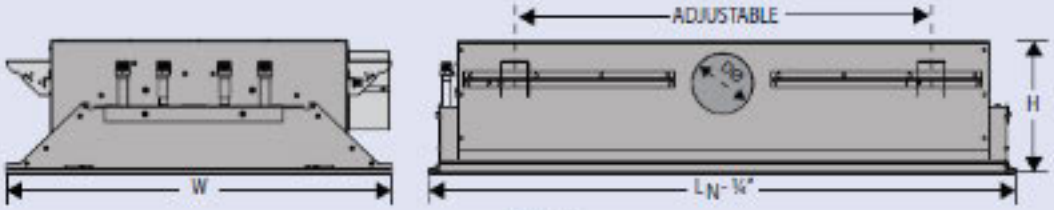

Standard border (Type 0) shown is designed for flush mounting in a 9/16" or 15/16" T-bar ceiling grid.

Optional border styles are shown below.

Available nominal lengths (L_N):
See chart at right

DID632
Height/Nozzle Type Table

Beam Length L_N	Nozzle Type							
	Z		M		G/J		H/U	
	H	DØ	H	DØ	H	DØ	H	DØ
4'	8½"	3¼"	8½"	3⅛"	8½"	4⅛"	8½"	5⅛"
5'							11"	7⅛"
6'								
7'				4⅛"		5⅛"		
8'		4⅛"						
9'								
10'								

T-BAR BORDER STYLE OPTIONS

Type B1

Designed for flush mounting with regular ceiling tiles for use in a 9/16" wide t-bar grid.

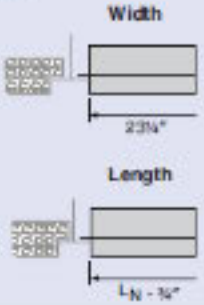

Type B2

Designed for flush mounting with regular ceiling tiles for use in a 15/16" wide t-bar grid.

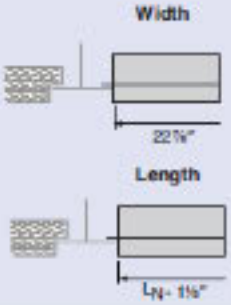

Technical data

Designation	Value
Primary air volume flow rate	6 – 85 l/s, 22 – 306 m³/h
Cooling capacity	Up to 2450 W
Heating capacity	Up to 2970 W
Max. operating pressure, water side	6 bar
Max. operating temperature	75 °C (55 °C when using flexible connecting hoses)
Minimum operating temperature	6 °C

Dimensions

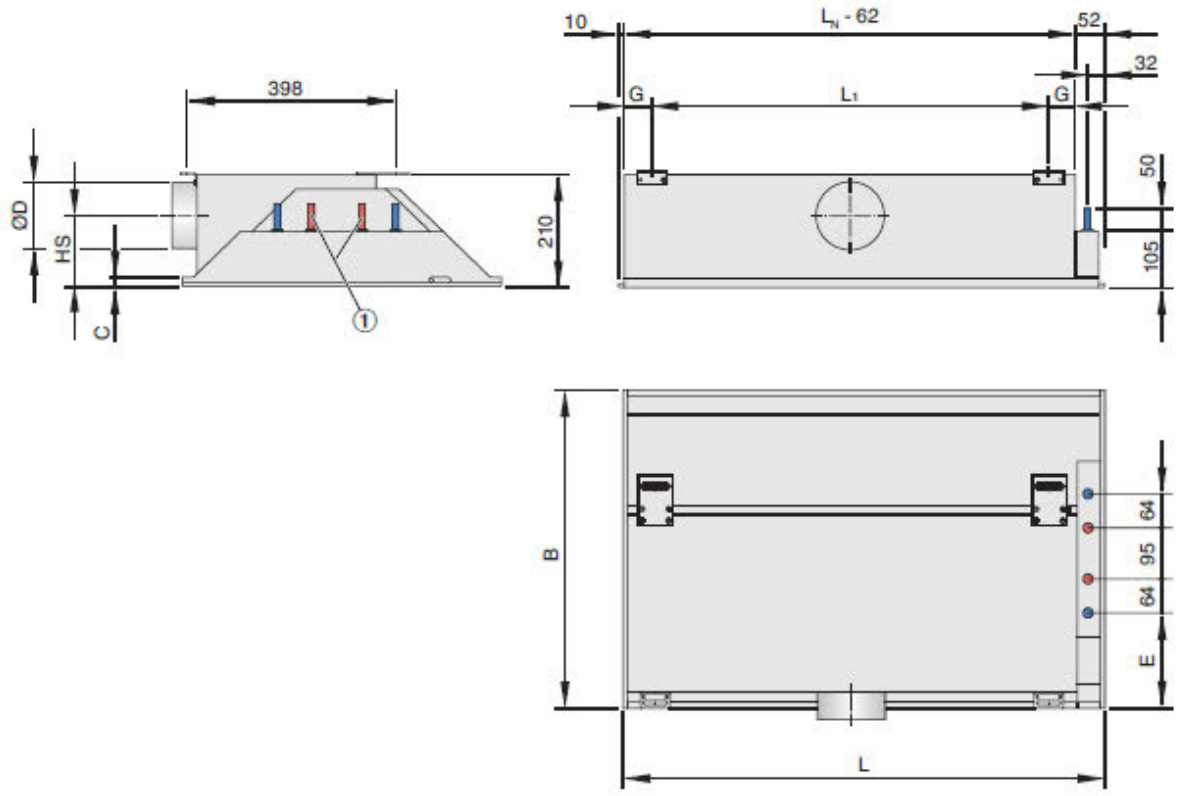

Fig. 2: Dimensional drawing of DID632

Dimensions [mm]		
B	C	E
593	18	177
598	8	179
618	18	189
623	8	192

B = Width of front frame

Dimensions [mm]					
L_N	L	L_1	ØD	HS	G
900	893 – 1500	735	123	134	51.5
1200	1193 – 1800	1035	123	134	51.5
1500	1493 – 2100	1335	123	134	51.5
1800	1793 – 2400	1035	123	134	351.5
2100	2093 – 2700	1315	158	116	361.5
2400	2393 – 3000	1435	158	116	451.5
2700	2693 – 3000	1515	158	116	561.5
3000	2993 – 3000	1635	158	116	651.5

L_N = Nominal length

L = Total length (diffuser face)

Weight [kg]								
Variant	L_N) [mm]							
	900	1200	1500	1800	2100	2400	2700	3000
DID632-LR	18	22	27	32	39	47	54	61
DID632-LQ	17	21	26	31	38	46	53	60
DID632-GL	20	25	31	36	43	52	59	67
DID632-GQ	20	25	31	36	43	52	59	67
Contained water (max.)	1.8	2.4	3	3.6	4.2	4.8	5.4	6